

**INVESTIGATION OF FLOW BOILING
HEAT TRANSFER AND FRICTION
COEFFICIENT ON COMPACT
PLATE-FIN HEAT EXCHANGER
SURFACES FOR R134a**

Thesis

Submitted in partial fulfilment of the requirements for the degree of

DOCTOR OF PHILOSOPHY

by

MUPPALA. AMARANATHA RAJU
(Reg. No. ME09P09)

RESEARCH GUIDES

Dr. T. P. ASHOK BABU
&
Dr. C. RANGANAYAKULU



**DEPARTMENT OF MECHANICAL ENGINEERING
NATIONAL INSTITUTE OF TECHNOLOGY
KARNATAKA, SURATHKAL, MANGALORE-575025**

JULY, 2017

DECLARATION

by the Ph.D. Research Scholar

I hereby *declare* that the Research Thesis entitled “**Investigation of flow boiling heat transfer and friction coefficient on compact plate-fin heat exchanger surfaces for R134a**” which is being submitted to the **National Institute of Technology Karnataka, Surathkal** in partial fulfillment of the requirements for the award of the Degree of **Doctor of Philosophy** in Department of **Mechanical Engineering** is a *bonafide report of the research work carried out by me*. The material contained in this Research Thesis has not been submitted to any University or Institution for the award of any degree.

Muppala. Amaranatha Raju

Registered No. 092008ME09P09

Department of Mechanical Engineering

Place: NITK-Surathkal

Date:

CERTIFICATE

This is to *certify* that the Research Thesis entitled “**Investigation of flow boiling heat transfer and friction coefficient on compact plate-fin heat exchanger surfaces for R134a**” submitted by **Muppala. Amaranatha Raju** (Register Number: **092008ME09P09**) as the record of the research work carried out by him, *is accepted as the Research Thesis submission* in partial fulfilment of the requirements for the award of degree of **Doctor of Philosophy**.

Research Guides

(Dr. C. Ranganayakulu)

(Dr. T. P. Ashok Babu)

Chairman - DRPC
(Signature with Date and Seal)

ACKNOWLEDGEMENT

I would like to express my deep sense of gratitude and respect to my supervisor **Dr. T. P. Ashok Babu**, Professor, Dean (FW) & former head of Mechanical Engineering Department, NITK, Surathkal for his excellent support, guidance and suggestions. I consider myself extremely lucky to be able to work under the guidance of such a dynamic personality.

My sincere and heartfelt thanks to my co-supervisor **Dr. C. Ranganayakulu**, Outstanding Scientist/Scientist 'H', Aeronautical Development Agency (ADA), Bangalore for his enormous encouragement, enlightening discussions and guidance at every stage of my research programme. I thank him for sparing his invaluable time and motivating me to complete the dissertation work.

I express my sincere thanks to my RPAC members **Dr. A. V. Adhikari**, Professor, Department of Chemistry, NITK, Surathkal and **Dr. Kumar. G. N.**, Assistant Professor, Mechanical Engineering Department, NITK, Surathkal for their motivation and encouragement to achieve my goal. I would like to thank present and past HOD's of Mechanical department, present and past Deans, present and past Directors of NITK, Surathkal for their encouragement.

I record my deepest gratitude to the Aeronautical Development Agency (ADA), Bangalore for allowing to carry out the research work on boiling heat transfer. I am grateful to **PGD (CA) & Director-ADA and R. Swaminathan, APGD (CP) & TD (GS)**, Aeronautical Development Agency (ADA), Bangalore for permitting me to carryout research work compact heat exchangers for boiling applications. I am deeply indebted to **Mr. A. Panigrahi** of M/s BHEL-HPVP, Vizak, who have taken keen interest in development of brazed test sections.

I would like to convey my sincere thanks to **Shri. K Nagaraja, Sc-'F'** and **Shri. K V Raman Murthy, Sc-'D'**, ADA, Bangalore for their valuable support and help during my entire course of research.

I would like convey special thanks to **Shri. Atmanand C M, PA-II, B. Mahesh, PA-II, Shri. M. Raghu**, Engineer, **Shri. A. Govardhan, M. Prakash Raju**, who have helped me in carryout work.

I record my special thanks to National Aerospace Laboratories (NAL), Bangalore for allowing to setup test facility and to carry out the research work. I am thankful to **Director–NAL and especially to Head (Propulsion Division)**. I would like convey special thanks to NAL team, **Dr. R. Rajendran, Shri. E. Rajesh, Shri Janakiram Reddy, Shri Pandyan, Shashidhar**, who have supported me in carryout work.

Words cannot express the feelings I have for my parents, I thank my **mother** and **father** for their constant unconditional support. I would like to thank my **mother-in law** and **father-in law** for their encouragement.

With a deep sense of gratitude I acknowledge the help rendered by my wife **Radhika**, who took care of every small detail at home. I am ever grateful to my daughter **Shishira** and my son **Chaitanya Shirish** who were deprived of my privileges and outings for several months.

Last but not least, I thank those who helped me directly or indirectly during my research work.

I thank **Lord Ganesha** who gave me all the strength and energy to undergo the uphill task and complete the PhD thesis. Without his blessings I would not have completed this milestone.

-Muppala. Amaranatha Raju

ABSTRACT

Compact plate-fin heat exchangers are extensively used in refrigeration industry, cryogenics and various process plants. Intensification of industrial thermal processes on one side as well as energy efficiency considerations on the other side has led to considerable interest in compact heat exchangers for applications of evaporation and condensation, which call for a low temperature difference between the fluids and thus for high heat transfer coefficients. In addition, compact heat exchangers are being used in aircraft industry for all electric ECS (Environmental Control System), utilizing phase change for design of evaporator and condenser. The hydraulic diameter of flow passages is usually less than 3 mm in compact heat exchangers. The two-phase flow regimes which, occur in these passages differ from those in general heat exchangers. In phase change heat transfer, in addition to fluid properties and geometrical parameters, fluid flow parameters are also affecting the heat transfer and frictional coefficients. Present study aims to extend the knowledge of performance of compact evaporator's and to develop a model which can be used for evaluating the heat transfer and pressure drop over a wide range of operating conditions as possible.

In the present study the two-phase phase frictional pressure drop and heat transfer performance characteristics of compact plate fin heat exchangers used as evaporators over R134a were investigated. Two-phase heat transfer coefficient and friction coefficient of the finned surfaces constitute the most important parameters for design of compact evaporator. These parameters are functions of fin geometry, mass flux, heat flux and vapour quality. An experimental test facility has been constructed to study the 2 offset strip and 2 wavy fin surfaces of plate fin heat exchangers and for generation of two-phase heat transfer and friction data.

A cross flow heat exchanger of specified dimension (150 x150 mm) has been designed and manufactured using vacuum brazing technique. It serves as the experimental test section/test evaporator. One channel of the test section, R134a refrigerant is passed and another channel of test section is passed with water. The heat is exchanged between these fluids. R134a absorbs the heat from water and gets evaporated due to latent heat of evaporation. Water gets cooled.

Experiments were carried out on evaporator test sections under two-phase flow conditions using R134a on one side and water on another side of the test section to investigate the two-phase heat transfer coefficients and friction coefficients on the wavy and offset strip fin surfaces. Refrigerant flow boiling heat transfer and two-phase pressure drop data were obtained over a range of refrigerant mass flux from 30 to 100 kg/m²s, heat flux from 11 to 24 kW/m², outlet vapour quality from 0.24 to 0.9 and saturation temperatures from -5 to 5 °C. The data was obtained under steady state conditions during evaporator performance tests. Inlet and exit temperatures, pressures as well as refrigerant flow rates, water flow rates, pressure drops across the test section has been measured and recorded. Experimental data was reduced and analysed for effect of quality, mass flux and heat flux and presented in the report.

The correlations were developed in terms of Reynolds number factor (F) and Martenelli parameter (X) for flow boiling heat transfer and in terms two-phase frictional multiplier ϕ_f and Martenelli parameter (X) for frictional pressure drop using the regression analysis.

Two-phase forced convective heat transfer coefficient is a multiplication of single-phase heat transfer coefficient, h_l by Reynolds number factor (F). Before conducting two-phase heat transfer experiments single-phase flow and heat transfer experiments were conducted on these fin surfaces to validate the test facility and testing procedure and also to find out single-phase heat transfer coefficient h_l and frictional factor f . The measured single-phase flow and heat transfer data for each fin surface is estimated in terms of the Colburn j factor and Fanning friction factor f as a function of Reynolds number.

Single phase flow and heat transfer analysis of R134a refrigerant (liquid phase) has also been carried out using Computational fluid dynamics (CFD) approach for wavy and offset strip fin surfaces. The results were validated with the single phase experimental results. Colburn j factor and Fanning friction factor f are predicted for both the fins. The correlations are developed at Reynolds number range of 100-15000. The effects of fin geometry on the enhanced heat transfer and pressure drops were investigated.

Keywords: Boiling, Evaporator, Fin surface, Fluid, Heat exchanger, Heat transfer, Refrigerant, Offset strip, Two-phase, Wavy.

CONTENTS

CHAPTER NO.	TITLE	PAGE NO.
	ACKNOWLEDGEMENT	i
	ABSTRACT	iii
	LIST OF FIGURES	xi
	LIST OF TABLES	xvi
	NOMENCLATURE	xvii
1	INTRODUCTION	1
	1.1 BOILING HEAT TRANSFER	3
	1.1.1 Flow boiling	4
	1.2 COMPACT HEAT EXCHANGERS	6
	1.2.1 Plate fin heat exchangers	6
	1.2.2 Materials	7
	1.2.3 Manufacture	8
	1.2.4 Applications	8
	1.2.5 Flow arrangement	9
	1.3 HEAT TRANSFER FIN SURFACES	9
	1.3.1 Offset strip fins	10
	1.3.2 Wavy fins	11
	1.4 TWO-PHASE FLOW HEAT TRANSFER AND FRICTION CHARACTERISTICS.	12
	1.5 SCOPE AND OBJECTIVES OF THE PRESENT STUDY	13
	1.6 ORGANIZATION OF THE THESIS	14
2	LITERATURE REVIEW	15
	2.1 EXPERIMENTAL STUDIES ON TWO-PHASE HEAT TRANSFER AND PRESSURE DROP	17
	2.1.1 Experimental studies in multichannel arrangements of offset strip and perforated fin passages	17
	2.1.2 Experimental studies in small circular and rectangular channels	21
	2.1.3 Experimental studies in plate heat exchangers	29

2.2	STUDIES ON SINGLE PHASE HEAT TRANSFER AND PRESSURE DROP IN COMPACT PLATE FIN SURFACES	31
3.0	CONCLUSION FROM THE LITERATURE SURVEY AND MOTIVATION	33
3	COMPUTATIONAL APPROACH FOR SINGLE PHASE HEAT TRANSFER AND FRICTIONAL ANALYSIS OF FIN SURFACES	35
3.1	CFD ANALYSIS	35
3.2	CFD APPROACH	36
3.3	METHODOLOGY	37
3.4	MATHEMATICAL MODEL AND GOVERNING EQUATIONS	37
3.5	ASSUMPTIONS	39
3.6	BOUNDARY CONDITIONS	40
3.7	ANSYS CFD PACKAGE	41
3.8	COMPUTATION OF j AND f FACTORS	42
3.9	HEAT TRANSFER AND FRICTIONAL ANALYSIS OF WAVY FINSURFACE	43
3.9.1	Numerical Model	43
3.9.2	CFD analysis	45
3.9.2.1	Computational domain	45
3.9.2.2	Dimensionless parameters	45
3.9.2.3	Grid independency	46
3.9.2.4	CFD simulation studies	47
3.9.2.5	Velocity and temperature fields	47
3.9.2.6	Validation	51
3.9.2.7	Generation of f and j data	53
3.9.3	Effect of geometry parameters and Reynolds number	54
3.9.3.1	Effect of h/s ratio on ' j ' and ' f '	54
3.9.3.2	Effect of a/s ratio on ' j ' and ' f '	55
3.9.3.3	Effect of λ/a ratio on ' j ' and ' f '	57
3.9.4	Generation of flow friction and heat transfer correlations	59
3.9.5	Determination of indices	60

3.10	HEAT TRANSFER AND FRICTIONAL ANALYSIS OF OFFSET STRIP FIN SURFACE	61
3.10.1	Numerical Model	61
3.10.2	CFD analysis	62
3.10.2.1	Computational domain	62
3.10.2.2	Dimensionless parameters	62
3.10.2.3	Grid independency	63
3.10.2.4	CFD simulation studies	63
3.10.2.5	Velocity and temperature fields	64
3.10.3	Generation of f and j data	65
3.10.4	Effect of geometry parameters and Reynolds number.	65
3.10.4.1	Effect of h/s ratio on ' j ' and ' f '	65
3.10.4.2	Effect of t/s ratio on ' j ' and ' f '	67
3.10.4.3	Effect of t/l ratio on ' j ' and ' f '	69
3.10.5	Generation of flow friction and heat transfer correlations	70
3.10.6	Determination of indices	71
3.11	SUMMARY	72
4	DEVELOPMENT OF EXPERIMENTAL SET UP FOR INVESTIGATION OF TWO-PHASE HEAT TRANSFER AND PRESSURE DROP ON FIN SURFACES	73
4.1	DETAILED SPECIFICATION OF THE TEST RIG	73
4.1.1	Refrigerant circuit	73
4.1.2	Condensation / Evaporation secondary circuit	74
4.2	STANDARDS	74
4.3	DESIGN AND DEVELOPMENT OF TEST RIG	75
4.3.1	Refrigerant loop	79
4.3.2	Evaporator loop	81
4.3.3	Super heater loop	83
4.3.4	Condenser loop	83
4.3.5	De-Super heater loop	84
4.3.6	Single phase flow and heat transfer loop	85
4.3.7	Details of major rig components	87

	4.3.7.1 Compressor	87
	4.3.7.2 Evaporator and Condenser	88
	4.3.7.3 Expansion Valve-Electronic	88
	4.3.7.4 Oil separators	89
	4.3.7.5 Chiller units	89
	4.3.7.6 Solenoid valves	89
	4.3.7.7 Flow regulating valves (FRV)	90
	4.3.7.8 Piping	90
	4.3.7.9 Evacuation and Gas charging system	90
4.4	INSTRUMENTATION OF THE TEST RIG	91
	4.4.1 Coriolis flow meter	91
	4.4.2 Turbine flow meter	91
	4.4.3 Pressure transducers and Differential pressure transducers	92
	4.4.4 Temperature sensors with digital indicator	93
4.5	DATA ACQUISITION SYSTEM	93
	4.5.1 Display details	95
	4.5.2 Electrical system	96
	4.5.2.1 MCC panel	96
4.6	MEASURING INSTRUMENT CALIBRATION	96
5	EXPERIMENTAL PROCEDURE AND DATA REDUCTION	97
	5.1 TEST SECTION/TEST EVAPORATOR	97
	5.2 TEST ARTICLE MOUNTING	101
	5.3 TESTING PROCEDURE	102
	5.3.1 Single phase heat transfer and pressure drop testing	102
	5.3.2 Two-phase heat transfer and pressure drop testing	104
	5.4 EXPERIMENTATION	105
	5.4.1 Single phase heat transfer experimentation	105
	5.4.2 Single phase pressure drop experimentation	107
	5.4.3 Two-phase flow and heat transfer experimentation	107

5.5	DATA REDUCTION	109
5.5.1	Single phase heat transfer and pressure drop	109
5.5.1.1	Single phase heat transfer coefficient	109
5.5.1.2	Single phase pressure drop coefficient	110
5.5.1.3	Estimation of single phase heat transfer and friction factor using CFD	110
5.5.2	Two-phase heat transfer and pressure drop coefficients	111
5.5.2.1	Two-phase heat transfer coefficient	111
5.5.2.2	Two-phase pressure drop coefficient	113
5.6	MEASUREMENT OF LUBRICATING OIL CONCENTRATION	123
5.7	ERROR AND UNCERTAINTY ANALYSIS	124
5.8	SUMMARY	128
6	RESULTS AND DISCUSSIONS	129
6.1	SINGLE-PHASE HEAT TRANSFER AND PRESSURE DROP CHARACTERISTICS	129
6.2	TWO-PHASE HEAT TRANSFER CHARACTERISTICS	131
6.2.1	Heat transfer characteristics of offset fin surfaces	131
6.2.1.1	Influence of flow properties on heat transfer coefficient	138
6.2.2	Heat transfer characteristics wavy fin surfaces.	140
6.3	Two Phase Pressure drop characteristics	147
6.3.1	Pressure drop characteristics of offset strip fin surfaces.	148
6.3.2	Pressure drop characteristics wavy fin surfaces	150
6.4	DEVELOPMENT OF TWO-PHASE CORRELATIONS FOR COMPACT PLATE FIN SURFACES.	151
6.4.1	Two-phase heat transfer correlations	151
6.4.1.1	Generation of heat transfer correlations for offset strip fin, OSF1	151
6.4.1.2	Generation of heat transfer correlations for offset strip fin, OSF2	154
6.4.1.3	Generalized heat transfer correlation	157

	for offset strip fin surfaces	
	6.4.1.4 Generation of heat transfer correlations for wavy fin, WF1	158
	6.4.1.5 Generation of heat transfer correlations for wavy fin,WF2	160
	6.4.1.6 Generalized correlation for wavy fin surfaces	162
6.4.2	Two-phase frictional pressure drop correlations	163
	6.4.2.1 Generation of frictional correlations for offset strip fin, OSF1	164
	6.4.2.2 Generation of frictional correlations for offset strip fin,OSF2	165
	6.4.2.3 Generalized frictional correlation for offset strip fin surfaces	166
	6.4.2.4 Generation of frictional correlations for wavy fin, WF1	166
	6.4.2.5 Generation of frictional correlations for wavy fin, WF2	167
	6.4.2.6 Generalized frictional correlation for wavy fin surfaces	168
6.5	SUMMARY	169
7	CONCLUSIONS AND SCOPE FOR FUTURE WORK	171
7.1	CONCLUSIONS	171
7.2	SCOPE FOR FUTURE WORK	173
	REFERENCES	175
	APPENDIXES	
I.	MEASURING INSTRUMENTS CALIBRATION	182
	PUBLICATIONS	191
	CURRICULUM VITAE	

LIST OF FIGURES		
FIGURE NO.	TITLE	PAGE NO
1.1	Flow boiling in a uniformly heated circular tube	5
1.2	Plate fin heat exchanger assembly	7
1.3	Heat exchanger flow arrangements	9
1.4	Types of fin geometries	10
1.5	Photograph of offset strip fin	11
1.6	Photograph of smooth wavy fin surface	12
3.1	Flow chart of methodology	38
3.2	Numerical model for wavy fin	43
3.3	Geometry parameters of wavy fin	44
3.4	Computational fluid domain for the smooth wavy fin surface.	45
3.5	Grid independency graph for wavy fin	47
3.6	Velocity profiles of wavy fin at h/2 a) liquid refrigerant R134a b) water	48
3.7	Total pressure profiles of wavy fin at h/2 a) liquid refrigerant R134a b) water	49
3.8	Static temperature profiles of wavy fin near the wall a) liquid refrigerant R134a b) water	50
3.9	Validation with experimental results for the fin 2.8h-3.5s-0.2t a) Water b) R113	52
3.10	Validation with experimental results for the fin 6.77h-1.411s-0.152t	53
3.11	Effect of h/s ratio on performance of wavy fin a) Colburn j factor b) Friction factor ' f '	55
3.12	Effect of a/s ratio on performance wavy fin a) Colburn j factor b) Friction factor ' f '	57
3.13	Effect of λ/a ratio on performance wavy fin a) Colburn j factor b) Friction factor ' f '	58
3.14	Numerical model for offset strip fin	61
3.15	The computational fluid domain for the offset strip fin surface	62
3.16	Grid independency graph for offset strip fin	63
3.17	Velocity profiles of offset strip fin at h/2 liquid refrigerant R134a	64
3.18	Static pressure profiles of offset strip fin at h/2 liquid refrigerant R134a	64

3.19	Static temperature profiles of offset strip fin at h/2 liquid refrigerant R134a	65
3.20	Effect of h/s ratio on performance of offset strip fin a) Friction factor ' f ' b) Colburn j factor	67
3.21	Effect of t/s ratio on performance of offset strip fin a) Friction factor ' f ' b) Colburn j factor	68
3.22	Effect of t/l ratio on performance of offset strip fin a) Friction factor ' f ' b) Colburn j factor	70
4.1	Schematic of the experimental rig for measurement of two-phase heat transfer and frictional characteristics of compact plate fin surfaces.	77
4.2a	Photograph of experimental test rig	78
4.2b	Photograph of experimental test rig in another view with test section	78
4.3	Photograph of experimental test section view in the test facility	79
4.4	Photograph of data acquisition system of test rig	79
4.5	Schematic layout of refrigerant loop	81
4.6	Schematic layout of evaporator loop	82
4.7	Schematic layout of super heater loop	83
4.8	Schematic layout of condenser loop	84
4.9	Schematic layout of de-super heater loop	85
4.10	Schematic layout of single phase loop	86
4.11	Facility with major component locations	87
4.12	Block diagram of data acquisition system	94
5.1	Test section block a) 3D-Model b) Brazed block	99
5.2	Thermocouples arrangements in test section	99
5.3	Cut section of thermocouples inserted in test section	100
5.4	Test Section/test evaporator	100
5.5	Figure depicting temperature, flow and pressure measurement a) Line diagram b) Picture of measurement	102
5.6	Pictorial Representation of data reduction for two-phase heat transfer coefficient	118
5.7	Pictorial Representation of data reduction for two-phase pressure drop	119
5.8	Measurement of % of lubricating oil mixing	123
6.1	Flow friction factor f and j factor for OSF1	130
6.2	Flow friction factor f and j factor for WF1	130
6.3	Measured local two-phase heat transfer coefficient h_{tp} Vs vapour quality x at heat flux $q = 16 \text{ kW/m}^2$ for mass fluxes \dot{G} (63, 73 and $82 \text{ kg/m}^2\text{s}$) for fin surface OSF1	131

6.4	Measured local two-phase heat transfer coefficient h_{tp} Vs vapour quality x at heat flux $q = 18 \text{ kW/m}^2$ for mass fluxes \dot{G} (63, 73 and $82 \text{ kg/m}^2\text{s}$) for fin surface OSF1	132
6.5	Measured local two-phase heat transfer coefficient h_{tp} Vs vapour quality x at heat flux $q = 21 \text{ kW/m}^2$ for mass fluxes \dot{G} (63, 73 and $82 \text{ kg/m}^2\text{s}$) for fin surface OSF1	132
6.6	Measured local two-phase heat transfer coefficient h_{tp} Vs vapour quality x at mass flux $\dot{G} = 63 \text{ kg/m}^2\text{s}$ for three heat fluxes q (16, 18 and 21 kW/m^2) for fin surface OSF1	133
6.7	Measured local two-phase heat transfer coefficient h_{tp} Vs vapour quality x at mass flux $\dot{G} = 73 \text{ kg/m}^2\text{s}$ for three heat fluxes q (16, 18 and 21 kW/m^2) for fin surface OSF1	133
6.8	Measured local two-phase heat transfer coefficient h_{tp} Vs vapour quality x at mass flux $\dot{G} = 82 \text{ kg/m}^2\text{s}$ for three heat fluxes q (16, 18 and 21 kW/m^2) for fin surface OSF1	134
6.9	Measured local two-phase heat transfer coefficient h_{tp} Vs vapour quality x at heat flux $q = 16 \text{ kW/m}^2$ for mass fluxes \dot{G} (48, 63 and $73 \text{ kg/m}^2\text{s}$) for fin surface OSF2	134
6.10	Measured local two-phase heat transfer coefficient h_{tp} Vs vapour quality x at heat flux $q = 21 \text{ kW/m}^2$ for mass fluxes \dot{G} (48, 63 and $73 \text{ kg/m}^2\text{s}$) for fin surface OSF2	135
6.11	Measured local two-phase heat transfer coefficient h_{tp} Vs vapour quality x at heat flux $q = 24 \text{ kW/m}^2$ for mass fluxes \dot{G} (48 and $73 \text{ kg/m}^2\text{s}$) for fin surface OSF2	135
6.12	Measured local two-phase heat transfer coefficient h_{tp} Vs vapour quality x at mass flux $\dot{G} = 48 \text{ kg/m}^2\text{s}$ for three heat fluxes q (16, 21 and 24 kW/m^2) for fin surface OSF2	136
6.13	Measured local two-phase heat transfer coefficient h_{tp} Vs vapour quality x at mass flux $\dot{G} = 63 \text{ kg/m}^2\text{s}$ for four heat fluxes q (13, 16, 21 and 24 kW/m^2) for fin surface OSF2	136
6.14	Measured local two-phase heat transfer coefficient h_{tp} Vs vapour quality x at mass flux $\dot{G} = 73 \text{ kg/m}^2\text{s}$ for three heat fluxes q (16, 21 and 24 kW/m^2) for fin surface OSF2	137
6.15	Measured local two-phase heat transfer coefficient h_{tp} Vs vapour quality x at heat flux $q = 13 \text{ kW/m}^2$ for mass fluxes \dot{G} (30, 35 and $40 \text{ kg/m}^2\text{s}$) for fin surface WF1	140
6.16	Measured local two-phase heat transfer coefficient h_{tp} Vs vapour quality x at heat flux $q = 16 \text{ kW/m}^2$ for mass fluxes \dot{G} (30 and $35 \text{ kg/m}^2\text{s}$) for fin surface WF1	141
6.17	Measured local two-phase heat transfer coefficient h_{tp} Vs vapour	141

	quality x at heat flux $q = 18 \text{ kW/m}^2$ for mass fluxes \dot{G} (30, 35 and $40 \text{ kg/m}^2\text{s}$) for fin surface WF1	
6.18	Measured local two-phase heat transfer coefficient h_{tp} Vs vapour quality x at mass flux $\dot{G} = 30 \text{ kg/m}^2\text{s}$ for three heat fluxes q (13, 16 and 18 kW/m^2) for fin surface WF1	142
6.19	Measured local two-phase heat transfer coefficient h_{tp} Vs vapour quality x at mass flux $\dot{G} = 35 \text{ kg/m}^2\text{s}$ for three heat fluxes q (13, 16 and 18 kW/m^2) for fin surface WF1	142
6.20	Measured local two-phase heat transfer coefficient h_{tp} Vs vapour quality x at mass flux $\dot{G} = 40 \text{ kg/m}^2\text{s}$ for two heat fluxes q (13 and 18 kW/m^2) for fin surface WF1	143
6.21	Measured local two-phase heat transfer coefficient h_{tp} Vs vapour quality x at heat flux $q = 16 \text{ kW/m}^2$ for mass fluxes \dot{G} (35, 40 and $50 \text{ kg/m}^2\text{s}$) for fin surface WF2	143
6.22	Measured local two-phase heat transfer coefficient h_{tp} Vs vapour quality x at heat flux $q = 19 \text{ kW/m}^2$ for mass fluxes \dot{G} (35, 40 and $50 \text{ kg/m}^2\text{s}$) for fin surface WF2	144
6.23	Measured local two-phase heat transfer coefficient h_{tp} Vs vapour quality x at heat flux $q = 21 \text{ kW/m}^2$ for mass fluxes \dot{G} (35, 40 and $50 \text{ kg/m}^2\text{s}$) for fin surface WF2	144
6.24	Measured local two-phase heat transfer coefficient h_{tp} Vs vapour quality x at mass flux $\dot{G} = 35 \text{ kg/m}^2\text{s}$ for four heat fluxes q (16, 19, 21 and 23 kW/m^2) for fin surface WF2	145
6.25	Measured local two-phase heat transfer coefficient h_{tp} Vs vapour quality x at mass flux $\dot{G} = 43 \text{ kg/m}^2\text{s}$ for three heat fluxes q (16, 19 and 21 kW/m^2) for fin surface WF2	145
6.26	Measured local two-phase heat transfer coefficient h_{tp} Vs vapour quality x at mass flux $\dot{G} = 51 \text{ kg/m}^2\text{s}$ for four heat fluxes q (16, 19, 21 and 23 kW/m^2) for fin surface WF2	146
6.27	Measured two-phase pressure drop ΔP Vs exit vapour quality x at mass fluxes \dot{G} (63, 73 and $82 \text{ kg/m}^2\text{s}$) for fin surface OSF1	148
6.28	Measured two-phase pressure drop ΔP Vs exit vapour quality x at mass fluxes \dot{G} (48, 63 and $73 \text{ kg/m}^2\text{s}$) for fin surface OSF2	149
6.29	Measured two-phase pressure drop ΔP Vs exit vapour quality x at mass fluxes \dot{G} (32, 35, 45 and $50 \text{ kg/m}^2\text{s}$) for fin surface WF1	150
6.30	Measured two-phase pressure drop ΔP Vs exit vapour quality x at mass fluxes \dot{G} (35, 40 and $50 \text{ kg/m}^2\text{s}$) for fin surface WF2	150
6.31	Measured local heat transfer coefficients for convective boiling in OSF1	152

6.32	Comparison of measured and predicted two-phase heat transfer coefficient for OSF1	153
6.33	Comparison of OSF1, F data with the predictions of referred correlations	154
6.34	Measured local heat transfer coefficients for convective boiling in OSF2	155
6.35	Comparison of measured and predicted two-phase heat transfer coefficient for OSF2	156
6.36	Comparison of OSF2, F data with the predictions of referred correlations	157
6.37	Combined measured local heat transfer coefficients for convective boiling in offset fin surfaces (OSF1 and OSF2).	157
6.38	Measured local heat transfer coefficients for convective boiling in WF1 and comparison with predictions reported for round tubes.	158
6.39	Comparison of measured and predicted two-phase heat transfer coefficient for WF1	160
6.40	Measured local heat transfer coefficients for convective boiling in WF2 and comparison with predictions reported for round tubes.	161
6.41	Comparison of measured and predicted two-phase heat transfer coefficient for WF2	162
6.42	Combined measured local heat transfer coefficients for convective boiling in wavy fin surfaces (WF1 and WF2)	163
6.43	Measured two-phase frictional coefficient for OSF1 and comparison with predictions reported	164
6.44	Measured two-phase frictional coefficient for OSF2 and comparison with predictions reported.	165
6.45	Combined measured two-phase frictional coefficient in offset fin surfaces (OSF1 and OSF2).	166
6.46	Measured two-phase frictional coefficient for WF1 and comparison with predictions reported	167
6.47	Measured two-phase frictional coefficient for WF2 and comparison with predictions reported	168
6.48	Combined measured two-phase frictional coefficient in wavy fin surfaces (WF1 and WF2).	169

LIST OF TABLES

TABLE NO.	TITLE	PAGE NO
2.1	Summary of literature studies with multichannel arrangements of offset strip and perforated fin passages	20
2.2	Summary of literature studies with small circular and rectangular channels	27
2.3	Summary of literature studies on plate heat exchangers	29
3.1	Description of variables Φ , Γ and S_Φ for conservation of mass, momentum and energy	39
3.2a	Wavy fin coefficients or indices for R134a	60
3.2b	Wavy fin coefficients or indices for water	60
3.3	offset strip fin coefficients or indices for R134a	71
4.1	Specification of compressor	87
4.2	Specification of evaporator and condenser heat exchangers	88
4.3	Specification of expansion valve	88
4.4	Specification of chiller unit	89
4.5	Specification of Coriolis flow meter	91
4.6	Specification of turbine flow meter	92
4.7	Specification of pressure transducer	92
4.8	Specification of differential pressure transducers	92
4.9	Specification of temperature transducers	93
4.10	Specification of data acquisition system	94
5.1	Test section geometry	101
5.2	Fin geometry parameters of 4 test sections	106
5.3	Measured single phase heat transfer of offset strip fin, OSF1	106
5.4	Measured single phase pressure drop of offset strip fin, OSF1	107
5.5	Dimensions and test range offset strip fins	107
5.6	Dimensions and test range of wavy fins.	108
5.7	Measured two-phase data of offset strip fin, OSF1	108
5.8	Measured two-phase pressure drop data of offset strip fin, OSF1	109
5.9	Sample results data of j and f factors	
	a) j factor data	120
	b) f factor data	120
5.10	Sample results data of two-phase heat transfer coefficient	121
5.11	Sample results data of two-phase pressure drop coefficient	122
5.12	Measurement of weight oil mixing	124
5.13	Accuracy of measuring instruments provided by manufacturer	124
5.14	Summary of uncertainty estimated using EES Program	128
6.1	Summary of correlations developed for offset and wavy fins	170

NOMENCLATURE

A	heat transfer area, m ²
A _p	primary surface area, m ²
A _s	secondary/fin surface area, m ²
A _F	frontal area, m ²
A _{ff}	free flow area, m ²
a	wave amplitude, m
C	constant in Martinelli parameter, dimensionless
C _p	specific heat at constant pressure, (J/kg K)
D _h	hydraulic diameter, m
F	Reynolds number factor, dimensionless
<i>f</i>	Fanning friction factor, dimensionless
\dot{G}	mass flux, kg/m ² s
g	gravitational acceleration, m/s ²
H	specific enthalpy, (J/ kg)
h	fin height, m
h _{tp}	two-phase heat transfer coefficient, W/m ² K
h _l	single phase liquid heat transfer coefficient, W/m ² K
<i>j</i>	Colburn factor, dimensionless
K _c	contraction coefficient, dimensionless
K _e	expansion coefficient, dimensionless
k	thermal conductivity of fin, W/m K
L	length of test section, m
<i>l</i>	lance length, m
M	molecular weight, g/mol
\dot{m}	mass flow rate, kg/s
Nu	Nusselt number, dimensionless
Pr	Prandtl number, dimensionless
P	pressure, bar
ΔP	pressure difference, mbar
Q	heat transfer rate, W

q	heat flux, W/m ²
Re	Reynolds number, dimensionless
S	nucleate boiling suppression factor, dimensionless
s	lateral fin spacing, m
T	temperature, °C
ΔT	temperature difference, K
t	fin thickness, m
U	overall heat transfer coefficient W/m ² K
V	velocity, m/s
v	specific volume, m ³ /kg
X	Lockhart and Martinelli parameter, dimensionless
x	vapour quality, dimensionless

Abbreviations:

CFD	Computational Fluid Dynamics
ECS	Environmental Control System of Aircraft
EES	Engineering Equation Solver
FPI	Fins per inch
LPM	Litres per minute
OSF	Offset strip fin
TC	thermocouple
WF	Wavy fin

Greek symbols

η	fin efficiency
ρ	density, kg/m ³
σ	surface tension, N/m
σ _A	header min flow area to max flow area ratio
σ _B	free flow area to frontal area ratio
α	ratio of fin height to fin spacing ; void fraction
β	ratio of wave amplitude to fin spacing
γ	ratio of wave length to wave amplitude
δ	ratio of fin thickness to fin spacing

ϵ	ratio of lance length to fin thickness
ϕ_f	two-phase frictional multiplier
Φ	generalized transport variable
κ	turbulent kinetic energy, m^2/s^2
Γ	effective diffusivity, m^2/s^2
ϵ	turbulent dissipation rate, m^2/s^2
μ	dynamic viscosity, Ns/m^2
λ	wave length, m

Subscripts

1,2,3,4	locations of thermocouple in the test section
1,2	test section inlet/outlet; fin numbers
i, o	inlet, outlet
A	acceleration
C	exit
c	critical
cb	convective boiling
E	entrance
exp	experiment
expo	expansion valve outlet
e	exit of test section
ev	evaporation
evi	evaporator inlet
evo	evaporator outlet
F	friction
G	gravitational
fg	latent heat of vaporization
IH	inlet header
l	liquid
m	mean
nb	nucleate boiling
OH	outlet header

p	primary surface
pre	prediction
pb	pool boiling
r	refrigerant
sat	saturated state
s	secondary surface
tp	two-phase
v	vapour
w	water
wall	wall temperature
z	axial location of channel

CHAPTER 1

INTRODUCTION

Heat exchanger is a device which exchanges heat between hot and cold fluids. Heat exchangers are widely used in process industries, chemical industries, Oil & Gas, cryogenics, automobiles and aerospace applications. Since the space and weight are the main design drivers in aircraft applications, compact heat exchangers have become vital compared to other conventional type of heat exchangers. Heat exchanger is called compact when heat transfer area per unit volume is greater than $700 \text{ m}^2/\text{m}^3$ in either one or more channels of a two-stream or a multi-stream heat exchanger. Development of compact heat exchangers for aircraft applications started well before 1980's and technology is well established now. But availability of Colburn ' j ' and friction factors ' f ' for the fin geometries in the open literature is limited though Shah and London(1969) & Keys and London (1984) carried out extensive research work and developed the correlations for fin geometries in 1960's. The Colburn ' j ' and Fanning friction factors ' f ' are most important parameters in design of compact plate fin heat exchangers for sensible heat transfer cases. Recently many authors published the generalized correlations for fin geometries through numerical analysis as well as experimental. This has made industries possible to develop compact heat exchangers for sensible heat transfer applications.

Demand for new cooling systems are increasing constantly due to increase in packing densities and power levels of electronic devices in aircraft avionics and electronics. For cooling high power electronics devices typical cooling devices based on conduction and single-phase forced or natural convection are not sufficient. Even though liquid-cooling, especially water cooling, has received attention for replacing air-cooling as a more energy-efficient solution, two-phase cooling is another promising technology for power electronics cooling and high heat flux devices. This is the reason why systems based on phase-change have been introduced in electronic cooling technology in recent years.

Heat exchangers with internally finned rectangular channels have been introduced in electronic chip sets than round tubes/ducts in order to accomplish a good contact. Different fin geometries such as offset strip fins, wavy fins, plain fins, perforated fins and louvered fins have been widely used for many years in compact heat exchangers for single-phase applications. Recently, however, it has become increasingly apparent that geometries of this type may also provide weight savings or improved performance in applications involving convective boiling. This has resulted in the increasing use of these fin surfaces for evaporators in refrigeration, air-conditioning, and cryogenic systems.

During the last few years, flow boiling and condensation heat transfer of refrigerants in rectangular channels with fins have received more attention due to their effectiveness and compactness, which are the key factors with regard to modern engineering design. For that reason, an increasing interest has been directed in order to characterize flow boiling heat transfer and pressure drop in these types of surfaces.

Although miniaturization offers many benefits in terms of compactness, portability and high efficiency, flow boiling in rectangular channels with fins involves a very complex combination of thermo-physical processes which are still far from being entirely understood at present, particularly under technically relevant conditions. This is more evident with reviewing the existing heat transfer prediction methods that basically posed further empirical or semi-empirical solutions rather than theoretical treatments. Therefore, experiments still play the major role at the present state of the art to meet the needs of practicing engineers for achieving realistic designs, together with efforts to advance the fundamental understanding of the physical phenomena taking place during the phase change process in the rectangular channels with fin geometries. The need to understand the performance characteristics of these configurations has prompted several recent studies of convective boiling in rectangular channel fin geometries. In rectangular channels, nucleate and convective boiling regimes are known to be the heat transfer mechanisms that co-exist during flow boiling. While forced convective boiling is admitted to be the dominant heat transfer mechanism in large diameter tubes, the nature of heat transfer regime in rectangular channels with fins is not yet completely identified.

The environmental concern over ozone depletion and global warming has brought the refrigeration industry to come up with new environmentally acceptable refrigerants. Among the alternatives R134a have zero ozone depleting potential. It is user friendly and environmental friendly. It has very good thermodynamic and transport properties. R134a is one alternative until new refrigerant with zero ODP and zero GWP properties invented.

Fewer data relating to two-phase flow and boiling heat transfer in compact heat exchangers are available in open literature compared to single phase flow. Lack of validated design correlations to predict the heat transfer coefficient is a significant barrier to the application of compact evaporators and condensers in the process industries. To develop the design correlations an accurate data base, knowledge of the prevailing flow regimes and the understanding of relationship between flow and heat transfer and of the physical mechanisms involved is required. It is also important to know the dominant heat transfer mechanism, convective flow boiling or nucleate boiling heat transfer for proper design of evaporators.

Driven by the need for thermal management solutions that can satisfy the evermore demanding needs of the various industries, the research proposed here is generation of two-phase flow boiling heat transfer coefficient ' h_{tp} ' and two-phase frictional coefficients ϕ_f for some specific fin surfaces and thus enrich the database on ' h_{tp} ' and ϕ_f coefficients for wavy and offset strip fin geometries and aimed at ultimate goal of successful design and optimization of enhanced geometries for boiling heat transfer in high performance aircraft industry, electronics and other applications.

1.1 BOILING HEAT TRANSFER

Boiling is the liquid-to-vapour phase change process that occurs at a solid-liquid interface when the surface is heated above the saturation temperature of the liquid. The formation and rise of the bubbles and the liquid entrainment coupled with the large amount of heat absorbed during liquid-vapour phase change at essentially constant temperature are responsible for the very high heat transfer coefficients associated with nucleate boiling.

Boiling is classified as pool boiling or flow boiling, depending on the presence of bulk fluid motion. Boiling is called pool boiling in the absence of bulk fluid flow and flow boiling (or forced convection boiling) in the presence of it. In pool boiling, the fluid is stagnant, and any motion of the fluid is due to natural convection currents and the motion of the bubbles is due to influence of buoyancy. In flow boiling, the fluid has velocity relative to heating surface and is forced to move in a heated pipe or over a surface by external means such as a pump. Therefore, flow boiling is always accompanied by other convection effects.

There are three different boiling heat transfer mechanisms. Nucleate boiling, in which heat is transferred by means of vapour bubbles nucleating, growing and finally detaching from the surface. Convective boiling, in which heat is conducted through the liquid and this one evaporates at the liquid-vapour interface and there won't be any bubble formation. Film boiling, in which the heat is transferred by conduction and radiation through a film of vapour that covers the heated surface and the liquid vaporizes at the vapour liquid interface. Nucleate boiling and film boiling may occur in both pool boiling and flow boiling, where as forced convective boiling occurs only in flow boiling. Pool boiling and flow boiling further classified into sub cooled boiling and saturated boiling. Boiling is called sub-cooled when the temperature of the liquid is below the saturation temperature and it is called saturated when the liquid temperature is equal to saturation temperature of the liquid.

1.1.1 Flow boiling

In flow boiling, the fluid is forced to move by an external source as it undergoes a phase-change process from liquid to vapour phase. The boiling in this case exhibits the combined effects of convection and pool boiling. The different stages encountered in flow boiling in a heated tube are illustrated in Fig. 1.1 together with the variation of the heat transfer coefficient, wall temperature, flow patterns and liquid temperature along the tube. Initially, the liquid is sub cooled and heat transfer to the liquid is by single-phase forced convection. Then bubbles start forming on the inner surfaces of the tube, and the detached bubbles are drafted into the mainstream. This gives the fluid flow a bubbly appearance, and thus the name bubbly flow regime. As the fluid is heated further, the bubbles grow in size and eventually coalesce into slugs of vapour.

Up to half of the volume in the tube in this slug flow regime is occupied by vapour. After a while the core of the flow consists of vapour only, and the liquid is confined only in the annular space between the vapour core and the tube walls. This is the annular-flow regime, and very high heat transfer coefficients are realized in this regime. As the heating continues, this annular liquid layer gets thinner and thinner, and eventually dry spots start appear on the inner surfaces of the tube. The appearance of dry spots is accompanied by a sharp decrease in the heat transfer coefficient. This transition regime continues until the inner surface of the tube is completely dry. Any liquid at this moment is in the form of droplets suspended in the vapour core, which resembles a mist, and we have a mist-flow regime until all the liquid droplets are vaporized. At the end of the mist-flow regime there is saturated vapour, which becomes superheated with any further heat transfer.

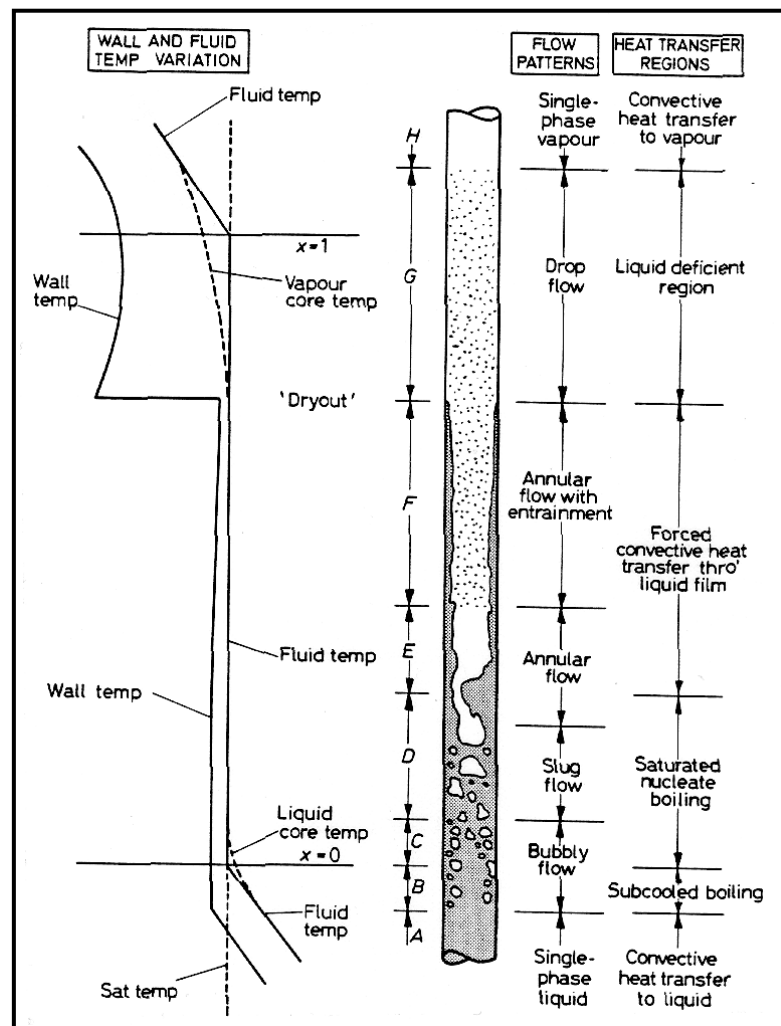


Fig.1.1: Flow boiling in a uniformly heated circular tube
(Collier, J.G and Thome, J.R 1994)

1.2 COMPACT HEAT EXCHANGERS

A compact heat exchanger is one which has large heat transfer surface area per unit volume of the exchanger. The compact heat exchangers occupy less space, low in weight, highly efficient and low in cost compared to typical heat exchangers. Compact heat exchangers can be used for liquid-liquid, liquid to gas and gas to gas type heat transfer applications. They are used in automobile heat exchangers, condensers and evaporators in refrigeration and air-conditioning industry, aircraft oil coolers, air heaters, intercoolers of compressors, aircraft and space applications. They are also used in cryogenics process, electronics, energy recovery, conservation and conversion and other industries.

To minimize the operating cost, maintenance free operation and effective utilization of energy resources are the main reasons behind the development of efficient heat exchangers like compact heat exchangers. By providing the extended surfaces i.e. fins on the flow passages, high compactness in heat exchangers can be achieved. Fins on the flow passages works as a secondary heat transfer area.

Various techniques can be used to make heat exchangers more compact. Three general types of extended surface geometries which can be used to increase gas-side heat transfer coefficients. These include: a) a plate-fin type heat exchanger (b) tube-finned type heat exchanger with flat fins, (b) tube-finned type heat exchanger with individually finned tubes. The most common compact heat exchangers among these are plate fin heat exchangers.

1.2.1 Plate fin heat exchangers

A plate fin heat exchanger is a formed by stacking the alternated layers of fins, separating sheets, known as parting sheets, side bars and covering plates. Fig.1.2 shows the schematic view of a compact heat exchanger. The fins serve as secondary heat transfer surface and as well as mechanical support against internal pressure between the two layers. Fluids streams exchange the heat across the parting sheets by flowing through the alternate fins passages. The heat exchanger block formed by the fins, side bars, cap sheets, and parting sheets are brazed in the brazing furnace holding rigidly in the fixture. The first and the last sheets, called cap sheets or covering sheets

are usually of thicker material than the separating sheets. These cap sheets provide support against the excess pressure and physical damage. Finally after brazing, inlet and outlet headers are welded to the block. Fluid stream enters the heat exchanger block at the inlet header via ports and leaves from the outlet header.

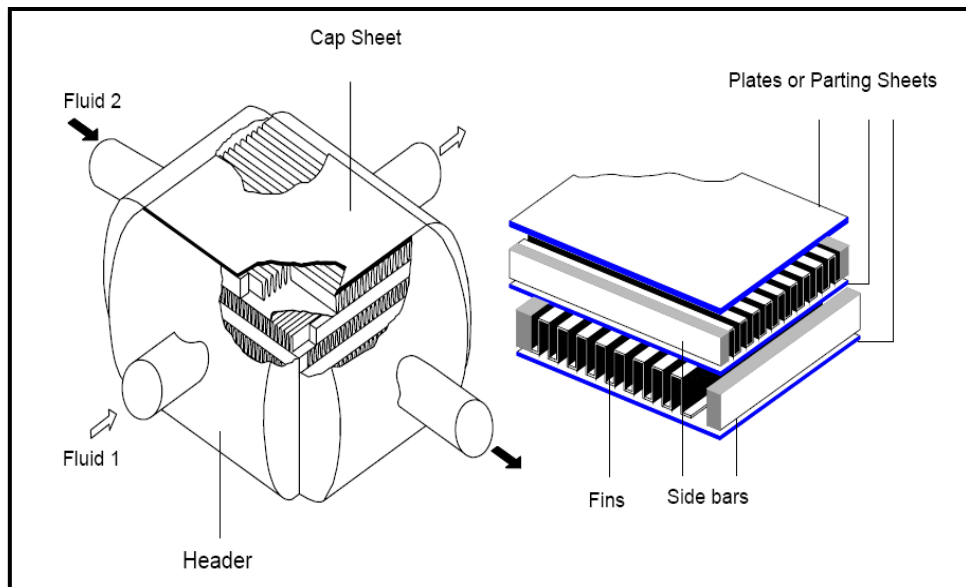


Fig.1.2: Plate fin heat exchanger assembly (Maiti, D.K, 2002)

The proposed geometries for the research are having compactness of order $1800-2000 \text{ m}^2/\text{m}^3$. Compact heat exchangers shall have higher effectiveness compared to shell and tube heat exchangers. Efficiency of more than 90% is achievable in case of compact heat exchangers where as max of 60% is achievable in case of shell and tube heat exchangers.

1.2.2 Materials

Generally plate fin heat exchangers are made up of from Aluminium and Stainless Steel. There are other materials, nickel and copper alloys also used depend upon the applications. Aluminium is preferred at low temperature and pressure applications, i.e. aerospace and cryogenic applications. It is preferred because of its high thermal conductivity, low density and high strength at low temperature. For higher temperature applications, above $500 \text{ }^\circ\text{C}$ Stainless steels, nickel and copper alloys have been used. Aluminium alloy of lower melting point is used as a brazing material for aluminium exchangers and nickel based alloy with appropriate melting

and welding characteristics used as a brazing material for stainless steel heat exchangers.

1.2.3 Manufacture

The fins, sidebars, parting sheets and covering plates are held together in a fixture under a load, placed in a furnace and brazed to form the plate fin heat exchanger block. The nozzles and header are then welded to the block, taking care that the brazed joints remain intact during the welding process. There are different brazing processes in which the brazing is carried out. The most common methods are salt bath brazing and vacuum brazing. The stacked assembly is preheated and dipped in the salt bath in salt bath brazing process. The furnace temperature shall be maintained at about 550°C. Molten salt works as flux as well as heating agent, maintaining the furnace at a uniform temperature. When temperature raises above the melting point of the brazing alloy, brazing takes place in the bath. The brazed block is cleansed and then thoroughly dried.

Vacuum brazing process, produces high quality braze joints, since no flux is used. Brazing takes place at high vacuum (Pressure approximately 10^{-6} mbar) condition. This ensures the absence of oxygen in the brazing environment. After brazing no washing or drying of the brazed block is required. The assembled block is heated by radiation to brazing temperature from electric heaters. All metals, such as stainless steel, aluminium, copper and nickel alloys can be brazed in vacuum furnace satisfactorily.

1.2.4 Applications

Plate-fin and tube-fin heat exchangers have found application in a wide variety of industries such as:

- a. Defence applications
- b. Aerospace applications
- c. Domestic refrigerators
- d. All types air-conditioning systems
- e. Automobile/ locomotive air conditioning systems
- f. Process industries

1.2.5 Flow arrangement

Multi stream flow arrangements are possible in a plate fin heat exchanger which may flow in directions parallel or perpendicular to one another. There are 3 primary flow arrangements (i) parallel flow (ii) counter flow and (iii) cross flow which in general used in engineering practice. Thermodynamically, parallel flow geometry gives the lowest while the counter flow arrangement provides the highest heat (or cold) recovery. The cross flow arrangement offers superior heat transfer properties and easier mechanical layout. Fig.1.3 shows the three configurations in general used in engineering practice: (a) cross flow, (b) counter flow and (c) cross-counter flow.

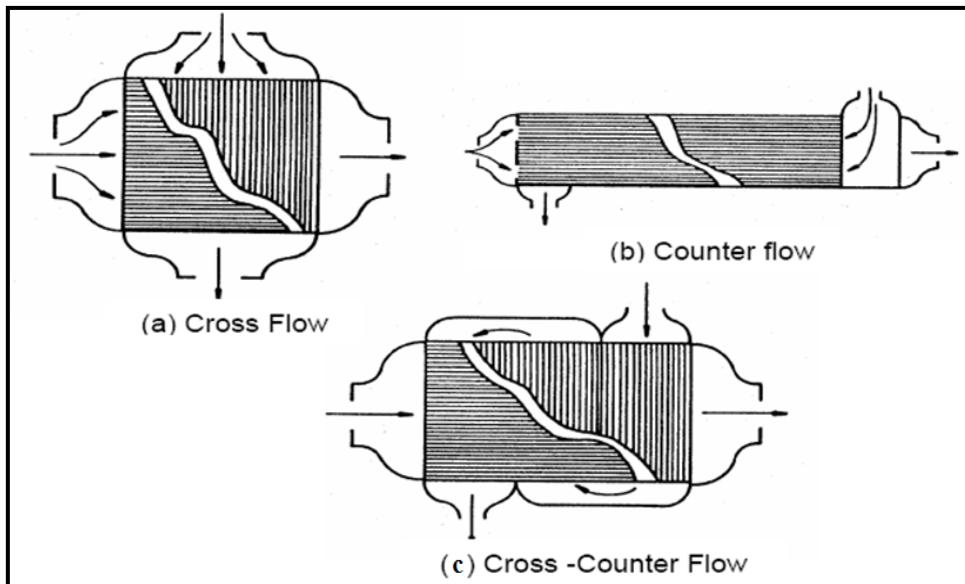


Fig.1.3: Heat exchanger flow arrangements (Maiti, D.K, 2002)

1.3 HEAT TRANSFER FIN SURFACES

The performance of a plate fin heat exchanger is determined by the type of the fin geometry, among other things. The most common fin types are: (1) plain fins with rectangular, trapezoidal or triangular passages (2) uninterrupted wavy fins and (3) interrupted fins such as offset strip, perforated, louvered and pin fins. Fig.1.4 shows types of fin geometries..

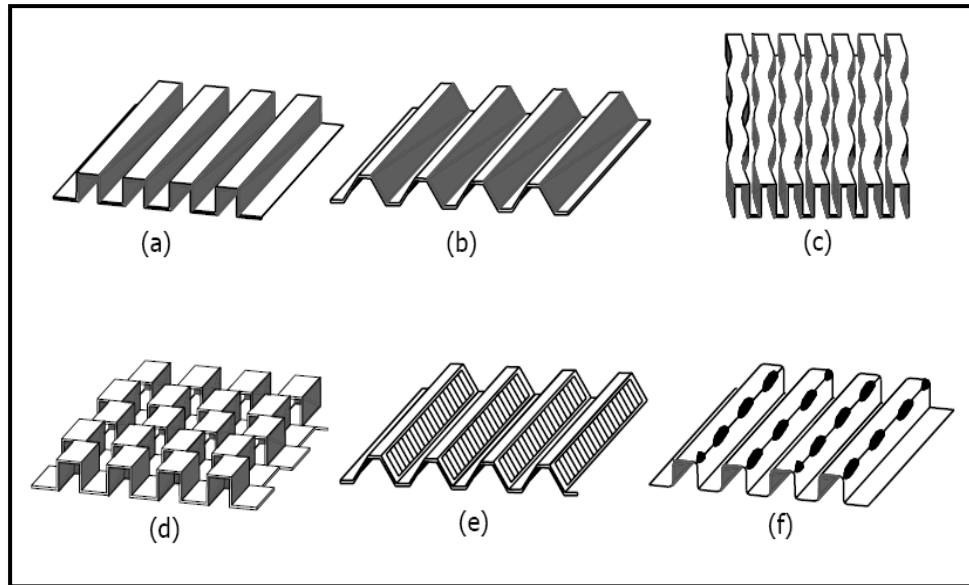


Fig. 1.4: Types of fin geometries: a) plain rectangular b) plain trapezoidal c) wavy d) serrated or offset strip fin e) louvered f) perforated
(Maiti, D.K, 2002)

1.3.1 Offset strip fin

This fin geometry is widely used in high performance plate fin heat exchangers. It consists of a type of interrupted surface, which may be visualized as a set of plain fins cut normal to the flow direction at regular intervals, each segment being offset laterally by half the fin spacing. Interruption in fin surface enhances heat transfer by two independent mechanisms. First, it prevents the thermal boundary layer growth by periodically interrupting it. Due to breaking up off boundary layer on the fin length increases the heat transfer coefficient. The thinner boundary layer offers lower thermal resistance. Interrupted surfaces offer an additional mechanism of heat transfer enhancement above a critical Reynolds number. Oscillations in the flow field in the form of vortices shed from the trailing edges of the interrupted fins enhance local heat transfer by continuously bringing in fresh fluid towards the heat transfer surfaces but with a penalty on pressure drop Maiti (2002). Fig 1.5 shows photograph of the offset strip fin.

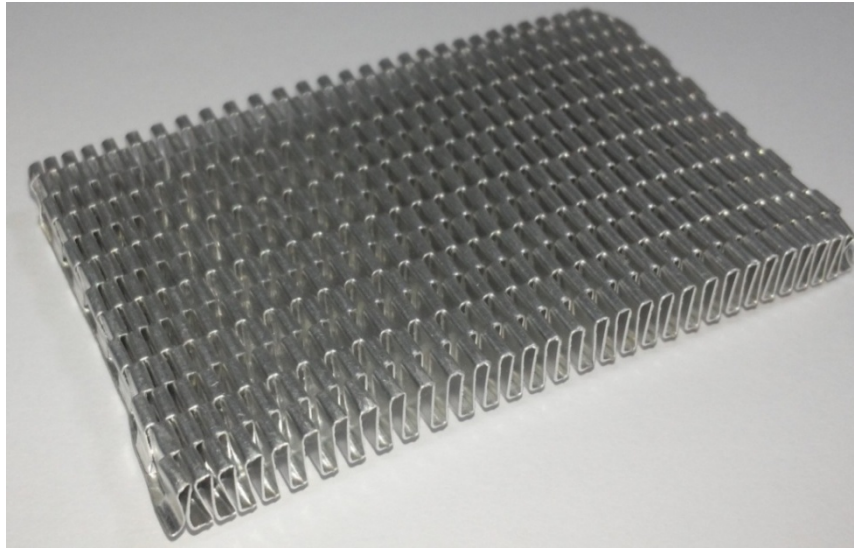


Fig.1.5: Photograph of offset strip fin

1.3.2 Wavy fins

The wavy fins are uninterrupted fin surfaces with cross-sectional shapes similar to those of plain fins, but with cyclic lateral shifts perpendicular to the flow direction. The wavy geometry lengthens the flow path, creates turbulence and promotes better mixing. The heat transfer and flow friction performance of wavy fin surfaces lies between those of plain and offset strip fins. Wavy fins are common in hydrocarbon industry where exchangers must cope with high mass velocities and moderate thermal duties. In aircraft applications, it is the preferred fin type on the ram air side, where available pressure drop allowance is rather small. Fig.1.6 shows photograph of the wavy fin.

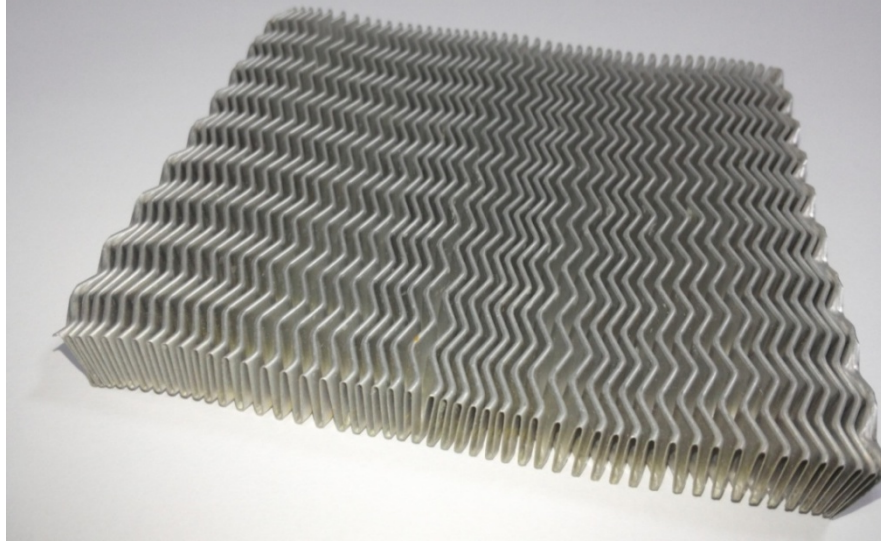


Fig.1.6: Photograph of smooth wavy fin surface

1.4 TWO-PHASE HEAT TRANSFER AND FLOW FRICTION CHARACTERISTICS

Reliable and accurate heat transfer and pressure drop characteristics of a fin surface are key inputs for design of compact evaporator. Two-phase heat transfer coefficient can be estimated by experimentally.

$$q = \frac{Q}{A} = h_{tp} (T_{wall} - T_{sat}) \quad (1.1)$$

T_{wall} is the local wall temperature measured using thermocouples inserted in a test section; T_{sat} is the bulk saturation temperature.

The two-phase pressure drop in the flow boiling channel is mainly due to frictional, acceleration and gravitational pressure gradients. The overall pressure drop in the test section is the summation of these three gradients.

$$\left[\frac{dp}{dz} \right]_{tp} = \left[\frac{dp}{dz} \right]_F + \left[\frac{dp}{dz} \right]_G + \left[\frac{dp}{dz} \right]_A \quad (1.2)$$

Where the suffix F, G, A, represents the frictional, gravitational and acceleration components. Among these three components, two-phase frictional pressure gradient is the one which contributes the highest. Generally it is expressed in terms of single-phase pressure gradient for the liquid phase flowing alone in the channel.

1.5 SCOPE AND OBJECTIVES OF THE PRESENT STUDY

The aim of the present study is to develop the technical expertise to enable new types of compact heat exchangers to be used for evaporation duties and to provide design information required to produce advanced compact heat exchangers especially for aerospace applications. A fundamental requirement of the heat exchanger designer is the ability to predict the heat transfer coefficients and friction coefficients under the conditions of interest with confidence. Hence the proposed research is carried out to investigate the flow boiling heat transfer coefficient and friction coefficients on few selected offset strip and wavy fin geometries and also to develop the correlations for the each fin geometry. An experimental test facility has been set up for generation of flow boiling heat transfer and friction coefficient data. Using the test facility the data will be measured and calculated to develop the correlations.

The objectives of the present work is

1. To obtain single-phase refrigerant heat transfer and pressure drop data for a range of fin surfaces using experiments as well as CFD approach. This serves to provide a quantitative understanding of the performance of compact plate fin surfaces in single-phase applications and to provide accurate refrigerant heat transfer and frictional coefficient information.
2. To develop the single-phase heat transfer and frictional correlations in terms of Colburn j factor and friction factor f for offset strip and wavy fin surfaces and investigation of effect of fin geometry on heat transfer and frictional data.
3. To obtain the flow boiling heat transfer and pressure drop data on wavy and offset strip fin geometries, over a range of mass flux, heat flux and vapour quality.
4. To obtain the local boiling heat transfer and pressure drop characteristics and analyse the trends with respect to mass flux, vapour quality and heat flux. Study the influence of these parameters on two-phase heat transfer and pressure drop.
5. As the final and principal aim, to extend the present knowledge of the thermo-hydraulic performance of plate fin heat exchangers for use of evaporators. It is the task of this study to develop correlations for different types fin surfaces (offset strip and wavy fins) for R134a. The correlations must be able to predict the

refrigerant flow boiling heat transfer and frictional pressure drop with reasonable accuracy.

1.6 ORGANIZATION OF THE THESIS

Present thesis is organised in 7 chapters. Chapter 1 provides general introduction to boiling heat transfer and compact heat exchangers, plate fin heat exchangers, applications and defines the scope and objectives of the work. With the motivational and introductory aspects of the work addressed in earlier sections of this chapter, Chapter 2 continues the analysis of published studies to explore the underlying physics and fundamental phenomena encountered in flow boiling heat transfer in a rectangular channel with wavy fin, offset strip fin surfaces, rectangular channels, round tubes and plate heat exchangers. Thus, Chapter 2 lays the foundation on which experimental and theoretical investigations, which comprise the core of this dissertation, have been built.

Chapter 3 presents the CFD approach and development of single-phase heat transfer and frictional correlations for compact heat exchanger fin surfaces, wavy and offset strip fins using R134a (liquid phase).

The experimental apparatus design, fabrication, testing, details of components used in the test facility and measurement system are detailed in Chapter 4.

Chapter 5 presents details of the test section, manufacturing procedure of test sections, experimentation details, data reduction, analysis and measurements recorded during the experimentation, complete with detailed estimates of measurement errors and uncertainties.

Results of the basic two-phase flow boiling and pressure drop characterization experiments are presented and discussed in Chapter 6. Also discusses the results of the data analysis, and presents the development of two-phase heat transfer and frictional correlations for fin surfaces over a refrigerant R134a.

Chapter 7 contains a summary of the key contributions of the dissertation and recommendations for the future work.

CHAPTER 2

LITERATURE REVIEW

Over the past two to three decades compact heat exchangers have become popular in cooling and heating applications across industries especially in automobile, aerospace and electronics. The demand for miniaturization of components is high in these industries to reduce weight, size and save the cost. Due to its high effectiveness compact heat exchangers will have low weight and occupy less space compared to other type of heat exchangers. Applications involving the phase changes, compact heat exchangers are using more and more widely, mainly due to their multi-stream capabilities, design flexibility, high thermal efficiencies and energy savings, Mandrusiak and Carey et al. (1986,1988 and 1989). Compact heat exchangers can be designed to operate in a pure counter flow mode. They can also accommodate multiple fluid streams. Compact heat exchangers allow a reduction in the quantity of the fluid in the evaporator. This increases safety in the case of refrigeration systems, an increase in environmental acceptability. Recently requirement of smaller evaporators is growing for the benefits of process intensification, the reduction in plant size, for a given capacity Kew and Cornwell (1997).

Transportation industry is the one using compact heat exchangers extensively as evaporators and condensers in vapour-compression refrigeration and air conditioning, Carey (1993). Today, there is widespread interest in expanding these heat exchangers for range of applications mainly to include phase change heat transfer in chemical process industries, among others, Mandrusiak and Carey et al. (1986, 1988, 1989), Carey (1993), Kew and Cornwell (1997).

The operating conditions in the small passages of compact heat-exchangers are dissimilar compared to large round tubes. There are several features of the operating characteristics that strongly affect of compact surfaces in vaporisation and condensation applications. First, compact heat-exchangers have a small hydraulic diameter and a very large surface-area-to-volume ratio. The second feature is the complexity of the passage and its impact on pressure drop, Carey (1993). Compact evaporators and condensers typically operate through the laminar, transition and

turbulent flow regimes, which makes the two phase heat transfer more complex. Channel geometry and size have direct effect on the heat transfer coefficient in addition to fluid properties in compact heat exchangers Kew and Cornwell (1997). There are different fin geometries such as offset strip fins, wavy fins, plain fins, perforated fins and louvered fins. Among these fins offset strip fins have higher heat transfer coefficient but with a penalty on pressure drop. The higher heat transfer coefficient is due to breaking up off boundary layer on the fin length and increase in pressure drop is due to increased form and friction drag.

Barbara (2003) performed extensive survey on local boiling heat transfer on small circular, rectangular and multi channel arrangements of serrated and perforated fins. She has highlighted the effect of vapour quality, mass flux, heat flux; channel geometry/size, fin type, gravity and surface tension in each boiling region. She has also discussed the different flow patterns observed during flow boiling in small passages and presented the typical trends of heat transfer coefficient in the two regions of boiling, nucleate and convective boiling. Webb and Gupte (1992) performed critical review of correlations for convective vaporization in tubes and tube banks. They critically assessed the three types of phenomenological models, the superposition, asymptotic and enhancement which are used for calculating heat transfer coefficient in convective vaporization and established the rational basis for modified model.

In the refrigeration/air conditioning industry, including automobile environment control, a fundamental understanding of multiphase flow and heat transfer involving boiling and condensing of refrigerants in small rectangular channels is important. In particular, there is need for a validated design correlation for two-phase pressure drop and heat transfer coefficient that will facilitate the design and optimization of compact heat exchangers for use with refrigerants.

Nevertheless, extensive applications exist in the aircraft industries, where phase-change heat transfer allows more compact heat exchanger designs with better performance than those used for single-phase operation. However, there have been only a few studies in the literature reporting on phase-change heat transfer and two-phase flow in compact heat exchangers. Validated design correlations are lacking in this area.

In this chapter the published literature on the subject reviewed, focusing on experimental evaluation of two-phase heat transfer and flow friction characteristics for each study channel geometry, test conditions and fluids used. Literature survey carried out in the following aspects.

- Experimental studies on flow boiling heat transfer and pressure drops in fin surfaces, round tubes and channels.
- Single phase heat transfer and pressure drop studies in plate fin surfaces.

2.1 EXPERIMENTAL STUDIES ON TWO- PHASE HEAT TRANSFER AND PRESSURE DROP

Saturated flow boiling studies in small passages are categorized as following

- Multichannel arrangements of compact plate-fin heat exchanger passages
- Small, circular and rectangular channels

2.1.1 Experimental studies in multichannel arrangements of offset strip and perforated fin passages

Table 2.1 provides the summary of the fin geometries, test conditions and fluids used in experimental researches to determine the flow boiling heat transfer coefficients in multichannel arrangements of heat exchanger passages. Initially only overall heat transfer coefficients in compact heat exchangers with offset strip or perforated fins were determined. But in more recent studies local boiling heat transfer coefficients (i.e., at given axial positions) were measured and presented against vapour quality, over a large range mass and heat fluxes in offset strip and perforated fin passages.

Robertson and Lovegrove (1983) performed experiments on R11 and measured the local boiling coefficients in a vertical serrated plate-fin passage. He has observed the high wall and bulk liquid super heating peaks at the beginning of boiling in the R11 as well as Nitrogen. He proposed a boiling coefficient in a simple correlating parameter Re_L . Robertson and Wadekar (1998) and Wadekar (1992) carried out experiments on vertical perforated plate-fin passage at a low pressure of 150 kPa using cyclohexane and heptanes respectively. They reported the findings of boiling heat transfer characteristics against vapour quality and mass flux in the study.

Carey et al. (1986, 1988, 1989 and 1993) performed studies of flow boiling heat transfer and single-phase of different fluids in offset strip fins test sections. The test section is made up of copper slabs. Tests were performed by orienting test section horizontally as well as vertically. They reported local boiling heat transfer coefficients for different mass fluxes against vapour quality. Empirical relationship proposed by Mandrusiak and Carey (1989) for these fins as a function of convective boiling parameter, F and Martinelli parameter is

$$F = \left[1 + \frac{28}{X^2}\right]^{0.372} \quad (2.1)$$

Ranganayakulu et al. (2013, 2015) reported experimental results for flow boiling of the R134a in a plate-fin heat exchanger with a high density offset strip fins. Water was used to heat the refrigerant. The experiments are conducted at different heat and mass fluxes. The overall heat transfer coefficient and the boiling heat transfer coefficient are plotted against heat fluxes. They reported that flow boiling heat transfer is contributed by both a convective and a nucleate boiling. The convection term has a significant contribution in the total heat transfer at high Reynolds number. They have proposed new constant for the nucleate boiling heat transfer coefficient for the offset strip fin for modified Forster and Zuber's equation.

$$h_{nuc} = 0.00916 \frac{k_l^{0.79} c_{pl}^{0.45} \Delta T^{0.24} \Delta P^{0.75} S}{\sigma^{0.5} \mu_l^{0.29} \Delta H_{iv}^{0.24} \rho_v^{0.24}} \quad (2.2)$$

Feldman et al. (2000) conducted laboratory experiments with CFC114 flowing in an electrically heated, serrated-fin and perforated fin test section of different sizes to measure local boiling heat transfer coefficients over a wide range of vapour quality, at a saturation pressure of 3 bar and different heat and mass fluxes. They have reported two kinds of mechanism in their findings, a nucleate boiling regime and a convective boiling regime. The nucleate boiling component was obtained from pool boiling data and the forced convective component of the two-phase heat transfer coefficient was found to be well represented by the F and Martinelli parameter X . Nucleate boiling regime where the heat transfer coefficient depends on heat flux but is independent of quality and mass flux. The convective boiling depends on quality and mass flux but is completely independent of heat flux. The effect of geometry parameters, fin length, height and density on the boiling regime is emphasized in the paper. It appeared clearly that the decrease of fin height

or length suppresses the nucleate boiling regime. They reported that the influence of fin density is not so evident in the boiling regime. They have proposed semi-empirical model, based on the asymptotic model in the form of

$$F = 1 + 1.8X^{-0.79} \quad (2.3)$$

Pulvirenti et al. (2010) studied experimentally the saturated flow boiling heat transfer of HFE-7100 in vertical rectangular channels with offset strip fins. The local boiling heat transfer coefficient has been obtained from experiments and analysed by means of Chen superposition method. Experimental measured local heat transfer value and predicted by his correlations lies within $\pm 25\%$. They have also studied effect of quality, mass flux and heat flux and reported that in convective boiling regime, heat transfer coefficient depends on quality and mass flux but is independent of heat flux where as in nucleate boiling regime heat transfer coefficient depends on heat flux but is independent of quality and mass flux. They have also obtained experimentally the single phase heat transfer coefficient for HFE-7100 and reported that j factor proposed in literature over predicts for liquids.

Kim and Sohn (2006) performed experimental studies on vertical rectangular channel with offset strip fins using R113. They measured the two-phase pressure gradients and local boiling heat transfer coefficients for electrically heated test section and proposed correlations for frictional multiplier (ϕ_f) as a function of Martinelli parameter X , and the local boiling heat transfer coefficient as a function of Reynolds number factor (F) and Martenelli parameter, X .

$$\phi_f^2 = 1 + \frac{23.4}{X} + \frac{4.17}{X^{2.66}} \quad (2.4)$$

$$F = \left[1 + \frac{2.52}{X^{1/2}} + \frac{15.1}{X^2} \right]^{0.5} \quad (2.5)$$

The experiments are conducted at very low Reynolds number that is at laminar regions. The predictions of local flow boiling heat transfer coefficients were found to be in good agreement with experimental data.

Saad et al. (2012) conducted experimental studies to study the flow behaviour in vertical up-flow in a small rectangular channel with offset strip fin. They reported the distribution of the two-phase flow depends on the gas and liquid superficial velocities.

Table 2.1: Summary of literature studies with multichannel arrangements of offset strip and perforated fin passages

Reference	Fin geometry (h/s/t/l) mm	FPI (inch)	Dh (mm)	\dot{G} (kg/m ² s)	q (kW/m ²)	Fluids	Fin type
Ranganayakulu and Kabelac (2015)	2.54/1.079/0.101/1.58	30	1.14	<20	<5.5	R134a	Offset-Strip
Pulvirenti et al.(2010)	2.8/2.0/0.2/5	12		0.07-0.23	<3.5	HFE7100	Offset-Strip
Kim and Sohn (2006)	2.8/3.5/0.2/1.5		2.84	17-43	<3.0	R113	Offset-Strip
Feldman et al.(2000)	6.93/1.21/0.2/3.18	18	2.06	19-49	1.4-3.54	R114	Offset-Strip
	6.93/1.16/0.2/9.52	22	1.98	19-49	1.4-3.54		
	6.93/1.21/0.2/-	18	2.06	19-49	1.4-3.54	R114	Perforated
	3.23/1.21/0.2/-	18	1.78	19-49	1.4-3.54		
	6.93/0.95/0.2-	25	1.67	19-49	1.4-3.54		
Carey and Mandruciak (1986)	3.8/7.94/1.59/12.7	2.62	5.14	3-100	-	Methanol Butanol and Water	Offset-Strip
Mandruciak and Carey (1989)	3.8/7.93/1.59/12.7	2.62	5.14	3-320	-	Methanol Butanol, Water and R113	Offset-Strip
	9.52/8.29/1.91/2.7	2.45	8.16	3-320	-		
	1.91/7.93/1.59/12.7	2.62	3.08	3-320	-		
Robertson and Lovegrove (1983)	6.16/1.49/0.2/3.18	15	2.4	34-150	<4	R11	Offset-Strip
Saad et al.(2012)	7.13/0.77/0.2/3.175	26	1.397		-	Air and Water	Offset-Strip
Wadekar (1992)	6.15/1.49/0.2/-	15	2.4	50-290	<4	n-heptane	Perforated
Robertson and Wadekar (1988)	6.15/1.49/0.2/-	15	2.4	50-290	1-10	Cyclohexane	Perforated
Mandruciak et al.(1988)	3.8/7.93/1.59/12.7	2.62	5.14	4-60	-	Methanol Butanol and Water	Offset-Strip

2.1.2 Experimental studies in small circular and rectangular channels

Studies on flow boiling in small channels may provide interesting information to understand the heat transfer mechanisms occurring in compact heat exchangers. Most of the studies presented below relate to the boiling in individual, small, circular and rectangular channels. Table 2.2 provides the summary of channel geometry, test conditions and fluids used in those studies.

Peng and Wang (1993) experimentally investigated the single-phase forced flow convection and boiling characteristics of rectangular cross section 0.6×0.7 mm. Sub-cooled water used for the study varying the temperature from 40 to 70 K. Uniform heat fluxes were applied on three sides of channels. Influences of liquid velocity and sub-cooling on the experimental boiling curves inspected by the authors.

Kew and Cornwell (1997) measured local boiling heat transfer coefficients and pressure drop in a narrow horizontal single-tube test sections made up of stainless steel for R141b. The diameters of the tube varied from 1.39–3.69 mm. Kew and Cornwell (1997) have presented the variation in boiling heat transfer coefficient with respect to vapour quality, for fixed mass and heat fluxes. Authors reported that heat transfer coefficient increases with heat flux at low quality. But at higher qualities the heat transfer coefficient is a function of quality and is essentially independent of heat flux. At high mass flux the heat transfer coefficient falls rapidly with increasing quality. They identified three flow patterns through flow visualization experiments. They are the isolated bubbles (IB), confined bubbles (CB) and the annular-slug flow (ASF). They proposed confinement number as

$$N_{CONF} = \frac{\left(\frac{\sigma}{g(\rho_L - \rho_G)}\right)^{0.5}}{D_h} \quad (2.6)$$

They also proposed heat transfer coefficient correlations for each region as follows

$$\text{IB region} \quad : \quad Nu = C_1 Re_{Lo}^{0.8} Bo^{0.7} \quad (2.6a)$$

$$\text{CB region} \quad : \quad Nu = C_2 Re_{Lo}^{0.8} Bo^{0.3} N_{CONF}^{0.5} Pr_L^{0.4} \quad (2.6b)$$

$$\text{ASF region} \quad : \quad Nu = C_3 F Nu_{Lo} \quad (2.6c)$$

Tran et al. (1996) experimentally studied the R12 refrigerant flow boiling heat transfer coefficients with respect to vapour quality and boiling curves. They have used small rectangular brass channel with hydraulic diameter of 2.4 mm for the study.

They have also studied local flow boiling heat transfer coefficients of R134a against vapour quality and mass flux as well as boiling curves for circular channel having hydraulic diameter of 2.46 mm. They proposed a correlations corresponds nucleate dominant region as

$$Nu = 770 (Re_{Lo} N_{CONF} Bo)^{0.62} \left(\frac{\rho_G}{\rho_L} \right)^{0.297} \quad (2.7)$$

Chen (1966) formulated a mechanism of micro and macro convective heat transfer to represent boiling heat transfer with net vapour generation to saturated, non metallic fluids in convective flow. He proposed correlations in terms two-phase Reynolds number function, F, and a bubble-growth suppression function, S. He tested his correlations with available data in the literature for water and organic fluids. The correlations proposed by Chen for tube flow for total heat transfer coefficient is

$$h_{TP} = h_{mic} + h_{mac} \quad (2.8)$$

$$h_{mic} = h_{Forster-Zuber} X S \quad (2.9)$$

$$h_{mac} = h_{Dittus-Boelter} X F \quad (2.10)$$

F and S are functions of Reynolds number and Martinelli parameters.

He has proposed the following equations for tube

$$F = 2.35 \left[0.213 + \frac{1}{X} \right]^{0.736} \quad (2.11)$$

Lee and Lee (2001) studied experimentally R113 flow boiling in a rectangular channels, oriented horizontally. They reported the local boiling heat transfer coefficients with respect to vapour quality, heat flux, mass fluxes and channel gap size. They reported that heat transfer coefficient increases with mass flux and local quality, however the effect of heat flux is minor. For the smaller the gap size and lower flow rate conditions, the heat transfer is primarily controlled by the film thickness.

Lockhart and Martinelli (1949) proposed two-phase pressure drop correlations for round tubes. They have used simultaneous flow of air and liquids including benzene, kerosene, water and oils pipes with varying diameters. The pressure drop resulting from various flow mechanisms is correlated by means of parameter X.

Kandlikar et al. (2006) investigated the saturated flow boiling critical heat flux (CHF) in micro channels using water as the working fluid. The experimental test section has six parallel micro channels with each having a cross sectional area of 1054

× 157 micrometers. The test section formed from copper block was uniformly heated by resistive cartridge. They reported the trends in CHF with mass flux and quality. CHF is found to increase with increasing Weber number, which indicates that as the mass flux increased, the CHF increased. The vapour mass fraction at the micro-channel outlet decreases with increasing CHF.

Qu and Mudawar (2003) measured CHF for a water-cooled heat sink containing 21 parallel, 0.215 mm x 0.821 mm channels. The authors found that flow reversal caused by flow instabilities have resulted in a CHF independent of inlet temperature but which increases with increasing mass velocity.

Kandlikar (1990) proposed generalized correlations for saturated two-phase flow boiling heat transfer inside a horizontal and vertical tube based on model utilizing contributions of due nucleate and convective boiling. He has considered the data base of 24 experimental investigations by various authors and 12 fluids. He proposed following generalized correlation for tubes with different fluids (ten fluids).

$$\frac{h_{TP}}{h_l} = C_1 Co^{C_2} (25Fr_{10})^{C_5} + C_3 Bo^{C_4} F_{fl} \quad (2.12)$$

Hamdar et al. (2010) investigated two-phase pressure drop and boiling heat transfer of HFC 152a in horizontal square mini-channel with diameter of 1 mm. The test section is uniformly heated using silicon electrical resistances. Electric current is supplied to electrical resistances by variable AC voltage controller. They presented the local boiling heat transfer coefficients against vapour quality, heat and mass fluxes. Also reported the two-phase overall frictional losses in the test section. They have proposed the following new correlations based on Trans et al. correlations.

$$Nu = (We_L Bo^2)^b \left(\frac{\rho_L}{\rho_V} \right)^c \quad (2.13)$$

Vakili-Farahani et al. (2013) were carried out the upward flow boiling experiments in a flat extruded multiport tube, composed of 7 parallel rectangular channels (1.1 mm x 2.1 mm) with hydraulic diameter of 1.4 mm. Two refrigerants, R245fa and R1234ze, were used for testing. Hot water heating technique that accounts for either uniform or non-uniform local heat flux distribution along the channel was used to heat the evaporator. Effects of heat flux, mass flux, vapour quality, and saturation temperature on flow boiling heat transfer in multiport tubes were reported in their paper.

Wang et al.(2013) measured experimentally the heat transfer coefficient and pressure drop of the two-phase saturated flow boiling for propane in a smooth horizontal tube at different mass fluxes, heat fluxes and saturated temperatures from -35.0 to -1.9°C. The test section was heated by electric heaters adhered to the tube outer surface. Heat transfer coefficients and frictional coefficients against mass and heat flux were reported. For saturation temperature and vapour quality, distinct variation trends were reported at different test conditions.

Lazarek and Black (1982) measured R113 local boiling heat transfer coefficient, pressure drop coefficient and critical heat flux for saturated flow condition. Vertical circular tube with inner diameter inner of 3.15 mm is used for the study. They reported that conventional Lockhart-Martenelli correlation can be used with the value of C being 30 for turbulent (liquid)-turbulent (gas) regime. They also found that quality had no influence upon the heat transfer rate and proposed a correlation

$$Nu = 30Re_{Lo}^{0.857}Bo^{0.714} \quad (2.14)$$

Marchitto et al. (2008) reported the measurements of the two-phase air–water distributions occurring in a cylindrical horizontal header supplying 16 vertical channels for upward flow. The effects of the operating conditions, of the header-channel distribution area ratios and of the inlet port orifice plates were investigated. The flow rates of each phase flowing in the different channels were measured. Time varying, void fraction data were also analysed to characterise the two-phase flow patterns.

Tibirica and Ribatski (2010) presented the experimental results in a horizontal 2.3mm ID stainless steel tube with heating length of 464 mm using R134a and R245fa as working fluids. The experiments were carried out at mass velocities of 50-70 kg/m²s and heat fluxes of 5-55 kW/m² exit saturation temperatures of 22, 31 and 41°C and vapour qualities of 0.05-0.99. They reported that heat transfer coefficient is a strong function of heat flux, mass velocity and vapour quality. They have also characterized the flow patters through images obtained from the high speed filming.

Charnay et al. (2015) presented experimental data concerning flow boiling heat transfer in mini-channel at high saturation temperatures. The experimental data were obtained in a horizontal 3 mm inner diameter stainless steel tube with R-245fa as

working fluid. The mass velocity ranges from 100 to 1500 kg/m²s, the heat flux varies from 10 to 50 kW/m² and the inlet vapour quality from 0 to 1. This experimental work is characterized by a saturation temperature ranging from 100 °C to 120 °C. They have studied the effect of flow mechanisms on heat transfer coefficients. Also they have investigated the influence of the mass velocity and the heat flux heat transfer coefficient. They have reported that at high saturation temperatures nucleate boiling dominated over a wide range of vapour quality.

Xu et al. (2015) carried out an experimental study on flow boiling of R134a under hyper-gravity for assessing the effect of gravity on two-phase flow boiling heat transfer coefficient. The experiments were conducted with a horizontal smooth copper tube with an inner diameter of 2.168 mm under both hyper-gravity (1.12–3.16 g) and normal gravity (1 g), with mass flux of 725 and 910 kg/m²s, heat flux of 19.0 and 28.5 kW/m², saturation pressure of 0.71 and 0.82 MPa (saturation temperature of 27.2 and 32.2 °C), and vapour quality from 0 to 0.65. The hyper-gravity environment was generated with a centrifugal acceleration machine. The experimental data under hyper-gravity are compared with those under normal gravity and with the predictions of 11 outstanding existing correlations developed for normal gravity. The results indicate that the heat transfer coefficient under hyper-gravity is greater than that under normal gravity and increases with increasing hyper-gravity.

Prajapati et al. (2015) carried out an experimental investigation to compare the flow boiling characteristics of de-ionized water in three different configurations of micro-channels. Experiments have been conducted with sub-cooled liquid state at the entry. Coolant mass is varied in the range of 100–350 kg/m²s and heat fluxes varied in the range of 10–350 kW/m². Different regimes of two-phase boiling have been observed based upon the heat flux and coolant flow rate. They have used three configurations for the study and comparison has been made in terms of heat transfer coefficient, pressure drop characteristics and affinity towards back flow or flow reversal in the channels. They have reported that for entire operating conditions, segmented finned channels demonstrate the highest heat transfer coefficient with negligible higher pressure drop compared to other two configurations of channels.

Kundu et al. (2014) conducted the experiments in horizontal tube to measure flow boiling heat transfer coefficients and pressure drops of R134a and R407C. The

size of the horizontal tube is 9.52 mm outside diameter and 1.2 m in length. Experiments were conducted at a refrigerant mass flux range of about 100–400 kg/m²s varying the inlet temperature between 5–9 °C. Heat fluxes are varied between 3–10 kW/m². The experimental data plotted against vapour quality for heat transfer coefficients and pressure drop gradient. They have reported that R134a exhibits higher heat transfer coefficients than those of R407C for same operating conditions.

Kim and Mudawar (2013) developed a universal predictive tools for pressure and heat transfer coefficient for mini/micro-channel flows that are capable of tackling fluids with drastically different thermo physical properties and very broad ranges of all geometrical and flow parameters of practical interest.

Table 2.2: Summary of literature studies with small circular and rectangular channels

Reference	Channel size mm	D_h , (mm)	\dot{G} (kg/m ² s)	q (kW/m ²)	Fluids	Geometry type
Kew and Cornwell (1997)	Ø1.39-3.69 x 500	1.39-3.69	188-1480	9.7-90	R141b	Circular Single channel
Tran et al. (1996)	1.7 x 4.06	2.46 2.4	63-832 44-505	3.6-59.5 5.6-129	R12 R12	Circular Rectangular Single channel
Lee and Lee (2001)	0.4 x 20 1 x 20 2 x 20	0.78 1.9 3.63	50-200	<15	R113	Rectangular channels
Kandlikar et al. (2006)	1.054 x 0.157 x 63.5	-	0.4-231.7	203.6-538.9	Water	Rectangular Multi channels
Peng et al. (1993)	0.6 x 0.7	0.647	1500-4000	20-1000	Water	Rectangular Multi channels
Hamdar et al. (2010)	1 x 1 x 381	1	200-600	10-60	R152a	Square Single channel
Farahani et al. (2013)	1.1 x 2.1 x 260	1.4	50-400	3-107	R245fa R1234ze	Rectangular Multi channels
Wang et al. (2013)	Ø 6 x 1550	6	62-104	11.7-87.1	Propane	Circular Multi Channel
Lazarek and Black (1982)	-	3.15	127-750	14-380	R113	Circular Single channel
Marchitto et al. (2008)	Ø 26 x 2000	26	-	-	Air-Water	Circular Single channel
Tibirica et al. (2010)	Ø 2.3 x 464	2.3	50-700	5-55	R134a R245fa	Circular Single channel

Reference	Channel size, mm	D_h (mm)	\dot{G} (kg/m ² s)	q (kW/m ²)	Fluids	Geometry type
Charnay et al.(2015)	Ø 2.3 x 185	3.00	100-1500	10-50	R-245fa	Circular Single channel
Xu et al.(2015)	Ø 2.168 x 200	2.168	725-910	19-28.5	R134a	Circular Single channel
Prajapati et al.(2015)	25.7 x 12.02	-	100–350	10–350	Deionized water	Rectangular channel
Kundu et al. (2014)	Ø 9.52 x 1200	7	100–400	3–10	R134a R407C	Circular Single channel

2.1.3 Experimental studies in plate heat exchangers

Table 2.3 presents the summary of the experimental studies on flow boiling in plate heat exchangers.

Table 2.3: Summary of literature studies on plate heat exchangers

Reference	Geometry type	\dot{G} (kg/m ² s)	q (kW/m ²)	Fluids
Han et al. (2003)	Plate heat exchanger with 45,35,20 chevron angles	13-34	2.5-8.5	R410a, R22
Longo et al. (2004)	Plate heat exchanger with Cross grooved herringbone corrugations	25.5–36.3	14.7–21.9	R22
Longo et al. (2007)	Plate heat exchanger with herringbone corrugations	13-36.7	4.5-19.7	R134a
Taboas et al. (2010)	Plate Heat exchanger	70-140	20-50	Ammonia-Water mixture
Vlasogianniset et al. (2002)	Plate Heat exchanger	-	-	Air-Water mixture
Kabelac et al. (2008)	Chevron-pattern Plate heat exchanger	50-60 80-90 10-20	9-15 10-20	R134a and Ammonia

Han et al. (2003) experimentally measured the evaporative heat transfer and pressure drop in the brazed plate heat exchangers with refrigerants R410A and R22. The plate heat exchangers with different 45°, 35° and 20° chevron angles are used. They have measured the evaporation heat transfer coefficients and pressure drops at varying mass flux of refrigerant, evaporating temperature, vapour quality and heat flux. They have reported that heat transfer coefficient increases with increasing vapour quality and decreasing evaporating temperature at a given mass flux in all plate heat exchangers. The pressure drop increases with increasing mass flux and quality and with decreasing evaporating temperature and chevron angle. They have also found that the heat transfer coefficients of R410A are larger than those of R22 and the pressure drops of R410A are less than those of R22.

Longo et al. (2004) carried out experimental work on “cross-grooved” surfaces to refrigerant vaporisation and condensation for R22. Plate heat exchanger with herringbone macro-scale corrugation is used for experimentation. Measured heat transfer coefficient and total pressure drops for different cross-grooved geometry. They also investigated the effect surface roughness of the plate on refrigerant two-phase heat transfer inside PHE. Their experimental results show that the cross-grooved surface has effect both in vaporisation and condensation. Surface roughness has effect only in vaporisation. An increase in the heat transfer coefficient from 30% to 40% in vaporisation to 60% in condensation with respect to a PHE is observed in cross-grooved surface. They have also reported heat transfer coefficients and frictional coefficients against mass and heat flux.

Longo et al. (2007) carried out experimental work on “herringbone” surfaces inside brazed plate heat exchangers (BPHE) using R134a refrigerant and measured heat transfer coefficient and pressure drops. Effects of heat flux, refrigerant mass flux, and saturation temperature and outlet conditions are investigated. They have reported that heat transfer coefficients show great sensitivity both to heat flux and outlet conditions and weak sensitivity to saturation temperature.

Taboas et al. (2010) experimentally investigated the saturated flow boiling heat transfer and frictional pressure drop of ammonia/water mixture flowing in a vertical plate heat exchanger. They presented the effects of heat flux, mass flux, mean vapour quality on boiling coefficient and frictional coefficient at pressures and ammonia concentration. They reported that the boiling heat transfer coefficient is highly dependent on the mass flux. The influence of heat flux and pressure are negligible at higher vapour qualities. The pressure drop increases with increasing mass flux and quality. However, the pressure drop is independent of the imposed heat flux.

Vlasogiannis et al. (2002) tested the plate heat exchanger under two-phase flow conditions by using an air/water mixture as the cold stream. The heat transfer coefficient of the air/water stream is measured as a function of air and water superficial velocities.

Kabelac et al. (2008) conducted the evaporation experiments on chevron-pattern plate heat exchanger using R134a and Ammonia and presented local heat

transfer coefficient. Saturation temperature varied from 268-283K for ammonia and between 265-283 for R134a. They reported that the heat transfer coefficient rises for high values of mass flux but decreases for low mass fluxes after a minimum value at vapour qualities about $x \sim 0.5$. Ammonia has higher heat transfer than the R134a.

2.2 STUDIES ON SINGLE PHASE HEAT TRANSFER AND PRESSURE DROP IN COMPACT PLATE FIN SURFACES

Research on single phase heat transfer in plate fin surface is also reviewed in relationship to two-phase heat transfer occurring in compact heat exchangers, since two-phase heat transfer coefficient is related with single phase heat transfer coefficient.

There are different types of fins like offset strip fins, wavy fins, plain fins, perforated fins, pin fins and louvered fins to provide the high density area and to enhance the heat transfer coefficient in compact heat exchangers. The most common among them are offset strip and wavy fins. Predicted or measured dimensionless parameters (Colburn ' j ' factor and fanning friction ' f ' vs. Reynolds number Re) of these fins are essential for design of heat exchangers. Kays and London (1984) conducted the experiments and compiled the results for 3 wavy fins and 21 offset strip fins. Joshi and Webb (1987) developed empirical correlations for heat transfer coefficient and friction factor in the offset strip fin heat exchanger surface geometry. Friction factor data were taken on eight scaled-up, idealized geometries. Wieting (1975) developed empirical relations by correlating experimental heat transfer and flow friction data for 22 offset strip fin surfaces over two Reynolds number ranges $Re_d < 1000$ and $Re_d > 2000$. For predicting Colburn ' j ' and Fanning friction ' f ' factors in the transition region ($1000 < Re_d < 2000$), he suggested extrapolating the equations up to their intersection point. Manglik and Bergles (1995) used an asymptotic method to establish their correlations for offset strip fin surfaces. They have considered 18 offset strip fin surfaces and analyzed for heat transfer and friction data. They also have analyzed effect of fin geometry parameters and proposed correlations in terms of geometry parameters. Ranganayakulu and Pallavi (2011) carried out numerical analysis on offset strip fins using air as a media and proposed correlations. They have

analyzed the fin geometry on ' j ' and ' f ' factors. Zhang et al.(2004) numerically simulated the two dimensional wavy plate fin channels with sinusoidal wall corrugations at low Reynolds number for air and presented velocity and temperature fields, isothermal Fanning friction factor, and Colburn j factor for different flow rates, wall-corrugation severity and fin spacing. Awad and Muzychka (2010) proposed the new models for prediction of Fanning friction factor ' f ' and Colburn j factor for air cooled compact wavy fin heat exchangers. The new models are developed by combining the asymptotic behaviour for the low Reynolds number and laminar boundary layer regions. The models are developed by taking into account the geometric variables such as fin height, fin spacing, wave amplitude, fin wavelength, Reynolds number, and Prandtl number. They have compared the models with numerical and experimental data for air at different values of the geometric variables. Asadi (2013) presented a study in terms of pressure drop and heat transfer coefficient for different types of compact heat exchangers. Ciofalo et al. (1996) mentioned that the condition yielded lower ' j ' values compared to those for the constant heat flux boundary condition but agreed well with the experimental values. Beale (1993) explored fluid flow and heat transfer in inline and staggered tube banks. Fully developed cross flow was assumed throughout. Both constant wall temperature and constant heat flux boundary conditions were considered and compared with existing experimental and numerical data. Dong Junqi et al. (2013) presented experimental correlation equations of the wavy fin about the heat transfer and pressure drop set up using the multiple regression method. Shah (2006) discussed significant advances in the theory, analysis, design and optimization, manufacturing and technology of compact heat exchangers.

All the studies carried out above used air as the coolant medium. Only few studies performed using liquid as coolant. Hu and Herold (1995) carried out studies both analytically and experimentally using liquid water and polyalphaolefin for Prandtl number ranges from 3 to 150 on offset strip fin surface. They have presented that the Prandtl number had a significant effect on the heat transfer factor j of the fin. They also observed that air models over predict the j factor for liquids. However the Prandtl number was found to have little on the Fanning friction factor. Ranganayakulu et al. (2013) performed numerical analysis on offset fins using CFD approach. He

found that the ' j ' of water is lower by about 30% when compared with air, where as there is no significant deviation in ' f ' values. Even though ' j ' is lower for water, the heat transfer coefficient (h_1) is much higher when compared to air. Kim and Sohn (2006) carried out experiments using water and R113 as a test fluid on offset strip fins by considering fin geometry effect. In their experimental findings noted that there is no significant variation of ' f ' factor. However, the j factor measured in their study was about 25% smaller, when compared with the prediction of Manglik and Bergles (1995) for Reynolds number less than 1000. For Reynolds number greater than 1000, the difference between the measured data and the prediction of Manglik and Bergles (1995) reduced with the increase in Reynolds number. Maiti (2002) carried out numerical analysis on wavy fin using air as medium and proposed correlations. Ranganayakulu et al. (2008) carried out numerical study of flow patterns of compact plate fin heat exchangers. Design data for wavy fins using computational fluid dynamics method was obtained. Correlations were proposed for ' f ' and ' j ' by considering the geometrical parameters.

3.0 CONCLUSION FROM THE LITERATURE SURVEY AND MOTIVATION

Evaporator should be compact and efficient to save weight, space and cost. To design the evaporator determination of heat transfer and friction data is essential. Hence determination of design data experimentally will help in design of compact plate-fin heat exchangers for evaporator applications. Due to compactness (large heat transfer area/unit volume) of these heat exchangers will led reduction in size and weight of the heat exchangers compared to present day heat exchangers of shell & tube, plate heat exchangers and plate & tube. Apart from compactness, using refrigerant R134a, which is user friendly and environmental friendly, having the high COP and heat transfer rates due to latent heat of vaporization, the size and weight of heat exchangers shall be further reduced. Hence, there is lot of scope for improvements of performance of systems, which have involved evaporation. Hence the determinations of boiling heat transfer and friction coefficients will help in design of compact evaporator. From the literature study it is observed that design information to produce advanced compact heat exchanger with fin surfaces having hydraulic diameter lower

than 3 mm and eco friendly refrigerant R134a is rather limited today. Present study is aimed to produce the design data on fin surfaces (offset strip and wavy type fins) using R134a as a working medium to extend the knowledge of compact evaporator performance.

It is also observed from the literature that, many authors are attempted to develop j and f correlations for offset strip and wavy fins using air as the working medium. Conversely, only few studies performed using liquid as working medium on these fin surfaces. Few authors presented that the Prandtl number had a significant effect on the heat transfer factor j of the fin. They have also reported that air models over predict the j factor for liquids and Prandtl number was found to have little effect on the Fanning friction factor. Hence, generation j correlation for offset strip and wavy fins using liquid as the working medium is necessary to enrich the data bank. Most of the authors attempted to develop j and f correlations experimentally which is expensive and time consuming. Numerical analysis is the new approach used to develop single phase heat transfer and friction correlations on these type of fin surfaces. Hence numerical analysis (CFD approach) is used in the present study for development generalized correlations for laminar and turbulent regions, in the form j and f by considering all geometrical and flow parameters. The numerical data is compared with the experimental data for validation.

Based on summary of the literatures reviewed, conclusion can be made that the research related to two -phase flow heat transfer and flow friction characteristics using compact plate fin surfaces (hydraulic diameter lower than 3 mm) and with eco-friendly refrigerants is a future area. A large scope is available for the research in this emerging area of heat transfer.

CHAPTER 3

COMPUTATIONAL APPROACH FOR SINGLE PHASE HEAT TRANSFER AND FRICTIONAL ANALYSIS OF FIN SURFACES

Chen (1966) proposed that the two-phase heat transfer coefficient of the fluid (h_{tp}) is sum of the convective term (h_{cb}), and the nucleate boiling term (h_{nb}). Convective heat transfer coefficient (h_{cb}) is related with single-phase heat transfer coefficient (h_l) by the Reynolds number factor (F). Hence to find out single phase heat transfer coefficient h_l and friction coefficient of fluid, numerical analysis using Computational fluid dynamics (CFD) has been carried out for fin geometry of wavy and offset strip fins using fluid R134a (liquid phase) and developed a generalized correlations. CFD also carried out for wavy fin surface using water as working medium and generated generalized correlations. With objective of reducing the volume of expensive experiments this method is being employed for single phase, since numerical analysis is well established for single phase Ranganayakulu et al. (2003, 2008, 2013).

3.1 CFD ANALYSIS

Generally CFD used as a tool for design aid to predict the performance of equipment involving heat transfer and fluid/gas flow. Numerical simulation of heat transfer and fluid flow problems before a prototype is built reduces the cost and time of development. However, CFD results must be validated by experimentation to ensure that the numerical predictions are reliable. Thus always a cycle is formed involving theoretical predictions, CFD and followed by experimentation. Validity of new mathematical models can be tested within the context of this relationship, with resulting improvements in the accuracy of CFD analysis.

CFD software mainly contains three elements (i) Pre-processor (ii) Solver and (iii) Post-processor. In pre-processing construction of geometry, generation of mesh on the surfaces or volumes shall be carried out. Solver used to solve the equation set

based on options chosen by the user and compute the flow field. Post-processor helps the user to examine the results and extract data in the flow fields, graphs etc.

3.2 CFD APPROACH

The CFD approach for analysis of heat transfer and pressure drop in the fin surfaces is explained in this section.

Initially the fin is modelled and mesh generated. Next, mesh finalization is done by taking different mesh configurations across the computational domain, starting with coarse to fine mesh at a particular Reynolds number. The grid independence check is carried out for each fin surface to find out the optimum number of elements for the analysis. Finally graph is plotted between the number of elements and the performance parameter i.e. pressure drop of the fin. Analyze the graph for minimum number of elements required for consistent results and hence, further analysis is conducted with more than minimum number of grid elements.

The CFD analysis shall be done in two-phases. In first phase the fin is analysed for friction factor ' f ' for a range of Reynolds number. In second phase the Colburn ' j ' factor is estimated for the same range of Reynolds number using energy equation. The model of periodic fully developed flow as suggested by Patankar et al. (1977) is used for the flow analysis in order to overcome the entrance effect. Kays and London (1984) method is used for estimation of friction factor f . In this method initially pressure drop for unit length is estimated which is used for estimation of the f . The same procedure is repeated for 100 to 15000 Reynolds numbers in order to draw the effect of Reynolds number on friction factor.

In the second phase the “velocity” is used as an inlet boundary condition and “outflow” is used as a outlet boundary conditions for the fin geometry. This analysis takes heat conduction into account. Weimer and Hartzog (1977) and Hasseler (1993) suggested a simplified assumption of the constant wall temperature boundary condition over all section of the fin. At particular Reynolds number pressure, temperature and velocity profiles are taken at the various fin sections. The ΔT between inlet and outlet of the fin, in turn, is used for estimating the ' j ' factor using the Kays and London (1984) methodology. Similarly, the same procedure is repeated

for 100-15000 Reynolds numbers in order to draw the ' j ' versus Re characteristic curve.

3.3 METHODOLOGY

To carryout numerical analysis for generation of Colburn j factor and friction factor f for wavy and offset fins, the following steps are used. Fig.5.1 shows the flow chart of methodology.

- Modeling and numerical grid generation for the fin
- Applying the boundary conditions
- Analysis using ANSYS CFD software, Ver 14
- Computation of ' j ' and ' f ' factors
- Validation of results with open literature.
- Generation of j and f correlations

3.4 MATHEMATICAL MODEL AND GOVERNING EQUATIONS.

Finite volume method is used for solving the conservation of mass, momentum and energy equations. Semi-implicit SIMPLER method as mentioned in Versteeg and Malalasekera (1995) algorithm is used for calculation of turbulent flow in the velocity and pressure conjugated problem. For the approximation of the convection terms second order upwind differential scheme is applied.

A standard κ - ϵ model mentioned by Versteeg and Malalasekera (1995) with enhanced wall treatment is used for predicting the turbulent flow in the plate-fin heat exchanger and in fin geometry. The standard k - ϵ model is a two equation model based on model transport equations for the turbulence kinetic energy (k) and its dissipation rate (ϵ). The model transport equation for k is derived from the exact equation. This model is widely used in industrial flow simulation due to robustness, economy, and reasonable accuracy for a wide range of turbulent flows. It is the workhorse of practical engineering flow calculations. In the derivation of the k - ϵ model, the assumption is that the flow is fully turbulent, and the effects of molecular viscosity are negligible. In this simulation work, molecular viscosity effects are assumed as negligible and only turbulence effects are considered, hence the standard k - ϵ model has been selected.

The generalized form of Reynolds transport equations as given in Anderson (1995) and Patankar (1980) is.

$$\text{div}(\rho u \Phi) = \text{div}(\Gamma \text{grad} \Phi) + S_{\Phi} \quad (3.1)$$

Where Φ is a generalized transport variable, Γ represents the effective diffusivity, S_{Φ} is the source term for the respective dependent variable. The meaning assigned to Φ , Γ and S_{Φ} are listed in Table 3.1. The convergent criteria is specified to absolute residuals ($\leq 1.0 \times 10^{-6}$).

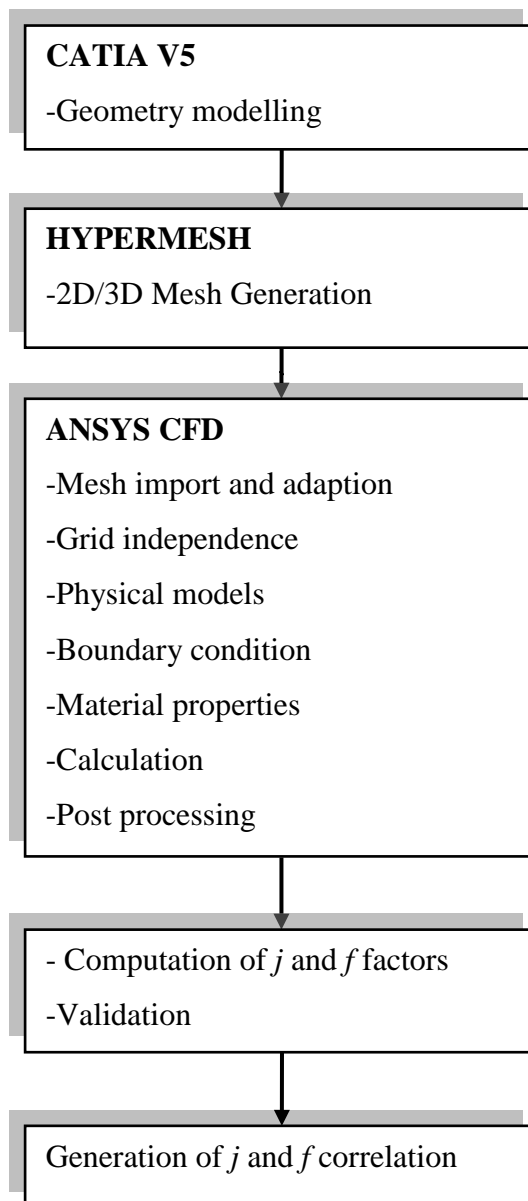


Fig 3.1: Flow chart of methodology

Table 3.1: Description of variables Φ , Γ and S_Φ for conservation of mass, momentum and energy

Conservation of law		Φ	Γ	S_Φ
Conservation of mass		1	0	0
Conservation of momentum	X-direction	u	μ	$-\frac{\partial \psi}{\partial x} + \rho g_x + \text{fluid friction} + S_u$
	Y-direction	v	μ	$-\frac{\partial \psi}{\partial y} + \rho g_y + \text{fluid friction} + S_v$
	Z-direction	w	μ	$-\frac{\partial \psi}{\partial z} + \rho g_z + \text{fluid friction} + S_w$
Conservation of Energy		θ	$\frac{k}{c_p}$	$-\frac{D\psi}{D\lambda} + \text{Viscous dissipation} + \text{Other heat sources}$

Substitution of the variable Φ in equation (3.1) by those defined in Table 3.1 leads to the general governing equations (3.2), (3.5) and (3.6) of fluid dynamics as follows.

Conservation of mass

$$\frac{D\rho}{D\lambda} = -\rho(\nabla \cdot \mathbf{u}) \quad (3.2)$$

$$\text{Where } \frac{D}{D\lambda} = \frac{\partial}{\partial \lambda} + u \frac{\partial}{\partial x} + v \frac{\partial}{\partial y} + w \frac{\partial}{\partial z} \quad (3.3)$$

$$\text{And } \nabla \cdot \mathbf{u} = \frac{\partial u}{\partial x} + \frac{\partial v}{\partial y} + \frac{\partial w}{\partial z} \quad (3.4)$$

Conservation of Momentum

$$\rho \frac{Du}{D\lambda} = -\nabla \rho - [\nabla \cdot \boldsymbol{\tau}] + \rho g \quad (3.5)$$

Conservation of energy

$$\rho \frac{DU}{D\lambda} = -(\nabla \cdot \mathbf{q}) - \psi(\nabla \cdot \mathbf{u}) - (\boldsymbol{\tau} \cdot \nabla \mathbf{u}) \quad (3.6)$$

3.5 ASSUMPTIONS

The assumptions made in the simulation are:

- The flow is steady and incompressible. The fluid density is constant throughout the computational domain.
- The fluid flow meets the Boussinesq assumption
- The effect of heat conduction through the fin and plate material is considered

- R134a (liquid phase) used as a working medium. Water medium also used for wavy fins.
- The flow is periodically developed both hydro-dynamically and thermally. Patankar et al. (1977) have shown that it is indeed the case in most practical situations.
- No slip boundary condition is considered on the wall
- The CAD model does not include the burrs, sharp edges etc.

3.6 BOUNDARY CONDITIONS

Proper boundary conditions are needed for a successful computational work. The following Boundary conditions are used for analyzing the models.

(a) No slip condition

No-slip condition indicates that the fluid sticks to the wall and moves with the same velocity as the wall, it is moving.

(b) Isothermal condition for pressure drop cases

Heat transfer effects are not considered.

(c) Periodicity condition

When the flow passage has features repeating at regular intervals periodic boundary condition is employed. This situation occurs in offset strip and wavy fin passages. The concept of periodicity and periodic boundary conditions were given by Patankar et al. (1977). Since the heat exchanger channel is characterized by a geometry periodically repeating in the flow direction, and the expected flow pattern would have a periodically repeating nature, the usage of such type of boundary conditions is valid. Fluent treats the flow at a periodic boundary as though the opposing periodic plane is a direct neighbor to the cells adjacent to the first periodic boundary. Thus, when calculating flow through the periodic boundary adjacent to a fluid cell, the flow conditions at the fluid cell adjacent to the opposite periodic plane are used.

(d) Total flow at the inlet

(e) Bulk temperature of fluid at inlet

(f) Symmetry boundary condition

Symmetric boundary conditions are used when the physical geometry of interest, such as the outlined heat exchanger channel, and the expected pattern of the flow/thermal solution are symmetric. When using this type of boundary condition in such regions no additional boundary conditions are required. Fluent assumes zero flux of all quantities across a symmetric boundary.

(g) Wall boundary conditions

In most of the flows either it may be internal flow or the external flow, the solid boundaries are encountered. The wall boundary conditions are then used. The wall boundary conditions play very significant roles especially whenever the energy equation is switched on and the heat transfer is to be properly determined. This is particularly important for the turbulence modelling. The walls should be properly captured and very fine mesh should be taken at the wall. The conduction or the convection or the radiation or the mixture of any two or three types and the other parameters can be defined in the wall boundary conditions. For the heat transfer, there are two types of boundary conditions that can be specified at the wall for the fully developed flows. They are:

- Constant wall heat flux
- Constant wall temperature

In the constant wall heat flux boundary condition, a constant specified heat flux is defined over the length while in the constant wall temperature the wall temperature is defined to be constant.

3.7 ANSYS CFD PACKAGE

Commercially available software ANSYS CFD is used to solve the CFD equations along with appropriate boundary conditions. ANSYS CFD uses finite volume numerical procedures to solve the governing equations for fluid velocities, mass flow, pressure, temperature, turbulence parameters and fluid properties. Numerical techniques involve the sub-division of the domain into a finite set of neighbouring cells known as "control volumes" and applying the discretized governing partial differential equations over each cell. This yields a large set of

simultaneous algebraic equations, which are highly non-linear. These equations are in turn solved by iterative means until a converged solution is achieved. There are five turbulence models available in ANSYS CFD

1. Spalart-Allmaras model
2. $\kappa - \varepsilon$ models
3. $\kappa - \omega$ models
4. Reynolds Stress Model (RSM)
5. Large Eddy Simulation Model (LES)

In present study standard κ - ε model is selected for these types of extended surfaces.

3.8 COMPUTATION OF j AND f FACTORS

The friction factor f is computed from the area averaged mean pressure drop over the periodic length 'L' using the relation.

$$\Delta P = \frac{4f L \dot{G}^2}{2\rho D_h} \quad (3.7)$$

Where \dot{G} is mass velocity ($\text{kg}/\text{m}^2\text{s}$), L = length of the passage (mm)

For wavy fin surfaces L is ' λ ', and offset strip fins L is lance length ' l '

Eqn 3.7 can be rewritten as by replacing \dot{G} as ρw_m

$$f = \frac{\Delta P D_h}{2w_m^2 \rho L} \quad (3.8)$$

Where w_m is area averaged mean velocity at any cross section, D_h = hydraulic diameter

$\Delta P = P_m(0) - P_m(L)$, $P_m(y)$ being the mean pressure over the cross section at axial coordinate y .

The Colburn j factor is defined as

$$j = \frac{h_l}{G C_p} Pr^{\frac{2}{3}} \quad (3.9)$$

Eqn3.9 can be written in terms of the output variables of CFD simulation

$$j = \frac{D_h}{4L} \ln \left[\frac{T_{wall} - T_m(0)}{T_{wall} - T_m(L)} \right] Pr^{\frac{2}{3}} \quad (3.10)$$

Where T_{wall} is the wall temperature, assumed uniform around the computational domain. The mean variables $w_m(y)$, $p_m(y)$, and $T_m(y)$ are computed from the following expressions.

$$\text{Frontal area of section } y, A_F(y) = \iint dx. dz \quad (3.11)$$

$$\text{Mean velocity, } w_m(y) = \frac{1}{A_F(y)} \iint w(x, y, z) dx. dz \quad (3.12)$$

$$\text{Mean pressure, } P_m(y) = \frac{1}{A_F(y)} \iint P(x, y, z) dx. dz \quad (3.13)$$

$$\text{Mean Temperature, } T_m(y) = \frac{1}{A_F(y)w_m(y)} \iint T(x, y, z)w(x, y, z) dx. dz \quad (3.14)$$

All the double integrals in Eqn (3.11), (3.12), (3.13) and (3.14) are evaluated by summing over the available flow cross section at axial position y .

3.9 HEAT TRANSFER AND FRICTIONAL ANALYSIS OF WAVY FIN SURFACE.

CFD analysis was carried out on wavy fin surface using liquid R134a and water. Generalized correlations were developed in terms Colburn j and f factor. The effect fin geometry and Reynolds number on j and f is investigated.

3.9.1 Numerical model

The numerical model shown in the Fig. 3.2 of the smooth wavy fin is defined by the following parameters.

- fin thickness (t),
- fin height (h),
- wave length (λ),
- wave amplitude (a),
- fin spacing (s).

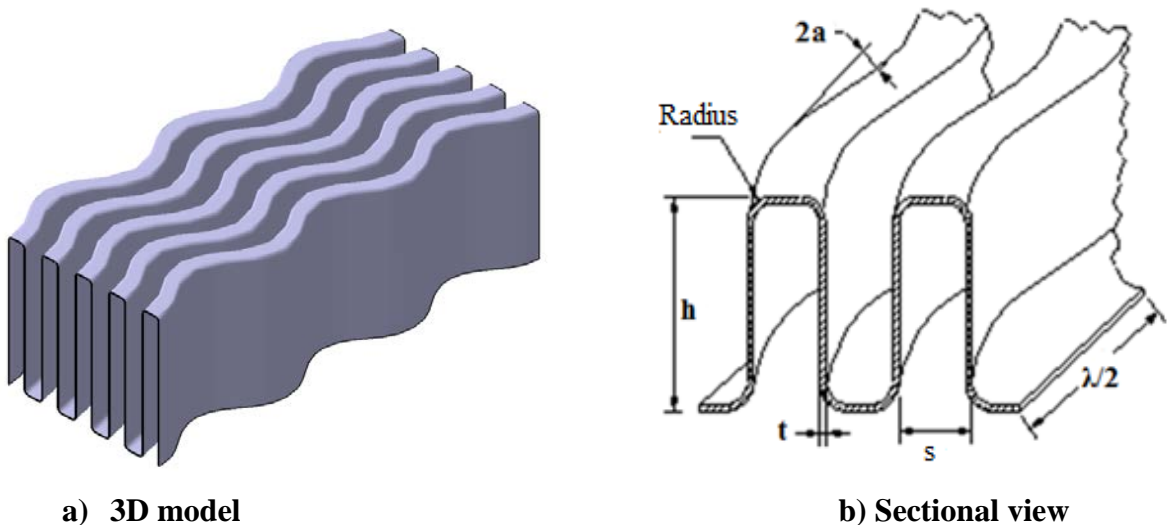


Fig. 3.2: Numerical model for wavy fin

Fig. 3.3 defines the geometric parameters smooth wavy fin surface considered for analysis.

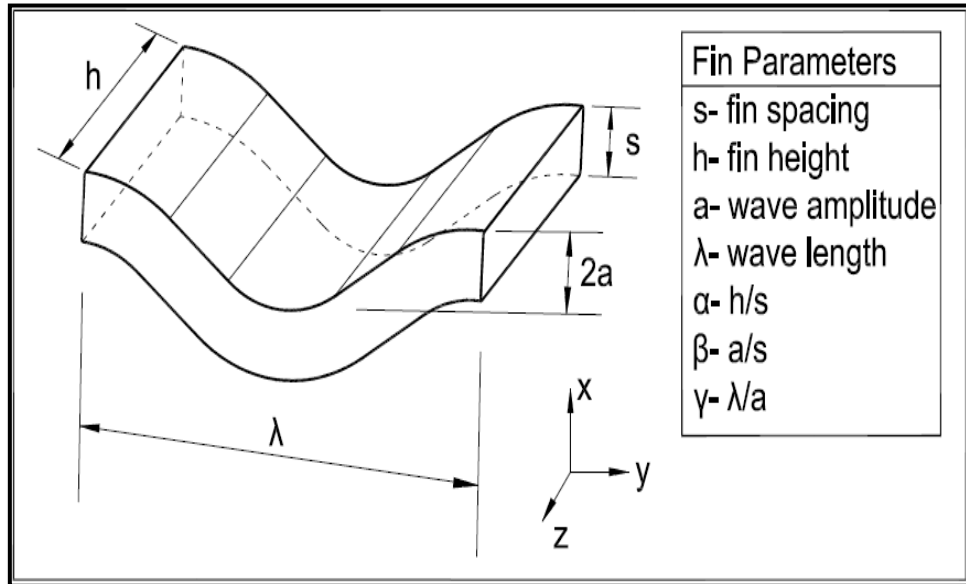


Fig. 3.3: Geometry parameters of wavy fin

Wavy fin was modelled using CATIA software. The wavy fin geometry initially considered for the analysis is

- fin height, $h = 6.77\text{mm}$,
- wave length, $\lambda = 9.525\text{mm}$,
- fin spacing, $s = 1.411\text{mm}$,
- fin thickness, $t = 0.152\text{mm}$,
- wave amplitude, $a = 1.95\text{mm}$
- hydraulic diameter, $D_h = 2.123\text{mm}$

Grid is generated using Hyper Mesh software. Initially 2D elements generated using quad elements. Hexa elements used for 3D domain for computation. The quality of the grid used in the computations directly influences the solution obtained. Lot of care has been taken in choosing the desirable features in the grid like orthogonality, control of spacing and skewness. Apart from these, very low aspect ratios of grid cells and highly stretched grids have been avoided to get better results.

3.9.2 CFD analysis

3.9.2.1 Computational domain

Fig. 3.4 shows the computational domain taken for modelling of heat transfer and fluid flow for a wavy fin surface. Fin spacing ‘ s ’ in the x-direction, wave length ‘ λ ’ in the y-direction and fin height ‘ h ’ in the z-direction constitutes the computational domain.

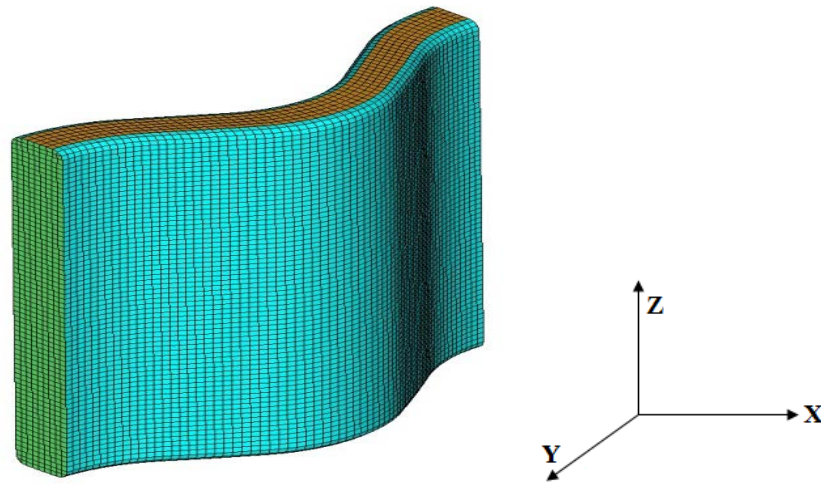


Fig. 3.4: The computational fluid domain for the smooth wavy fin surface.

3.9.2.2 Dimensionless parameters

The wavy fin geometry parameters are expressed in terms non-dimensional parameters α , β and γ . The effect of fin thickness is neglected in the analysis. Colburn j and f correlations are expressed in terms of these non-dimensional parameters.

$$\alpha = \frac{h}{s} \quad (3.15)$$

$$\beta = \frac{a}{s} \quad (3.16)$$

$$\gamma = \frac{\lambda}{a} \quad (3.17)$$

Hydraulic diameter D_h is used as the characteristic dimension in expressing the heat transfer and flow friction data.

Geometry parameters are varied and a total of 103 sets of wavy fin surfaces are considered and modelled for CFD analysis for developing the correlations. Two fluids liquid water and refrigerant R 134a (liquid phase) are used as medium for the

analysis. The following ranges of fin geometries and Reynolds numbers are taken for analysis.

$$2.83 \leq \frac{h}{s} \leq 11.24 \quad (3.18)$$

$$1.13 \leq \frac{a}{s} \leq 2.53 \quad (3.19)$$

$$4.14 \leq \frac{\lambda}{a} \leq 8 \text{ and} \quad (3.20)$$

$$100 \leq \text{Re} \leq 1000 \text{ for laminar region} \quad (3.21)$$

$$1000 \leq \text{Re} \leq 15000 \text{ for turbulent region} \quad (3.22)$$

3.9.2.3 Grid independency

The main objective of the grid independence study is

- Verification of mesh correctness for the problem
- Refinement of mesh and
- Selection of the optimal mesh.

This is carried out in the first step in each and every analysis. Mesh sizes ranging from coarse to fine mesh are taken first and solved with same boundary conditions. Pressure drop is taken as standard benchmark to determine the independency of the mesh and the graph between number of elements and the pressure drop is drawn in Fig. 3.5. Then the mesh size is finalized based upon the value where there is no significant change in the pressure drop. This mesh size is taken for further analysis. From the figure it is quite clear that the value beyond the 2 million mark has no significance change in the pressure drop. Hence the number of elements of 2 million is taken as final mesh because of computation time and convergence.

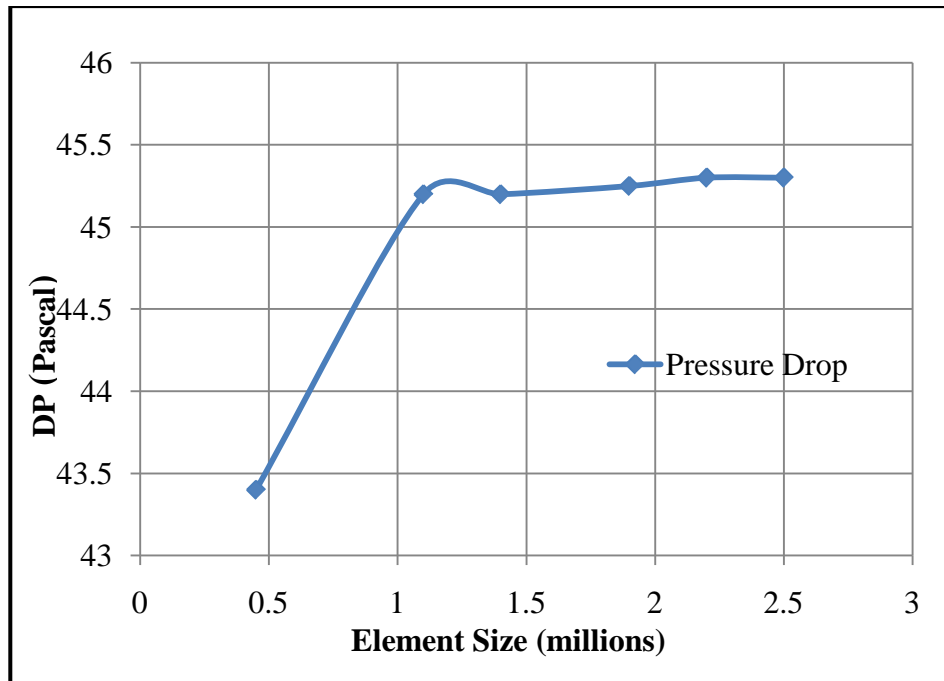


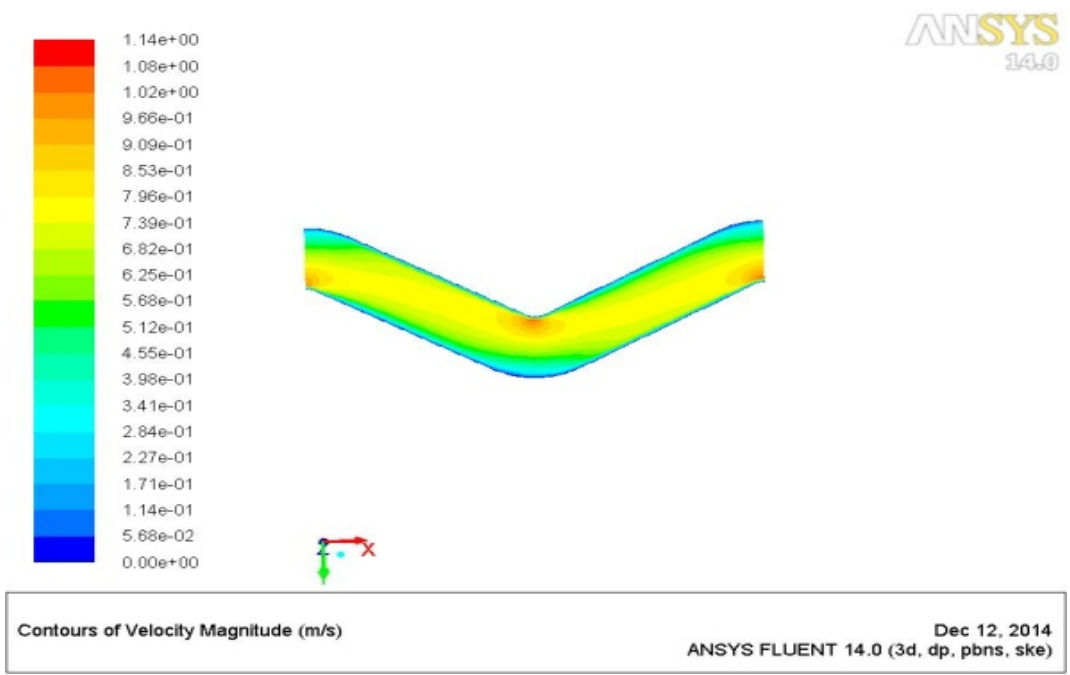
Fig.3.5: Grid independency graph for wavy fin

3.9.2.4 CFD simulation studies

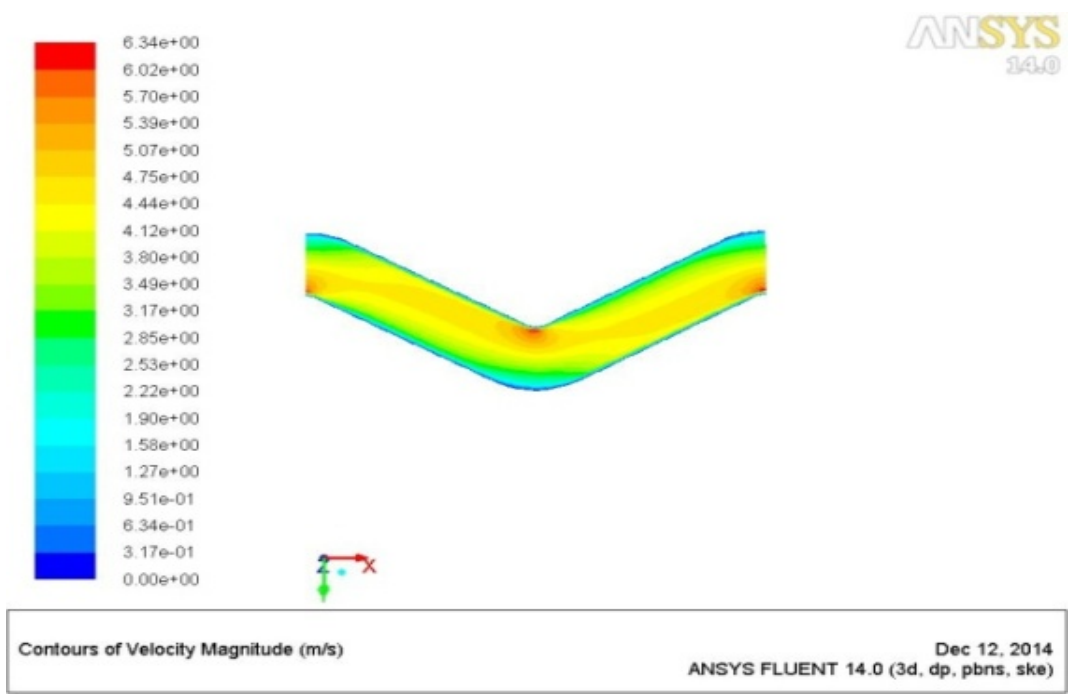
The CFD studies were carried out on the smooth wavy fin at different Reynolds number ranging from 100 to 15000 by applying the boundary conditions. The analysis was carried out in two-phases. In first phase the fin characterized for friction factor ' f ' over above range of Reynolds number. In second phase the Colburn ' j ' factor is estimated for the same range of Reynolds number using energy equation.

3.9.2.5 Velocity and temperature fields

Fig. 3.6-3.8 shows the velocity, pressure and temperature fields for flow over the wavy fin surface at Reynolds number, $Re=10000$ based on the ANSYS CFD output data.

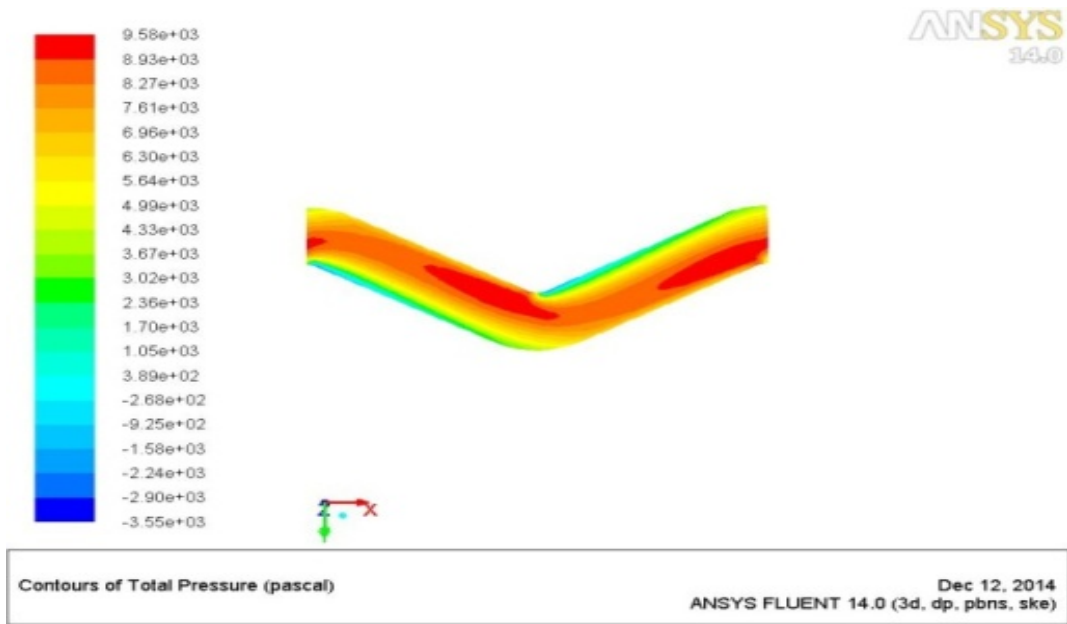


a) R134a

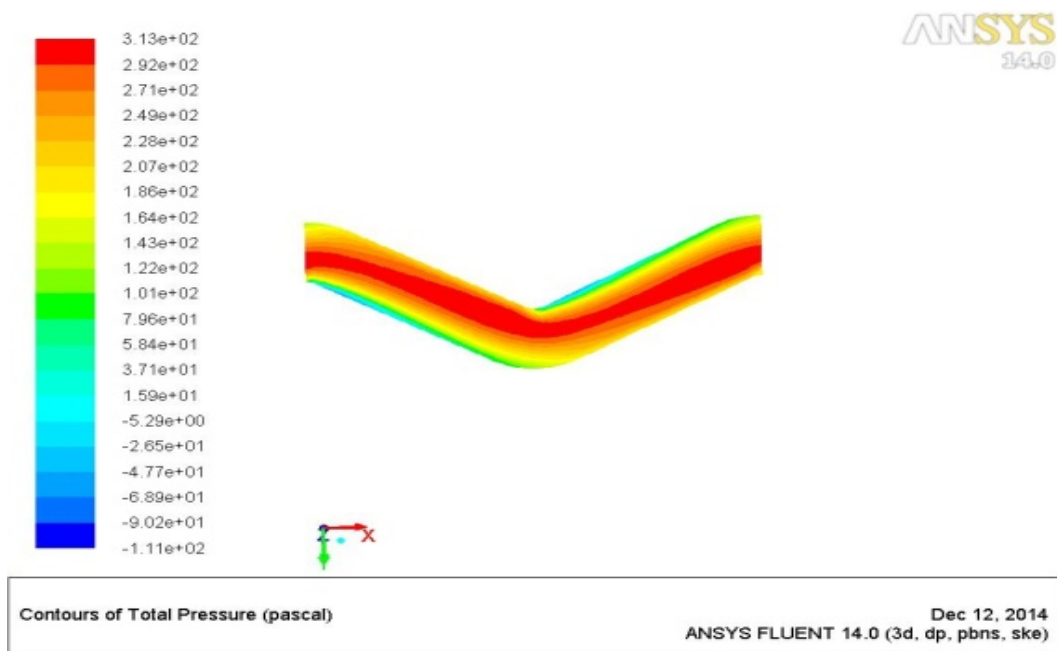


b) Water

Fig. 3.6: Velocity profiles of wavy fin at $h/2$ a) liquid refrigerant R134a b) water

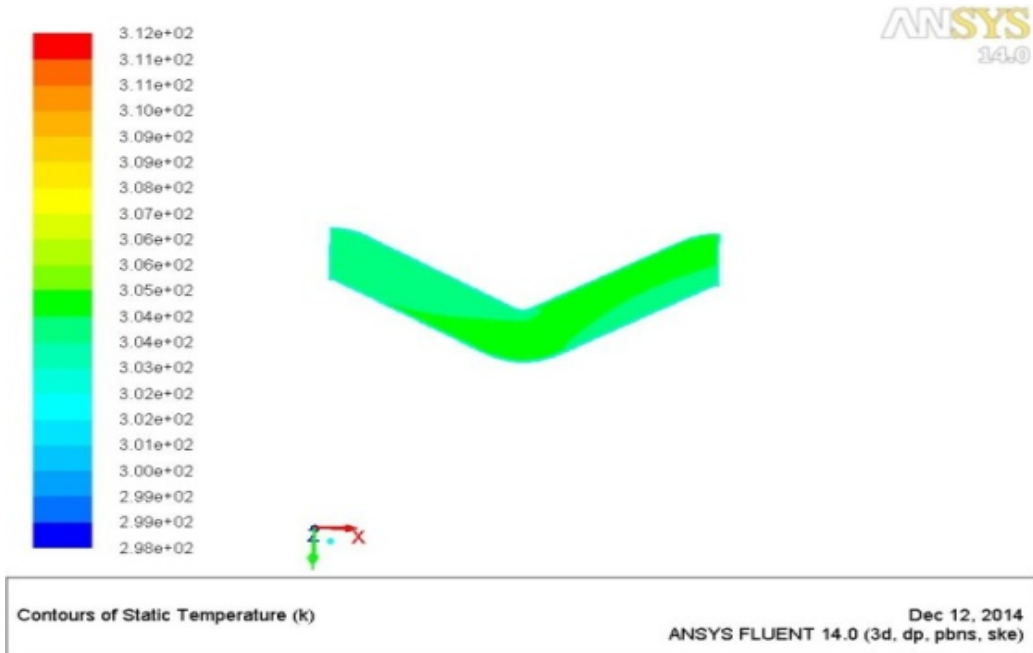


a) R134a

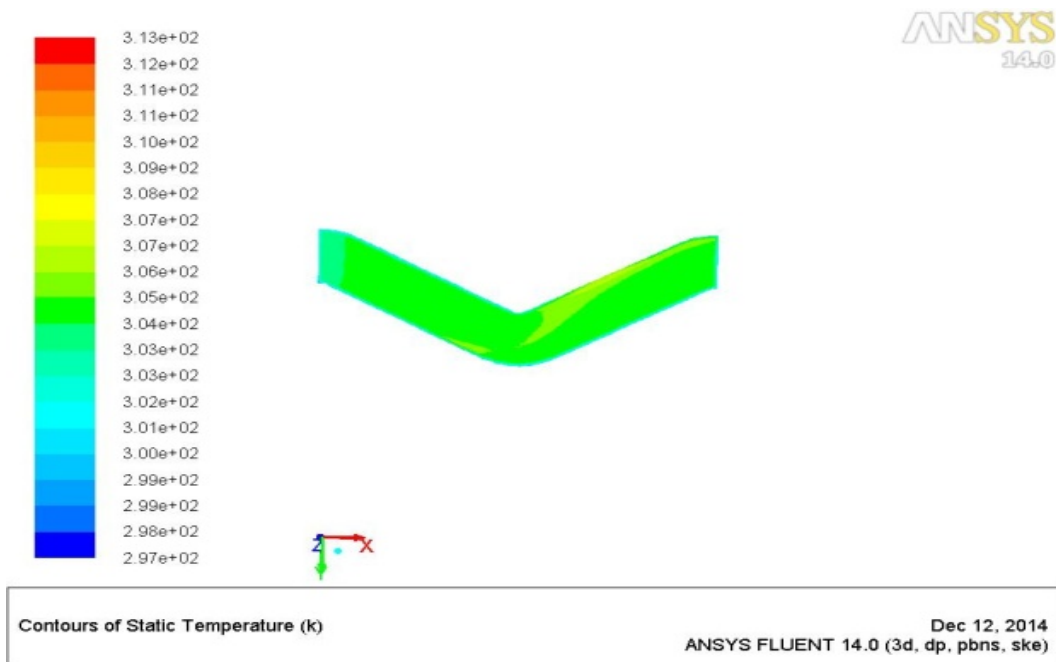


b) Water

Fig.3.7: Total pressure profiles of wavy fin at $h/2$ a) liquid refrigerant R134a



a) R134a



b) Water

Fig. 3.8: Static temperature profiles of wavy fin near the wall a) liquid refrigerant R134a b) water

From the plots it is observed that flow separates from the wall near concave faces on the flow path. It separates from diverging flank and reattaches on to a converging flank, thus creating a recirculation flow at the corrugation trough. This

phenomenon is even more clearly visible with velocity profile plots given in Fig.3.6. The reason behind the flow separation is the inability of the fluid to turn around sharp bends. The maximum velocity occurs near the valleys of the corrugations.

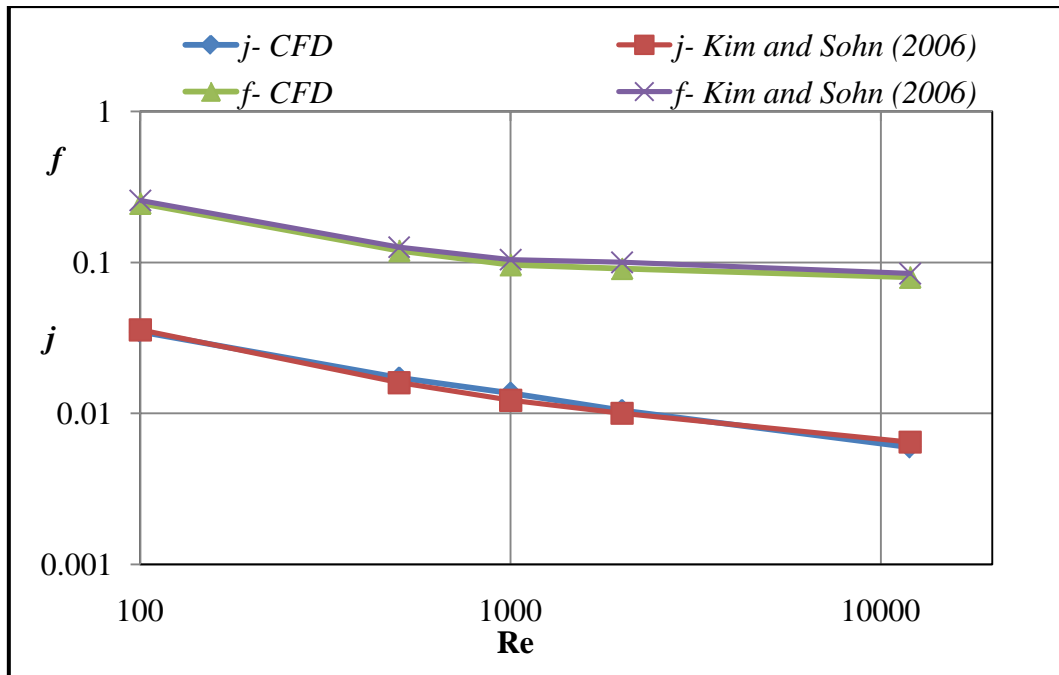
Fig. 3.7 shows the pressure contours in the x-z plane. The highest pressures occur near the wave troughs and downstream from the wave peaks. The minimum pressure occurs just upstream of the concave surfaces in the flow passage.

Fig.3.8 shows the temperature distribution in the x-z plane. The enhancement in heat transfer rate may be observed from the temperature contours over the recirculation zone.

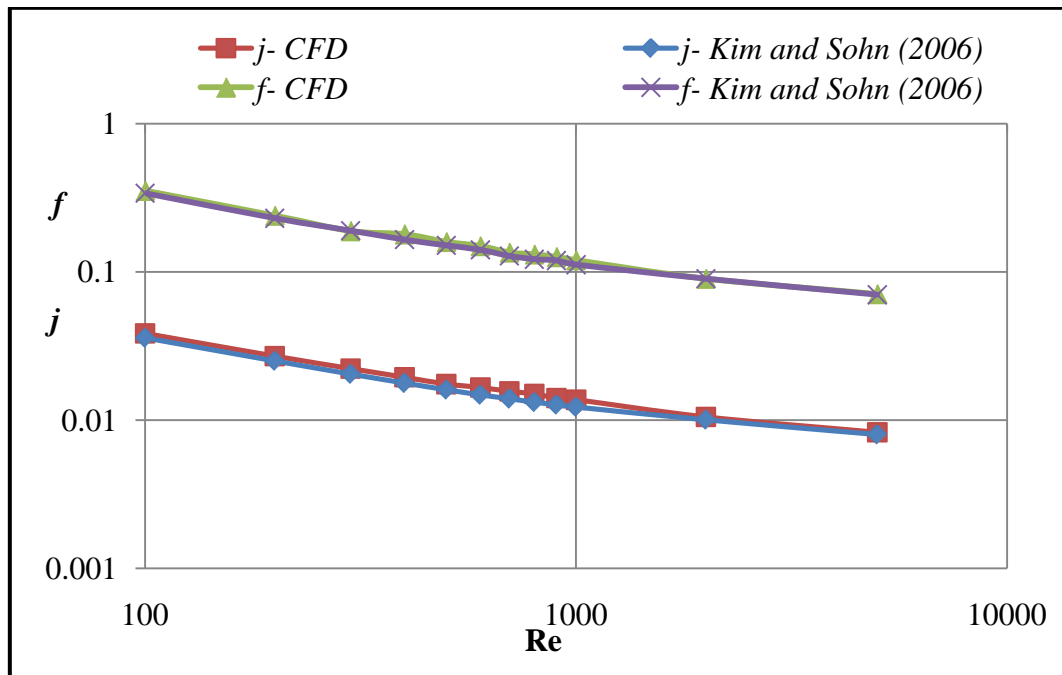
3.9.2.6 Validation

To validate the CFD results, offset strip fin geometry from Kim and Sohn (2006) has been taken for the CFD analysis and modelled; since experimental results with wavy fin and liquid water/refrigerant R134a as working medium is not available in the open literature.

Water and R113 is used as working fluid for analysis. The above fin geometry was modelled; grid generated and carried out CFD analysis using ANSYS CFD. The results were analyzed and compared with experimental results of Kim and Sohn (2006) and plotted in Figs. 3.9a & 3.9b. The CFD results are found in good agreement with experimental results. The variation is found to less than 5% in both '*f*' and '*j*' values. Uniform wall temperature boundary conditions are used for the analysis. Before carrying out the analysis grid independence check was carried out to optimize the mesh size.



a) Water as a working fluid



b) R113 as a working fluid

Fig.3.9: Validation with experimental results for the fin2.8h-3.5s-0.2t
a) Water b) R113

The CFD results also validated with wavy fin and air medium, by considering the wavy fin geometry from Kays and London (1984). The wavy fin geometry considered for the analysis is $6.77h-1.411s-0.152t$.

The above fin geometry was modelled; grid generated and carried out CFD analysis using ANSYS CFD. The results were analyzed and compared with experimental results of Kays and London (1984) and plotted in Fig.3.10. The CFD results are found in good agreement with experimental results. The variation is found to be less than 5% in both ' f ' and ' j ' values. Uniform wall temperature boundary conditions are used for the analysis. Before carrying out the analysis grid independence check was carried out to optimize the mesh size.

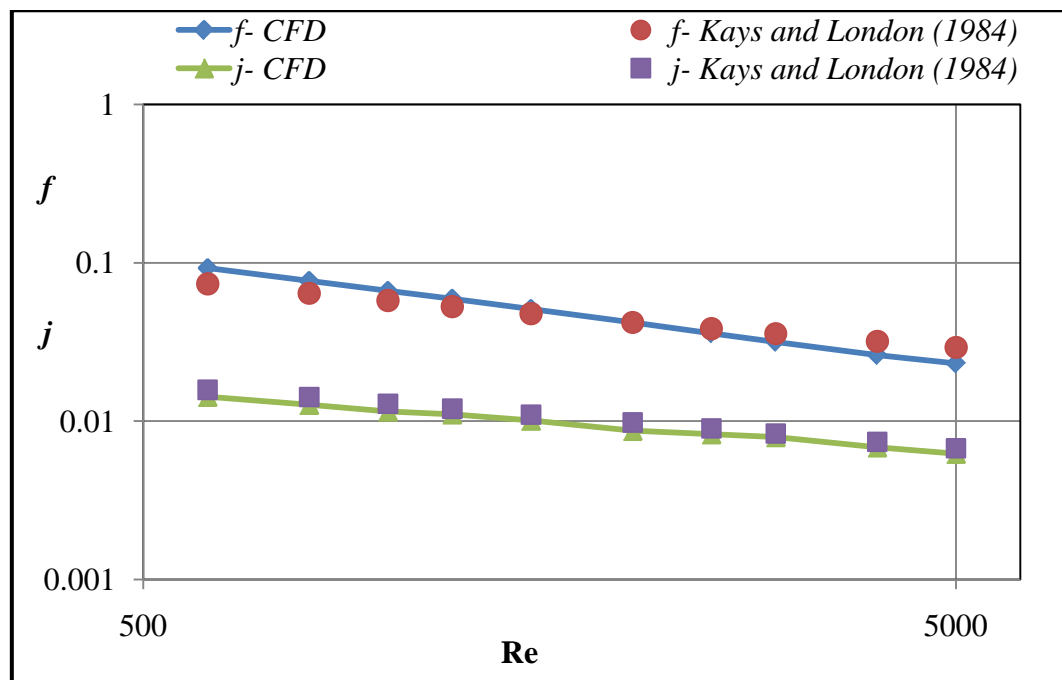


Fig. 3.10: Validation with experimental results for the fin $6.77h-1.411s-0.152t$

3.9.2.7 Generation of f and j data

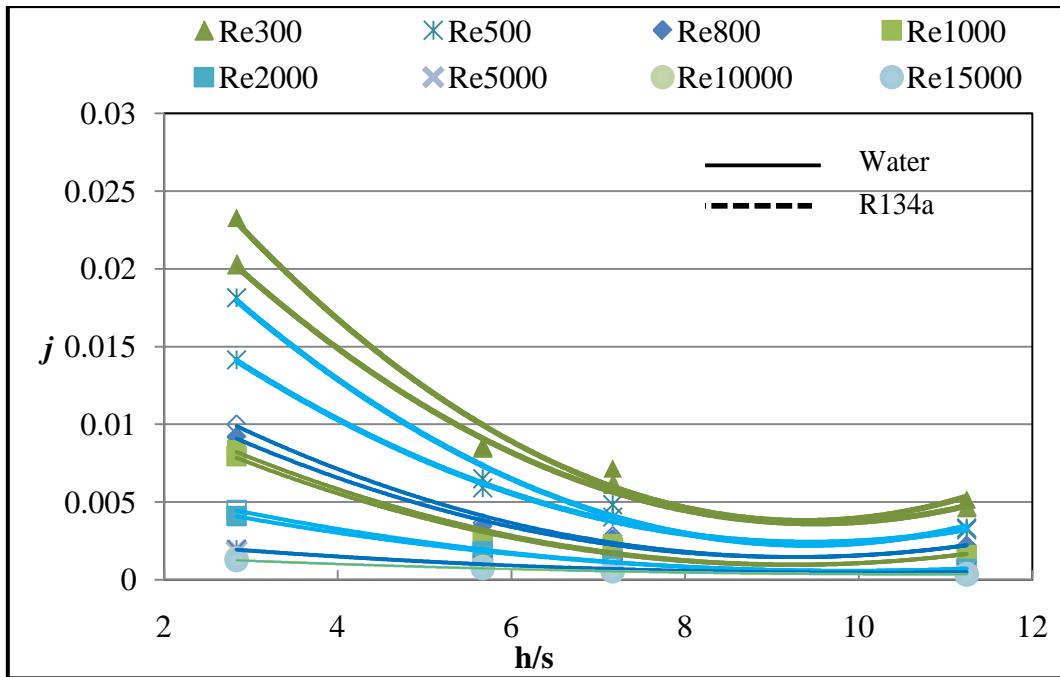
A total of 103 wavy surfaces are modelled and simulated in CFD to find out the j and f factors. Based on these results correlations have been developed between f , j , Re and geometrical fin parameters.

3.9.3 Effect of geometry parameters and Reynolds number

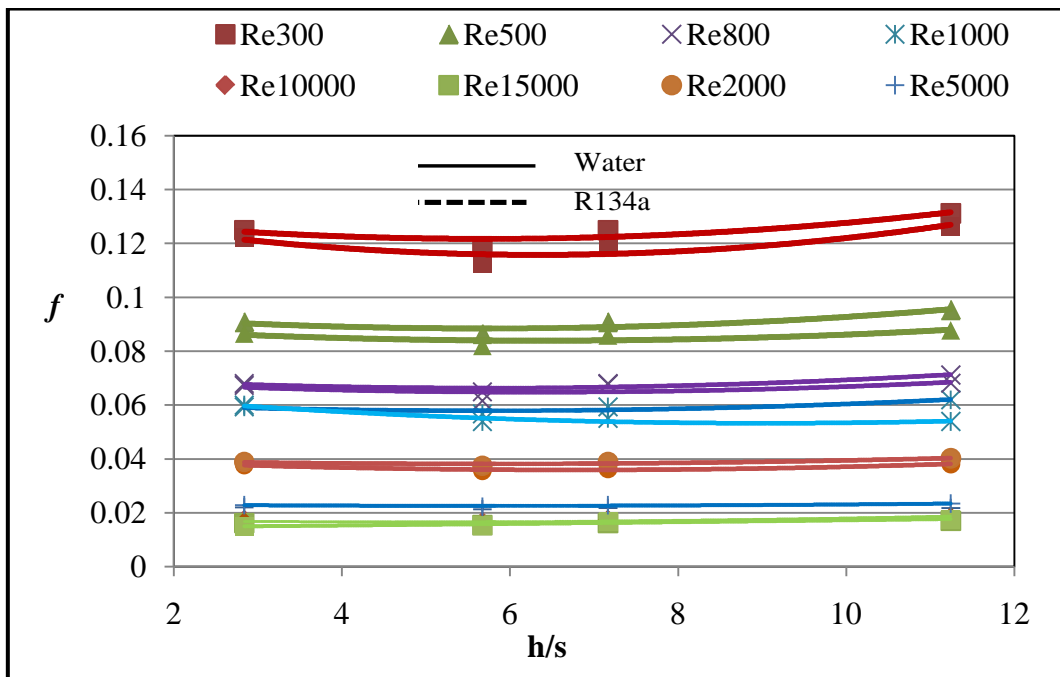
The effect of Reynolds number and variations of non-dimensional parameters on wavy fin surface performance are presented. Velocity, pressure and temperature fields' response to changes in Reynolds number and geometric parameters is clearly manifested. Fig 3.11-3.13 shows the role of geometric parameters h/s , a/s , λ/a vs ' j ' and parameters h/s , a/s , λ/a vs ' f ' for determining the heat transfer and flow friction performance. The individual effects due to variations in geometrical parameters are explained below.

3.9.3.1 Effect of h/s ratio on ' j ' and ' f '

The Colburn j factor and friction factor f are plotted against the fin height (h)-to-fin spacing (s) ratio (h/s) for varying Reynolds number in Fig. 3.11a & 3.11b for water and liquid refrigerant R134a. Both ' f ' and ' j ' decrease with increase in Re as expected. The effect of h/s is clearly discernable; the effect is same in both laminar and turbulent flows. For higher values of h/s , lower the j and f values and become constant or even tends increase for constant Re. Increase of h/s ratio narrow down the passage, causing increase of j and f values. It is observed more effective after h/s ratio of 5.67. Hence h/s ratio is called critical ratio where change in j and f values at constant Re is observed. There is no significant variation of ' f ' factor for both liquid water and liquid refrigerant R134a at constant Reynolds number. The difference is found to be less than 5% for both liquids. However the variation in ' j ' factor is found for water and liquid refrigerant R134a about 15%.



a) Effect of fin height/spacing on ' j '

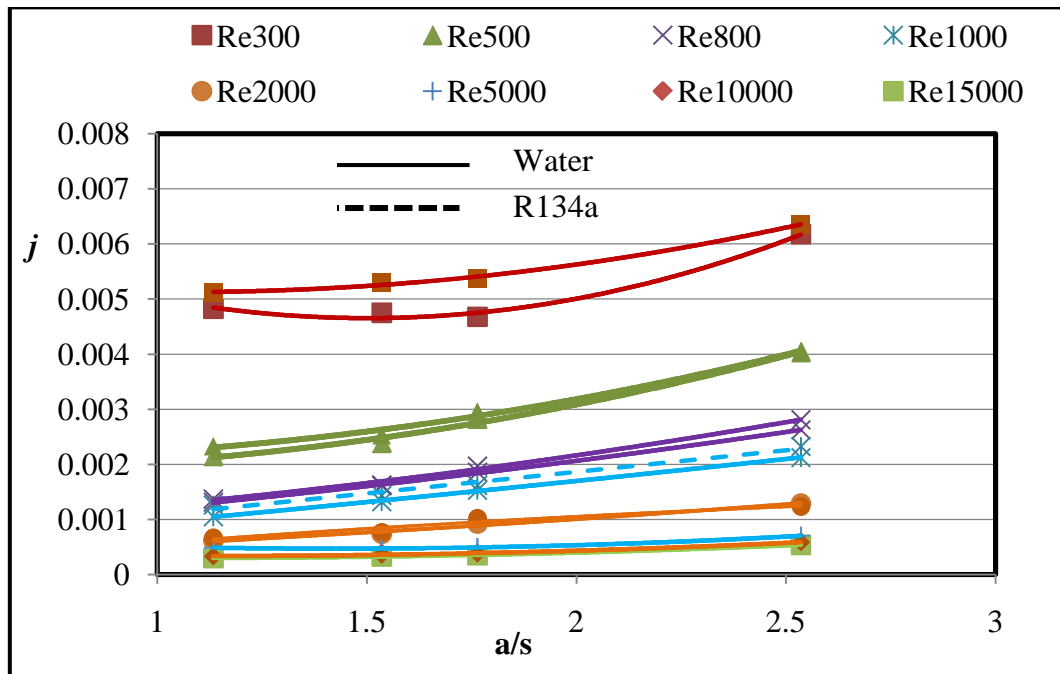


b) Effect of fin height/spacing on ' f '

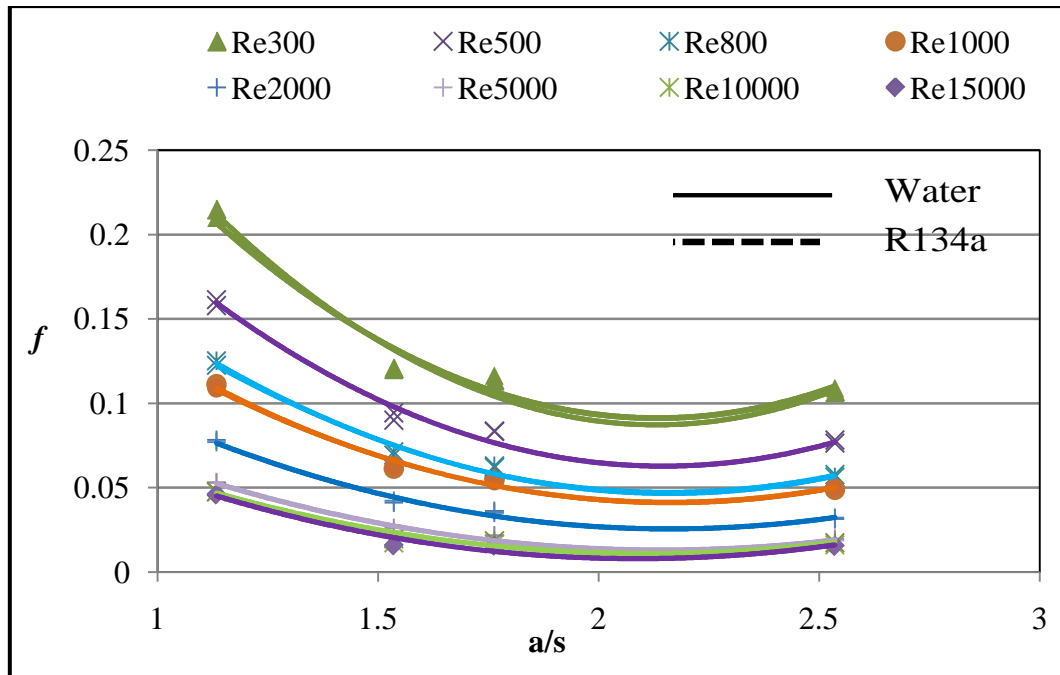
Fig. 3.11: Effect of h/s ratio on performance of wavy fin a) Colburn j factor b) Friction factor ' f '

3.9.3.2 Effect of a/s ratio on 'j' and 'f'

The Colburn j factor and friction factor f are plotted against the wave height (a)-to-fin spacing (s) ratio (a/s) for varying Reynolds number in Fig.3.12a & 3.12b. Both ' f ' and ' j ' decrease with increase in Re as expected. Friction factor f decreases with the increase of a/s up to 1.53 and become constant or tends increase for constant Re. Colburn j factor increases with the increase of a/s. Larger the wave height leads to recirculating flow in the wavy passages, which increases the heat transfer coefficient. Friction factor f decreases up to a/s=1.53 for constant Re and become almost constant or increase at higher Re beyond this ratio. This ratio is a critical ratio after which the slope has become constant for particular Re. This is because higher wave height introduces the form drag causing increase in friction factor. There is no significant variation of ' f ' factor for both liquid water and liquid refrigerant R134a at particular Reynolds number. The difference is found to be less than 5% for both liquids. However the variation in ' j ' factor is found about 15%.



a) Effect of fin wave height/spacing on 'j'

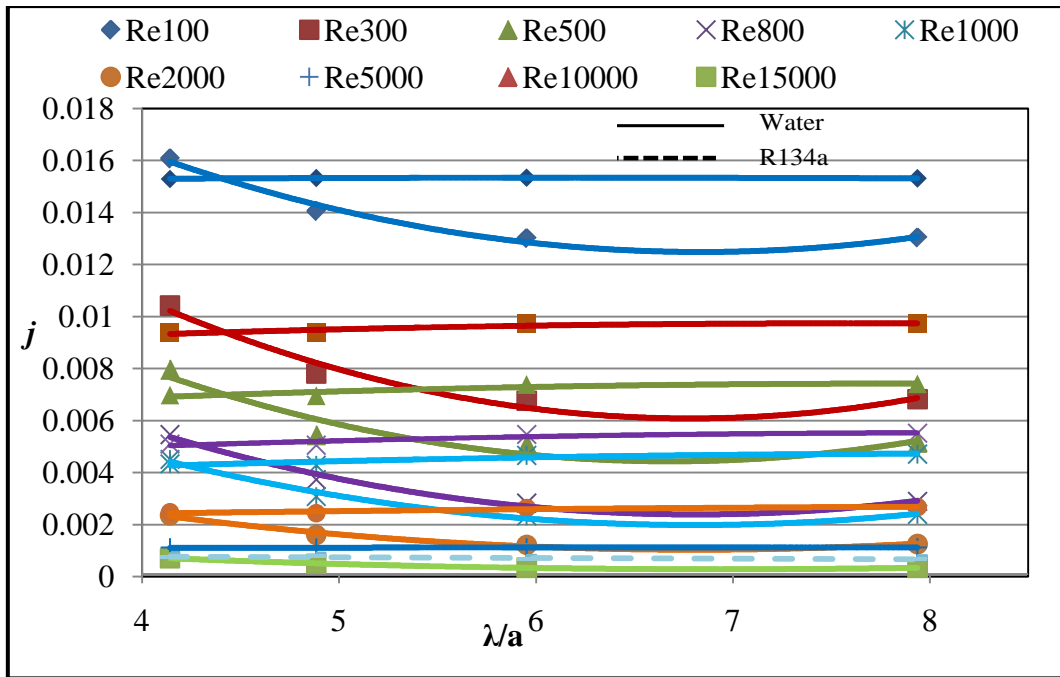


b) Effect of fin wave height/spacing on ' f '

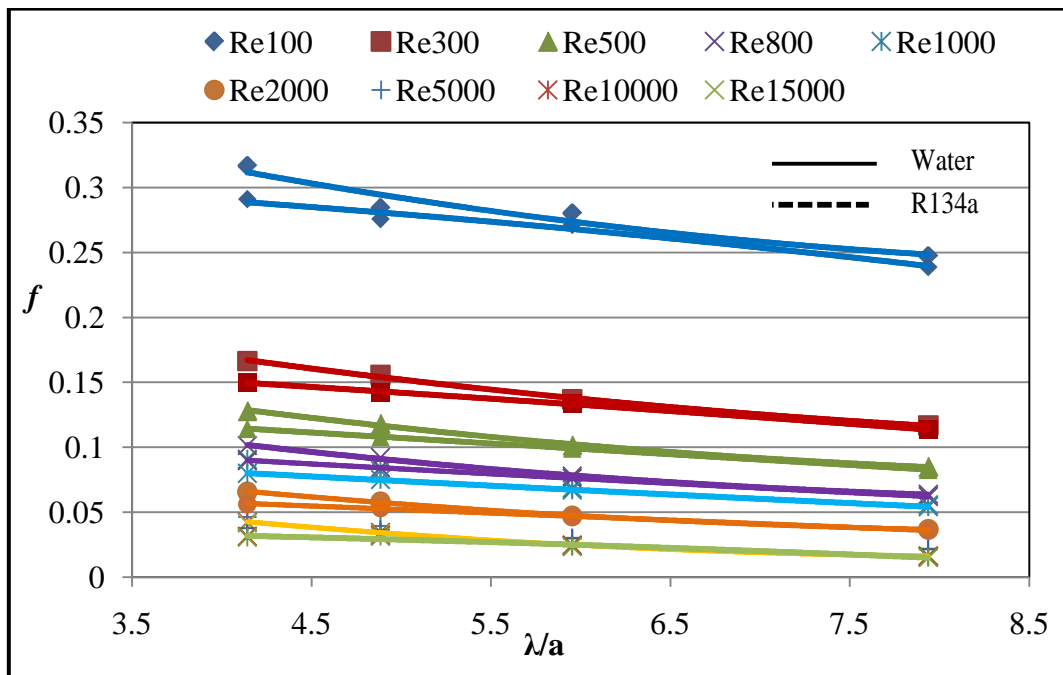
Fig. 3.12: Effect of a/s ratio on performance wavy fin a) Colburn j factor b) Friction factor ' f '

3.9.3.3 Effect of λ/a ratio on ' j ' and ' f '

The Colburn j factor and friction factor f are plotted against the wave length (λ) - to-wave height (a) ratio (λ/a) for varying Reynolds number in Fig 13a & 13b. Both ' f ' and ' j ' decrease with increase in Re as expected. Both Friction factor f and Colburn j factor decrease with the increase of λ/a for constant Re. Increase of λ/a with constant wave height means increase of wave length. As the wave length increases, the extent and strength of re-circulating flow diminishes. This affects both heat transfer coefficient and friction coefficient. There is no significant variation of ' f ' factor for both liquid water and liquid refrigerant R134a at particular Reynolds number. The difference is found to be less than 5% for both liquids. However the variation in ' j ' factor is found about 15%.



a) Effect of fin wave length/wave height on j'



b) Effect of fin wave length/wave height on f'

Fig. 3.13: Effect of λ/a ratio on performance wavy fin a) Colburn j factor b) Friction factor f'

3.9.4 Generation of flow friction and heat transfer correlations

An extensive numerical study was carried on the heat transfer and pressure drop phenomena with wavy fins. From the Fig 3.11 to 3.13 it can be observed significant non-linearity in ' f ' vs Re and ' j ' vs Re curves. The correlations are expressed for j and f in terms non-dimensional parameters. Two separate equations expressed at low and high Re regions. Using power law expressions Colburn factor j and friction factor ' f ' is determined since, variations in ' f ' and ' j ' with Re, h/s, a/s and λ/a follow constant slope log-linear lines in both laminar and fully turbulent flow regions.

The Colburn factor j and friction factor f are functionally related to Re, h/s, a/s and λ/a . It can be represented in general form as:

$$f \text{ or } j = C (Re)^{a_0} (\alpha)^{a_1} (\beta)^{a_2} (\gamma)^{a_3} \quad (3.23)$$

Where C, a0, a1, a2, a3 are constants depends on the type of fin surface and geometry. The ' j ' vs Re data for wavy fin surfaces show significant non linearity at Reynolds number range of $100 \leq Re \leq 15000$. Two separate equations have been proposed over low and high Re regions as below. Also the variation in ' j ' factor is found large for water and liquid refrigerant R134a. Hence, separate ' j ' correlations have proposed for water and liquid R134a. This is due to significant effect of Prandtl number on heat transfer coefficient.

$$j = 2.989Re^{-0.54241} \alpha^{-0.72276} \beta^{-0.83914} \gamma^{-0.7588} \text{ for } 100 \leq Re \leq 1000 \quad (3.24)$$

$$j = 3.245Re^{-0.66388} \alpha^{-0.53614} \beta^{-0.80626} \gamma^{-0.6346} \text{ for } 1000 \leq Re \leq 15000 \quad (3.25)$$

$$j = 1.154Re^{-0.65938} \alpha^{-0.96698} \beta^{0.176702} \gamma^{0.28878} \text{ for } 100 \leq Re \leq 1000 \quad (3.26)$$

$$j = 0.323Re^{-0.69341} \alpha^{-0.9602} \beta^{0.633246} \gamma^{0.889252} \text{ for } 1000 \leq Re \leq 15000 \quad (3.27)$$

Eqn. (3.24) and (3.25) predict the j factor for R134a and Eqn. (3.26) and (3.27) predicts for the water. The above correlations predict the 96 percent of the j data for the turbulent regions and 99 percent of j data for laminar regions.

Similarly the f vs Re data for wavy fin surfaces show significant non linearity at Reynolds number range of $100 \leq Re \leq 15000$. Two separate equations have been proposed for the low and high Re regions as below. The deviation between ' f ' data of water and liquid R134a is less than 5%. Hence, single correlations have proposed for

both fluids. Prandtl number was found to have little effect on the Fanning friction factor.

$$f = 18.607Re^{-0.59381} \alpha^{-0.088954} \beta^{-0.46976} \gamma^{-0.92621} \text{ for } 100 \leq Re \leq 1000 \quad (3.28)$$

$$f = 24.413Re^{-0.46532} \alpha^{-0.226497} \beta^{-0.94256} \gamma^{-1.70937} \text{ for } 1000 \leq Re \leq 15000 \quad (3.29)$$

The above correlations predict the 96 percent of the f data for the turbulent regions and 99 percent of f data for laminar regions.

3.9.5 Determination of indices

Table 3.2a and 3.2b represents the indices C , a_0 , a_1 , a_2 and a_3 of equations (3.28) and (3.29) for fanning friction factor f and equations (3.24-3.25) and (3.26-3.27) for Colburn factor j by multiple regression method of wavy fin surfaces numerical data of Table 1 of APPENDIX-I.

Table 3.2a: Wavy fin coefficients or indices for R134a

Coefficient	f		j	
	≤ 1000	> 1000	≤ 1000	> 1000
C	18.607	24.413	2.989	3.245
a0	-0.59381	-0.46532	-0.54241	-0.66388
a1	-0.088954	-0.22649	-0.72276	-0.53614
a2	-0.46976	-0.94256	-0.83914	-0.80626
a3	-0.92621	-1.70907	-0.7588	-0.6346
	RMS=0.99		RMS=0.96	

Table 3.2b: Wavy fin coefficients or indices for water

Coefficient	f		j	
	≤ 1000	> 1000	≤ 1000	> 1000
C	18.607	24.413	1.154	0.323
a0	-0.59381	-0.46532	-0.65938	-0.69341
a1	-0.088954	-0.22649	-0.96698	-0.9602
a2	-0.46976	-0.94256	0.176702	0.63324
a3	-0.92621	-1.70907	0.28878	0.8892
	RMS=0.99		RMS=0.96	

3.10 HEAT TRANSFER AND FRICTIONAL ANALYSIS OF OFFSET STRIP FIN SURFACE

CFD analysis was carried out on offset strip fin surface using liquid R134a and generalized correlations were developed in terms Colburn j and f factor. The effect fin geometry and Reynolds number on j and f was investigated.

3.10.1 Numerical model

The numerical model shown in the Fig. 3.14 of the offset strip fin is defined by the following parameters.

- fin thickness (t),
- fin height (h),
- lance length (l), and
- fin spacing (s).

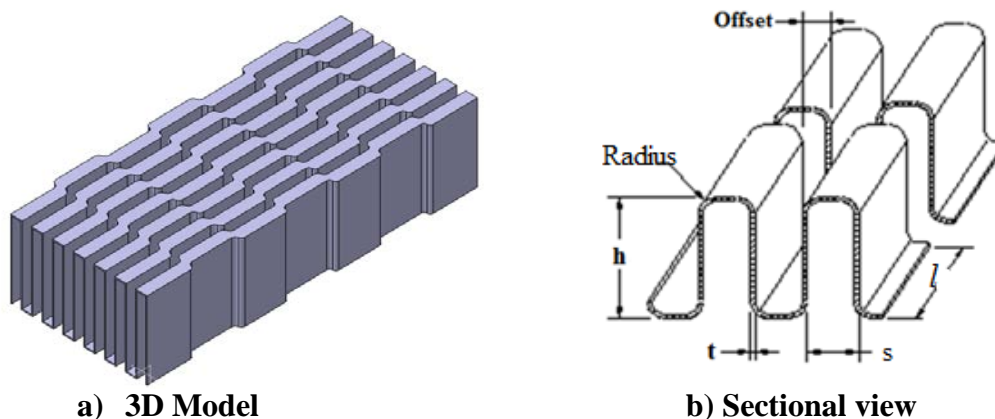


Fig. 3.14: Numerical model for offset strip fin

Offset strip fin was modelled using CATIA software. The offset strip fin geometry considered for the analysis is

$$h = 5 \text{ mm}, l = 3.525 \text{ mm}, s = 1.414 \text{ mm}, t = 0.254 \text{ mm}, D_h = 1.86 \text{ mm}$$

Grid is generated using Hyper Mesh software. Initially 2D elements generated using quad elements. Hexa elements used for 3D domain for computation. The quality of the grid used in the computations directly influences the solution obtained. Lot of care has been taken in choosing the desirable features in the grid like orthogonality, control of spacing and skewness. Apart from these, very low aspect ratios of grid cells and highly stretched grids have been avoided to get better results.

3.10.2 CFD analysis

3.10.2.1 Computational domain

Fig. 3.15 shows the computational domain taken for modelling heat transfer and fluid flow for an offset strip fin surface. Fin spacing 's' in the x-direction, lance length 'l' in they-direction and fin height 'h' in the z-direction constitutes the computational domain.

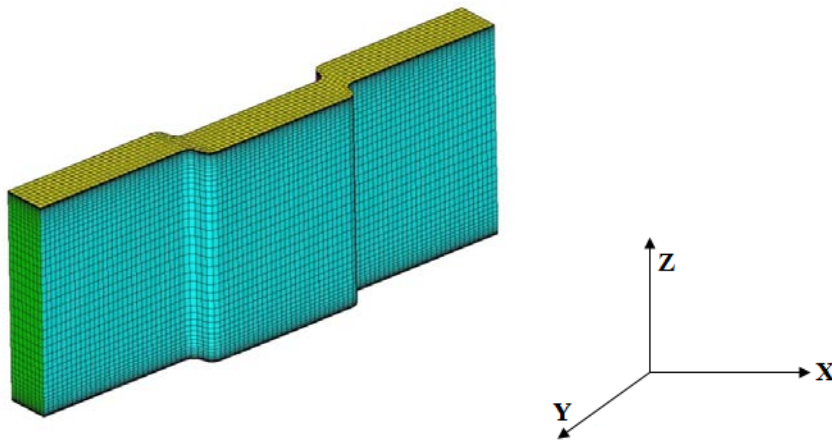


Fig. 3.15: The computational fluid domain for the offset strip fin surface

3.10.2.2 Dimensionless parameters

The offset strip fin geometry parameters are expressed in terms non-dimensional parameters α , δ and ϵ . The effect of fin thickness is considered for the analysis. Colburn j and f correlations are expressed in terms of these non-dimensional parameters.

$$\alpha = \frac{h}{s} \quad (3.30)$$

$$\delta = \frac{t}{s} \quad (3.31)$$

$$\epsilon = \frac{t}{l} \quad (3.32)$$

Hydraulic diameter D_h is used as the characteristic dimension in expressing the heat transfer and flow friction data.

A total of 133 sets of offset strip fin surfaces are considered and modelled for CFD analysis for developing the correlations. Refrigerant R 134a (liquid phase) is

used as working medium for the analysis. The following ranges of fin geometries and Reynolds numbers are taken for analysis.

$$1.74 \leq \frac{h}{s} \leq 6.476 \quad (3.33)$$

$$0.076 \leq \frac{t}{s} \leq 0.22 \quad (3.34)$$

$$0.0274 \leq \frac{t}{l} \leq 0.1 \text{ and} \quad (3.35)$$

$$100 \leq Re \leq 1000 \text{ for laminar region} \quad (3.36)$$

$$1000 \leq Re \leq 15000 \text{ for turbulent region} \quad (3.37)$$

3.10.2.3 Grid independency

Grid independency check was carried as per para 3.9.2.3 for offset strip fin. Plot between number of elements and the pressure drop is drawn in Fig. 3.16.

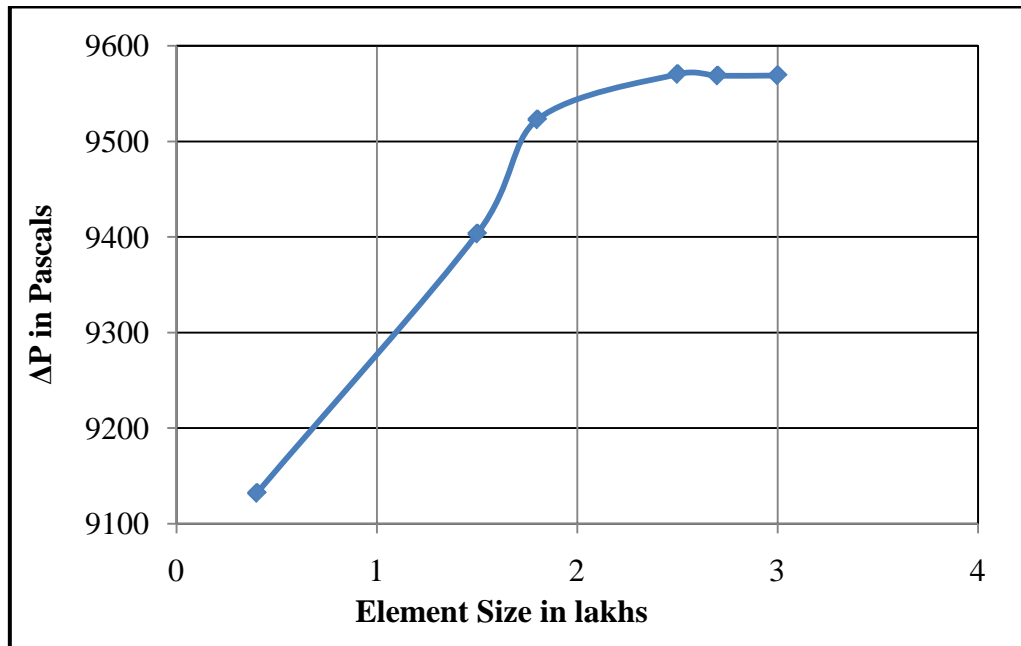


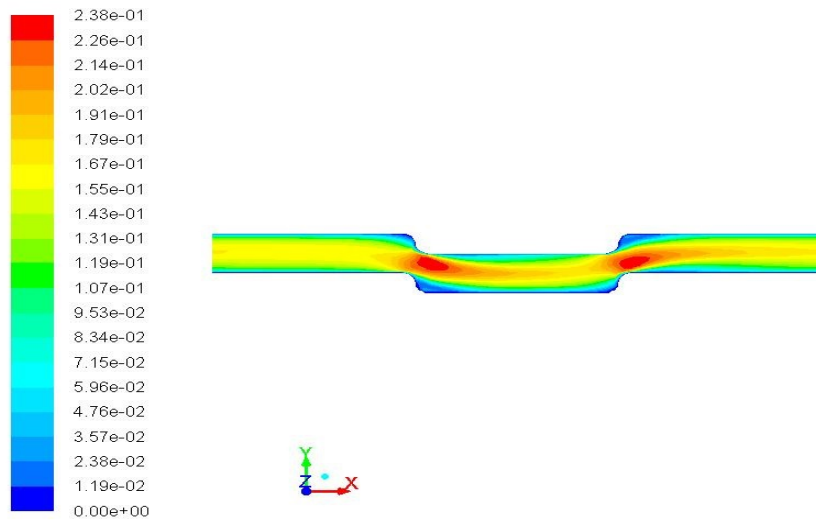
Fig. 3.16: Grid independency graph for offset strip fin

3.10.2.4 CFD Simulation studies

The CFD studies were carried out on the offset strip fin at different Reynolds number ranging from 100 to 15000 by applying the boundary conditions. The analysis was carried out in two-phases. In first phase the fin characterized for friction factor ' f ' over above range of Reynolds number. In second phase the Colburn ' j ' factor is estimated for the same range of Reynolds number using energy equation

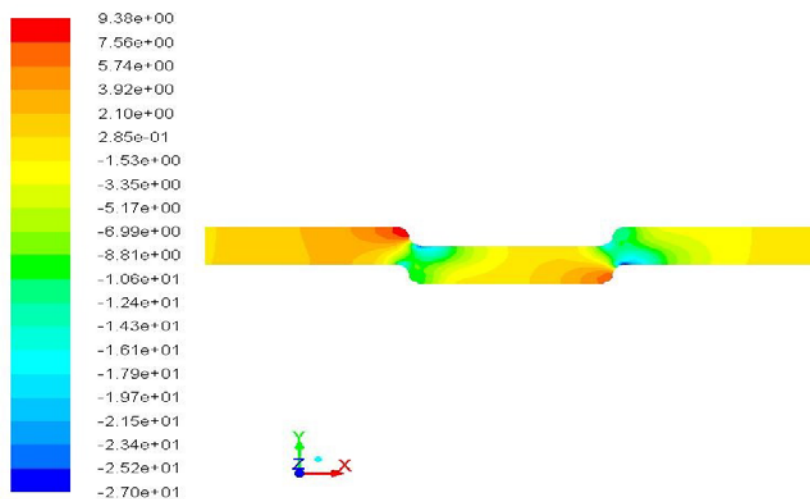
3.10.2.5 Velocity and Temperature fields

Fig. 3.17-3.19 shows the velocity, pressure and temperature fields for flow over the surface at Reynolds number 1000 based on the ANSYS CFD output data.



Contours of Velocity Magnitude (m/s)

Fig. 3.17: Velocity profiles of offset strip fin at $h/2$ liquid refrigerant R134a



Contours of Static Pressure (pascal)

Fig. 3.18: Static pressure profiles of offset strip fin at $h/2$ liquid refrigerant R134a

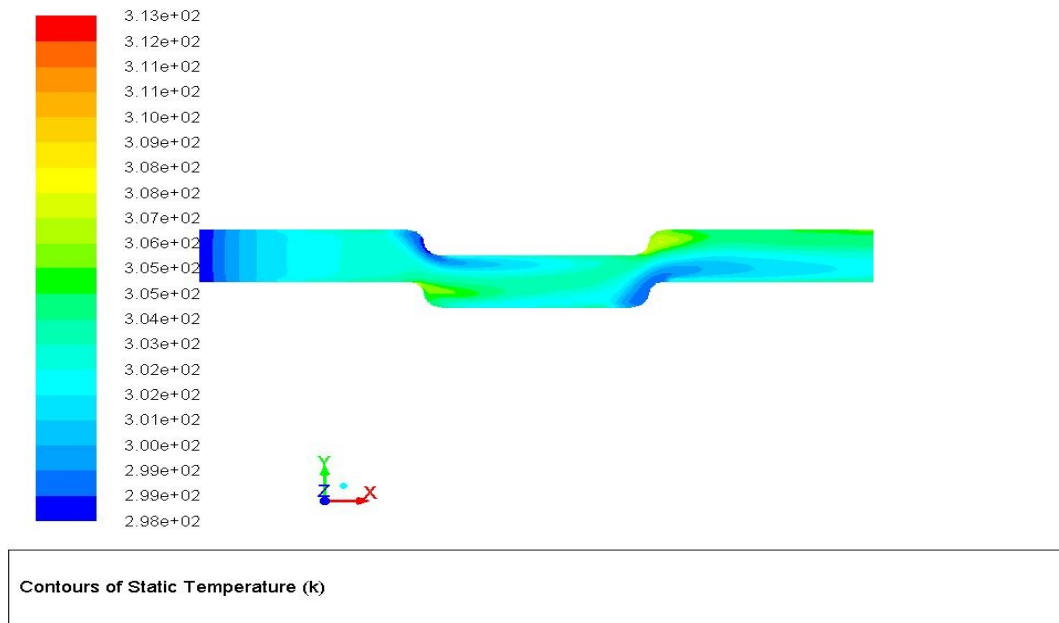


Fig. 3.19: Static temperature profiles of offset strip fin at h/2 liquid refrigerant R134a

3.10.3 Generation of f and j data

Total 133 sets offset strip fin surfaces are modelled and simulated in CFD to find out the j and f factors. Based on these results correlations have been developed between f , j , Re and geometrical fin parameters.

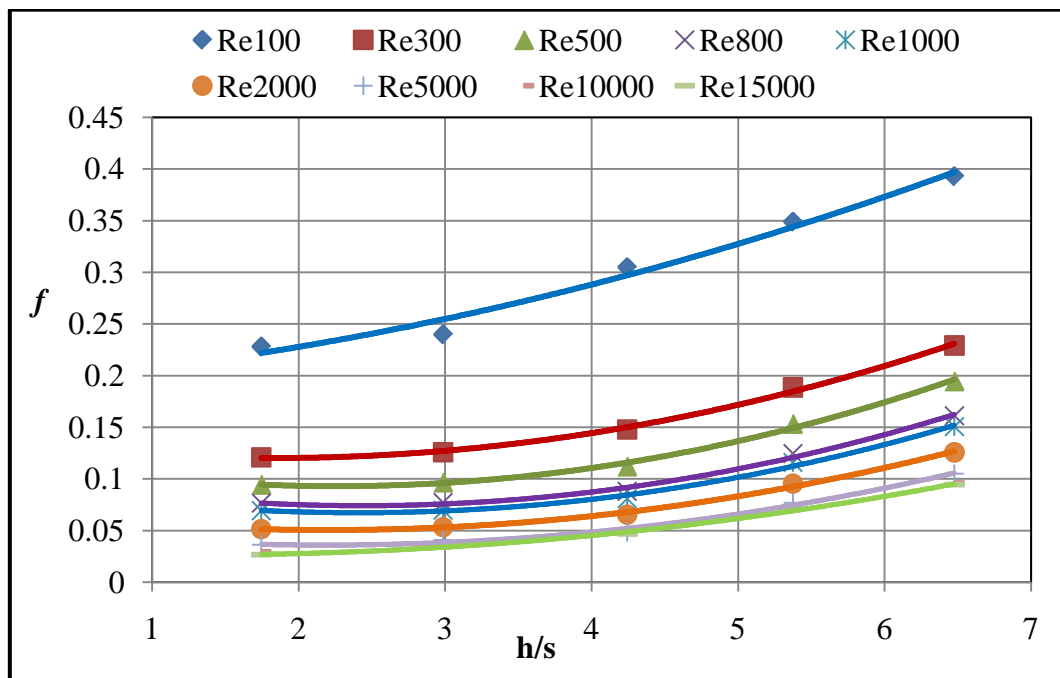
3.10.4 Effect of geometry parameters and Reynolds number

The effect of Reynolds number and variations of non-dimensional parameters on offset strip fin surface performance are presented. Velocity, pressure and temperature fields' response to changes in Reynolds number and geometric parameters is clearly manifested. Fig 3.20-3.22 shows the role of geometric parameters h/s , t/s , t/l vs ' j ' and parameters h/s , t/s , t/l vs ' f ' for determining the heat transfer and flow friction performance. The individual effects due to variations in geometrical parameters are explained below

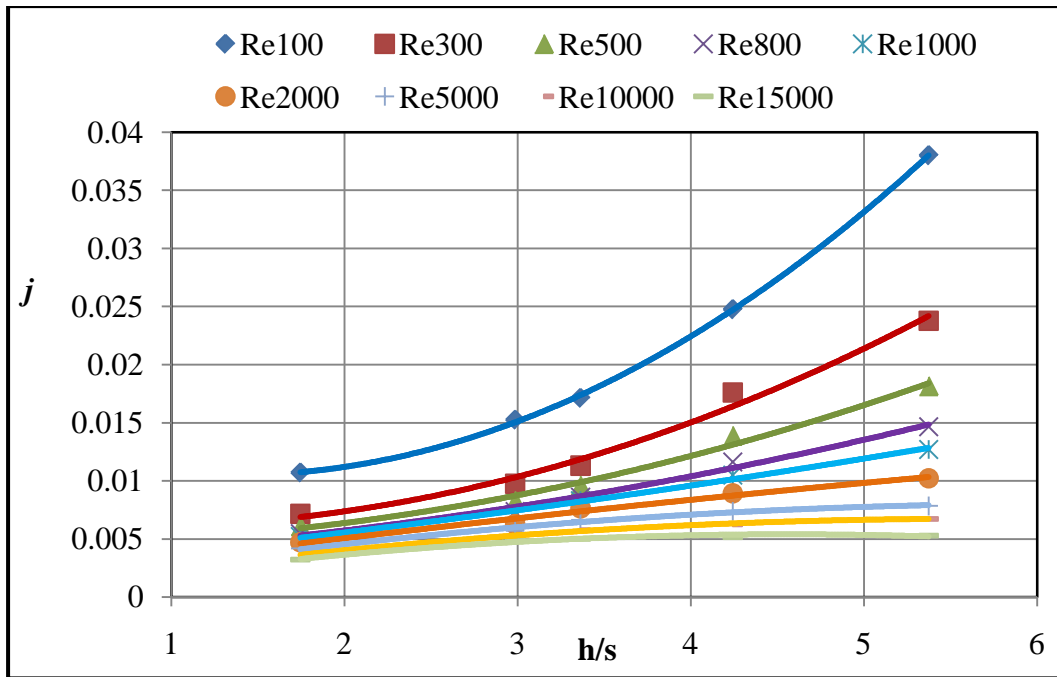
3.10.4.1 Effect of h/s ratio on ' j ' and ' f '

The friction factor f and Colburn j factors are plotted against the fin height (h)-to-fin spacing (s) ratio (h/s) for varying Reynolds number in Fig 3.20a & 3.20b for liquid refrigerant R134a. Both ' f ' and ' j ' decrease with increase in Re as expected. Friction

factor ' f ' and Colburn ' j ' factor increase with the increase of h/s for constant Re . The effect of h/s is clearly discernable; the effect is same in both laminar and turbulent flows, for higher values of h/s higher the j and f values. The rate of increase of j and f is low or even constant at high Re up to h/s ratio of 3 and rate of increase of heat transfer is high at h/s ratio of 3 and above. Hence h/s ratio is called critical ratio where change in j and f values at constant Re is observed. It is because the passages become narrower with increase of h/s , causing increase of j and f values.



a) Effect of fin height/spacing on ' f '



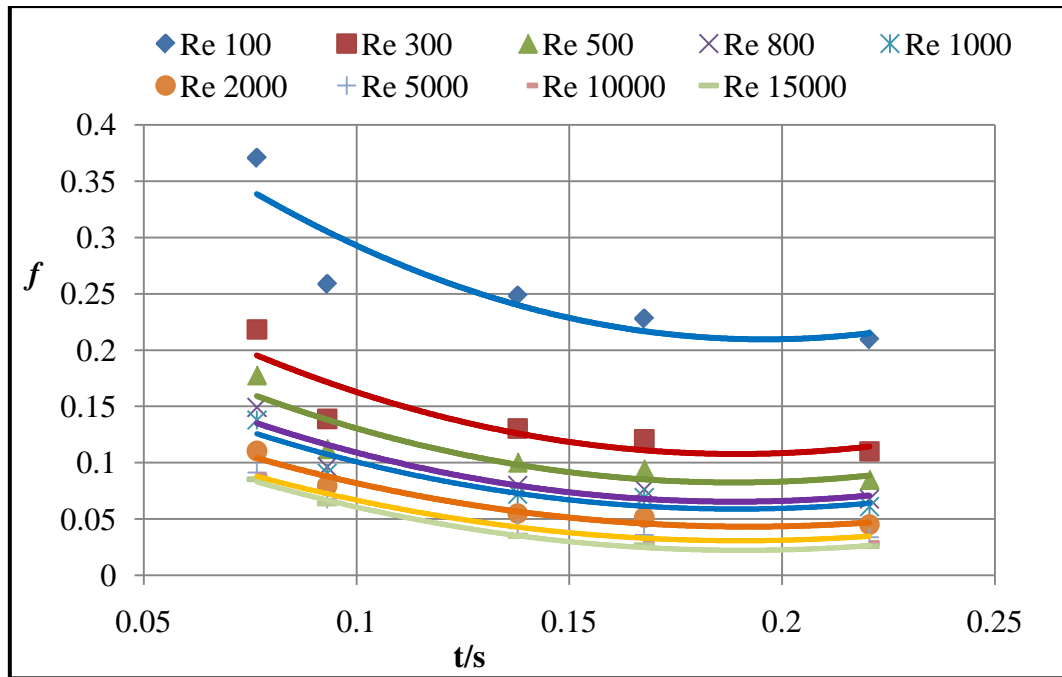
b) Effect of fin height/spacing on 'j'

Fig. 3.20: Effect of h/s ratio on performance offset strip fin

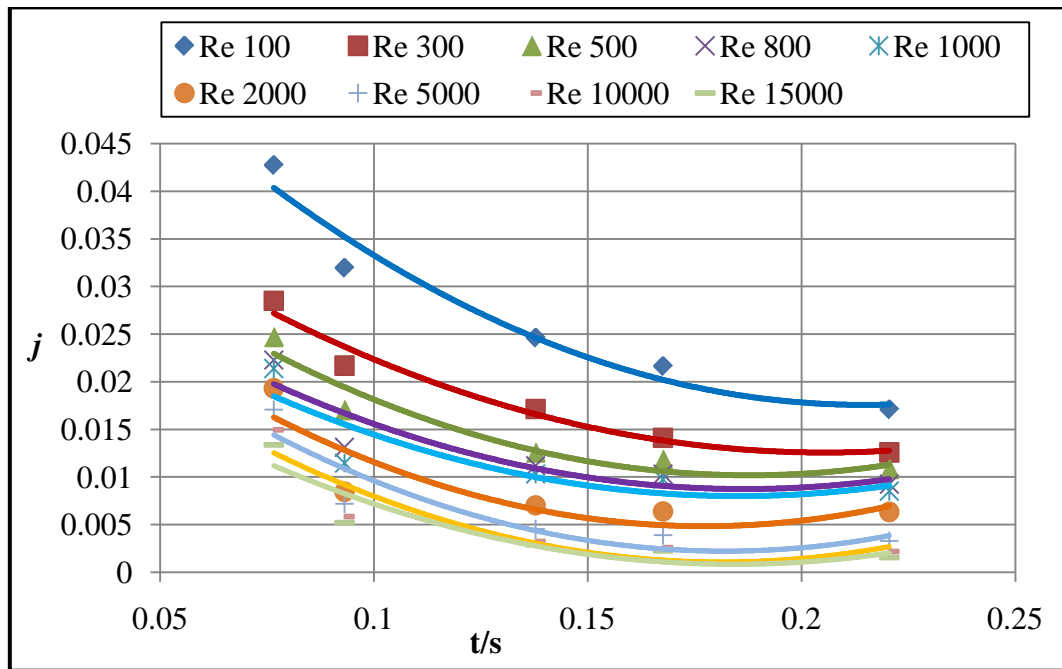
a) Friction factor 'f' b) Colburn j factor

3.10.4.2 Effect of t/s ratio on 'j' and 'f'

The friction factor f and Colburn j factors are plotted against the fin thickness (t)-to-fin spacing (s) ratio (t/s) for varying Reynolds number in Fig. 3.21a & 3.21b for liquid refrigerant R134a. Both ' f ' and ' j ' decrease with increase in Re as expected. Friction factor ' f ' and Colburn ' j ' factor decreases with the increase of t/s for constant Re. The fin thickness introduces the form drag and effects the heat transfer. Furthermore a thicker fin leads to smaller passages and smaller fin density. There is consequent reduction in free flow area. At low Re the curves have downward trends, while at high Re, the opposite is true. Because Re is determined largely by s, increase of t/s means primarily increase of fin thickness t. The total surface area includes the cross section of the fins on the leading and trailing edges. But this surface is not as effective for heat transfer as the lateral surface, particularly at low Re where the streamlines bend smoothly around the front surface of the fins. But at high Re, wider fins cause greater recirculation of flow near the leading edge and vortices near the trailing edge. This leads to significant increase of friction factor and heat transfer coefficient.



a) Effect of fin thickness/spacing on ' f '

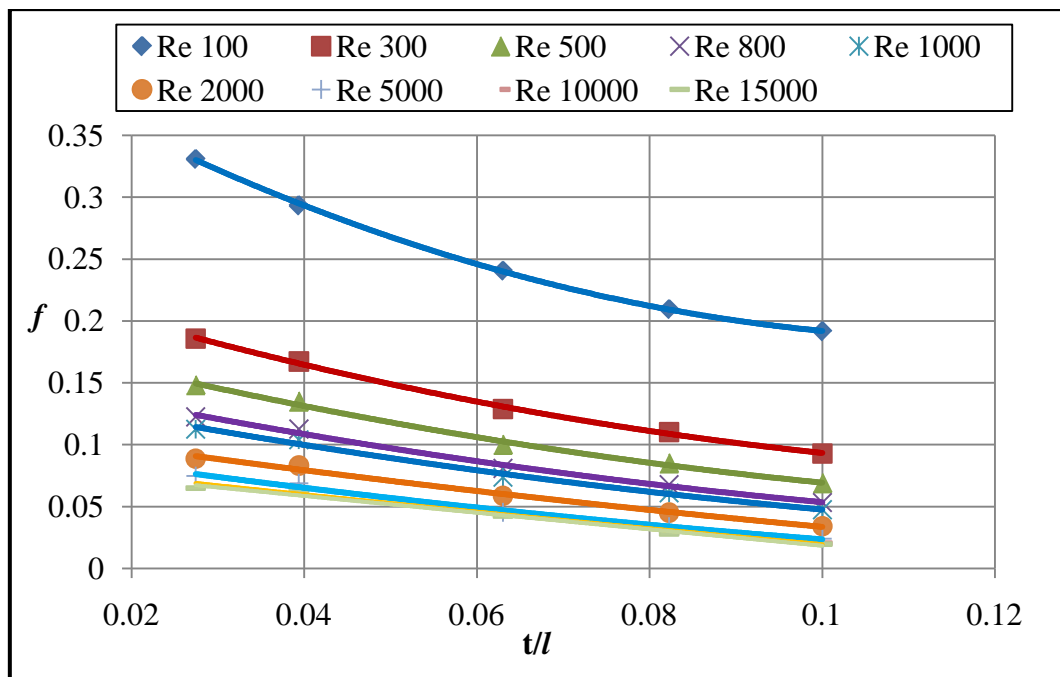


b) Effect of fin thickness/spacing on ' j '

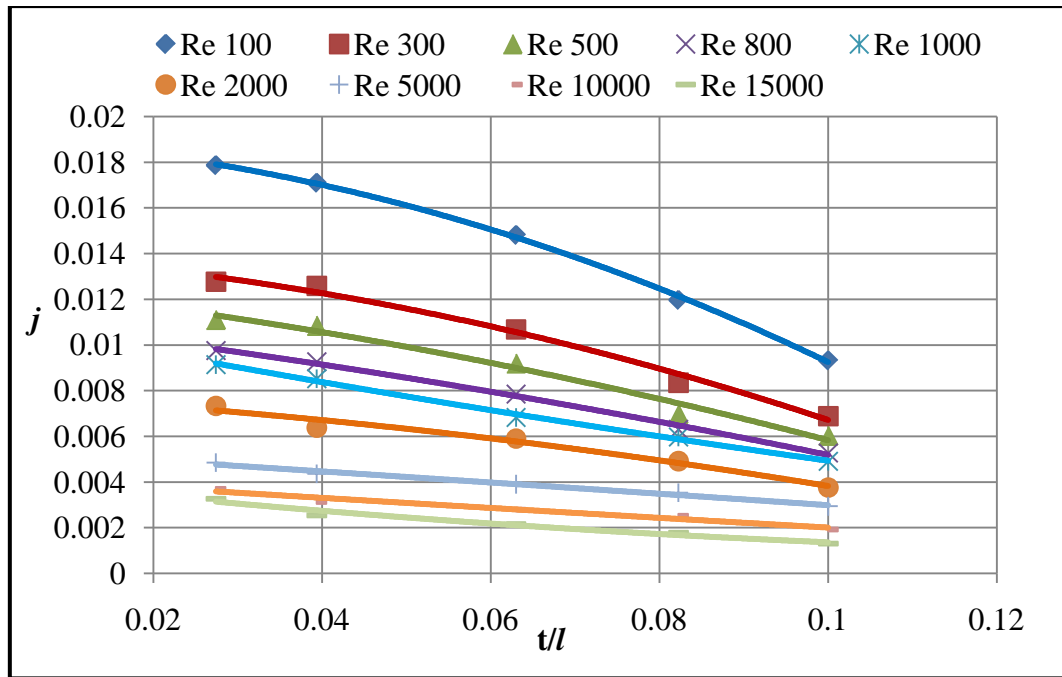
Fig. 3.21: Effect of t/s ratio on performance of offset strip fin a) Friction factor ' f ' b) Colburn j factor

3.10.4.3 Effect of t/l ratio on ' j ' and ' f '

The friction factor f and Colburn j factors are plotted against the fin thickness (t)-to-fin length (l) ratio (t/l) for varying Reynolds number in Fig 3.22a & 3.22b for liquid refrigerant R134a. Both ' f ' and ' j ' decrease with increase in Re as expected. Friction factor ' f ' and Colburn ' j ' factor decreases with the increase of t/l for constant Re. The fin thickness introduces the form drag and effects the heat transfer. Also, as the boundary layer grows over the fin surface. It is abruptly disrupted at the end of the fin offset length l . Essentially for flow over shorter lengths of fins of finite thickness, there is an outward displacement over the leading edge followed by local acceleration near the trailing edge and the eventual dissipation of boundary layer in the fin wakes. The fin thickness and offset fin length to have competing influence on the flow field. Moreover, thicker fins have larger form drag and heat transfer contributions from blunt fin edges, where with slender and longer fins, f and j are influenced only by the momentum and energy transfer from the fin sides.



a) Effect of fin thickness/fin length on ' f '



b) Effect of fin thickness/fin length on 'j'

Fig. 3.22: Effect of t/l ratio on performance of offset strip fin a) Friction factor 'f'
b) Colburn j factor

3.10.5 Generation of flow friction and heat transfer correlations

An extensive numerical study was carried on the heat transfer and pressure drop phenomena with offset strip fins. From the Fig 3.20 to 3.22 it can be observed significant non-linearity in 'f' vs Re and 'j' vs Re curves. The correlations are expressed for j and f in terms non-dimensional parameters. Two separate equations expressed at low and high Re regions. Using power law expressions Colburn factor j and friction factor 'f' is determined since, variations in 'f' and 'j' with Re, h/s, t/s and t/l follow constant slope log-linear lines in both laminar and fully turbulent flow regions.

The Colburn factor j and friction factor f are functionally related to Re, h/s, t/s, t/l. It can be represented in general form as:

$$f \text{ or } j = C (Re)^{a0} (\alpha)^{a1} (\delta)^{a2} (\epsilon)^{a3} \quad (3.38)$$

Where C, a0, a1, a2, a3 are constants depends on the type of fin surface and geometry.

The 'j' vs Re data for offset strip fin surfaces show significant non linearity at Reynolds number range of $100 \leq Re \leq 15000$. Two separate equations have been proposed for the low and high Re regions as below.

$$j = 0.01197 \times R_e^{-0.5375} \times \alpha^{0.1212} \times \delta^{-0.1906} \times \epsilon^{-0.8473} \text{ for } 100 \leq \text{Re} \leq 1000 \quad (3.39)$$

$$j = 0.0099 \times R_e^{-0.3744} \times \alpha^{-0.4331} \times \delta^{-0.5475} \times \epsilon^{-0.6931} \text{ for } 1000 \leq \text{Re} \leq 15000 \quad (3.40)$$

Eqn. (3.39) and (3.40) predict the j factor for R134a. The above correlations predict the 96 percent of the j data for the turbulent regions and 99 percent of j data for laminar regions.

Similarly the f vs Re data show significant non-linearity at Reynolds number range of $100 \leq \text{Re} \leq 15000$. Two separate equations have been proposed for the low and high Re regions as below.

$$f = 0.33648 \times R_e^{-0.5909} \times \alpha^{-0.1275} \times \delta^{-0.2356} \times \epsilon^{-0.6108} \text{ for } 100 \leq \text{Re} \leq 1000 \quad (3.41)$$

$$f = 0.00632 \times R_e^{-0.2163} \times \alpha^{0.2253} \times \delta^{-0.3799} \times \epsilon^{-0.9331} \text{ for } 1000 \leq \text{Re} \leq 15000 \quad (3.42)$$

The above correlations predict the 96 percent of the f data for the turbulent regions and 99 percent of f data for laminar regions.

3.10.6 Determination of indices

Table 3.3 represents the indices C, a0, a1, a2 and a3 of equations (3.41) and (3.42) for fanning friction factor f and equations (3.39) and (3.40) for Colburn factor j by multiple regression method of offset strip fin surfaces numerical data of Table 2 of APPENDIX-I

Table 3.3: Offset strip fin coefficients or indices for R134a

Coefficient	f		J	
	≤ 1000	> 1000	≤ 1000	> 1000
C	0.53648	0.00632	0.01697	0.0099
a0	-0.5909	-0.2163	-0.5375	-0.3744
a1	-0.1275	0.2253	0.1212	-0.4331
a2	-0.2356	-0.3799	-0.1906	-0.5475
a3	-0.6108	-0.9331	-0.8473	-0.6931
	RMS=0.99		RMS=0.96	

3.11 SUMMARY

Single phase heat transfer analysis and pressure drop was carried out using CFD on offset strip and wavy fin surfaces with varying fin geometry for R134a liquid phase and also using water in wavy fin surfaces. j and f factor are predicted for both the fins. Generalized correlations have been developed for these fin surfaces. The correlations are developed at Reynolds number range of 100-15000. The effect of fin geometry on the enhanced heat transfer and pressure drops are investigated in this chapter.

CHAPTER 4

DEVELOPMENT OF EXPERIMENTAL SET UP FOR INVESTIGATION OF TWO-PHASE HEAT TRANSFER AND PRESSURE DROP ON FIN SURFACES

Unconfined flow boiling and channel experiments will be required to explain the phenomenological aspects of channel boiling and provide heat transfer data and correlations with, which one can design and predict the performance of boiling structures in confined geometries. As the parametric domain of interest is focused on applications of evaporator design, an experimental system was constructed to facilitate the investigation of flow boiling heat transfer in compact plate fin surfaces of typical dimensions. The basic foundation of the various experiments is the same, and the following conditions should be assumed except where otherwise noted. Tests were conducted at atmospheric conditions outside. Experiments were performed with R134a as a working medium with particular attention paid to saturated conditions at the inlet of the test section.

This chapter begins with a description of the design and development of test rig in which the experiments were conducted. The construction and function of the test facility is discussed next, followed by an overview of the entire experimental system. This chapter ends with a description of the experimental measurements and data acquisition system.

4.1 DETAILED SPECIFICATION OF THE TEST RIG

The specification detail of each circuit is given below. Also, the instrumentation and safety protection requirements of each circuit mentioned.

4.1.1 Refrigerant circuit:

- Flow rate : 0.01 to 0.08 kg/sec (In steps of 0.005kg/s)
- Pressure range : 0-10 bar 'g'
- Working media : R134a
- Operating Temperature range: -10 °C to 100°C

- Capacity : 20 kW
- Power supply : 440 V, 3Phase, 50 Hz
- This circuit can be used to test experimental compact heat exchanger as an evaporator.
- This circuit is fully instrumented to read pressure, flow and temperature etc. All the indicators are digital type and are connected to data acquisition system to log the data.
- Safety measures for the protection of the test rig included to cut off if the set pressure is exceeded and provision to detect the refrigerant leakage.

4.1.2 Condensation / Evaporation secondary circuit:

- Flow rate : 1 to 60 LPM
- Pressure range : 0-2 bar 'g'
- Working media : DM Water
- Operating Temperature range
 Condensation Loop : 10°C to 40°C
 Evaporation Loop : 10°C to 40°C
- Power supply : 440 V, 3P, 50 Hz
- This circuit is fully instrumented to read pressure, flow and temperature etc. All the indicators are digital type and are connected to data acquisition system to log the data.
- Safety Measures for the protection of the test rig included to cut off if the set pressure is exceeded and Provision to detect the refrigerant leakage.

4.2 STANDARDS

The following are the applicable standards:

1. Thermodynamic property table for saturated R-134a (Temperature table), SI units ASHRAE Transaction 94, pp. 2095-2118
2. Thermodynamic property table for water (R718)
3. Compressor design as per Sea-Bird Refrigeration Pvt.Ltd.
4. Evaporator design as per PHE B3-030, Technical brochure from Danfoss Industries Pvt.Ltd.

5. Condenser design as per PHE B3-030, Technical brochure from Danfoss Industries Pvt.Ltd.
6. Chiller unit design as per Werner Finley Pvt.Ltd.
7. Pipe lines design as per ASME B-88, ASHRAE Guide and Data Book,
8. ASHRAE Handbook of Refrigeration.

4.3 DESIGN AND DEVELOPMENT OF TEST RIG

Experimental test facility shown in Fig. 4.1 has been designed and developed to carry out the experimental tests on the test section/test evaporator. Vapour Compression Refrigeration System test facility mainly consists of six interconnected loops. That is

1. Refrigerant Loop
2. Evaporator Loop
3. Condenser Loop
4. Super heater loop
5. De-Super heater loop
6. Single phase flow and heat transfer loop

Super heater loop is introduced to ensure dry compression at the compressor inlet. De-super heater loop (cooling loop / Heating) is provided to before condenser to maintain the saturated conditions.

The components and sub systems of the test facility are mounted on moveable platform and lifting screw jack assembly. The major components and sub systems of the test facility are variable speed reciprocating compressor, condenser, evaporator, cooling system, heating system, data acquisition and control system with instrumentation and digital display. Refrigerant R134a was used as refrigerant in this test facility. Refrigerant R134a was circulated in one side of the test section. Water was used to heat liquid refrigerant in evaporator as well as to cool the refrigerant gas in the condenser. Water is circulated in the test section from the chiller units. Chillers supply the water between 10 to 40°C temperatures. Test facility consists of two separate chiller units for evaporator and condenser. Sampling ports are provided for easy charge/discharging of the refrigerant. Suitable evacuation and charging system is provided to charge and discharge the refrigerant. Seamless copper tubes used as piping system in the test facility. The test facility is fully insulated to avoid heat loss

to the environment. Leak detection sensor is installed in the test facility, which gives an alarm whenever there is a refrigerant leak noticed in the test facility. Fig. 4.2a, 4.2b and Fig. 4.3 shows photograph of the actual test facility designed and developed where as Fig. 4.4 shows the data acquisition system of the test facility.

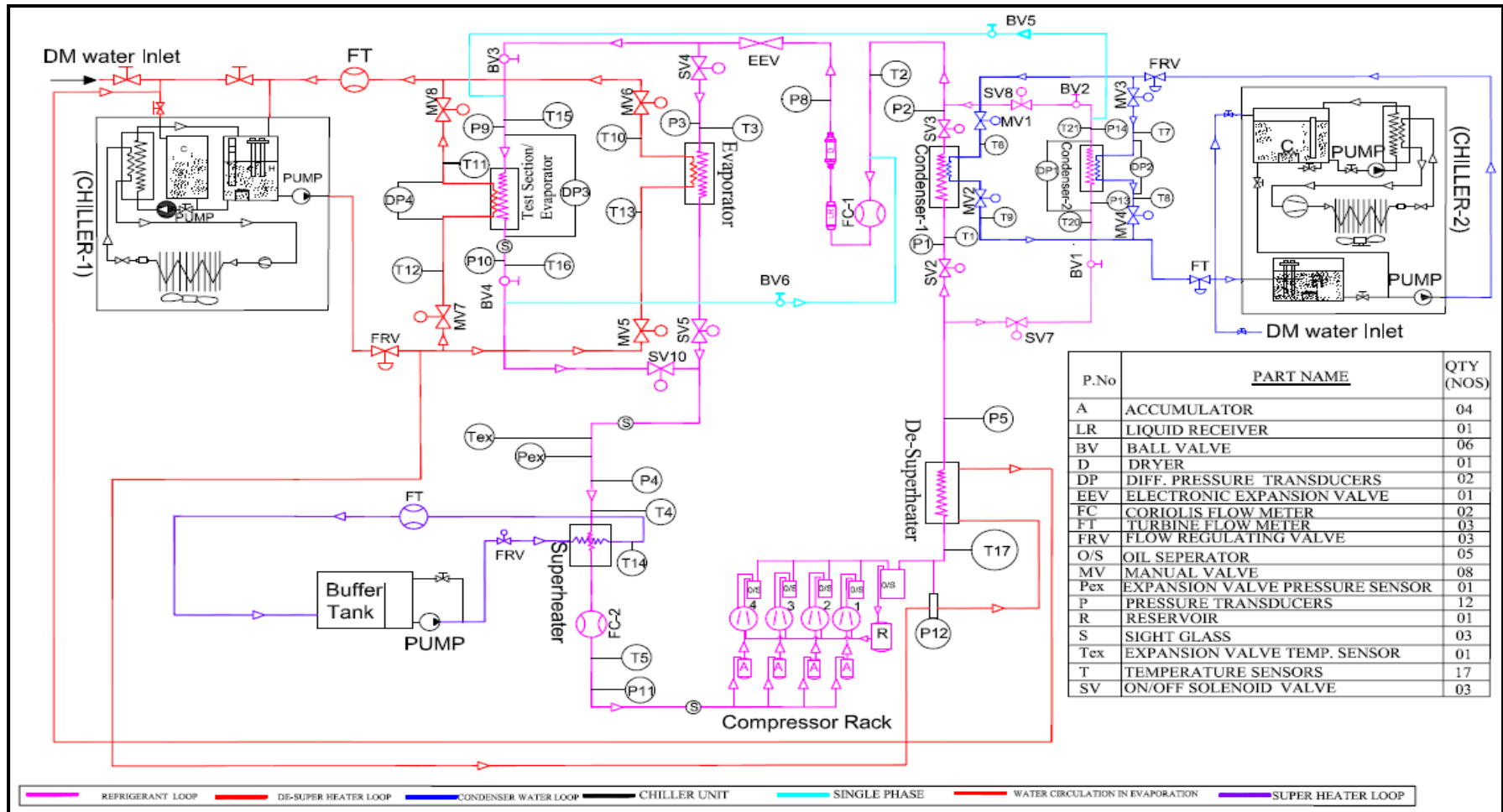


Fig.4.1: Schematic of the experimental rig for measurement of two-phase heat transfer and frictional characteristics of compact plate fin surfaces.

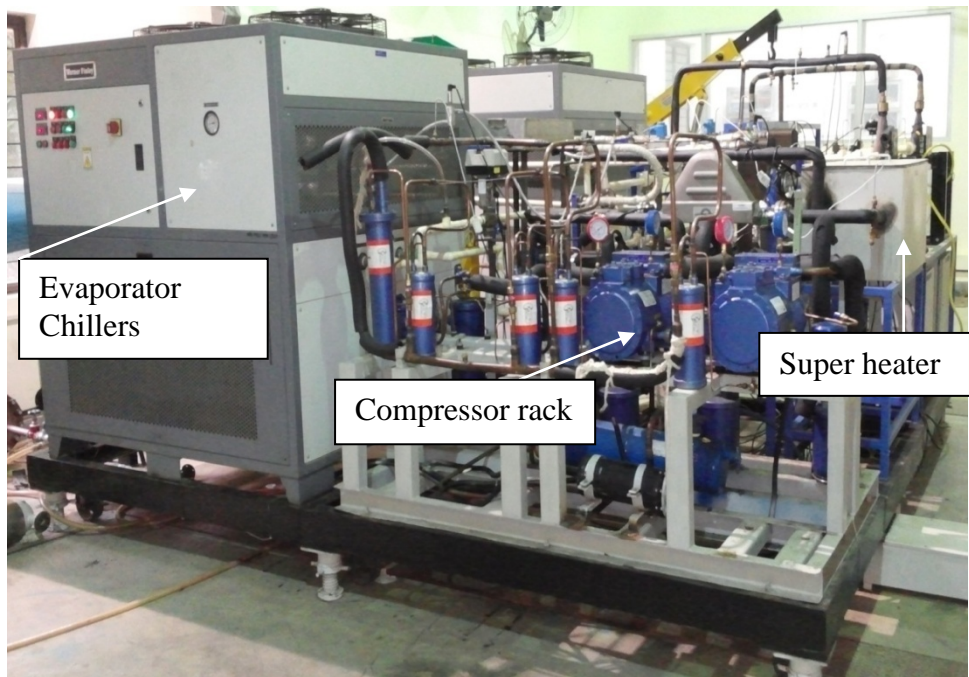


Fig.4.2a: Photograph of experimental test rig

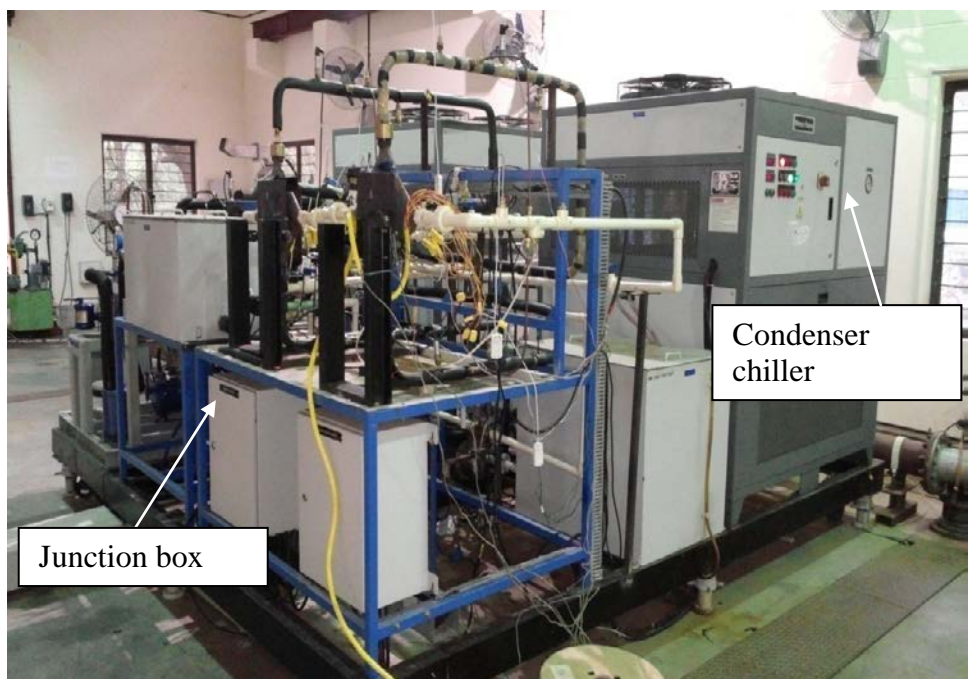
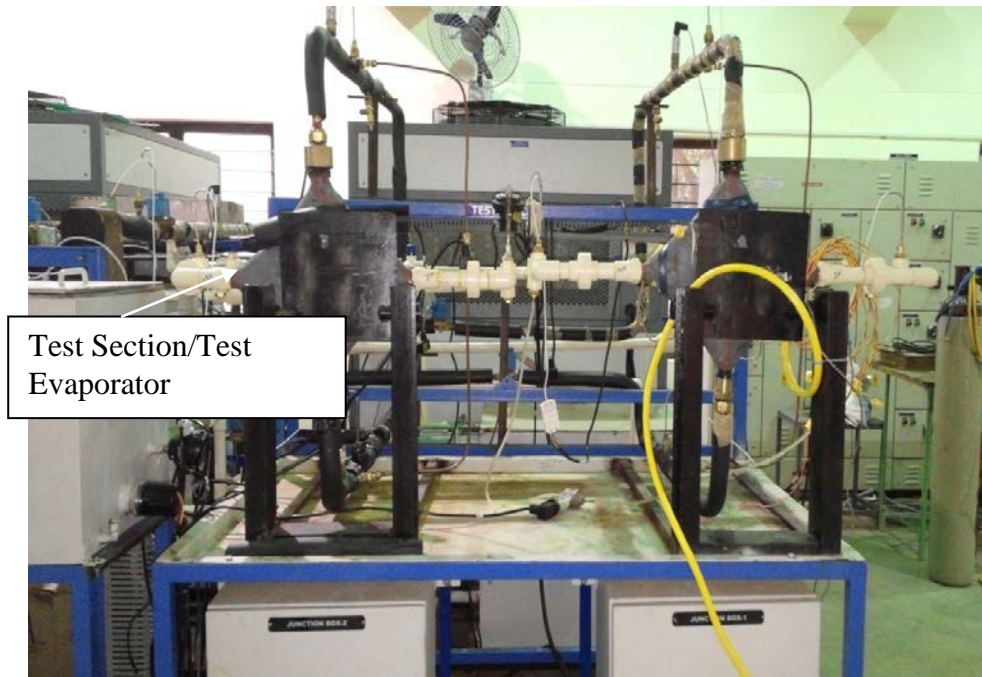


Fig. 4.2b: Photograph of experimental test rig in another view with test section



Test Section/Test Evaporator

Fig. 4.3: Photograph of experimental test section view in the test rig



Fig.4.4: Photograph of data acquisition system of test rig

4.3.1 Refrigerant loop

Refrigerant loop system employed in the test rig has shown schematically in Fig. 4.5. It is a basic vapour compression cycle system, consists of four semi hermitically sealed variable speed reciprocating compressors connected in parallel, condenser

(plate heat exchanger) , expansion valve, evaporator (plate heat exchanger) and test section. The variable speed compressors are designed to control flow rate between 0.01– 0.08 kg/sec variable in steps of 0.005 kg/sec. The refrigerant used in the circuit is Freon R134a. Drier is installed in the liquid line. The drier contains silica gel and absorbs traces of moisture present in the liquid refrigerant so that it does not enter the narrow cross-section of the expansion device causing moisture chocking by freezing. Collector tank which is installed in the liquid line collects the liquid. Temperature and pressure sensors across the compressor, condenser, expansion valve and evaporator are provided for measurement temperature and pressure and also the differential pressure sensors across the evaporator and condenser for measurement of differential pressure. Coriolis flow meter is installed in the circuit after evaporator to measure the vapour flow rate and after condenser to measure the liquid flow rate. The system also has sight glass for physical verification of state of the R134a.

Refrigerant loop consists of 4 compressors with different capacity connected in a parallel to vary the flow rates and keeping pressure same at the delivery section. The oil separator provided in the refrigerant loop intercepts the oil mixed with compressed gas and returns it to the crankcase of the compressor. This ensures the efficient lubrication of its moving parts. Separate oil separator for each compressor and a common oil separator are installed in the loop. Each compressor is provided with accumulators and gate valves or non return valves to avoid the backward flow. There are two sampling ports one at the evaporator side and another at the condenser side. These ports are used to charge the system as well as discharge the system. Sampling port also used to collect the refrigerant for checking the purity of the refrigerant at stipulated periods. Solenoid valves are installed before and after evaporator to bypass vapour refrigerant to the test evaporator/test section mounted in the loop. Test bench is provided for easy mounting and removing of the test evaporator unit in the test rig. Initially experiments were performed with evaporator in the loop closing the solenoid valves in the test evaporator side. Once the data stabilizes the solenoid valves in the evaporator side closes and passes the refrigerant through test evaporator unit (test section).

Cold water pump sucks the water from cold water tank circulated through the chiller evaporator and gets cooled before supplied back to the tank. Temperature in Cold water tank can be maintained up to 10 °C.

Hot water circuit consists of thermostat with heater system. The heaters heat the water in the tank to the desired temperatures and maintain the temperature. Hot water pump sucks the water from hot water tank and supplies hot water to the test evaporator unit. Temperature in hot water tank can be maintained up to 40 °C.

The water mass flow rate from the chiller unit to the evaporator/test section can be varied from 0.1 to 0.8 kg/s in steps of 0.05kg/s. Both the tanks (cold water tank and hot water tank) are interconnected. The thermostat and heater will control the inlet water temperature to evaporator from 10 °C to 40 °C in steps 1 °C with an accuracy of ± 0.2 °C.

The hot water at desired temperature is circulated through water circuit of the evaporator/test section. The water rejects the heat to the refrigerant R134a, which is circulating through refrigerant circuit of the evaporator/test section. The refrigerant becomes the vapour by absorbing heat from hot water in the evaporator and water gets cooled by rejecting the heat to refrigerant. The cooled water is supplied back to the water tank. Evaporator circuit consists of solenoid valves to bypass the water flow to evaporator or test section which is under test. It also consists of flow control valves and turbine flow meters to control water flow rate to the unit.

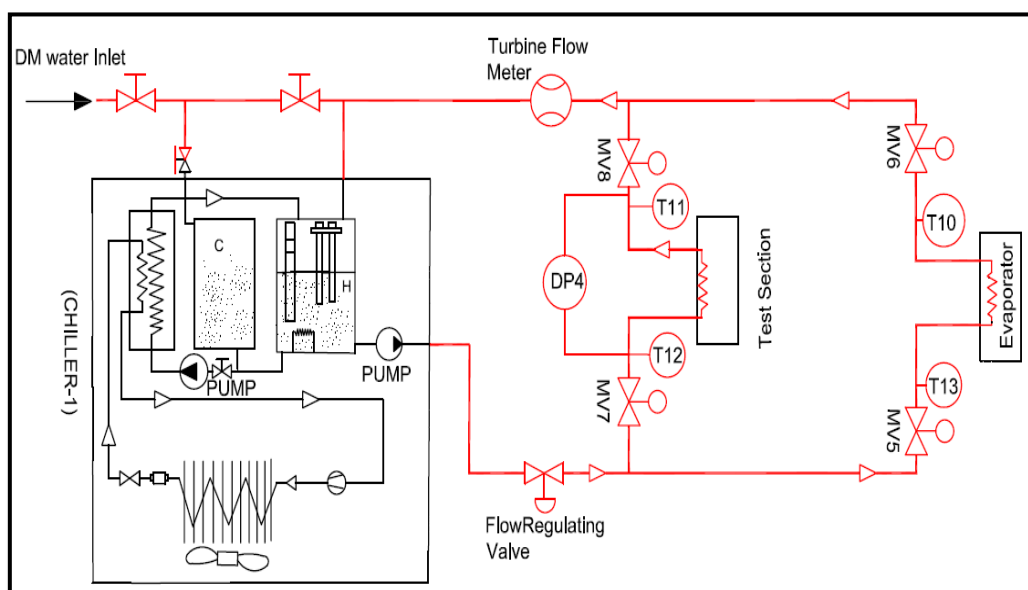


Fig. 4.6: Schematic layout of evaporator loop

4.3.3 Super heater loop

The R134a coming out of the evaporator should be in fully vapour form to safeguard the compressor. In case the refrigerant is not in fully vapour form, it will be converted to fully vapour form in the super heater loop before entering into compressor. The super heater loop consists of 3kW heating system, buffer tank, pump, heat exchanger, shut off valves, pressure, flow and temperature sensors. The schematic diagram of the super heater loop is shown in Fig. 4.7. Pump sucks the water from buffer tank and pumps through the heaters. Water is heated up in the heaters to a desired temperature and circulated to super heater tank. Any traces of liquid refrigerant present in the vapour refrigerant coming out of the evaporator is converted to vapour before entering into the compressor system. Super heater loop consist of flow regulating valve and turbine flow meter to control the flow to tank.

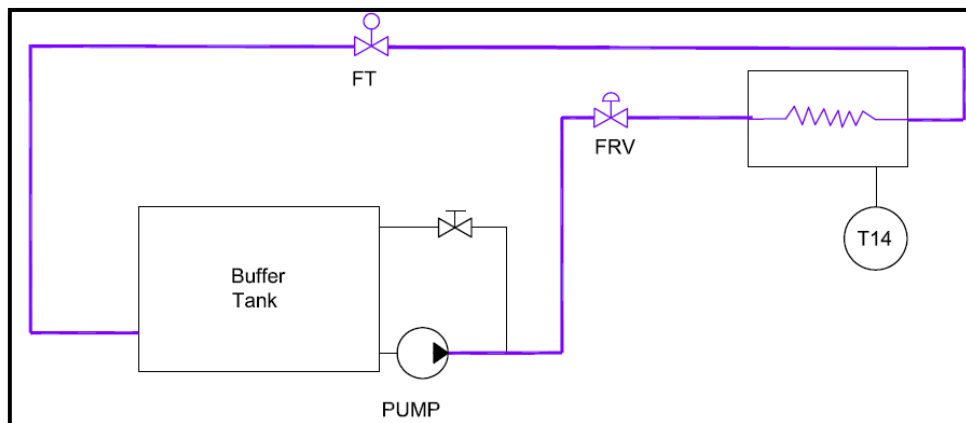


Fig. 4.7: Schematic layout of super heater loop

4.3.4 Condenser loop

Condenser loop system employed in the test rig has been shown schematically in Fig. 4.8. The condenser cooling loop consists of chiller unit (DM Water tank with pump, flow control valve and shut off valves). Water is circulated to condense the refrigerant vapour in the condenser. The water mass flow rate can be varied from 0.1 to 0.8 kg/s in steps of 0.05 kg/s. The chiller unit and heater will control the inlet water temperature to condenser from 10 °C to 40 °C. The chiller unit consists of two tanks, cold water tank and hot water tank as similar to evaporator chiller. Both the tanks are connected to the water pumps.

The cold water at desired temperature is circulated through water circuit of the condenser. The water absorbs the heat from refrigerant R134a, which is circulating through refrigerant circuit of the condenser unit. The refrigerant becomes the liquid by rejecting heat to the cold water in the condenser and water gets heated by absorbing the heat from the refrigerant. The heated water is supplied back to the water tank. Condenser circuit also consists of flow control valves and turbine flow meters to control water flow rate to the unit.

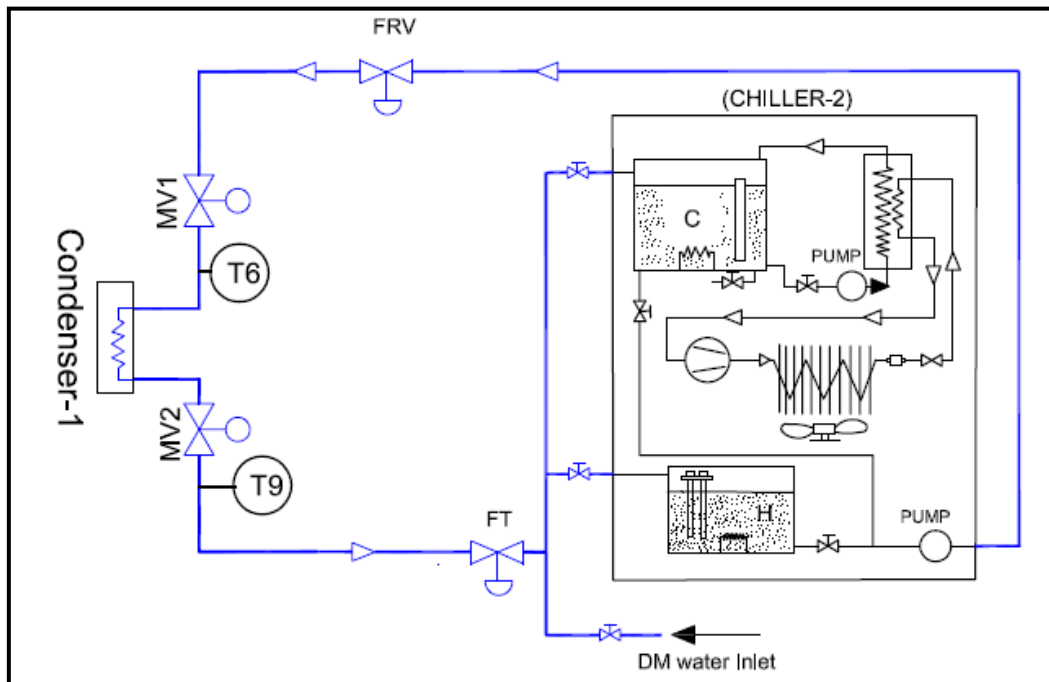


Fig. 4.8: Schematic layout of condenser loop

4.3.5 De-super heater loop

In general the refrigerant vapour coming out of the compressor will be in super heated condition. To bring down the vapour to saturated conditions at condenser inlet, de-super heater has been designed. De-super heater loop consists of plate heat exchanger, flow regulating valves, sight glass and instrumentation to measure temperature and flow rate. The schematic diagram of the de-super heater loop is shown in Fig. 4.9. Cold water is tapped from condenser chiller unit at a desired temperature and circulated through the water circuit of de-super heater plate heat exchanger. Water flow rate is regulated until the saturated conditions obtained at the inlet of the condenser. De-super heater loop consist of flow regulating valve and turbine flow meter to control the flow to tank.

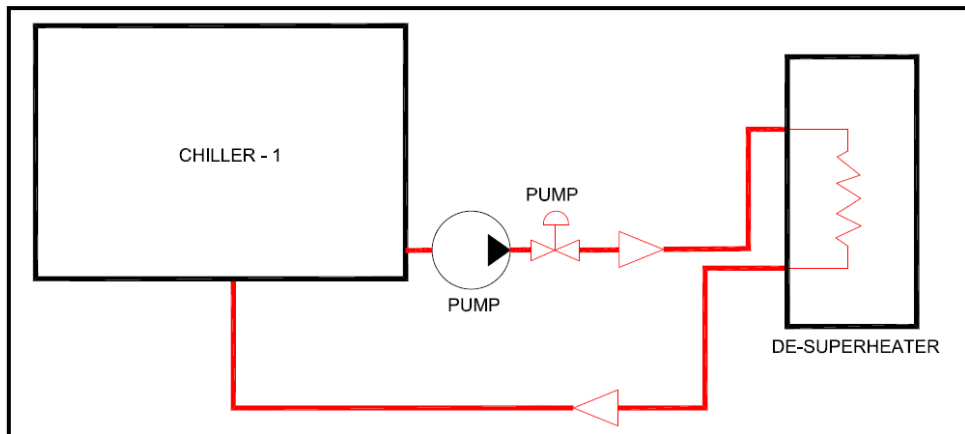


Fig. 4.9: Schematic layout of de-super heater loop

4.3.6 Single phase flow and heat transfer loop

Single phase heat transfer and friction characteristics are determined using the single phase flow and heat transfer loop. Single phase flow and heat transfer loop employed in the test rig is shown schematically in Fig. 4.10. The refrigerant coming from the compressor is sub-cooled by de-super heater and condenser loop (Condenser-2). Cold water coming from chiller-2 is used to condense the vapour refrigerant in the condenser-2. Sub-cooled liquid refrigerant is bypassed after condenser-2 and allowed to pass through the test evaporator, where it is heated by hot water circulated from chiller-1. The sub-cooled liquid refrigerant absorbs the heat from the hot water circulated in the test evaporator, where as hot water losses the heat. The liquid refrigerant from the test evaporator is again fed before expansion valve. The liquid refrigerant expands in the expansion valve and finally passed through evaporator in the main refrigerant loop. The refrigerant is evaporated in the evaporator by hot water circulated from the chiller-1. Chiller-1 supplies the hot water for both the test evaporator and evaporator simultaneously. The refrigerant vapour from evaporator passes through compressor rack. The procedure repeats for different mass flow rates of the refrigerant.

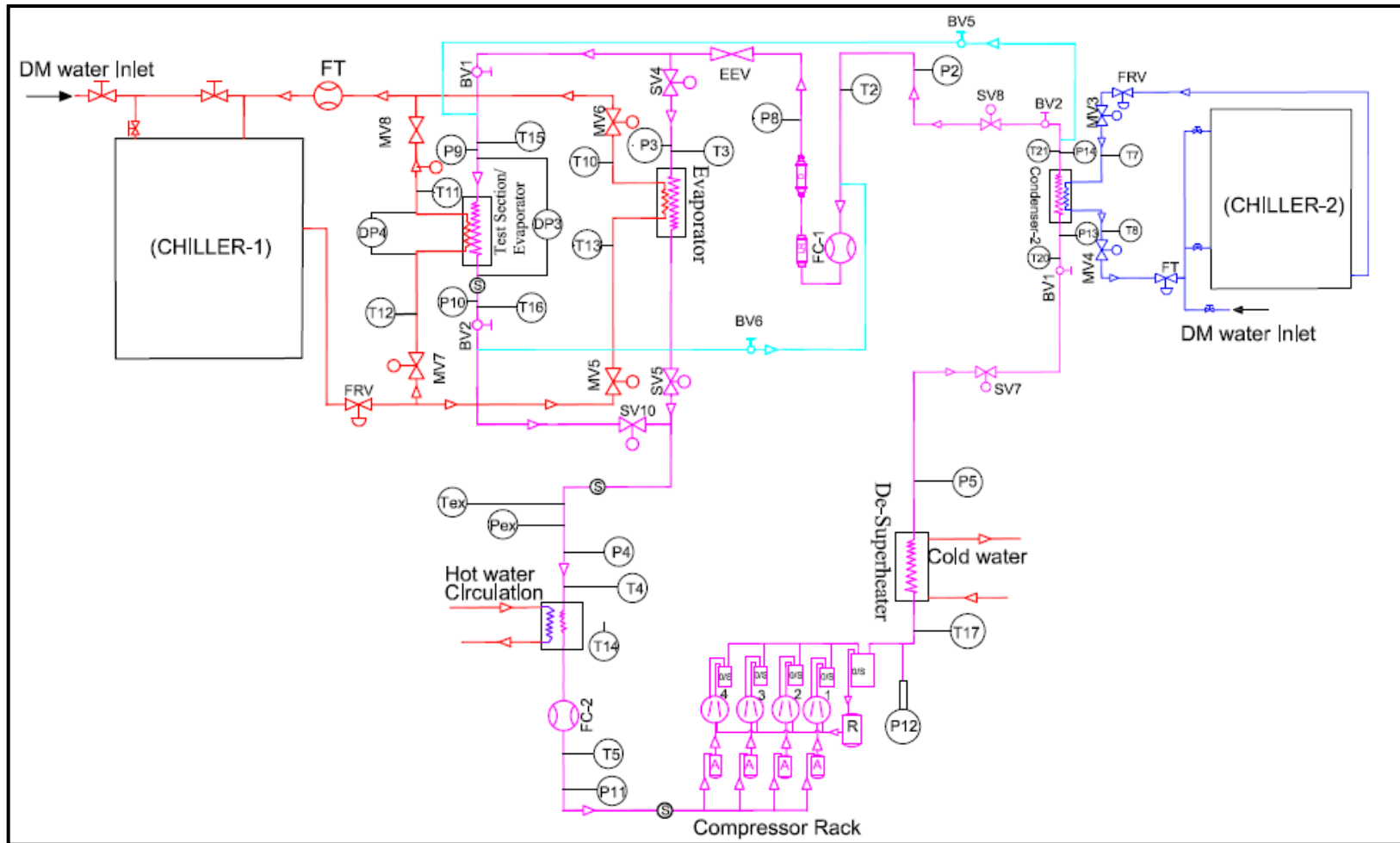


Fig. 4.10: Schematic layout of single phase loop

4.3.7 Details of major rig components

Fig. 4.11 shows the major components locations in the test facility

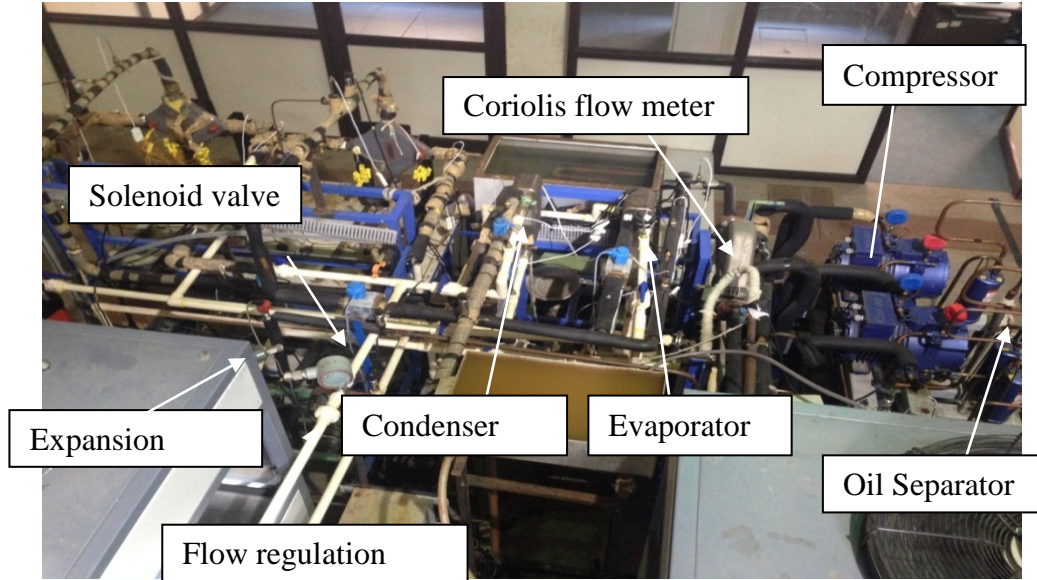



Fig. 4.11: Test facility with major component locations

4.3.7.1 Compressor

Compressor is one of the four essential parts of the vapour compression refrigeration system. The compressor operates in a cycle continuously, raising the refrigerant vapour pressure to the condenser pressure (corresponding to condensing temperature). Semi hermitically variable speed reciprocating compressor is used in the test facility. This type of compressor increases the vapour pressure by reducing the volume through the application of work. There is definite quantity of vapour delivered for each rotation of the crank shaft. Total 4 reciprocating compressors with different capacities are used in the test facility. The capacity of the compressor can vary by changing or controlling the speed of the each compressor. The specification of the compressor is given in the Table 4.1.


Table 4.1: Specification of compressor

Make	SEA-BIRD	
Model no.	200/IIL /1 H.P/ 400 to 500 RPM, Qty:1 250/IVL/2 H.P/ 425 to 620 RPM, Qty:1 300/ VL/3 H.P/ 355 to 635 RPM, Qty:2	
Capacity	1.2 kW, 2.2 kW, 3.7 kW	
Electric supply	440 V, 3P, 50 Hz	
Flow rate	0.0178 -0.02244 kg/s,0.04 - 0.058 kg/s 0.070 - 0.122 kg/s	

4.3.7.2 Evaporator and Condenser

Evaporator is a component of the refrigeration unit in which the refrigerant absorbs heat from the space (object) by changing its phase from liquid to vapour. Condenser is also component of refrigeration unit in which it rejects the heat and condenses the refrigerant to become liquid state. Plate heat exchanger is used as evaporator and condenser in the test facility. A plate heat exchanger is a heat exchanger constructed using metal plates to transfer heat between two fluids. The specification of the evaporator and condenser is given in the Table 4.2.


Table 4.2: Specification of evaporator and condenser heat exchangers

	Evaporator	Condenser	
Make	Danfoss	Danfoss	
Model no.	PHE B3-052-60-3.0-HQ	PHE B3-030-70-3.0-HQ	
Type	Plate heat exchanger	Plate heat exchanger	
Capacity	27 kW	30kW	
Design Pressure	45 bar	45 bar	

4.3.7.3 Expansion valve-Electronic

An expansion device is one of the main components of the test facility. It reduces the pressure of the liquid refrigerant and controls the flow of refrigerant from high pressure side to the low pressure side of the system. Electronic expansion valve (EEV) has been used in the test facility to control the flow of refrigerant entering the evaporator. EEV has chosen to open and close automatically without aid of an external device. It maintains constant refrigerant pressure in the evaporator. The specification of the EEV is given Table 4.3

Table 4.3: Specification of expansion valve

Make	CAREL	
Model no.	E ² V-24	
Capacity	20kW	
Flow rate	0.1kg/sec	
Maximum working pressure	40 bar	
Temperature range	-40°C to 65°C	

4.3.7.4 Oil separators




The SEA-BIRD oil separator is used in the test facility. It is an impingement screen type oil separator. Each compressor has a separate oil separator apart from common oil separator. Oil separation is done in two stages, first stage at individual compressor and second stage at common oil separator unit.

4.3.7.5 Chiller units

The test facility consists of two chiller units. It is an assembly of water tank with DM water, thermostat with heater, pump, flow control valve and shut off valves. The chiller unit consists of two tanks, cold water tank and hot water tank. Both the tanks are connected to the water pumps. Chiller working principle explained in Para no.4.3.2. The specification of the chiller unit is given in Table 4.4.

Table 4.4: Specification of chiller unit

Make	Werner-Finley	
Model no.	6TC10WC1X	
Capacity	6 TR	
Temperature range	10-40°C	
Flow rate	75 LPM	

4.3.7.6 Solenoid valves



Electromechanically operated Solenoid valves are used the test facility to bypass the refrigerant and water flow rates between evaporator and test section which is under test. The valve is controlled by an electric current through a solenoid. Two port type solenoid valves are used.

4.3.7.7 Flow regulating valves (FRV)

FRV are used mainly to regulate the water flow rate the test unit. These valves shall be directly controlled from the data acquisition through PLC.

4.3.7.8 Piping

Seamless copper tubes are used in the test facility. Sizing of the pipe lines is done based on the based on ASTM B-88 standard. The equivalent lengths of suction line, discharge line and liquid line are calculated after considering the effect of reducing tee, straight tee, elbow, solenoid valve, flow meter, sight glass, pressure sensor etc. All the pipe lines are insulated to avoid the temperature.

4.3.7.9 Evacuation and gas charging system

A separate evacuation and gas charging unit procured to evacuate the refrigerant gas and charge the gas when ever required. It is a movable unit consists of vacuum pump mounted on a wheels. Charging can be done in two ways liquid charging or gas charging. The test facility have both charging ports. Generally before changing the test section the gas is evacuated fully and stored in gas cyclinder. After changing the unit the gas is charged using the same unit.




4.4 INSTRUMENTATION OF THE TEST RIG

The instrumentation sub system comprises of instruments for measurement of flow rate, temperature, pressure and an electronic data acquisition system. Test facility consists of 16 temperature sensors, 10 pressure sensors, 8 differential pressure transducers, 4 turbine flow meters and 2 Coriolis flow meters.

4.4.1 Coriolis flow meter

Refrigerant flow rate is probably the most important quantity to be measured. It is desirable to use a flow meter that measures the total flow rate rather than the velocity at a particular point. Coriolis flow meter found suitable for accurate measurement of flow rate and used in the test facility. It measures the mass per unit time flowing through the device. Two Coriolis flow meters are installed in the test facility, one is at liquid line i.e. after condenser to measure liquid flow rate and another is at vapour line i.e. after the evaporator to measure the vapour flow rate. The specification of the Coriolis flow meter is given in Table 4.5.


Table 4.5: Specification of Coriolis flow meter

Make	Micro-Motion	
Model no.	CMFS015, CMFF100S	
Electric supply	18 to 100 VDC and 85 to 265 VAC; self switching	
Flow rate	0.003 to 0.09 kg/s	
Accuracy	±0.05% of rate for liquid, ±0.35% of rate for gas	
Working Pressure	40bar	
Working temperature	-15 to 70 °C	

4.4.2 Turbine flow meter

Turbine flow meters used in the test facility to measure the water flow rate. Four turbine flow meters are installed in the test facility, one is at evaporator line, second one at condenser line, third one at super heater line and fourth one at de-super heater line. The specification of the turbine flow meter is given in Table 4.6.

Table 4.6: Specification of turbine flow meter

Make	Rockwin	
Model no.	TFM1015	
Flow rate	1-60 LPM	
Accuracy	±3%	
Max Pressure	250kg/ cm ²	

4.4.3 Pressure transducers and differential pressure transducers

Pressure measurement in the refrigeration experiments is very important parameter for maintaining accurate conditions at the inlet/outlet of the evaporator. Diaphragm type pressure transducers have been employed to measure the pressure of refrigerant and water in the circuits at an entry and exits of test section, evaporator, condenser, expansion valve, and compressor. The test facility has extensively instrumented with pressure sensors to measure the all the data points. Differential pressure transducers are also installed in the test rig both in refrigerant circuit and water circuit to measure the pressure drops across the test section. The details of the pressure transducers and differential pressure transducers provided in the test facility are given in Table 4.7 and Table 4.8 respectively.

Table 4.7: Specification of pressure transducer



Make	Measurement specialties	
Model no.	M5100	
Pressure Range	0-20bars	
Accuracy	±0.25%	
Stability	±1% FS	

Table 4.8: Specification of differential pressure transducers

Make	Sesocon	
Model no.	251-01	
Capacity	0-5PSI	
Electric supply	12-36 VDC	
Accuracy	±0.25% F.S	

4.4.4 Temperature sensors with digital indicator

The accuracy of any heat transfer study depends on that of the temperature measurement. Platinum resistance RTD's are have been employed to measure the temperatures of refrigerant and water in the circuits at an entry and exits of test section, evaporator, condenser, expansion valve, compressors, super heater side and de super heater side. The test facility has extensively instrumented with temperature sensors to measure the all data points. The details of the temperature sensors provided in the test facility are given in Table 4.9.

Table 4.9: Specification of Temperature transducers

Make	RTD products, UK
Model no.	PT-100 wire thin film
Temperature Range	-40 to 100°C
Accuracy	±0.15 °C
Diameter	3mm
Sheath length	100 mm

4.5 DATA ACQUISITION SYSTEM

A data acquisition system with PC based data logging was developed. Data acquisition system consists of industrial PC with SCADA software of GE CIMPLICITY and PLC of GE VERSAMAX as shown in Fig. 4.12. It consists of 64 Analog, 32 digital input modules and 64 Analog, 32 digital output modules of GE make. All this I/O modules are connected to a GE VERSAMAX PLC which contains 2 No's of RS484 and RS232 communication ports. The PLC is connected to an industrial graded PC which is having GE CIMPLICITY SCADA software (Ver. 8.2) through RS 232 cable. The vapour compression refrigeration test rig module consists of various components like variable frequency drive (VFD) control compressors, motorised valves, solenoid valves, flow regulation valves and chillers. These components are controlled by SCADA system in order to obtain the satisfactory results. Pressure, differential pressure, temperature and flow sensors are connected to a PC through PLC and SCADA system. SCADA system monitor the temperature sensors, pressure sensors, thermocouples and flow meters data and for its smooth functionality and data gathering.

The variations occurring in different components of the rig is controlled by the PLC that stores the values for further process, this information is sensed by the SCADA software that regulates the movement of the valves, all the pressure sensors (Gauge and Differential), temperature sensors, chillers temperature settings, test section thermocouples and motorised and solenoid flow regulation valves are connected to a PLC in respective modules through line resistance compensation cable. The sensor values/readings can be recorded/monitored with the help of SCADA. Pressure, temperature and flow rate of refrigerant and water in condenser and evaporator loop can be varied using SCADA that is, by varying the valve positions and by switching on/off the compressors.

The SCADA system is programmed in such a way as to control valves position, data monitor and logging, report generation, trend analysis, graphical analysis of data, process flow diagrams, using ladder programming technique. Specification of data acquisition system is given Table 4.10.

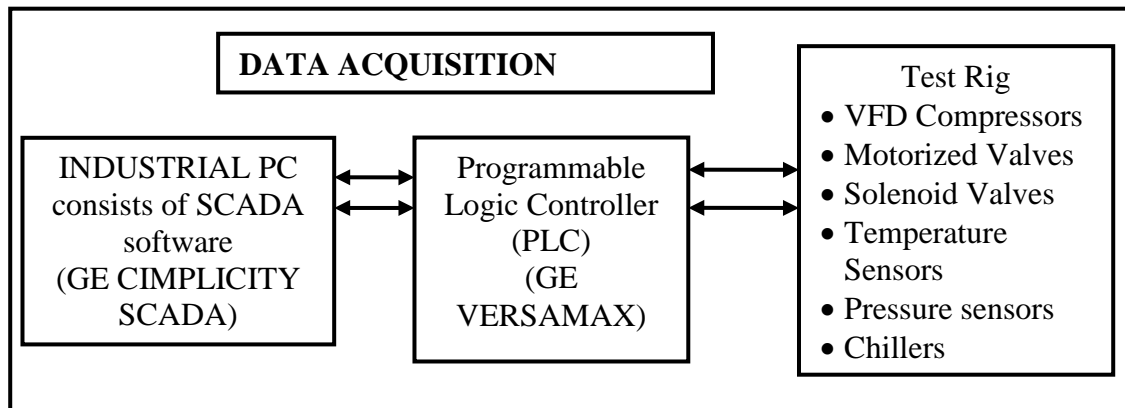


Fig.4.12: Block diagram of Data acquisition system

Table 4.10: Specification of data acquisition system

Parameter	RTD	Thermocouples	Pressure, Differential Pressure and flow
Analog Input Card	IC200ALG620	IC200ALG630	IC200ALG240
Channels	16 (4/card)	24 (8/card)	24 (8/card)
ADC Resolution	16 bits	16 bits	16 bits
Update rate	230ms/channel	70ms/channel	-
Measurement Accuracy	±0.15	±0.15	0.1%
Input current	-	-	1-20mA
Input voltage	-	-	±10 V DC

4.5.1 Display details

a) Display on main panel (Digital meters)

Rack mounting type control with following displays.

- Pressure, Flow rate and Temperature reading display,
- Input Voltmeter with Selector Switch
- Ammeter with Selector Switch
- 3-phase supply indications lamp

b) Facility on operator's panel

- Emergency (push Button)
- Mains ON/OFF indications
- Alarm for gas leak detection

c) Electrical control details

- It have MCCB as incomer, separate MCB for motor, MCB for control, circuit etc. with twice the capacity of load.
- Provided double earthing interconnections with suitable copper wire, earth-bus with all terminations and connections.
- All copper cables/wires have twice the capacity of the load.
- A four core suitable insulated copper cable of 10 meter long for incoming power connection is provided.
- Water-Glycol Thermostat with heater – 2 No's and Mini heater are controlled by PID controller.

d) Electrical control panel

Control panel Comprises of:

- Main power isolator, pumps and compressor on /off switches, mains indication, fuse units.
- Digital indication for pressures, temperature and flow of upstream and downstream refrigerant line and water lines
- All control circuit wiring was done with multi stand wires and multi core wire of standard brand.

- Earth connector terminal, neutral connector terminals and necessary controls was done as per the test unit demand and standards.
- The panel board is coloured with powder coating and internal wiring was done as per the requirements and standards

4.5.2 Electrical system

4.5.2.1 MCC panel

The MCC panel is intended to control the feeders listed below both in local and remote mode. It consists of

- Super heater feeder – 3kW
- Water circulation pump – 0.37kW
- Compressor 1 – 1.5kW (VFD Control)
- Compressor 2 – 2.2kW (VFD Control)
- Compressor 3 – 3.7kW (VFD Control)
- Water glycol feeder 1 – 15kW
- Water glycol feeder 2 – 15kW

4.6 MEASURING INSTRUMENTS CALIBRATION

Calibration of following measuring instruments carried out as per the standard procedure. The details of calibration and calibration certificates included in

APPENDIX-I

A. Pressure sensors

- Absolute pressure sensors
- Differential pressure sensors

B. Flow meters

- Turbine flow meters
- Coriolis flow meters

C. Temperature sensors

- Resistance Temperature Detectors (RTD's)
- Thermocouples

CHAPTER 5

EXPERIMENTAL PROCEDURE AND DATA REDUCTION

A detailed testing procedure, experimental results and data reduction for test sections (2 offset strip and 2 wavy fin surfaces) are presented in this chapter. The data were taken under following conditions.

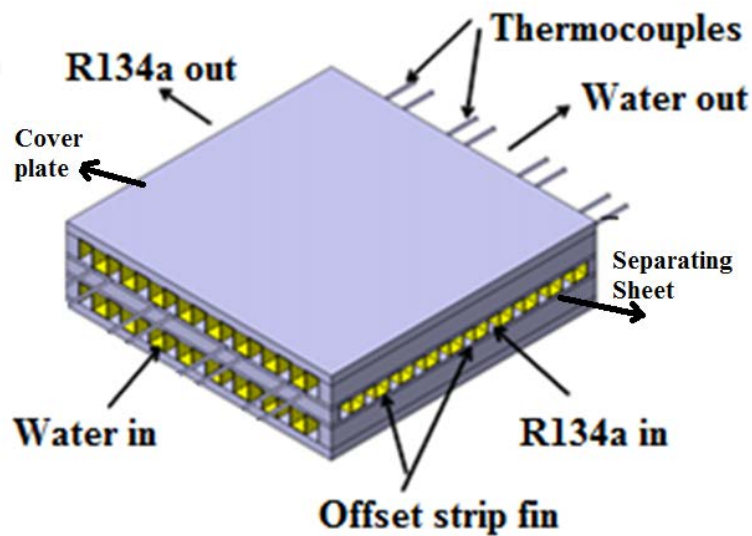
- All data for analysis were taken under steady-state conditions,
- For heat transfer data, evaporator exit refrigerant temperature was slightly lower than inlet temperature due to the pressure drop across the evaporator with a corresponding saturation temperature reduction.
- For pressure drop data, the differential pressure transmitter had a positive reading. Differential pressure transmitters are designed for the measurement of positive pressure differences.
- Uniform distribution of Heat flux is assumed across the surface.
- The effect of flow mal-distribution, for both water and refrigerant streams, was not considered

The experimental data were reduced to obtain the refrigerant side heat transfer coefficient and frictional pressure drop. To avoid lubricant oil mixing with refrigerant in the system, an oil separator was installed in the system. However, oil finds its way into the evaporator no matter how efficient the oil separator is. Oil concentration was measured in the system and found it is less than 0.5%.

5.1 TEST SECTION/TEST EVAPORATOR

The test section is two streams cross flow heat exchanger, where as one channel carries R134a as the working fluid while the second channel carries the water. The size of the test section is 150mm x 150 mm. The test section is a stack of three fins, one refrigerant side fin in which the boiling heat transfer and pressure drop coefficients is estimated and two water side fins. The size of the test section arrived based the heat loads coming in our application areas.

The test sections are manufactured by stacking fins, side-bars, parting sheets and cover plates, held together in a fixture under a placed in a brazing furnace and brazed to form the plate fin heat exchanger block. The 3-D model and brazed block is shown in Fig 5.1 a and b. The nozzles and header are then welded to the block, taking care that the brazed joints remain intact during the welding process. Before brazing the core, sufficient number of thermocouples is inserted between the separating sheets to measure the wall temperatures during testing. K-type thermocouples are used with 0.5 mm diameter stainless steel sheath. Fig 5.2 shows the thermocouples arrangements in test section to measure the wall temperatures at axial position along the refrigerant flow direction. 8 K type thermocouples are inserted in the test section at four locations as shown in Fig 5.3. Mean of two temperatures at each location is used for estimation of two -phase heat transfer coefficient. The local boiling two-phase heat transfer coefficient will be determined at these four locations. The picture shown in Fig 5.4 is one of the 4 test sections manufactured.



a) 3D-Model block



b) Brazed block

Fig.5.1: Test section block a) 3-D model b) Brazed block

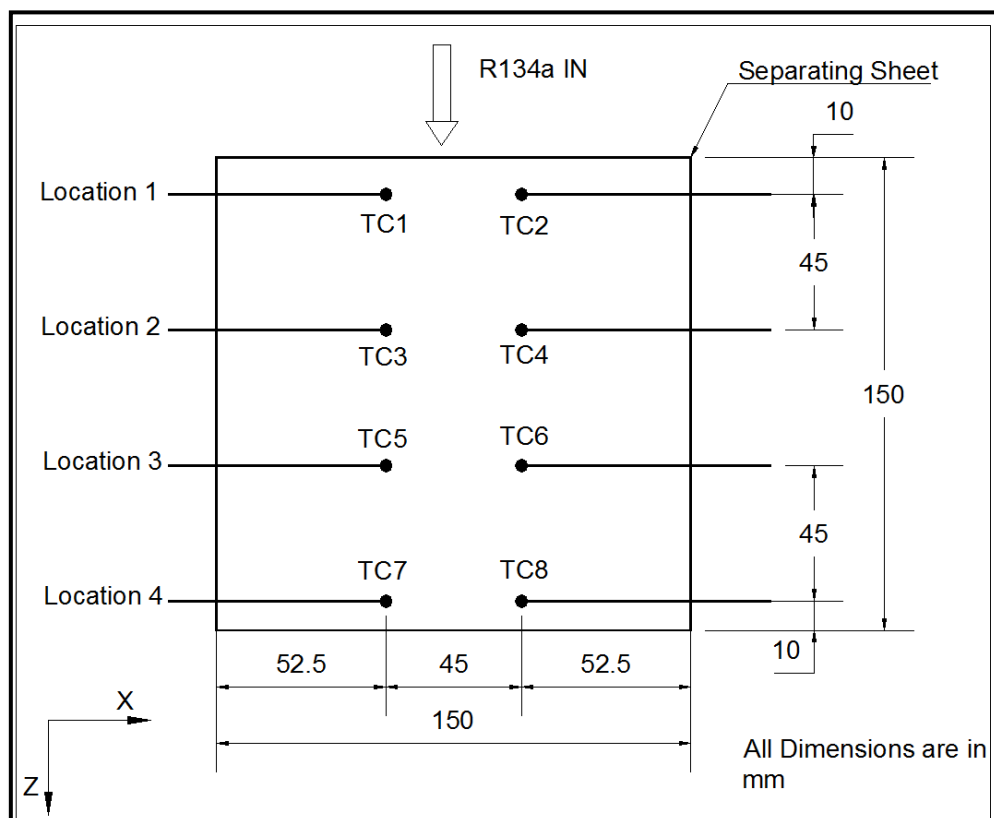


Fig. 5.2: Thermocouples arrangements in test section



Fig. 5.3: Cut section of thermocouples inserted in test section

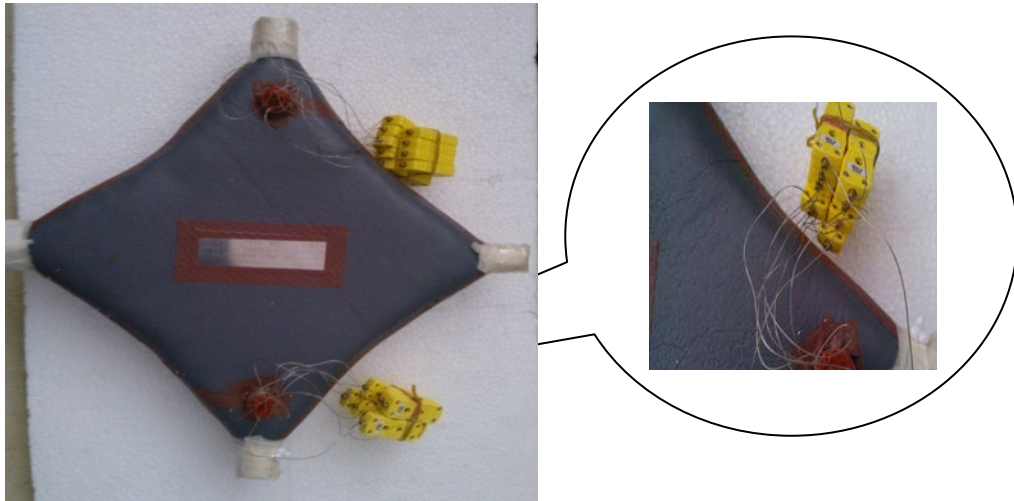


Fig.5.4: Test Section/Test evaporator

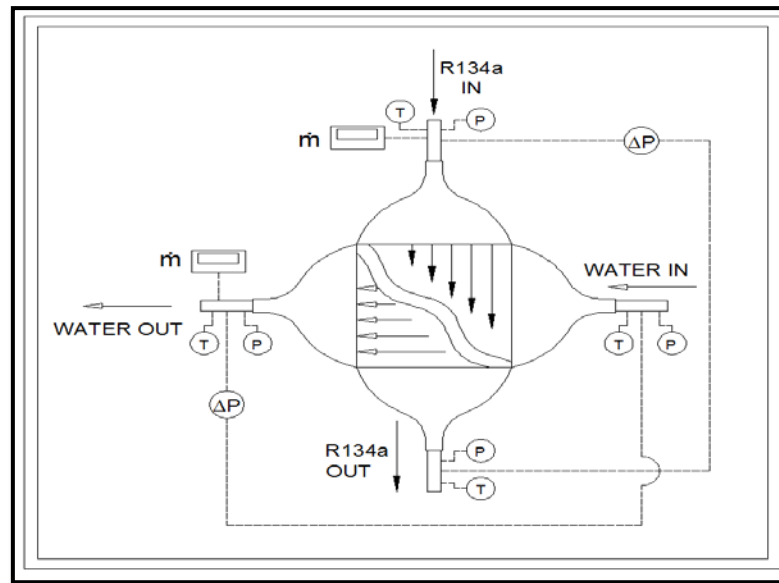
Total 4 test sections (2 offset strip and 2 wavy fin types) with different fin geometries have been identified for generation of boiling heat transfer and friction coefficients. All the test sections are made up Aluminium Alloy AA3003. These test sections are selected because of availability of these fin surfaces globally for supply and use in industrial applications. The Table 5.1 indicates the test sections and size of fins used, offset strip and wavy fins. Offset strip fin test section is named as OSF and wavy fin test section is named as WF for easy identification.

Table 5.1: Test section geometry

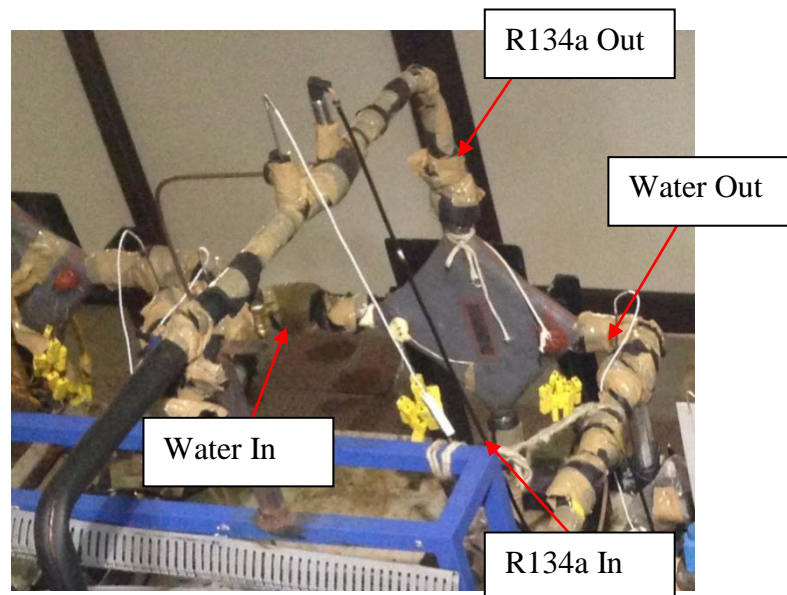
SI. No	Name	Fin Type	Fin density (FPI)	Height (mm)	No. of Fins	FIN Size cm			Test Section Height
						Flow Length	Width	Thickness	mm
1	WF1	Wavy	16	5	1	15	14.2	0.00762	36.15
		Wavy	18	10.2	2	15	14.2	0.0152	
2	WF2	Wavy	16	4.09	1	15	14.2	0.00762	35.25
		Wavy	18	10.2	2	15	14.2	0.0152	
3	OSF1	Offset strip	30	3.05	1	15	14.2	0.01016	23.8
		Offset strip	28	5	2	15	14.2	0.0127	
4	OSF2	Offset strip	18	3.8	1	15	14.2	0.0254	24.55
		Offset strip	28	5	2	15	14.2	0.0127	

5.2 TEST ARTICLE MOUNTING

Test section mounted vertically in the vapour cycle test facility for carrying out the experiments. Test section is mounted on a fixture to hold it firmly in a place and placed in test bench. The inlet and outlet pipe line connections of R134a and water pipe lines with test section were connected. Temperature and pressure sensors are mounted at the inlet and outlet pipe lines to measure the temperature and pressure of R134a and water. Fig. 5.5 a & b shows the line diagram of the test section and measurements recorded during the testing.



a) Line diagram of test section



b) Picture depicting measurement

Fig. 5.5: Figure depicting temperature, flow and pressure measurement a) Line diagram b) picture of measurement

5.3 TESTING PROCEDURE

5.3.1 Single phase heat transfer and pressure drop testing

Before conducting the two-phase experiments single phase heat transfer experiments were conducted on test section/test evaporator.

The test section was mounted in the circuit. Opened all the solenoid valves in the refrigerant loop. Refrigerant loop is then evacuated using the vacuum pump and filled with nitrogen gas at 6.5 bar'a'. Nitrogen gas charging is kept for 48 hrs. The leak test was carried out using soap solution after 48 hrs for any leaks in the refrigerant loop. The loop is again evacuated up to vacuum level of 759mm of Hg is kept for 24 hrs. Then the loop is charged with refrigerant R134a without switching on the power. For safety reasons, the test rig is located in a separate room and fully automated.

Switched on the main power and ensured proper voltage, current and health of the units. The solenoid valves before and after the test section in both the loops (Refrigerant loop and Evaporator loop) closed to avoid refrigerant flow and water flow to the test evaporator/test section and condenser-2. Switch on the compressor and continued the charging still the compressor inlet/out conditions achieved. At the same time switched on both evaporator and condenser chillers and allowed water to pass through the evaporator and condenser. Compressor running is continued still the conditions stabilized in the main loop. The condition stabilizes after 3 to 4 hours of running the system. After stabilization of the conditions the solenoid valves closed before and after condenser-1 and refrigerant flow is bypassed to the condenser-2. Opened the water side solenoid of the condenser-2 and closed the condenser-1 water side solenoid valves.

The refrigerant coming from the compressor is sub-cooled by de-super heater and condenser loop (Condenser-2). Cold water coming from chiller-2 is used to condense the vapour refrigerant in the condenser-2. Sub-cooled liquid refrigerant is bypassed after condenser-2 and allowed to pass through the test evaporator, where it is heated by hot water circulated from chiller-1. The sub-cooled liquid refrigerant is passed through one side of the test section and hot water from the chiller-1 at desired temperature is circulated through other side of the test section. The sub-cooled liquid refrigerant absorbs the heat from the hot water circulated in the test evaporator, where as hot water rejects the heat. The liquid refrigerant from the test evaporator is again fed before expansion valve. The liquid refrigerant expands in the expansion valve and finally passed through evaporator in the main refrigerant loop. The refrigerant is evaporated in the evaporator by hot water circulated from the chiller-1. Chiller-1 supplies the hot water for both the test evaporator and main evaporator

simultaneously. The refrigerant vapour from evaporator passes through compressor rack before further heated at super heater. The procedure repeats for different mass flow rates of the refrigerant. Temperatures, flow rates and absolute/differential pressures of R134a and water were recorded for the later analysis. Wall temperatures at parting sheets also recorded.

5.3.2 Two-phase heat transfer and pressure drop testing

Switched on the main power and ensured proper voltage, current and health of the units. The solenoid valves before and after the test section in both the loops (Refrigerant loop and Evaporator loop) closed to avoid refrigerant flow and water flow to the test evaporator/test section. Switch on the compressor and continued the inlet/out conditions achieved. At the same time switched on both evaporator and condenser chillers and allowed water to pass through the evaporator and condenser. Compressor running is continued still the conditions stabilized in the main loop. The condition stabilizes after 3 to 4 hours of running the system. After stabilization of the conditions in the test rig, solenoid valves closed before and after evaporator and refrigerant flow is bypassed to the test section, which is under test. Opened the water side solenoid of the test section and closed the main evaporator water side solenoid valves.

An experimental test was conducted as follows: By changing the RPM of the compressor the required flow rate of refrigerant liquid was obtained. The liquid temperature at the inlet of the test section was controlled by expansion valve and controlling the heat loads at evaporator and condenser. The refrigerant in the refrigerant circuit receives the heat from the hot water circulated in the water circuit from the chiller unit and boiling takes place in the heated length of the test section. The chiller unit supplies the hot water at set temperature and flow rate of water is controlled through flow regulating valve installed in the water circuit of evaporator loop. The boiling and evaporation of liquid refrigerant takes place in the test section to become the vapour. The hot water temperature and flow was controlled to maintain the heat flux at required value. The vapour coming from the test section was further heated in the super heater to ensure complete vapour at the suction side of the compressors. In the super heater the refrigerant vapour is further heated through a hot water circulation. The vapour sucked by the compressor, compressed in the

compressor. Both the pressure and temperature of the refrigerant vapour increases. Vapour from the compressor was sub-cooled to saturation vapour condition in the de-super heater. The vapour coming out off the de-super heater is condensed in the condenser of the refrigerant loop. Refrigerant vapour condensed in the condenser by continually adjusting the temperature and flow rate of the cooling water coming the chiller unit. Then the liquid refrigerant flows through a filter/dryer and collector tank before expanding in the electronic expansion valve. The flow rate was monitored by a Coriolis mass flow meter. Sight glasses are used to ensure the fluid condition at each stage. Temperatures, flow rates and absolute/differential pressures of R134a and water were recorded for the later analysis. The wall temperatures were measured using the K-type thermocouples inserted in the test section during brazing of test section. 16 temperature sensors are installed at each stage in the test facility for temperature measurement. Pressure drops of both circuits were measured. All the measurements have been performed in steady state condition that have reached within 60 min after operating conditions were fixed. All the experiments were conducted by ensuring saturated liquid R134a at the entry to the test section and boiling/vaporization occurred within the test section

The experiments were conducted on 4 test sections. Before every experiment the refrigerant circuit was evacuated using vacuum pump to remove the entrapped air in the circuit and leak checked with nitrogen gas.

5.4 EXPERIMENTATION

5.4.1 Single phase heat transfer experimentation

Single-phase experiments performed on 4 test sections (2 offset strip and 2 wavy fin surfaces) with sub-cooled liquid refrigerant. Energy balance verified and validated the measurement equipment, experimental procedure and technique. The geometrical parameters of the 4 test sections are presented in Table 5.2.

Table 5.2: Fin geometry parameters of 4 test sections

Variables	OSF1	OSF2	WF1	WF2
Fin height, h (mm)	3.05	3.8	5	4.09
Lance length, l (mm)	3.175	1.588	-	-
Wave length, λ (mm)	-	-	9.525	9.525
Fin spacing, s (mm)	0.847	1.411	1.639	1.639
Fin thickness, t (mm)	0.1016	0.254	0.076	0.076
Wave amplitude a (mm)	-	-	1.95	1.95
Hydraulic diameter, D_h (mm)	1.1894	1.7461	2.3127	2.2494
Fins per inch FPI	30	18	16	16

Single phase flow heat transfer experiments conducted in all test sections, using sub cooled liquid R-134a. Pressure drop experiments conducted using water as a test fluid. Tests were performed at different mass flow rates on each test section and data was recorded after reaching the steady state conditions. For each test section a number of tests were conducted over a range of Reynolds numbers. The test section is heated with water flowing in either side of the refrigerant flow.

Measured heat transfer data is presented in the Table 5.3 for offset strip fin (OSF1) test section. Measurements are noted at stabilized conditions and the measured data is used for further calculation and analysis.

Table 5.3: Measured single phase heat transfer of offset strip fin, OSF1

\dot{m}_r kg/s	\dot{m}_w LPM	T_{ri} °C	T_{ro} °C	T_{win} °C	T_{wout} °C	T_{wall} °C
0.0108	2.83	18.1	28.5	29.35	28.5	28.6
0.0124	2.84	18.2	28.9	29.2	28.2	29.0
0.0158	2.84	18.1	29.6	30.7	29.3	30.0
0.0175	2.84	18.1	30.0	31.0	29.5	30.2
0.0200	2.85	18.3	31.6	32.8	30.8	31.8
0.0225	2.67	18.1	32.1	33.3	30.8	32.5
0.0253	2.67	18.3	31.8	33.7	31.1	32.4
0.0280	2.65	18.2	32.2	33.6	30.9	32.7
0.0309	4.26	18.5	31.7	33.7	31.9	32.7

5.4.2 Single phase pressure drop experimentation

Single phase pressure drop experiments are conducted using water as testing fluid since friction factor does not vary with liquid or gases as reported by Hu et al. (1995). Measured pressure drop data is presented in the Table 5.4

Table 5.4: Measured single phase pressure drop of offset strip fin, OSF1

\dot{m}_w LPM	ΔP_{total} mbar
3.05	8.50
4.10	12.80
5.04	17.00
6.12	22.55
7.03	28.60
8.00	35.06
9.11	42.20
10.07	49.95
11.12	58.63

5.4.3 Two-phase flow and heat transfer experimentation

Experiments were performed on 4 test evaporator/test sections (2 offset strip fin and 2 of wavy fin) at different mass flux, heat flux and quality range. The details of test range and fin details used in refrigerant side are given in Table 5.5 and 5.6 for offset strip fin and wavy fin respectively.

Table 5.5: Dimensions and test range offset strip fins.

Variables	OSF1	OSF2
Saturation pressure, P_{sat} (bar a)	2.82-3.49	2.62-3.49
Saturation temperature, T_{sat} ($^{\circ}C$)	-1 to 5	-3 to 5
Mass flux, \dot{G} ($kg/m^2 s$)	50-82	48-100
Heat flux, q (kW/m^2)	14-22	13-24
Exit vapour quality, x	0.32-0.75	0.24-0.80
Fin height, h (mm)	3.05	3.8
Lance length, l (mm)	3.175	1.588
Fin spacing, s (mm)	0.847	1.411
Fin thickness, t (mm)	0.1016	0.254
Hydraulic diameter, D_h (mm)	1.1894	1.7461
Fins per inch FPI	30	18
Heat transfer area A , m^2	0.163178	0.12961
Free flow area A_{ff} , mm^2	368.4321	412.8962
Material	AA3003	AA3003

Table 5.6: Dimensions and test range of wavy fins.

Variables	WF1	WF2
Saturation pressure, P_{sat} (bar a)	2.50 -2.93	2.61 - 3.14
Saturation temperature T_{sat} ($^{\circ}\text{C}$)	-4.5 to -0.5	-3.5 to 2.0
Mass flux, \dot{G} ($\text{kg}/\text{m}^2 \text{ s}$)	30-50	35-50
Heat flux, q ($\text{kW}/\text{m}^2\text{s}$)	11-19	16-23
Exit vapour quality, x	0.26-0.80	0.38-0.90
Fin height, h (mm)	5	4.09
Wave length, λ (mm)	9.525	9.525
Fin spacing, s (mm)	1.639	1.639
Fin thickness, t (mm)	0.076	0.076
Wave amplitude a (mm)	1.95	1.95
Hydraulic diameter, D_h (mm)	2.3127	2.2494
Fins per inch FPI	16	16
Heat transfer area A , m^2	0.149994	0.130364
Free flow area A_{ff} , mm^2	665.619	543.9534
Material	AA3003	AA3003

Measured heat transfer data is presented in the Table 5.7 for offset strip fin (OSF1) test section. Measurements are noted at stabilized conditions and the measured data is used for further calculation and analysis.

Table 5.7: Measured two-phase data of offset strip fin, OSF1

SL.No	\dot{m}_r kg/s	\dot{m}_w kg/min	T_{sat} $^{\circ}\text{C}$	T_{wi} $^{\circ}\text{C}$	T_{wo} $^{\circ}\text{C}$	T_{wall1} $^{\circ}\text{C}$	T_{wall2} $^{\circ}\text{C}$	T_{wall3} $^{\circ}\text{C}$	T_{wall4} $^{\circ}\text{C}$
1	0.023	2.82	-0.70	18.20	6.50	5.40	4.60	4.50	3.90
	0.023	3.29	-0.40	19.60	8.10	5.60	4.50	4.00	3.80
	0.023	3.71	-0.50	20.40	8.60	6.20	4.50	4.30	4.20
	0.023	4.51	-0.20	21.90	10.90	6.50	5.10	4.85	5.00
2	0.027	3.29	2.10	18.80	9.20	7.00	6.10	5.70	5.40
	0.027	2.95	1.30	17.50	5.30	6.60	5.20	4.70	4.40
	0.027	4.78	3.20	18.10	9.10	8.90	7.20	6.80	6.60
	0.027	4.34	2.40	21.30	9.80	8.10	6.70	6.40	6.20
3	0.030	2.90	3.50	18.40	7.40	8.80	7.30	7.10	6.70
	0.030	4.21	4.60	19.30	10.00	9.80	8.00	7.60	7.50
	0.030	5.80	4.90	19.60	11.50	10.50	8.50	8.10	8.00
	0.030	6.36	4.90	19.20	11.70	10.60	8.70	8.40	8.40

Table 5.8 shows the experimental pressure drop data recorded during experimentation performed on offset strip fin (OSF1)

Table 5.8: Measured two-phase pressure drop data of offset strip fin, OSF1

SL.No	\dot{G} kg/m ² s	Exit vapour quality, x	Pressure drop, ΔP_{total} , mbar
1	63	0.350	82.073
		0.487	96.557
		0.572	98.626
		0.662	104.143
		0.754	108.282
2	73	0.356	90.349
		0.414	96.557
		0.487	104.833
		0.567	109.661
		0.656	118.627
3	82	0.320	94.488
		0.378	102.764
		0.452	111.040
		0.512	113.799
		0.588	100.007

5.5 DATA REDUCTION

5.5.1 Single phase heat transfer and pressure drop

5.5.1.1 Single phase heat transfer coefficient

Energy balance in the test section is verified by calculating the heat lost by water and heat gained by the liquid refrigerant.

$$\dot{m}_w C_p (T_{wi} - T_{wo}) = \dot{m}_r C_p (T_{ro} - T_{ri}) \quad (5.1)$$

Overall heat transfer coefficient can be determined with the measured data using to the following equations

$$Q = UA \Delta T_{LMTD} \quad (5.2)$$

Heat transfer between the refrigerant and water separated by plates with a thickness t , area A_p and thermal conductivity k , the overall heat transfer coefficient U is given as

$$\frac{1}{U} = \frac{1}{\eta_{or} h_l} + \frac{t}{k \left(\frac{A_p}{A_r} \right)} + \frac{1}{\eta_{ow} h_w \left(\frac{A_w}{A_r} \right)} \quad (5.3)$$

Where U is based on the refrigerant side area A_r , h_l and h_w are the refrigerant and water heat transfer coefficients, respectively, and η_o is the overall fin efficiency, which is defined as

$$\eta_o = 1 - a(1 - \eta_f) \quad (5.4)$$

In which a is the ratio of the fin area to the total area, η_f is fin efficiency

Single phase heat transfer coefficient h_l can be calculated using Eqn.5.3 or it can also be estimated using Colburn j factor.

Dimensionless parameter Colburn j factor is estimated using the following equation

$$j = \frac{D_h}{4L} \ln \left[\frac{T_{wall} - T_{ri}}{T_{wall} - T_{ro}} \right] \text{Pr}^{\frac{2}{3}} \quad (5.5)$$

5.5.1.2 Single phase pressure drop coefficient

The pressure drop in the channel geometry is due to mainly core friction, acceleration and entrance/exit effects. The relation for the flow stream pressure drop across the test sections is

$$\begin{aligned} \Delta P_{total} &= \Delta P_{IH} + \Delta P_E + \Delta P_A + \Delta P_F + \Delta P_C + \Delta P_{OH} \\ \Delta P_{total} &= \frac{\dot{G}^2 v_l}{2g_c} \left[-2 \sigma_A (1 - \sigma_A) + (K_c + (1 - \sigma_B^2)) + 2 \left(\frac{v_2}{v_1} - 1 \right) + f \frac{A}{A_c} \frac{v_m}{v_1} - (1 - \sigma_B^2 - \right. \\ &\quad \left. K_e) \frac{v_2}{v_1} + 1.5 (1 - \sigma_A^2) \right] \end{aligned} \quad (5.6)$$

The experimental friction factor, f is calculated from the pressure drop measured across the whole length of the test section using the above equation.

5.5.1.3 Estimation of single phase heat transfer and friction factor using CFD.

The single phase heat transfer and friction characteristics with offset strip fins and wavy fins were also determined for liquid phase R134a using CFD. The details are presented in Chapter 3. The measured single phase heat transfer and pressure drop data for R134a are given in terms of the Colburn factor j and Fanning friction factor f . Colburn j and f data are given as a function Re . Colburn j factor is calculated using the expression (3.24) and (3.25) for wavy fin and (3.39) and (3.40) for offset strip fin and

Friction factor f is calculated from the equation (3.28) and (3.29) for wavy fin and equations (3.41) and (3.42) for offset strip fins.

5.5.2 Two-phase heat transfer and pressure drop coefficients

5.5.2.1 Two-phase heat transfer coefficient

The evaporation temperature is saturation temperature and evaporation pressure is saturation pressure of the refrigerant,

$$T_{ev}=T_{sat}; P_{ev}= P_{sat} \quad (5.7)$$

The specific enthalpies of the refrigerant at the evaporator inlet and outlet, H_{evi} and H_{evo} , are calculated with the measured temperatures and pressures at the inlet and outlet of the evaporator.

$$H_{evi}=f(T_{evi}, P_{evi}) ; H_{evo}=f(T_{evo}, P_{evo}) \quad (5.8)$$

The evaporator inlet quality is controlled by the electronic expansion valve. The vapour quality at the inlet and outlet of the test channel is given by state variables enthalpy and pressure.

$$(x_{evo} - x_{evi}) = \frac{\dot{m}_w c_p (T_{wi} - T_{wo})}{\dot{m}_r h_{fg}} \quad (5.9)$$

$$x_{evi} = \frac{H_{expo} - (H_{evi})_{sat}}{(H_{evo} - H_{evi})_{sat}} \quad (5.10)$$

The local vapour quality inside test section at every position z from the channel inlet to the channel outlet are calculated from the equation.

$$x_z = x_{evi} + \frac{Q z}{\dot{m}_L h_{fg}} \quad (5.11)$$

Where

$$Q = \dot{m}_w c_p (T_{wi} - T_{wo}) \quad (5.12)$$

Energy balance in the test section was verified by calculating the heat lost by water and comparing it with latent heat of vaporization of refrigerant.

$$\dot{m}_w c_p (T_{wi} - T_{wo}) = (x_{evo} - x_{evi}) \dot{m}_r h_{fg} \quad (5.13)$$

The two- phase heat transfer coefficient on refrigerant is given by equation

$$h_{tp} = \frac{Q}{(A_p + \eta_f A_s)(T_{wall} - T_{ev})} \quad (5.14)$$

$$\text{Fin efficiency, } \eta_f = \frac{\tanh \left(\frac{mH}{m} \right)}{mH} \quad (5.15)$$

$$m = \left[\frac{2h_{tp}(t+1)}{k_s t l} \right]^{0.5} \quad (5.16)$$

T_{wall} is the mean wall temperature of two adjacent wall temperatures measured at each axial position in the refrigerant flow direction in the test section.

$$T_{wall11} = \frac{TC_1 + TC_2}{2} \quad (5.17)$$

$T_{ev} = T_{sat}$ = Inlet temperature of the test section

Heat is transferred from water to refrigerant liquid by nucleate boiling as well as by two-phase convective mechanisms. The boiling heat transfer coefficient on the refrigerant, h_{tp} , is sum of the convective term h_{cb} and the nucleate boiling term h_{nb} as proposed by Chen (1966)

$$h_{tp} = h_{cb} + h_{nb} \quad (5.18)$$

The convective heat transfer coefficient h_{cb} is related with single-phase heat transfer coefficient h_l by the Reynolds number factor F .

$$h_{cb} = F h_l \quad (5.19)$$

$$F = \frac{h_{cb}}{h_l} \quad (5.20)$$

Where h_l can be obtained from single phase experimental heat transfer data. The Reynolds number factor has generally been postulated to be a function of Lockhart and Martinelli parameter X

$$X = \left(\frac{(dp/dz)_{F,l}}{(dp/dz)_{F,v}} \right)^{0.5} = \left(\frac{\Delta P_l}{\Delta P_v} \right)_F^{0.5} = \frac{1-x}{x} \left(\frac{f_l v_l}{f_v v_v} \right)^{0.5} \quad (5.21)$$

Where f_l liquid friction factor and f_v is vapour friction factor.

Nucleate boiling heat transfer coefficient will be contributed both the primary and secondary surface are as Kim and Sohn (2006).

$$h_{nb} = \frac{h_{nb,p} A_p + h_{nb,s} \eta A_s}{A_p + \eta A_s} \quad (5.22)$$

Nucleate boiling component h_{nb} , is predicted by Suppression factor S and Pool boiling heat transfer coefficient proposed by Nishikawa et al. (1982)

$$h_{nb} = S h_{pb} \quad (5.23)$$

$$h_{pb} = 31.4 \left(\frac{P_c^{0.2}}{M^{0.1}} \frac{F_p}{T_c^{0.9}} \right) q^{0.8} \quad (5.24)$$

$$F_p = \left(\frac{p}{p_c}\right)^{0.23} / \left[1.0 - 0.99 \left(\frac{p}{p_c}\right)\right]^{0.9} \quad (5.25)$$

Where M is molecular weight and q is the local heat flux.

Suppression factor proposed by Bennett et al. (1980) is directly extended to the flow boiling in a channel with offset strip fins in the present study.

$$S = \frac{24.4}{N_B} [1 - \exp(-0.041N_B)] \quad (5.26)$$

$$N_B = \frac{h_l}{k_l} \left[\frac{\sigma}{g(\rho_l - \rho_v)} \right]^{0.5} \quad (5.27)$$

Where σ is the surface tension and ρ is the density

Flow boiling heat transfer coefficient measured by experimentally and predicted by equation (5.9) shall be compared and presented.

5.5.2.2 Two-phase pressure drop coefficient

The two-phase pressure gradient in the boiling channel mainly consists of the frictional, acceleration and gravitational pressure gradients. Sum of other form losses in the channel due inlet/outlet header, expansion and contraction are also included. Assumed fully liquid at the inlet of the test section and fully vapour at exit of the test section for the entrance loss and exit losses calculation. Neglected the entrance and exit effects. The overall pressure drop in the test section for a vapour–liquid mixture over a length L is estimated using equation.

$$\Delta P_{tp} = \Delta P_{IH} + \Delta P_F + \Delta P_A + \Delta P_G + \Delta P_{OH} \quad (5.28)$$

The acceleration pressure gradient can be expressed as

$$\Delta P_A = \dot{G}^2 \left[\frac{x^2 v_g}{\alpha} + \frac{(1-x)^2 v_l}{1-\alpha} - 1 \right] \quad (5.29)$$

Assuming the flow as a homogenous equilibrium model the void fraction α is expressed in terms of

$$\alpha = \frac{1}{1 + \left(\frac{1-x}{x}\right) \left(\frac{\rho_v}{\rho_l}\right)} \quad (5.30)$$

The gravitational pressure gradient can be expressed as

$$\Delta P_G = \left[\frac{\alpha}{v_g} + \frac{(1-\alpha)}{v_l} \right] gL \quad (5.31)$$

Inlet header enlargement pressure gradient can be expressed as

$$\Delta P_{IH} = -\frac{\dot{G}^2 v_l}{2} [2 \sigma_A (1 - \sigma_A)] \quad (5.32)$$

Outlet header contraction pressure gradient can be expressed as

$$\Delta P_{OH} = \frac{\dot{G}^2 v_g}{2} [1.5 (1 - \sigma_A^2)] \quad (5.33)$$

Two- phase frictional pressure gradient can be expressed as

$$\Delta P_F = \frac{2v_l \dot{G}^2 (1-x)^2 f \phi_f^2 L}{D_h} \quad (5.34)$$

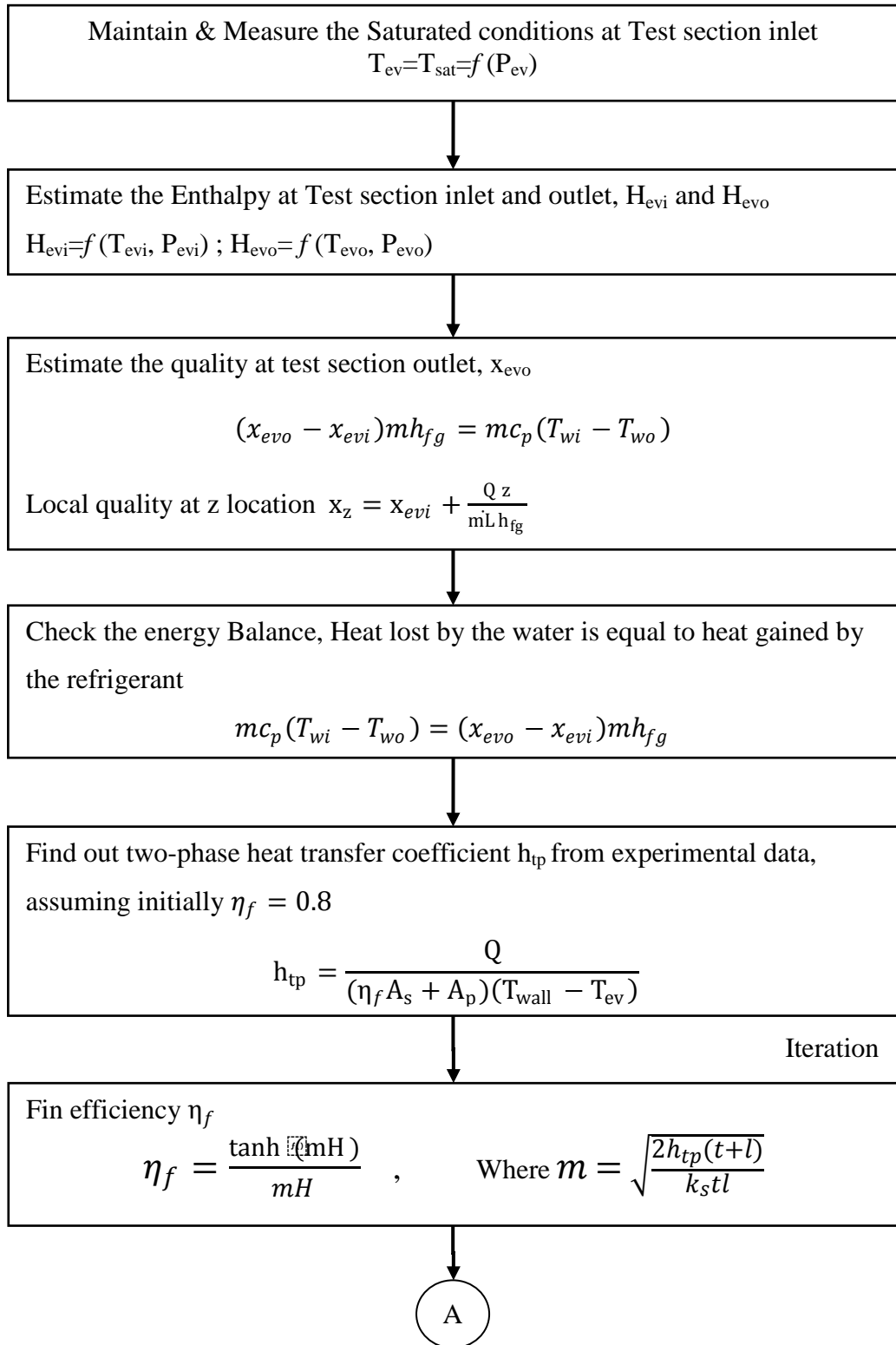
Where ΔP_{IE} is expansion losses in the inlet header, ΔP_{OH} is exit header contraction pressure losses, \dot{G} is the mass velocity, v is the specific volume, f is the fluid friction factor, α is the local void fraction, x is local quality and g denotes the gravitational acceleration.

The two-phase frictional multiplier in round tubes, ϕ_f^2 was uniquely correlated as a function of a parameter X by Lockhart and Martinelli (1949), where

$$\phi_f^2 = 1 + \frac{C}{X} + \frac{1}{X^2} \quad (5.35)$$

Where X is Martinelli parameter, X is calculated using equation (Eqn.5.14) and constant C depends upon the flow characteristics of each phase. In case of tubes, for fully turbulent vapour phase $C = 12$ when liquid is laminar, $C=20$ when liquid is turbulent. Two phase pressure drop coefficient of offset strip and wavy will be expressed in above form.

Pictorial representation of data reduction for two-phase heat transfer and pressure drop coefficients is shown Fig. 5.6 and 5.7 respectively.



A

$$h_{tp} = h_{tp-Exp} = h_{cb} + h_{nb}$$

The convective heat transfer coefficient h_{cb} is related with single-phase heat transfer coefficient h_f by the Reynolds number factor F,

$$F = \frac{h_{cb}}{h_l}$$

Find out single phase heat transfer coefficient h_l from the single phase correlations numerically developed or from experimental data.

$$j = C (R_e)^{a_0} (\alpha)^{a_1} (\beta)^{a_2} (\gamma)^{a_3}$$

Find out F by assuming h_{nb} as zero (neglecting the nucleate contribution) and substituting h_{tp} in h_{cb}

Find out Martinelli Parameter X by substituting f_f and f_v

$$X = \frac{1-x}{x} \left(\frac{f_l v_l}{f_v v_v} \right)^{0.5}$$

Two-phase Reynolds number generally been postulated to be a function of X. Plot the graph between F and $1/X$, for the case $1/X > 0$, Excluding the data for which the nucleate boiling was dominant, $1/X < 1$ and partial dry out heat transfer coefficient.

B

B

Find out the correlation for two-phase Reynolds number factor from the graph in the form of

$$F = \left[1 + \frac{1}{X} \right]^{0.5}$$

This gives the two-phase convective heat transfer coefficient

Estimation of h_{tp-Pre} and comparison with h_{tp-Exp}

$$\begin{aligned} h_{tp-Pre} &= h_{cb} + h_{nb} \\ h_{tp-Pre} &= F h_l + S h_{pb} \end{aligned}$$

Even though in flow boiling convective component is predominant, there will be small nucleate boiling effect due to wall super heat at low vapour qualities.

The nucleate boiling contribution can be estimated using expression

$$h_{nb} = \frac{h_{nb,p} A_p + h_{nb,s} \eta A_s}{A_p + \eta A_s}$$

The nucleate boiling component is expressed in terms of suppression factor S and pool boiling component

$$h_{nb} = S h_{pb}$$

Since there are no correlations available for fins for estimation S and h_{pb} , correlation available for round tubes is extended for estimation of pool boiling and suppression factor S

$$h_{pb} = 31.4 \left(\frac{P_c^{0.2}}{M^{0.1}} \frac{F_p}{T_c^{0.9}} \right) q^{0.8}, \quad F_p = \frac{\left(\frac{p}{p_c} \right)^{0.23}}{\left[1.0 - 0.99 \left(\frac{p}{p_c} \right) \right]^{0.9}}$$

C

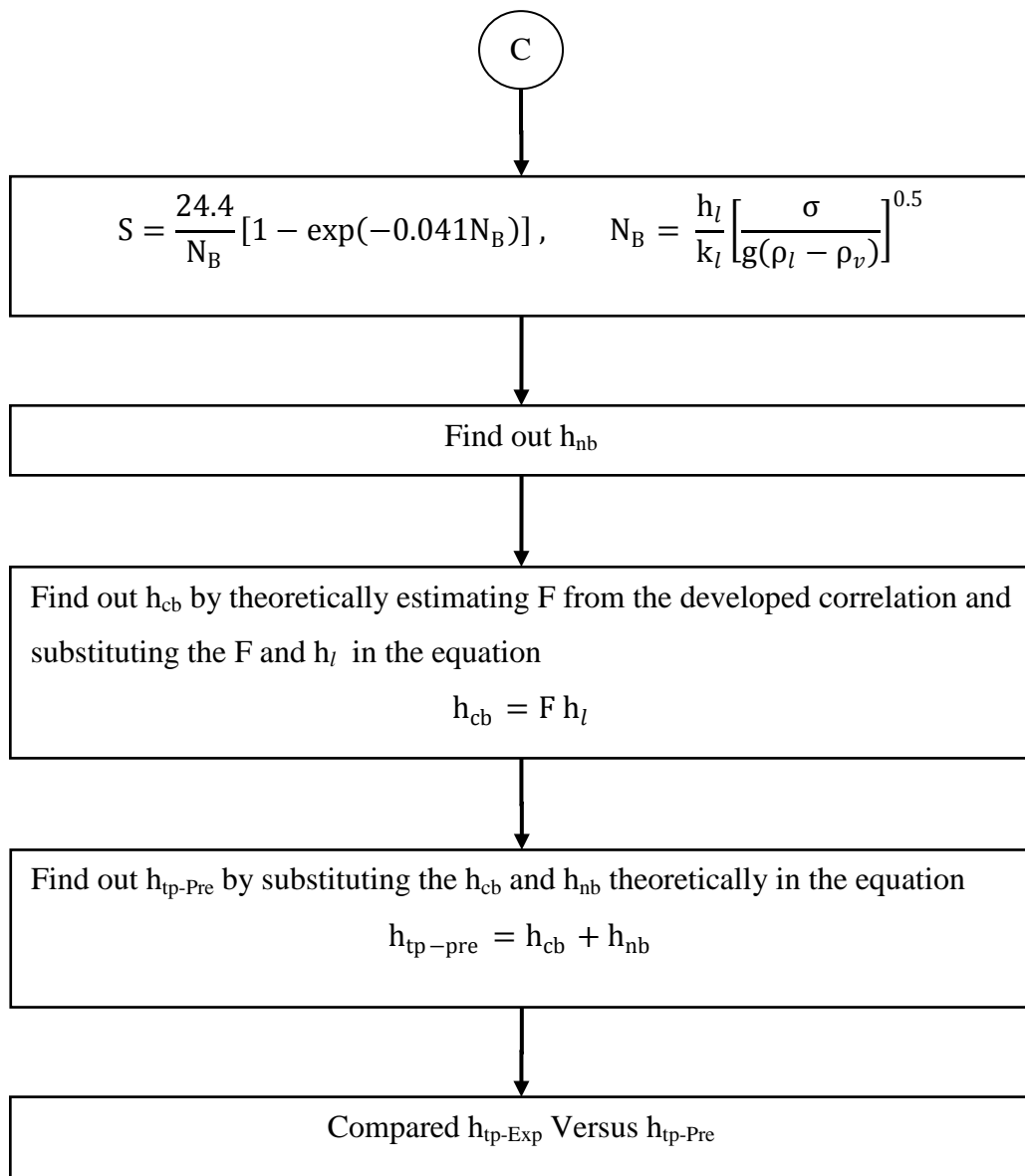


Fig 5.6: Pictorial Representation of data reduction for two-phase heat transfer coefficient

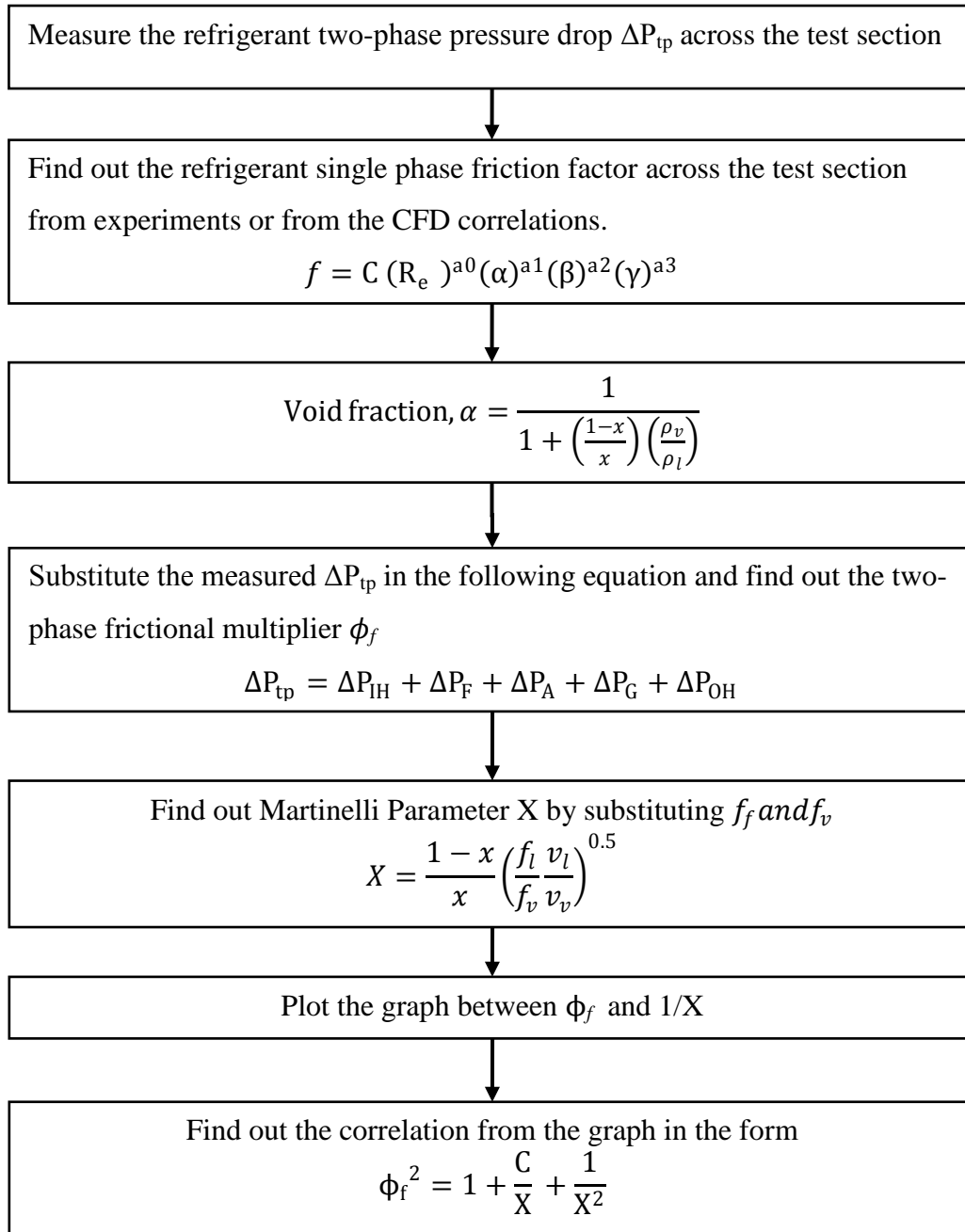


Fig 5.7: Pictorial Representation of data reduction for two-phase pressure drop

With the above steps the measured data is reduced to the results. The calculated values of some representative results of offset strip fin OSF1 presented in Table. 5.9 a & b for single phase j and f factors and in Table 5.10 and 5.11 for two-phase heat transfer coefficient and friction coefficient respectively.

Table 5.9: Sample results of j and f factors

Table 5.9a: j factor data

\dot{m}_r kg/s	\dot{m}_w LPM	T_{ri} °C	T_{ro} °C	T_{win} °C	T_{wout} °C	T_{wall} °C	\dot{G} kg/m ² s	Re	Pr	j	h_1 W/m ² K
0.0108	2.83	18.1	28.5	29.35	28.5	28.6	29	171.46	3.52	0.0213	383.20
0.0124	2.84	18.2	28.9	29.2	28.2	29.0	34	197.47	3.52	0.0196	405.03
0.0158	2.84	18.1	29.6	30.7	29.3	30.0	43	252.39	3.51	0.0193	509.46
0.0175	2.84	18.1	30.0	31.0	29.5	30.2	47	280.41	3.51	0.0188	548.56
0.0200	2.85	18.3	31.6	32.8	30.8	31.8	54	324.10	3.50	0.0192	645.36

Table 5.9b: f factor data

\dot{m} LPM	ΔP_{total} mbar	T_{in} °C	σ_A	σ_B	k_c	k_e	\dot{G} kg/m ² s	Re	f
3.05	8.50	30.00	0.0595	0.1090	1.20	0.70	138	164	0.1942
4.10	12.80	30.00	0.0595	0.1090	1.20	0.70	185	220	0.1606
5.04	17.00	30.00	0.0595	0.1090	1.20	0.70	228	270	0.1403
6.12	22.55	30.00	0.0595	0.1090	1.20	0.70	277	328	0.1254
7.03	28.60	30.00	0.0595	0.1090	1.20	0.70	318	377	0.1203

Table 5.10: Sample results data of two-phase heat transfer coefficient

SL. No	\dot{G} kg/m ² s	q kW/m ²	Vapour quality, x				x_{exit}	Two- phase heat transfer coefficient h_{tp} , W/m ² K				h_l W/m ² K
			x_1	x_2	x_3	x_4		h_{tp1}	h_{tp2}	h_{tp3}	h_{tp4}	
1	63	14	0.049	0.179	0.292	0.439	0.487	2152	2513	2566	2942	475.426
		16	0.057	0.210	0.343	0.515	0.572	2614	3279	3703	3905	475.457
		18	0.066	0.243	0.397	0.596	0.662	2719	3780	3961	4057	475.447
		21	0.075	0.277	0.453	0.679	0.754	3127	4080	4313	4170	474.351
2	82	14	0.038	0.138	0.227	0.340	0.378	2482	3604	3832	4386	549.221
		16	0.045	0.166	0.271	0.407	0.452	3085	5012	5802	6038	549.409
		18	0.051	0.188	0.307	0.461	0.512	3273	5435	6241	6480	550.467
		21	0.059	0.215	0.353	0.529	0.588	3741	5982	6592	6592	549.865

Martinelli Parameter X				Reynolds number factor F				N_B	F_p	S	h_{pb} W/m ² K	h_{nb} W/m ² K
X_1	X_2	X_3	X_4	F_1	F_2	F_3	F_4					
0.50	2.12	4.02	7.61	4.527	5.285	5.398	6.188	4.957	0.640	0.905	660.272	597.738
0.59	2.57	5.07	10.29	5.498	6.896	7.789	8.213	4.958	0.642	0.905	752.267	681.014
0.69	3.11	6.39	14.30	5.719	7.951	8.330	8.533	4.957	0.641	0.905	844.647	764.646
0.79	3.69	7.98	20.40	6.593	8.601	9.092	8.791	4.946	0.643	0.905	936.016	847.551
0.35	1.44	2.63	4.61	4.520	6.562	6.978	7.986	5.727	0.664	0.892	678.656	605.103
0.41	1.74	3.26	6.01	5.616	9.123	10.560	10.990	5.729	0.670	0.892	788.425	702.954
0.47	2.01	3.86	7.43	5.946	9.873	11.338	11.772	5.740	0.671	0.891	874.554	779.579
0.54	2.39	4.74	9.76	6.804	10.878	11.988	11.988	5.734	0.671	0.892	974.923	869.155

Table 5.11: Sample results data of two- phase pressure drop coefficient

SL.No	\dot{G} kg/m ² s	Exit vapour quality x	Pressure drop, ΔP_{total} mbar	σ_A	F	Void fraction α	Differential pressures in Pascals					1/X	ϕ_f
							ΔP_{IH}	ΔP_{OH}	ΔP_A	ΔP_G	ΔP_F		
1	63	0.350	82.073	0.060	0.1438	0.981	215.495	0.171	-3866.09	56.75	11801.313	5.23	16.100
		0.487	96.557	0.060	0.1440	0.989	216.769	0.171	-3822.26	40.83	13220.503	9.26	21.600
		0.572	98.626	0.060	0.1437	0.992	214.546	0.171	-3799.56	35.23	13412.530	12.96	26.101
		0.662	104.143	0.060	0.1438	0.995	215.287	0.171	-3773.44	30.43	13942.233	19.00	38.660
		0.754	108.282	0.060	0.1438	0.997	211.232	0.170	-3717.13	27.04	14307.185	29.62	47.082
3	82	0.320	94.488	0.060	0.1213	0.975	318.594	0.293	-6584.02	70.69	15643.796	4.25	14.857
		0.378	102.764	0.060	0.1212	0.980	312.507	0.291	-6513.38	60.96	16416.600	5.44	16.683
		0.452	111.040	0.060	0.1203	0.984	298.790	0.292	-6490.85	53.48	17242.913	7.23	19.484
		0.512	113.799	0.060	0.1198	0.988	297.013	0.294	-6512.84	47.98	17548.067	9.13	22.035
		0.588	100.007	0.060	0.1199	0.991	295.833	0.293	-6457.44	41.94	18120.609	12.40	28.537

Similarly single phase heat transfer and pressure drop coefficients, two-phase heat transfer and pressure drop coefficients are estimated for OSF2, WF1 and WF2 fin surfaces from measured experimental data.

5.6 MEASUREMENT OF LUBRICATING OIL CONCENTRATION

Poly ester oil is used in the vapour compression cycle system to provide lubrication for compressors. During system operation some % of lubrication oil mixes with refrigerant eventhough sytem is equipped with two levels of oil separting system. To estimate the concentration of oil mixed in the refrigerant R134a the following method was carryied out. During charging the system pure refrigerant was ensured. After completion of test points on each test section the % of oil mixing was measured as per procedure given below.

1. Taken the emty cylinder and evacuated. Masured the weight of the emty cyclinder using digital weight balance and noted.
2. Collected the refrigerant from the sampling port and stored in the cyclinder.
3. Measured the weight of cyclinder with refrigerant as shwon in the Fig 5.8 and noted the reading.



Fig 5.8: Measurement of % of lubricating oil mixing

4. Opened the cylinder cap and vented the refrigerant from the cylinder. The refrigerant was evaporated and lubricating oil was settled at bottom of the cyclinder.
5. After venting, the weight of the cylinder was measred. The measurements are provided in the Table 5.12.

Table 5.12: Measurement of weight of oil mixing

SL. No	Empty weight of the cylinder in gms	Weight of the cylinder + Refrigerant collected in gms	Net weight	Weight of the cylinder after venting in gms	%of oil mixed
1	775	1043gms	268 gms	776.2	0.5%
2	775	1040 gms	265 gms	776	0.3%
3	775	1055 gms	280 gms	776.3	0.4%

The procedure was repeated for all the test sections and estimated % of oil mixing. Oil mixing in the refrigerant was found less than 0.5% in all the cases.

5.7 ERROR AND UNCERTAINTY ANALYSIS

Errors and uncertainties are generated from disturbances, instrument selection and condition, calibration, environment, observation process. But it is important to find out accuracy level of the measuring instruments and method. It needs to find out propagated error in result due to error in measurement.

The parameters which are measured for the present study are mass flow rate, pressure and temperatures. The uncertainty associated with temperature, pressure and mass flow rate is specified by manufacturer is provided in Table 5.13

Table 5.13: Accuracy of measuring instruments provided by manufacturer

SL.No	Devices	Type	Range	Accuracy
1	Resistance thermometers	RTD	-40 to 100 °C	±0.15°C
2	Thermocouples	Type K	-40 to 250 °C	±0.5°C
3	Refrigerant flow meter	Coriolis	0.003 to 0.09 kg/s	±0.05% for liquid and ±0.035% for gas
4	Water flow meter	Turbine	1-60 LPM	±3%
5	Pressure transducers	Strain gage	0-20 bar abs	±0.25% F.S
6	Differential Pressure transducers	Strain gage	0-5PSI	±0.25% F.S

Uncertainty in mass flux, heat flux, quality and propagated error in two-phase heat transfer coefficient h_{tp} is presented in this section. Kline and McClintock method is used to find out the propagated error.

Suppose Y is function of several variables,

$$Y = f(y_1, y_2, y_3, y_4, \dots, y_n)$$

Where Y is the quantity of interest, $y_1, y_2, y_3, y_4, \dots, y_n$ are independent variables.

Let W_Y be the resultant uncertainty and $W_{y_1}, W_{y_2}, W_{y_3}, \dots, W_{y_n}$ be the uncertainties in the independent variables $y_1, y_2, y_3, \dots, y_n$ respectively. The uncertainty in the result is given by

$$W_Y = \sqrt{\left(\frac{\partial Y}{\partial y_1}\right)^2 W_{y_1}^2 + \left(\frac{\partial Y}{\partial y_2}\right)^2 W_{y_2}^2 + \left(\frac{\partial Y}{\partial y_3}\right)^2 W_{y_3}^2 + \dots + \left(\frac{\partial Y}{\partial y_n}\right)^2 W_{y_n}^2} \quad (5.36)$$

Uncertainties of the following parameters are estimated using EES (Engineering Equation Solver) programme and placed in Table 5.14.

Uncertainty in temperature difference

$$\Delta T_w = T_{wo} - T_{wi} = 17.0 - 7.4 = 9.6^\circ\text{C}$$

$$\Delta T_w = f(T_{wo}, T_{wi})$$

$$W_{\Delta T_w} = \sqrt{\left(\frac{\partial \Delta T}{\partial T_{wo}}\right)^2 W_{T_{wo}}^2 + \left(\frac{\partial \Delta T}{\partial T_{wi}}\right)^2 W_{T_{wi}}^2} \quad (5.37)$$

$$W_{\Delta T_w} = 0.2121$$

$$W_{\Delta T_w} = \pm 2.2\%$$

Similarly uncertainty in wall temperature and evaporator inlet temperature is estimated

$$\Delta T_r = T_{wall} - T_{ev}$$

$$\Delta T_r = f(T_{wall}, T_{ev})$$

$$W_{\Delta T_r} = 0.522$$

$$W_{\Delta T_r} = \pm 4.58\%$$

Uncertainty in heat lost by the fluid (Water)

$$Q = \dot{m}_w C_p \Delta T$$

$$Q = f(\dot{m}_w, \Delta T)$$

$$W_Q = \sqrt{\left(\frac{\partial Q}{\partial \dot{m}_w}\right)^2 W_{\dot{m}_w}^2 + \left(\frac{\partial Q}{\partial \Delta T}\right)^2 W_{\Delta T}^2} \quad (5.38)$$

$$W_Q = 110.6$$

$$W_Q = \pm 3.72\%$$

Uncertainty in water mass flux \dot{G}_w ,

$$\dot{G}_w = \frac{\dot{m}_w}{A_{ff}} \quad (5.39)$$

$$\dot{G}_w = f(\dot{m}_w, A_{ff})$$

$$W_{\dot{G}_w} = \sqrt{\left(\frac{\partial \dot{G}_w}{\partial \dot{m}_w}\right)^2 W_{\dot{m}_w}^2 + \left(\frac{\partial \dot{G}_w}{\partial A_{ff}}\right)^2 W_{A_{ff}}^2} \quad (5.40)$$

$$W_{\dot{G}_w} = 1.865$$

$$W_{\dot{G}_w} = \pm 2.9\%$$

Uncertainty in refrigerant mass flux \dot{G}_r ,

$$\dot{G}_r = \frac{\dot{m}_r}{A_{ff}} \quad (5.41)$$

$$\dot{G}_r = f(\dot{m}_r, A_{ff})$$

$$W_{\dot{G}_r} = \sqrt{\left(\frac{\partial \dot{G}_r}{\partial \dot{m}_r}\right)^2 W_{\dot{m}_r}^2 + \left(\frac{\partial \dot{G}_r}{\partial A_{ff}}\right)^2 W_{A_{ff}}^2} \quad (5.42)$$

$$W_{\dot{G}_r} = 0.03216$$

$$W_{\dot{G}_r} = \pm 0.0004\%$$

Uncertainty in quality x ,

$$x = \frac{Q}{\dot{m}_r h_{fg}}$$

$$x = f(Q, \dot{m}_r)$$

$$W_x = \sqrt{\left(\frac{\partial x}{\partial \dot{m}_r}\right)^2 W_{\dot{m}_r}^2 + \left(\frac{\partial x}{\partial Q}\right)^2 W_Q^2} \quad (5.43)$$

$$W_x = 0.02245$$

$$W_x = \pm 3.726\%$$

Uncertainty in two-phase heat transfer coefficient

$$h_{tp} = \frac{Q}{(\eta_f A_s + A_p)(T_{wall} - T_{ev})}$$

$$h_{tp} = \frac{Q}{(\eta_f A_s + A_p) \Delta T_r}$$

$$h_{tp} = f(Q, \Delta T_r)$$

$$W_{h_{tp}} = \sqrt{\left(\frac{\partial h_{tp}}{\partial Q}\right)^2 W_Q^2 + \left(\frac{\partial h_{tp}}{\partial \Delta T_r}\right)^2 W_{\Delta T_r}^2} \quad (5.44)$$

$$W_{h_{tp}} = 124.5$$

$$W_{h_{tp}} = \pm 5.9\%$$

Uncertainty in single phase friction coefficient

$$f = \frac{\rho_l D_h \Delta P}{2L\dot{G}^2} \quad (5.45)$$

$$f = f(L, \dot{G}, \Delta P)$$

$$W_f = \sqrt{\left(\frac{\partial f}{\partial L}\right)^2 W_L^2 + \left(\frac{\partial f}{\partial \dot{G}}\right)^2 W_{\dot{G}}^2 + \left(\frac{\partial f}{\partial \Delta P}\right)^2 W_{\Delta P}^2} \quad (5.46)$$

$$W_f = 0.00477$$

$$W_f = 2.6\%$$

Uncertainty in single phase heat transfer coefficient

$$j = \frac{D_h}{4L} \ln \left[\frac{T_{wall} - T_{ri}}{T_{wall} - T_{ro}} \right] Pr^{\frac{2}{3}}$$

$$j = j(L, T_{wall}, T_{ri}, T_{ro})$$

$$W_j = \sqrt{\left(\frac{\partial j}{\partial L}\right)^2 W_L^2 + \left(\frac{\partial j}{\partial T_{wall}}\right)^2 W_{T_{wall}}^2 + \left(\frac{\partial j}{\partial T_{ri}}\right)^2 W_{T_{ri}}^2 + \left(\frac{\partial j}{\partial T_{ro}}\right)^2 W_{T_{ro}}^2} \quad (5.47)$$

$$W_j = 0.009685$$

$$W_j = 4.5\%$$

Uncertainty in two-phase frictional coefficient (Two- phase frictional multiplier)

$$\phi_f^2 = \frac{D_h \Delta P}{2L\dot{G}^2 v_l (1-x)^2 f} \quad (5.48)$$

$$\phi_f^2 = \phi_f^2(\Delta P_F, G, x, f, L)$$

$$W_{\phi_f^2} = \sqrt{\left(\frac{\partial \phi_f^2}{\partial L}\right)^2 W_L^2 + \left(\frac{\partial \phi_f^2}{\partial G}\right)^2 W_G^2 + \left(\frac{\partial \phi_f^2}{\partial x}\right)^2 W_x^2 + \left(\frac{\partial \phi_f^2}{\partial \Delta P_F}\right)^2 W_{\Delta P_F}^2 + \left(\frac{\partial \phi_f^2}{\partial f}\right)^2 W_f^2} \quad (5.49)$$

$$W_{\phi_f^2} = 8.224$$

$$W_{\phi_f^2} = 6.02\%$$

Uncertainty in Reynolds number factor

$$F = \frac{h_{cb}}{h_l}$$

$$F = f(h_{cb}, h_l)$$

$$W_F = \sqrt{\left(\frac{\partial F}{\partial h_{cb}}\right)^2 W_{h_{cb}}^2 + \left(\frac{\partial F}{\partial h_l}\right)^2 W_{h_l}^2} \quad (5.50)$$

$$W_F = 0.321, W_F = 7.4\%$$

Table 5.14: Summary of uncertainty estimated using EES Program

Parameters	Uncertainty
Water mass flux, \dot{G}_w	$\pm 2.9\%$
Refrigerant mass flux, \dot{G}	$\pm 0.0004\%$
Water heat load, Q	$\pm 3.72\%$
Vapour quality, x	$\pm 3.726\%$
Temperature difference, ΔT_w	$\pm 2.2\%$
Temperature difference, ΔT_r	$\pm 4.58\%$
Two- phase heat transfer coefficient, h_{tp}	$\pm 5.9\%$
Colburn j factor	$\pm 4.5\%$
Two-phase frictional multiplier, ϕ_f^2	$\pm 6.02\%$
Single phase friction coefficient, f	$\pm 2.5\%$
Reynolds number factor, F	$\pm 7.4\%$

5.8 SUMMARY

Experiments were carried out as per procedure on 4 fin surfaces of different fin geometrical parameters (2 offset strip fins surfaces and 2 wavy fin surfaces) by mounting on test setup. Measurements are noted at stabilized conditions and the measured data is used for further calculation and analysis. Experimental data were obtained for the heat transfer and pressure drop analysis. Before conducting the two phase experiments single phase experiments were conducted to check the energy balance and validate the measurement equipment, experimental procedure and technique. Experiments were performed on at different mass flux, heat flux and quality range. Measured data has been reduced and analysed. A total of 30 experiments both single phase and two-phase were conducted on each of test section.

CHAPTER 6

RESULTS AND DISCUSSIONS

Experiments were performed to analyse the flow boiling heat transfer and friction characteristics on plate fin surfaces. Experiments are carried out on the experimental apparatus described in Chapter 4 to study 2 offset strip and 2 wavy fin surfaces, on which no experimental data was previously available. This chapter contains a presentation of results, discussion of observed trends, two-phase heat transfer and pressure drop correlations developed for each fin surface and comparisons with previously published flow boiling correlations on fin surfaces. The analysis was done independently on each fin surface and data plotted for each fin surface separately.

Two-phase flow heat transfer and pressure drop characteristics through offset strip fin and wavy fin surfaces are evaluated for refrigerant R134a by varying the heat flux and mass flux at different vapour quality. The results for each surface are presented in this chapter.

6.1 SINGLE-PHASE HEAT TRANSFER AND PRESSURE DROP CHARACTERISTICS

Before conducting flow boiling experiments, the single-phase flow and heat transfer characteristics of the offset strip fins and wavy fins were determined first to check the energy balance and validate the measurement equipment, experimental procedure and technique. The refrigerant R134a is passed through test core in one side and water was allowed to pass through another side. The test was conducted at different mass flow rates. The measured single phase flow and heat transfer data for each fin surface is plotted in terms of the Colburn j -factor and friction factor f as a function of Reynolds number. R134a used as a test fluid for obtaining the j factor and water used as test fluid for obtaining the f factor.

The data is presented in Fig. 6.1 for offset strip fin, OSF1 and in Fig. 6.2 for wavy fin, WF1.

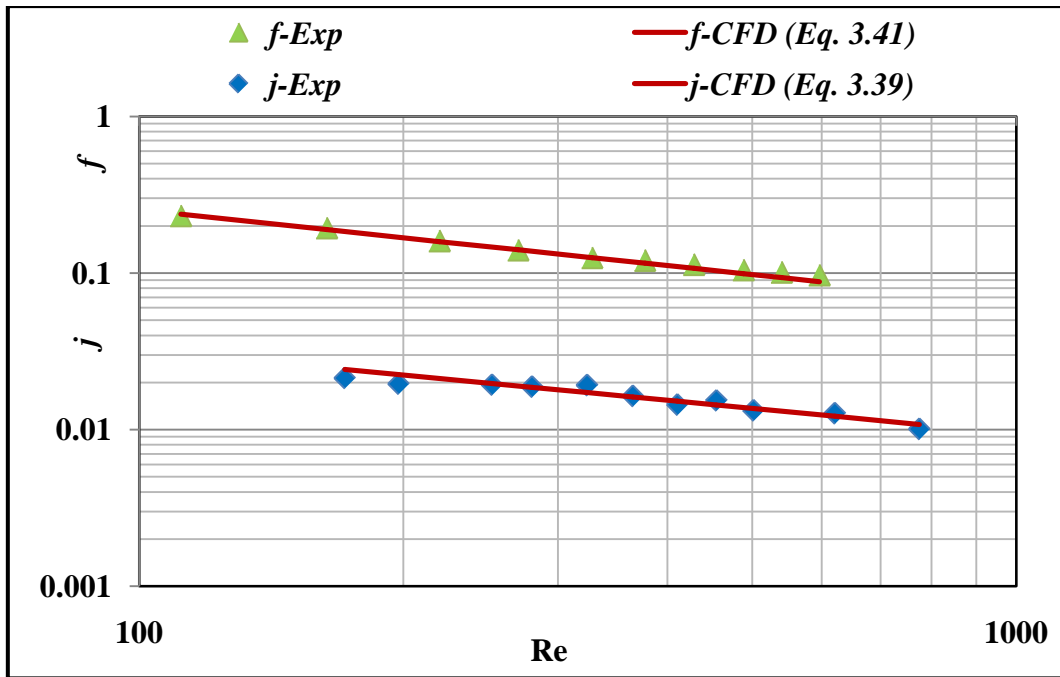


Fig 6.1: Flow friction factor f and j factor for OSF1

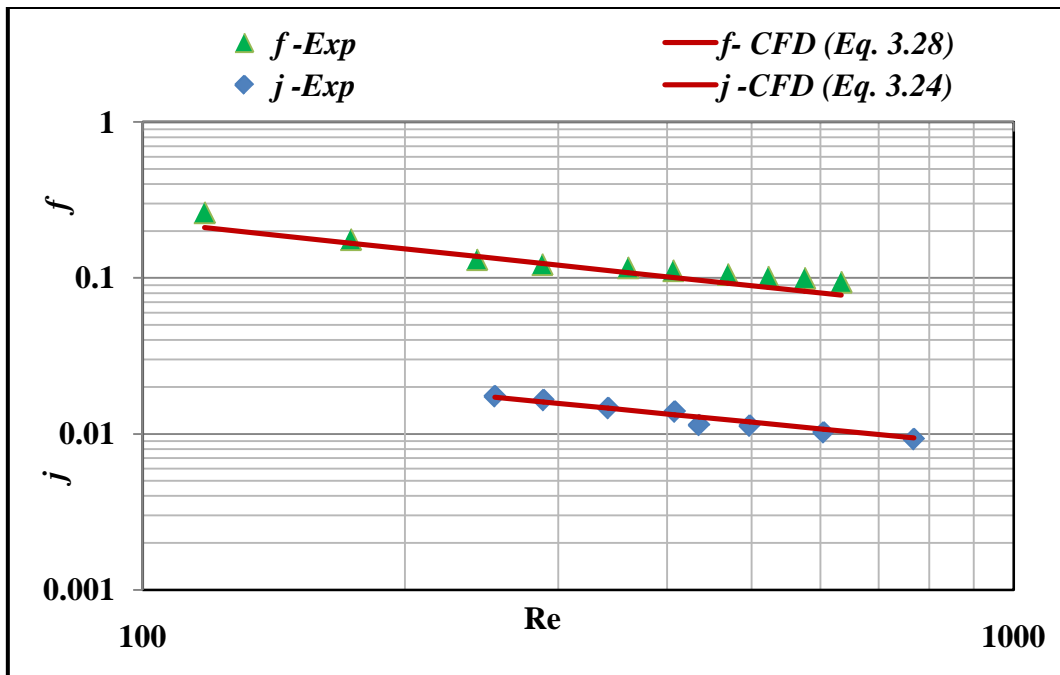


Fig 6.2: Flow friction factor f and j factor for WF1

From the above graphs it is observed that the Colburn j factor and friction factor decreases with increase Re . It is also found that CFD results are in good agreement with experimental results. The variation is found less than 5% in both ' f ' and ' j ' values.

6.2 TWO-PHASE HEAT TRANSFER CHARACTERISTICS

The primary interest in the heat transfer performance analysis is the refrigerant flow boiling heat transfer coefficient h_{tp} . The purpose of the analysis is the quantitative evaluation of this parameter, and its dependence on relevant flow properties (mainly \dot{G} , q and x). The experimental values of two-phase heat transfer coefficient, h_{tp} with quality at different mass fluxes and heat fluxes for flow boiling of R134a in the different types of fin are presented here.

Experimental results have been presented in Fig 6.3 to 6.26 in terms of h_{tp} vs quality plots. Fig 6.3 to 6.14 presents the results of experimented two offset strip fin surfaces, while Fig 6.15 to 6.26 presents the results for two wavy fins surfaces. The influence of the vapour quality x along the test section, z on the refrigerant heat transfer coefficient is shown in these graphs.

6.2.1 Heat transfer characteristics of offset fin surfaces.

Experiments were performed on 2 offset strip fin surfaces OSF1 and OSF2. Measured values of the local boiling heat transfer coefficient with vapour quality at selected heat inputs and mass velocities are plotted in the graphs. Fig. 6.3 to 6.14 shows plotted experimental data of two-phase heat transfer coefficient h_{tp} versus vapour quality x , for flow boiling in the test section/test evaporator.

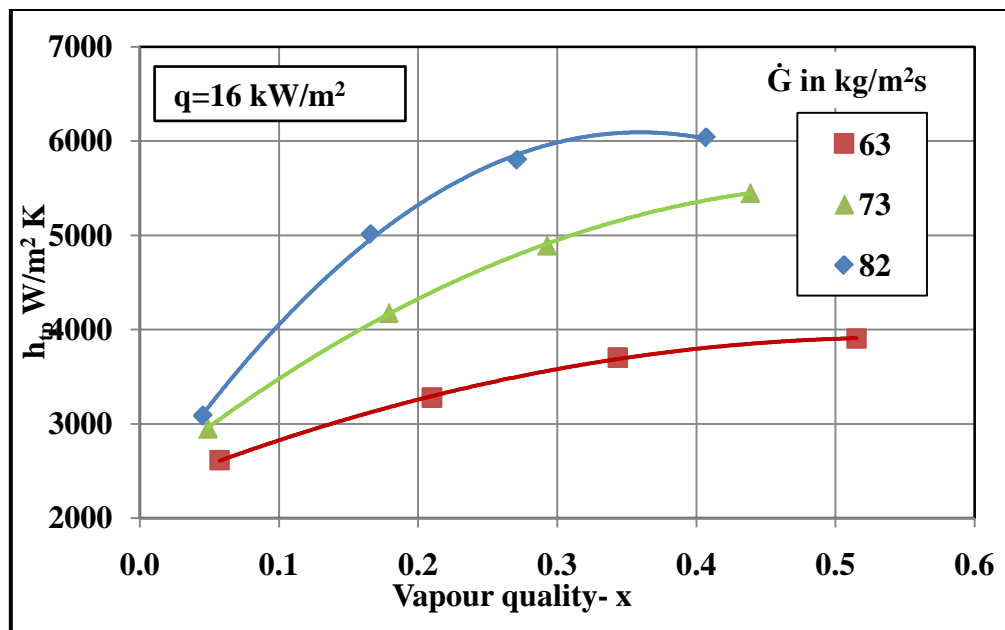


Fig. 6.3: Measured local two-phase heat transfer coefficient h_{tp} Vs vapour quality x at heat flux $q = 16 \text{ kW/m}^2$ for mass fluxes \dot{G} (63, 73 and 82 $\text{kg/m}^2\text{s}$) for fin surface OSF1

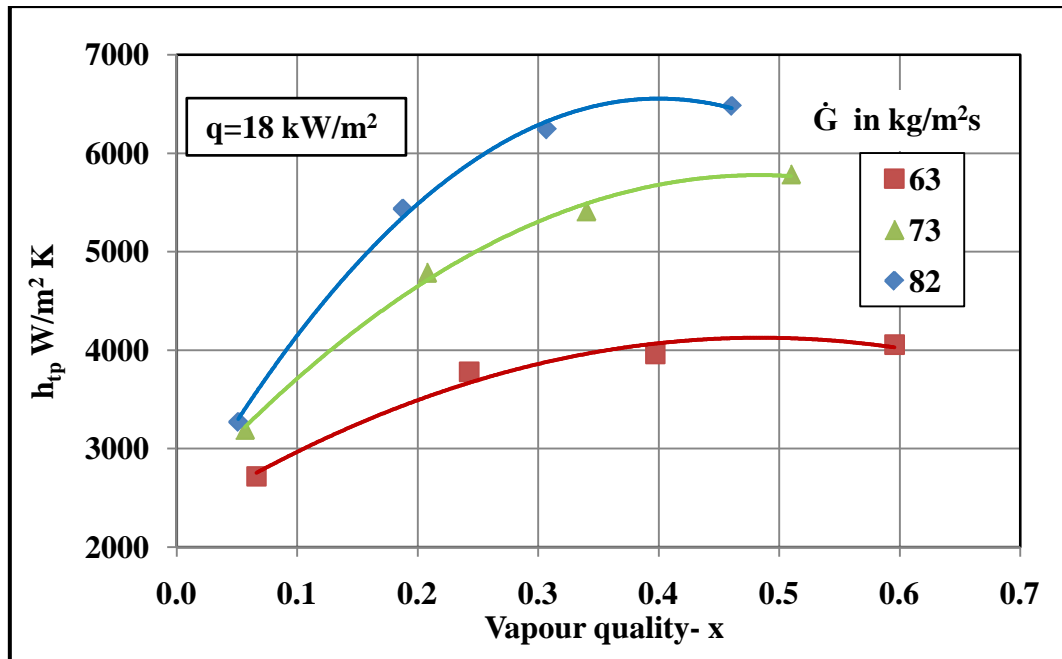


Fig. 6.4: Measured local two-phase heat transfer coefficient h_{tp} Vs vapour quality, x at heat flux $q = 18 \text{ kW/m}^2$ for mass fluxes \dot{G} (63, 73 and 82 kg/m²s) for fin surface OSF1

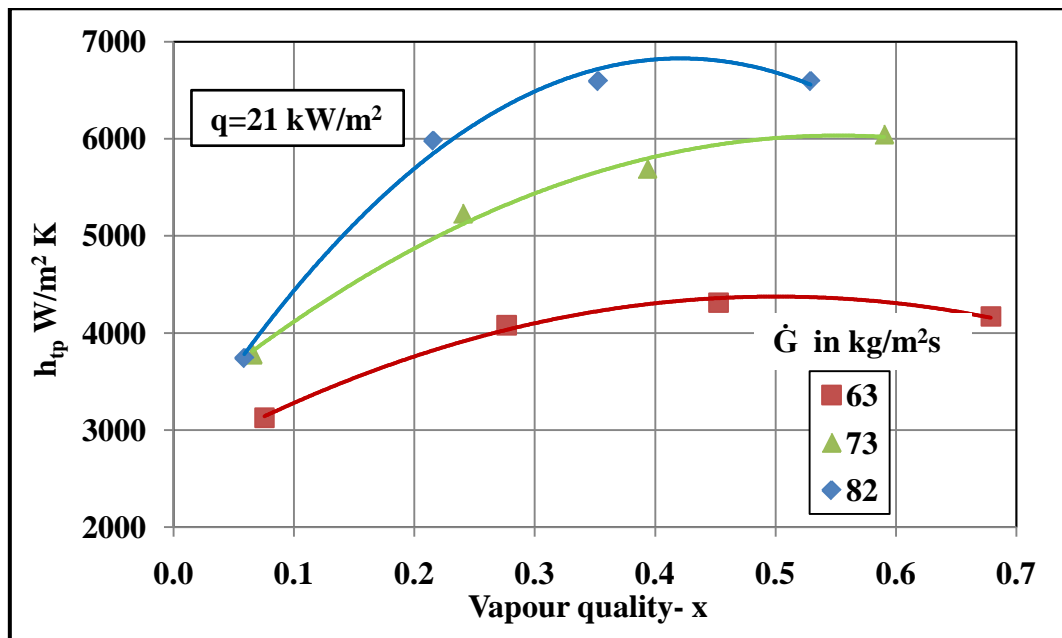


Fig. 6.5: Measured local two-phase heat transfer coefficient h_{tp} Vs vapour quality, x at heat flux $q = 21 \text{ kW/m}^2$ for mass fluxes \dot{G} (63, 73 and 82 kg/m²s) for fin surface OSF1

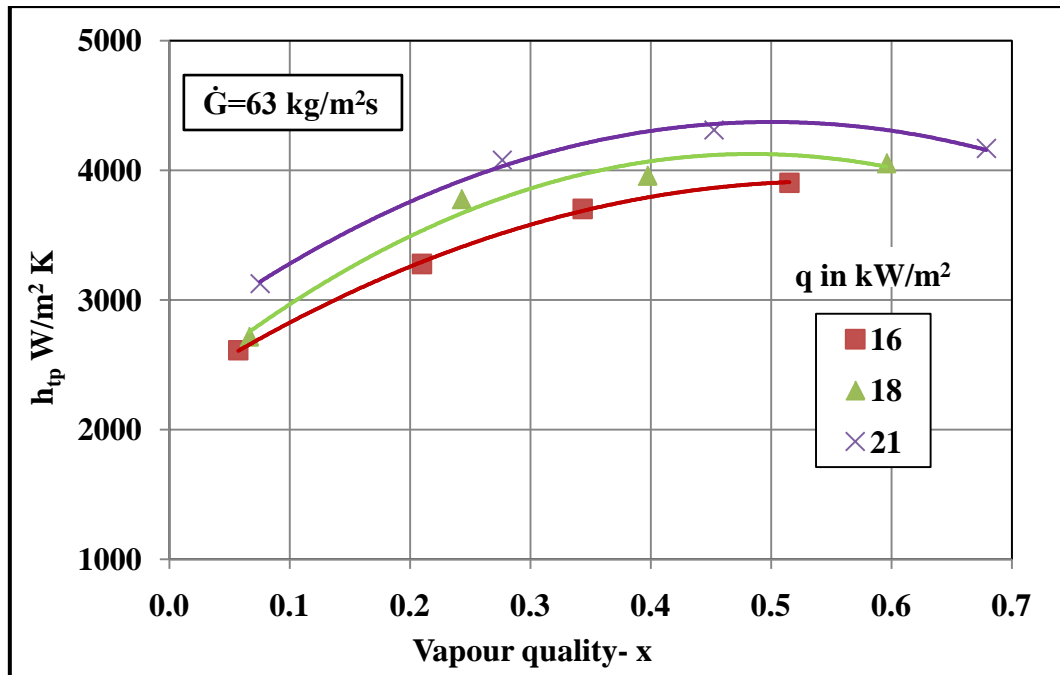


Fig. 6.6: Measured local two-phase heat transfer coefficient h_{tp} Vs vapour quality, x at mass flux $\dot{G}= 63 \text{ kg/m}^2\text{s}$ for three heat fluxes q (16, 18 and 21 kW/m^2) for fin surface OSF1

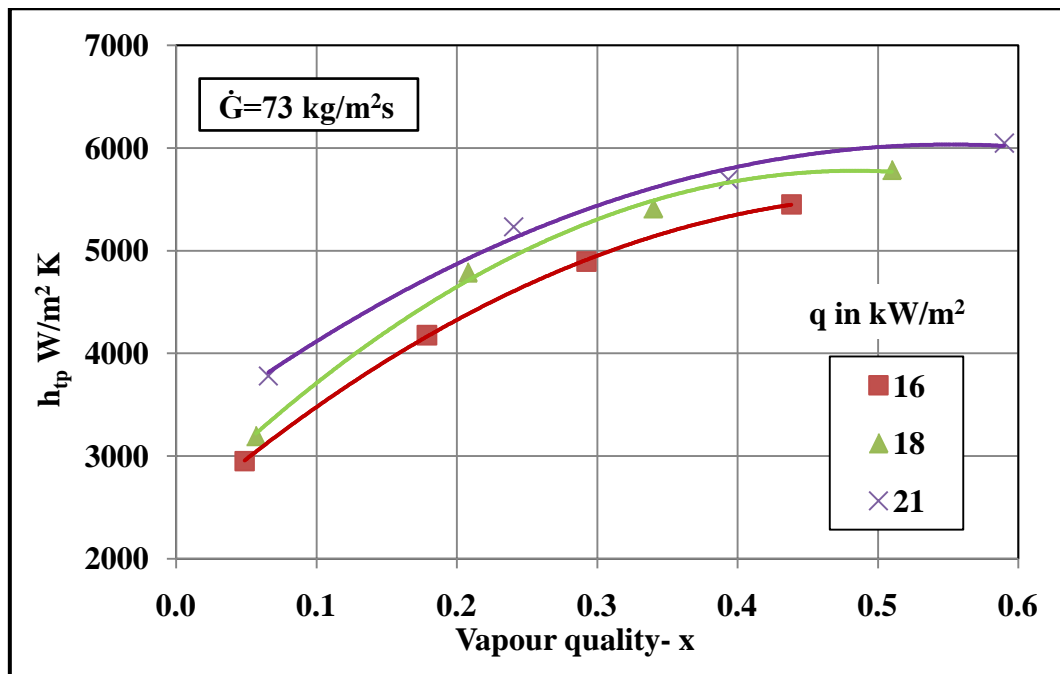


Fig. 6.7: Measured local two-phase heat transfer coefficient h_{tp} Vs vapour quality x at mass flux $\dot{G}= 73 \text{ kg/m}^2\text{s}$ for three heat fluxes q (16, 18 and 21 kW/m^2) for fin surface OSF1

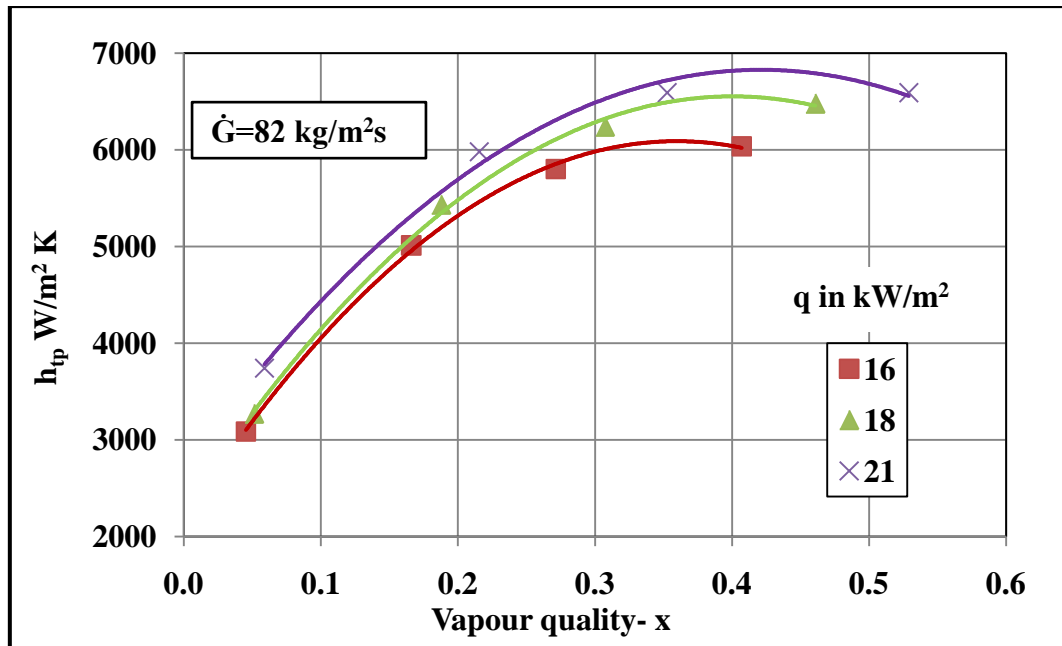


Fig. 6.8: Measured local two-phase heat transfer coefficient h_{tp} Vs vapour quality x at mass flux $\dot{G} = 82 \text{ kg/m}^2\text{s}$ for three heat fluxes q (16, 18 and 21 kW/m²) for fin surface OSF1

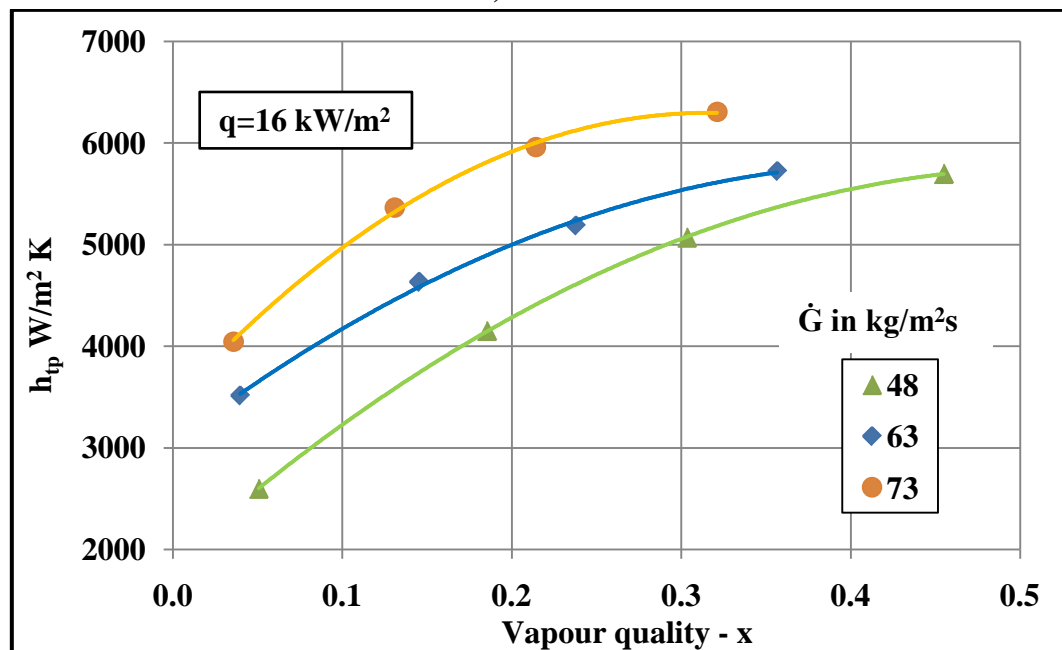


Fig. 6.9: Measured local two-phase heat transfer coefficient h_{tp} Vs vapour quality x at heat flux $q = 16 \text{ kW/m}^2$ for mass fluxes \dot{G} (48, 63 and 73 kg/m²s) for fin surface OSF2

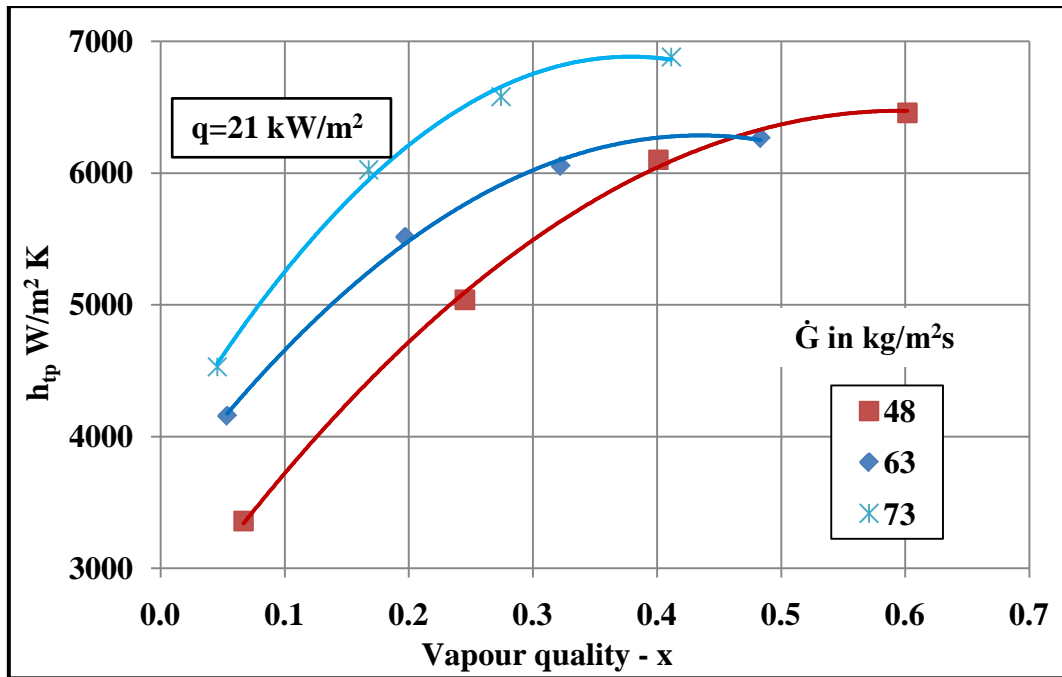


Fig. 6.10: Measured local two-phase heat transfer coefficient h_{tp} Vs vapour quality x at heat flux $q = 21 \text{ kW/m}^2$ for mass fluxes \dot{G} (48, 63 and $73 \text{ kg/m}^2\text{s}$) for fin surface OSF2

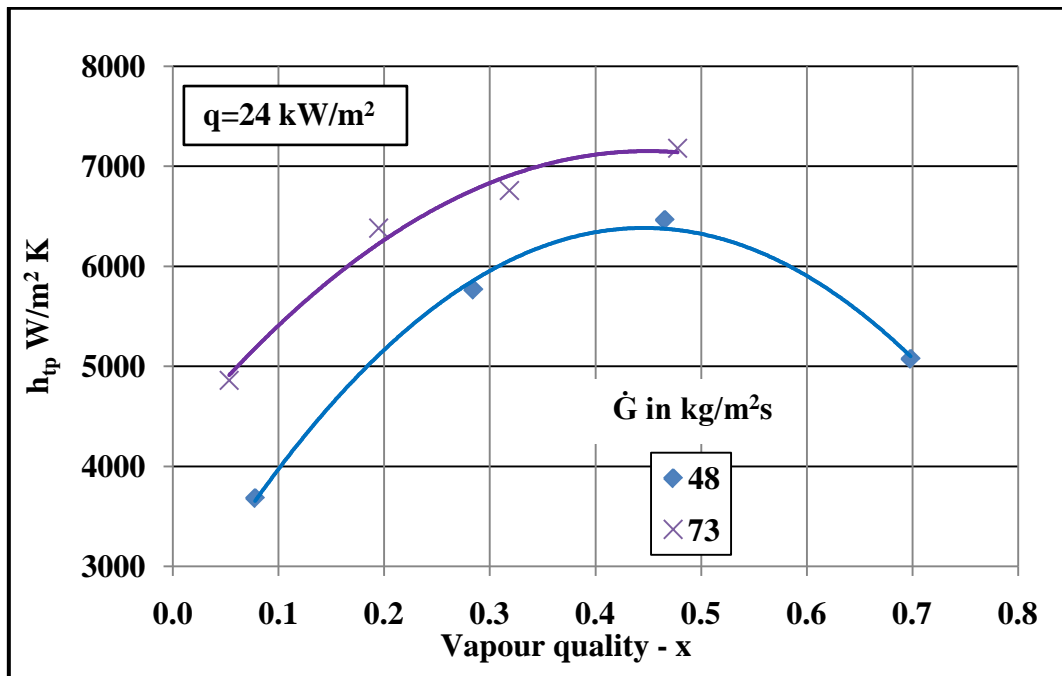


Fig. 6.11: Measured local two-phase heat transfer coefficient h_{tp} Vs vapour quality x at heat flux $q = 24 \text{ kW/m}^2$ for mass fluxes \dot{G} (48 and $73 \text{ kg/m}^2\text{s}$) for fin surface OSF2

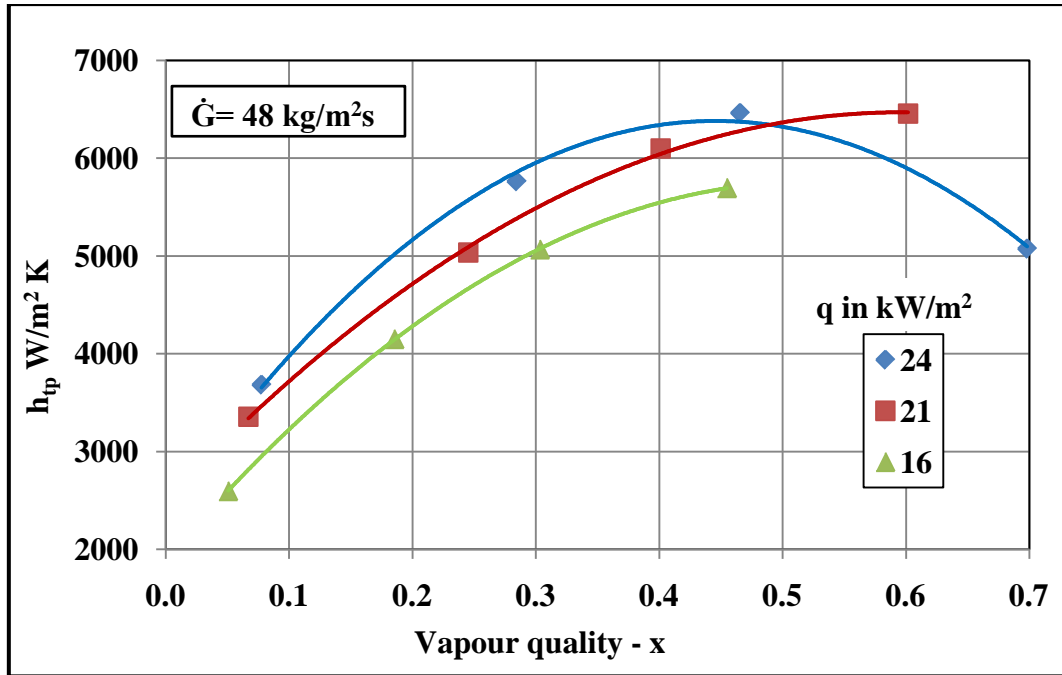


Fig. 6.12: Measured local two-phase heat transfer coefficient h_{tp} Vs vapour quality x at mass flux $\dot{G} = 48 \text{ kg/m}^2\text{s}$ for three heat fluxes q (16, 21 and 24 kW/m^2) for fin surface OSF2

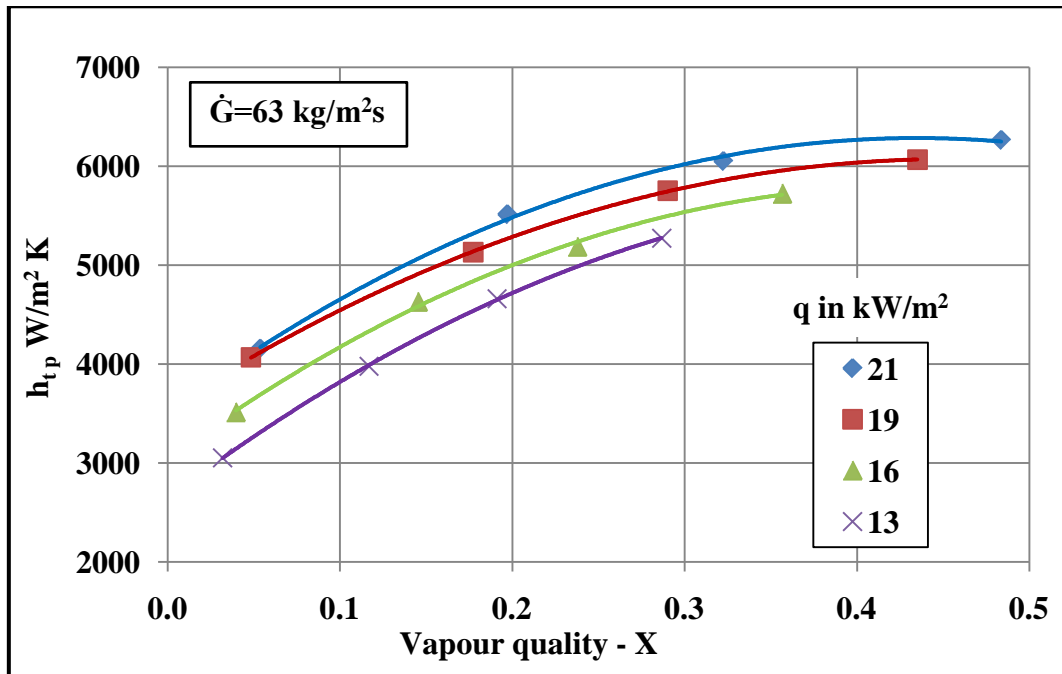


Fig. 6.13: Measured local two-phase heat transfer coefficient h_{tp} Vs vapour quality x at mass flux $\dot{G} = 63 \text{ kg/m}^2\text{s}$ for four heat fluxes q (13, 16, 21 and 24 kW/m^2) for fin surface OSF2

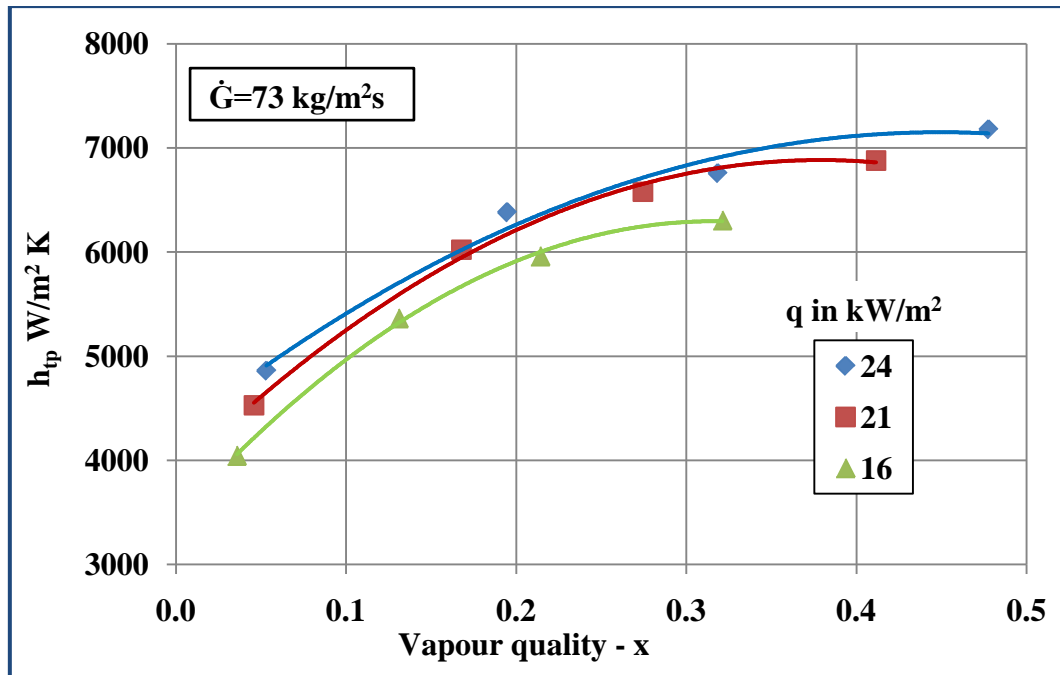


Fig. 6.14: Measured local two-phase heat transfer coefficient h_{tp} Vs vapour quality x at mass flux $\dot{G} = 73 \text{ kg/m}^2\text{s}$ for three heat fluxes q (16, 21 and 24 kW/m^2) for fin surface OSF2

From the above graphs, it is observed that two-phase heat transfer coefficient increases with the increase in mass flux and vapour quality. It is also observed that effect of heat flux is insignificant on two-phase heat transfer coefficient. Heat transfer coefficient shows a strong dependence on the mass flux and quality. Similar trends are observed in two test sections OSF1 and OSF2. The reasons for these trends are discussed in para 6.2.1.1.

Flow boiling heat transfer inside fin channels is governed by two mechanisms: nucleate boiling and convective boiling. Nucleate boiling is characterized by the formation of vapour bubbles at a heated surface when nucleation conditions i.e. a thin liquid layer near the surface superheated enough to allow nucleation, are reached. Convective boiling is characterized by heat transferred by conduction and convection through the liquid film and vaporization at the liquid/vapour interface. In nucleate-dominated flow boiling, the heat transfer coefficient increases with increasing heat flux (or wall super heat) and is independent of mass flux and vapour quality. On the other hand, in convective-dominated flow boiling (when nucleate boiling appears to be largely suppressed), the heat transfer coefficient is independent of heat flux (or

wall super heat) and increases with mass flux and vapour quality as discussed by Robertson and Wadekar (1988).

From the experimental tests, it is evident that heat transfer coefficient is depending on vapour quality. Flow boiling heat transfer coefficient is a resultant of nucleate boiling and liquid convection. At high heat fluxes and for low vapour qualities heat transfer is largely by the nucleate boiling, whereas at low heat fluxes and high vapour qualities convective boiling heat transfer is predominates as discussed in Kundu et al. (2014).

Nucleate boiling on the primary surface occurs concurrently with forced convection of liquid in fins. Hence, distinction between a nucleate boiling region and convective boiling region is very difficult with these types of fins in a channel. And also attaining uniform heat flux a channel with these type fins is difficult since the fin efficiency varies along the channel. It results in non uniform heat flux as explained by Kim and Sohn (2006). In the present study distinction between nucleate boiling region and convective boiling region is not able to identify.

6.2.1.1 Influence of flow properties on heat transfer coefficient

a) Influence of vapour quality:

Heat transfer coefficient increases with increase in vapour quality in the convective boiling region. This is due to the decrease in the liquid film thickness and an increased vapour phase velocity. Increase in heat transfer coefficient is mainly caused by the diminishing liquid film thickness at the liquid-vapour interface as the intense evaporation takes place in the channel. Diminishes the liquid film thickness, reduces the thermal resistance associated with heat conduction across the film. Thus nucleate boiling at high vapour qualities is suppressed due to significant cooling by the thinning of the annular flow. In the convective boiling region, for higher vapour quality a decrease of heat transfer coefficient supposed to be caused by disappearance of the liquid film covering the surface called emergence of the post dry out or total dry out region as explained by Mandrusiak et al. (1989). The heat transfer coefficient even falls toward the value of single-phase flow gas. The present study also shows the same occurrence. This phenomenon is seen in graphs Fig 6.5 & 6.6 of OSF1, Fig. 6.11 & 6.12 of OSF2. At higher qualities (approximately $x > 0.3$) correspond to

convective evaporation, the heat transfer coefficients increases stridently with quality. This increase proceeds until liquid film starts fading from fin surface (approximately $x > 0.5$), after that heat transfer coefficient starts decreasing even though the vapour quality increasing. In Fig. 6.3-6.8, the heat transfer coefficient of test evaporator OSF1 is evaluated as function of mass flux and heat flux over a range of vapour quality. In Fig. 6.9-6.14, the heat transfer coefficient of test evaporator OSF2 is evaluated as function of mass flux and heat flux over a range of vapour quality.

b) Influence of mass flux:

Local boiling heat transfer coefficients are reported for R134a in Fig. 6.3-6.5 and Fig. 6.9-6.11 against the mass velocity. The data reported at constant heat flux for varying mass fluxes. From the experimental data it can be clearly observed that the heat transfer coefficient increasing with respect to refrigerant mass flux. In fact increase of mass flux increases the fluid velocity, thus enhancing convective boiling heat transfer. The influence of mass flux is weak at very low quality region, i.e. corresponding to slug flow regimes, at which nucleate boiling is dominant. Increase in mass flux increases the interfacial shear stress; hence, the bubbles on the heated surface are carried forward from fin surface under influence of shear stress. The bubbles do not attain the larger diameters as seen in pool boiling. In Fig. 6.3-6.5, the heat transfer coefficient of test evaporator OSF1 is evaluated as function of mass flux of varying vapour quality at constant heat flux of 16, 18 and 21 kW/m² respectively. In Fig 6.9-6.11, the heat transfer coefficient of test evaporator OSF2 is evaluated as function of mass flux of varying vapour quality at constant heat flux of 16, 21 and 24 kW/m² respectively. It is understood that at higher mass flux and vapour quality the two-phase mixture flows at higher velocity, which promotes convective heat transfer.

c) Influence of heat flux:

The effect of heat flux over local boiling heat transfer coefficients are reported for R134a in Fig. 6.6-6.8 and Fig. 6.12-6.14. The data reported for refrigerant fluid at constant mass flux at different heat fluxes. In Fig. 6.6-6.8, the heat transfer coefficient of test evaporator OSF1 is evaluated as function of heat flux of varying vapour quality at constant mass flux of 63, 73 and 82 kg/m²s respectively. In Fig. 6.12-6.14, the heat transfer coefficient of test evaporator OSF2 is evaluated as function of heat flux of

varying vapour quality at constant mass flux of 48, 63 and 73 kg/m²s respectively. Heat flux affects more the heat transfer coefficient in low vapour quality region than the higher vapour quality region. At higher vapour quality the difference between low and high heat flux heat transfer coefficients diminishes and the curves converge as shown in Fig. 6.6-6.8 and Fig. 6.12-6.14. This effect highlights the occurrence of nucleate boiling at low vapour quality i.e. during intermittent flow. Furthermore, when the vapour quality increases i.e. annular flow region the nucleate boiling is gradually suppressed, where as the importance of convective boiling increases to become dominant.

6.2.2 Heat transfer characteristics wavy fin surfaces

Experiments were performed on 2 wavy fin surfaces WF1 and WF2. Measured values of the local boiling heat transfer coefficient with vapour quality at selected heat inputs and mass velocities are plotted in the graphs. Fig. 6.15 to 6.26 shows plotted experimental data of two-phase heat transfer coefficient h_{tp} versus vapour quality x , for flow boiling in the test section.

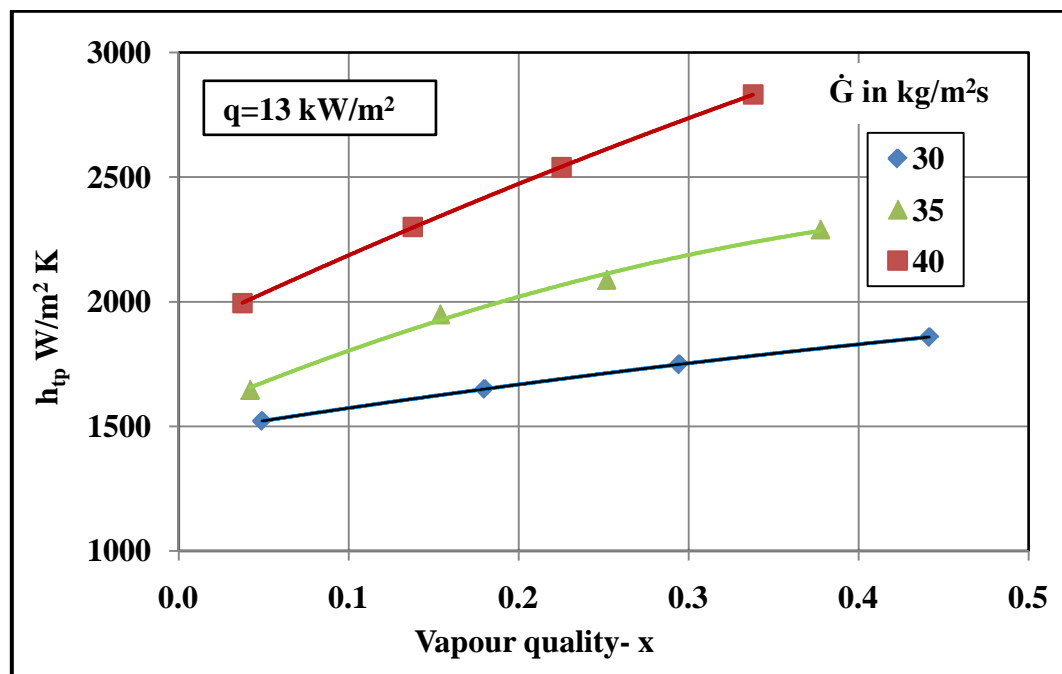


Fig. 6.15: Measured local two-phase heat transfer coefficient h_{tp} Vs vapour quality x at heat flux $q = 13$ kW/m² for mass fluxes \dot{G} (30, 35 and 40 kg/m²s) for fin surface WF1

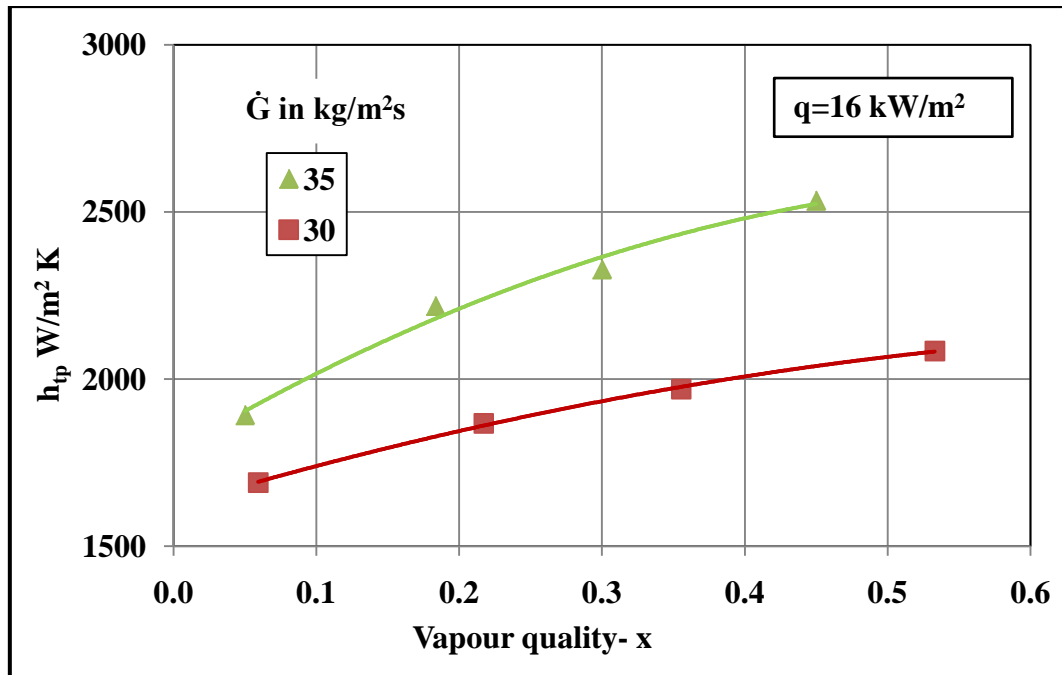


Fig. 6.16: Measured local two-phase heat transfer coefficient h_{tp} Vs vapour quality x at heat flux $q = 16 \text{ kW/m}^2$ for mass fluxes \dot{G} (30 and 35 kg/m²s) for fin surface WF1

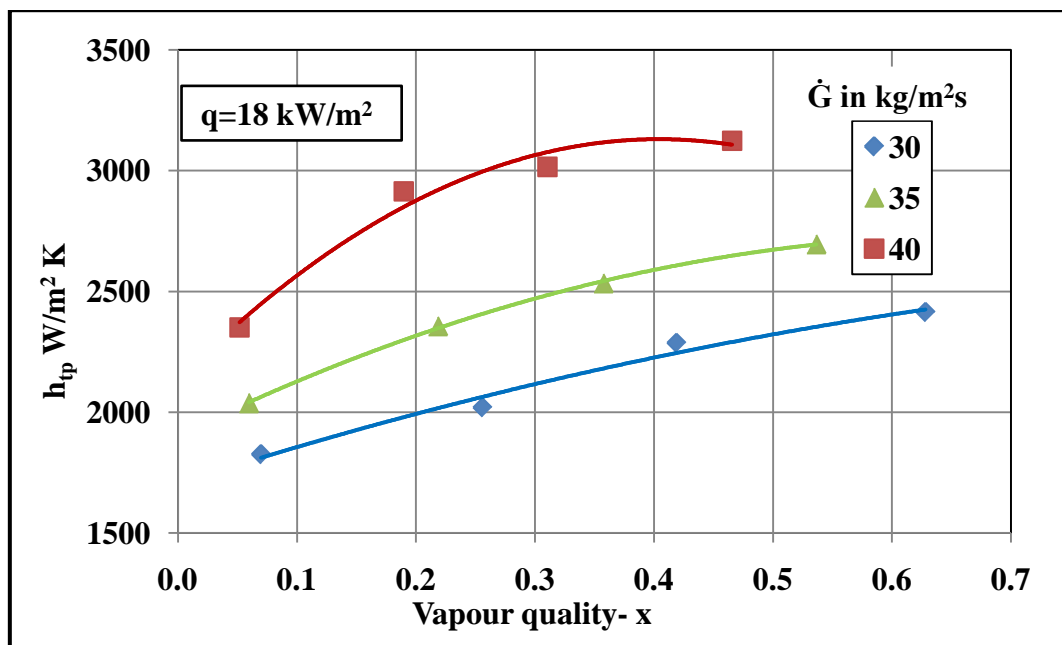


Fig. 6.17: Measured local two-phase heat transfer coefficient h_{tp} Vs vapour quality x at heat flux $q = 18 \text{ kW/m}^2$ for mass fluxes \dot{G} (30, 35 and 40 kg/m²s) for fin surface WF1

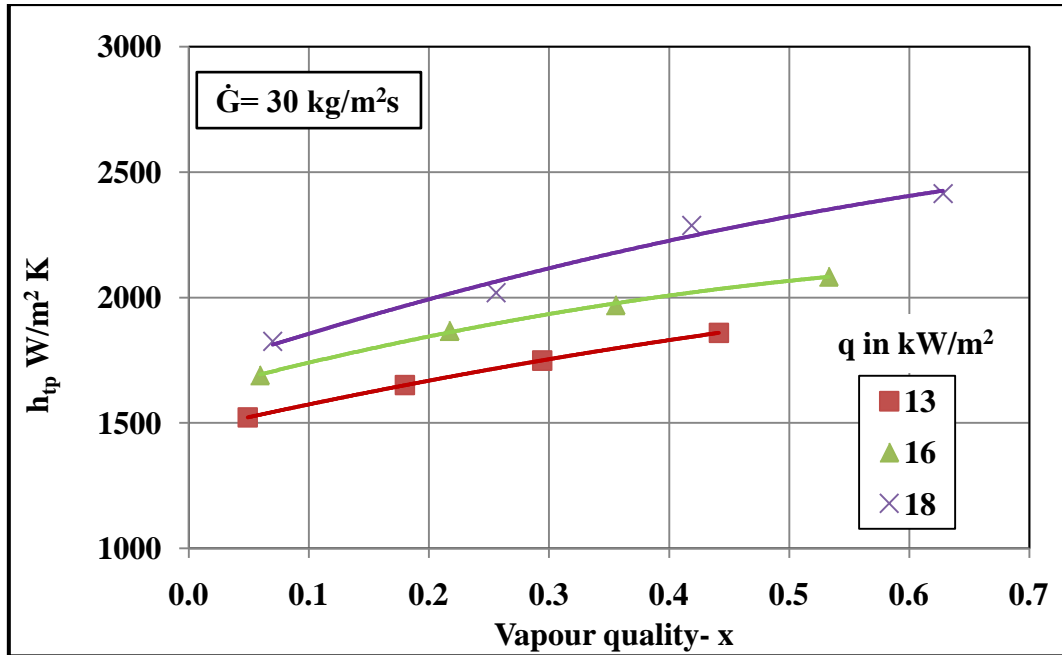


Fig. 6.18: Measured local two-phase heat transfer coefficient h_{tp} Vs vapour quality x at mass flux $\dot{G} = 30 \text{ kg/m}^2\text{s}$ for three heat fluxes q (13, 16 and 18 kW/m²) for fin surface WF1

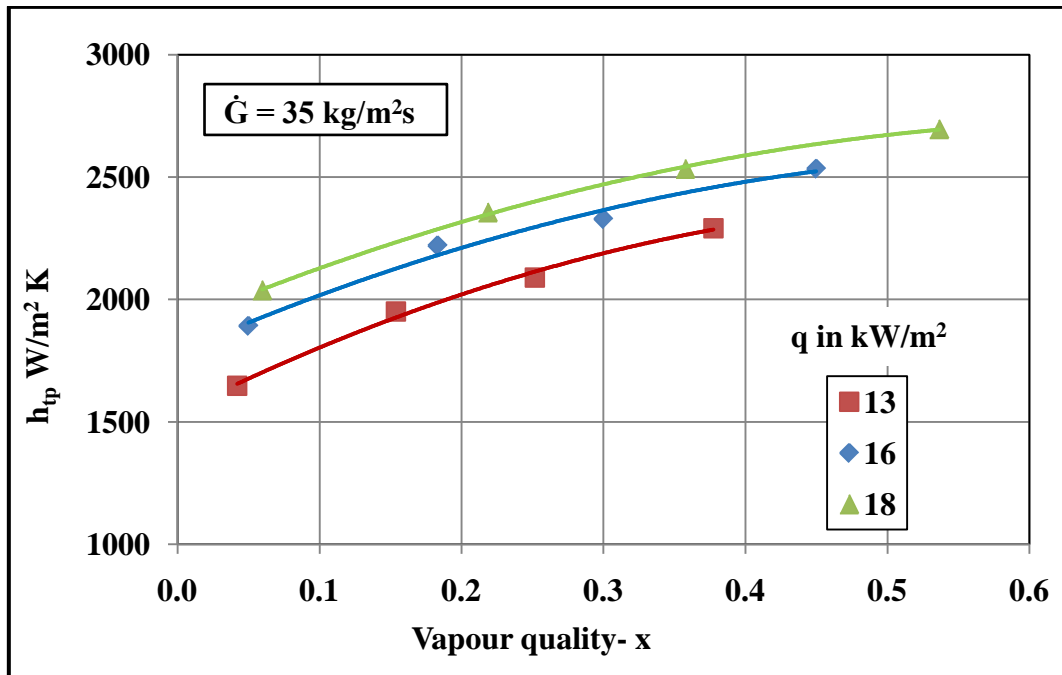


Fig. 6.19: Measured local two-phase heat transfer coefficient h_{tp} Vs vapour quality x at mass flux $\dot{G} = 35 \text{ kg/m}^2\text{s}$ for three heat fluxes q (13, 16 and 18 kW/m²) for fin surface WF1

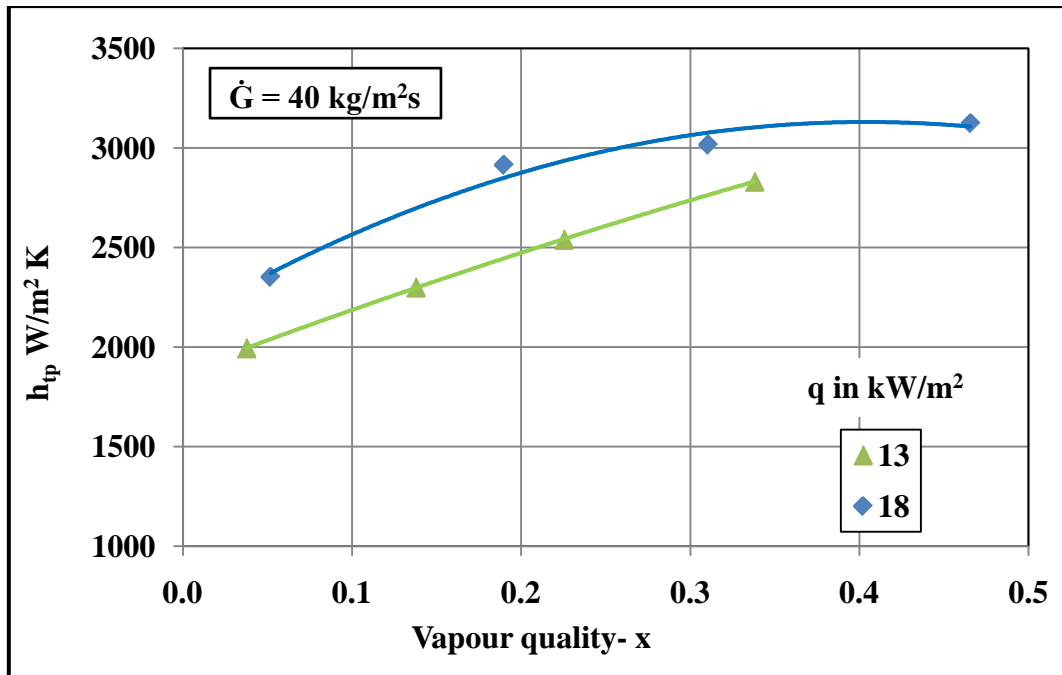


Fig. 6.20: Measured local two-phase heat transfer coefficient h_{tp} Vs vapour quality x at mass flux $\dot{G} = 40 \text{ kg/m}^2\text{s}$ for two heat fluxes q (13 and 18 kW/m^2) for fin surface WF1

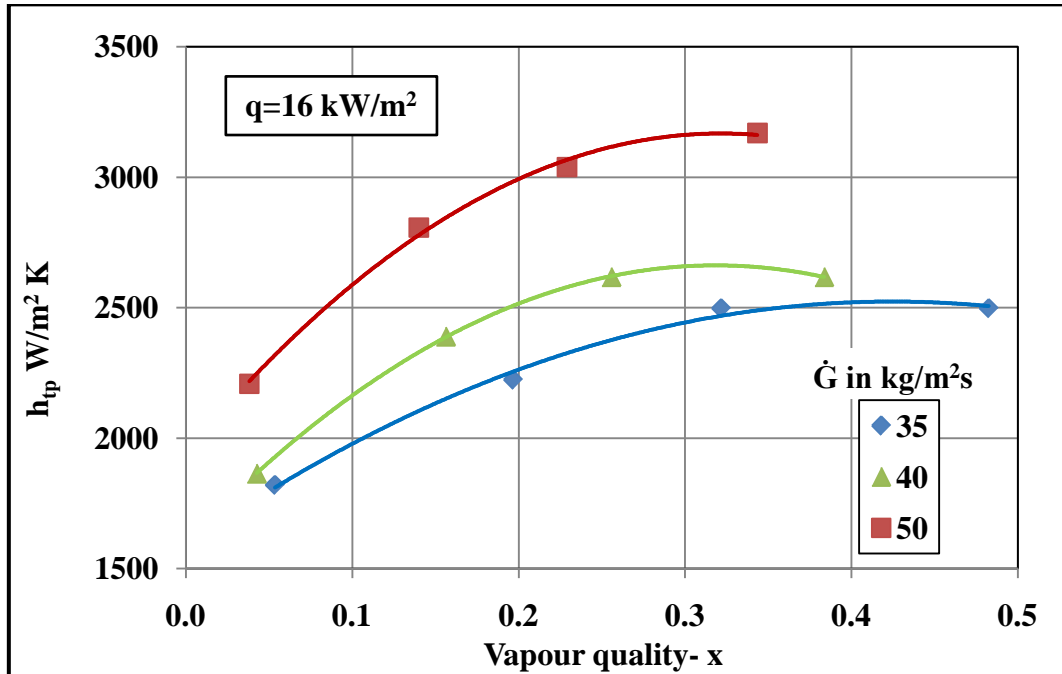


Fig. 6.21: Measured local two-phase heat transfer coefficient h_{tp} Vs vapour quality x at heat flux $q = 16 \text{ kW/m}^2$ for mass fluxes \dot{G} (35, 40 and 50 $\text{kg/m}^2\text{s}$) for fin surface WF2

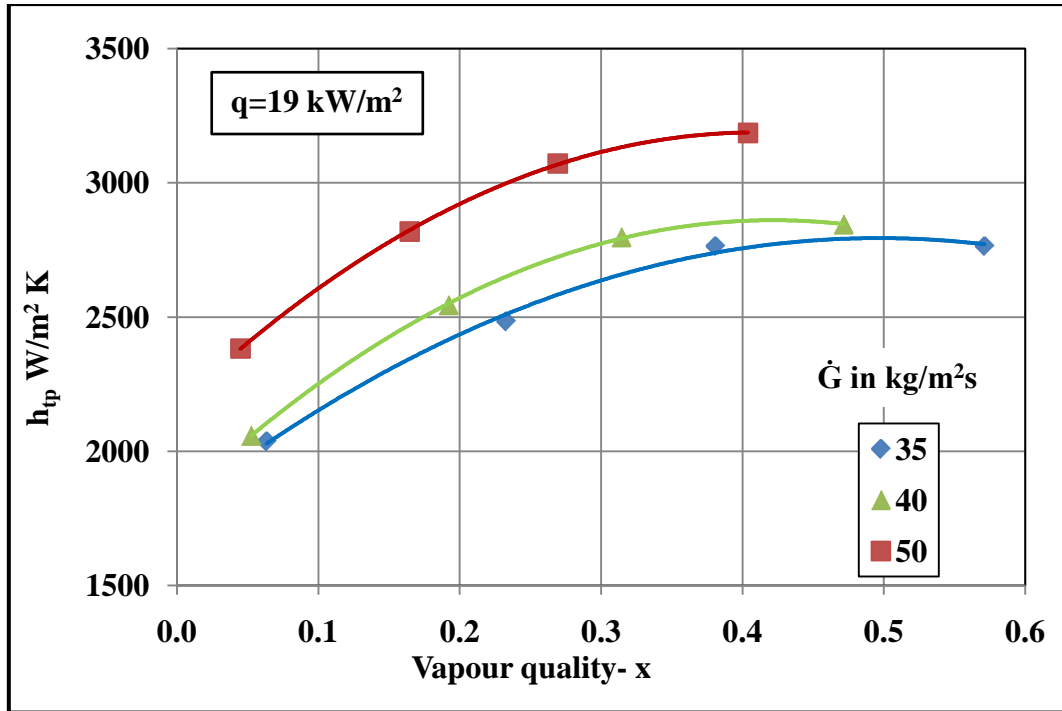


Fig. 6.22: Measured local two-phase heat transfer coefficient h_{tp} Vs vapour quality x at heat flux $q= 19 \text{ kW/m}^2$ for mass fluxes \dot{G} (35, 40 and $50 \text{ kg/m}^2\text{s}$) for fin surface WF2

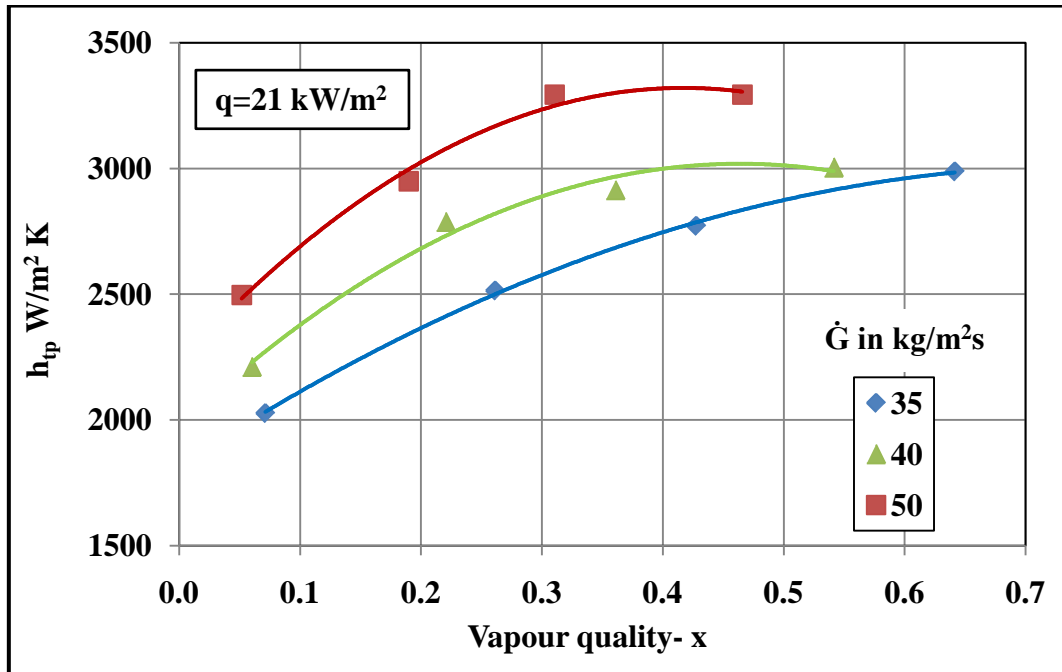


Fig. 6.23: Measured local two-phase heat transfer coefficient h_{tp} Vs vapour quality x at heat flux $q= 21 \text{ kW/m}^2$ for mass fluxes \dot{G} (35, 40 and $50 \text{ kg/m}^2\text{s}$) for fin surface WF2

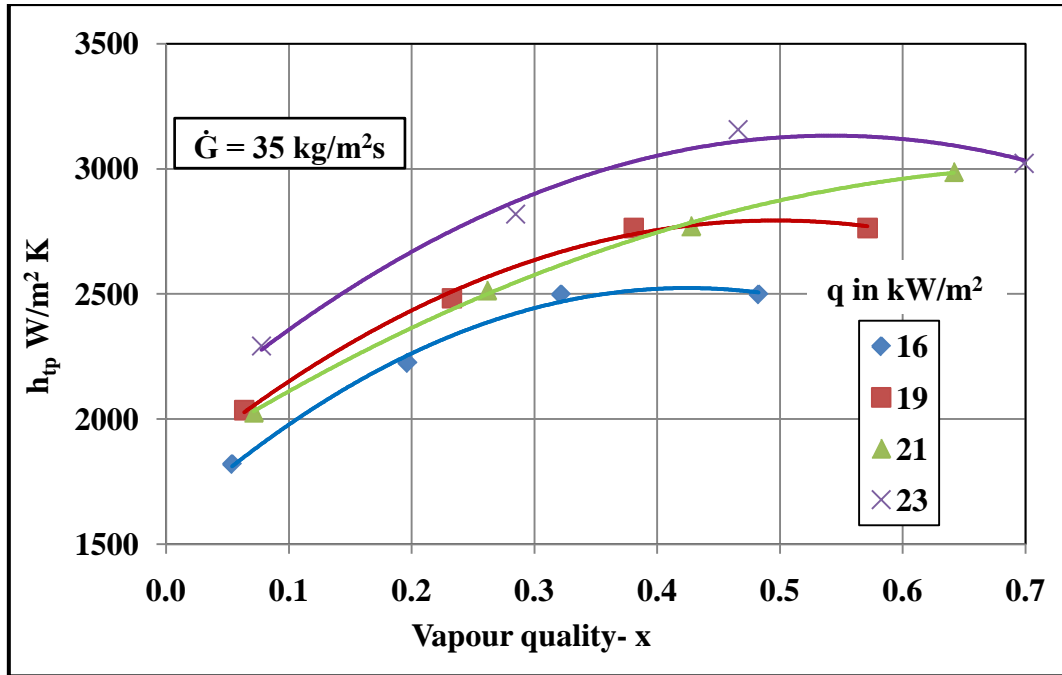


Fig. 6.24: Measured local two-phase heat transfer coefficient h_{tp} Vs vapour quality x at mass flux $\dot{G} = 35 \text{ kg/m}^2\text{s}$ for four heat fluxes q (16, 19, 21 and 23 kW/m^2) for fin surface WF2

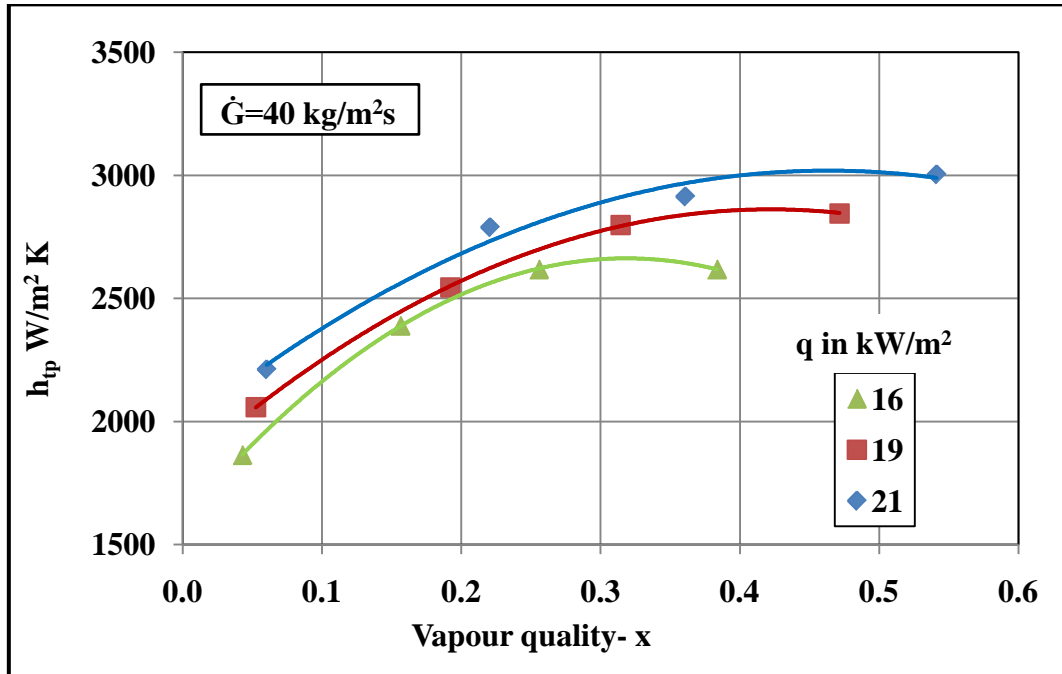


Fig. 6.25: Measured local two-phase heat transfer coefficient h_{tp} Vs vapour quality x at mass flux $\dot{G} = 43 \text{ kg/m}^2\text{s}$ for three heat fluxes q (16, 19 and 21 kW/m^2) for fin surface WF2

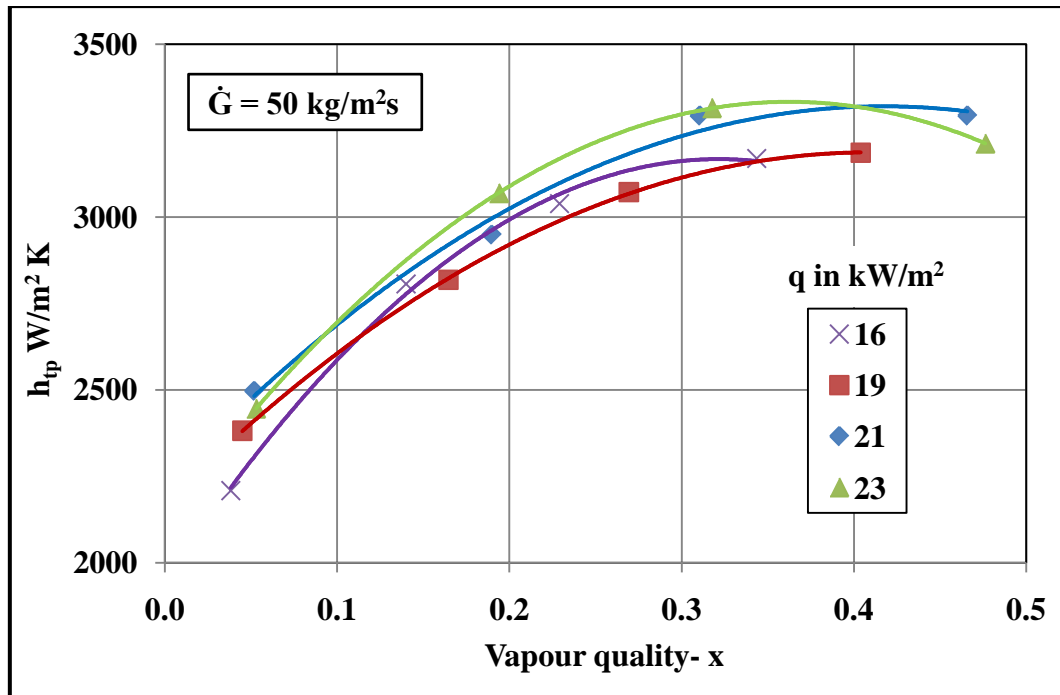


Fig. 6.26: Measured local two-phase heat transfer coefficient h_{tp} Vs vapour quality x at mass flux $\dot{G}= 51 \text{ kg/m}^2\text{s}$ for four heat fluxes q (16, 19, 21 and 23 kW/m^2) for fin surface WF2

In Fig. 6.15-6.17, the heat transfer coefficient of test evaporator WF1 is investigated as a function of mass flux over vapour quality at constant heat flux of 13, 16 and 18 kW/m^2 respectively. In Fig. 6.21-6.23, the heat transfer coefficient of test evaporator WF2 is investigated as function of mass flux over vapour quality at constant heat flux of 16, 19, 21 and 23 kW/m^2 respectively.

In Fig. 6.18-6.20, the heat transfer coefficient of test evaporator WF1 is investigated as function of heat flux over vapour quality at constant mass flux of, 30, 35 and 40 $\text{kg/m}^2\text{s}$ respectively. In Fig. 6.24-6.26, the heat transfer coefficient of test evaporator WF2 is investigated as function of heat flux over vapour quality at constant mass flux of 35, 40 and 50 $\text{kg/m}^2\text{s}$ respectively.

The influence of the vapour quality x along the test section z on the refrigerant heat transfer coefficient is shown above graphs. From the graphs in Fig. 6.15-6.20 of WF1 and Fig. 6.21-6.26 of WF2, it is observed that as vapour quality increases, the heat transfer coefficient increased. Heat transfer coefficient increases with quality, where liquid convection is the main mechanism. In fact, as the flow proceeds

downstream and vaporization takes place, the void fraction increases, thus decreasing the density of the liquid-vapour mixture. As a result, the flow accelerates enhancing convective transport from the heated wall surface. The consequent increase in heat transfer coefficient proceeds until the liquid film disappears, leaving the wall surface partially or totally dry. In this region the heat transfer coefficient decreases because of the low thermal conductivity of the vapour.

Lower heat transfer coefficient of wavy fins is observed compared to offset strip fins. In wavy fins surface remains continuous and no boundary layer breakup and liquid film disappears may be at later than offset strip fins. In offset strip fins boundary layers are interrupted frequently leading to enhancement of heat transfer. Close to the leading edge of the fins, heat transfer coefficient is very high due to generation of fresh boundary layer. Also through mixing of fluid enhances the heat transfer coefficient.

From Fig. 6.15-6.17 of WF1 and Fig. 6.21-6.23 of WF2, it is observed that, as the mass flux increases the heat transfer coefficient increases at constant heat flux. It is understood that at higher mass flux and vapour quality the two-phase mixture flows at higher velocity, which promotes convective heat transfer. Heat transfer coefficient shows a strong dependence on the heat flux and mass flux. Effect of heat flux is plotted in Fig. 6.18-6.20 of WF1 and Fig. 6.24-6.26 of WF2. It found that heat flux has less effect on heat transfer coefficient. The reasons for these trends are discussed at length in section 6.2.1.1 of this chapter.

6.3 TWO-PHASE PRESSURE DROP CHARACTERISTICS

The pressure drop across a refrigerant evaporator has many contributions like frictional, acceleration, gravitational, entrance and exit losses. Among which the two-phase frictional pressure drop is by far the largest. It is the purpose of this study to evaluate this pressure drop and find its dependency on relevant flow and geometrical parameters. The experimental values of two-phase pressure drop ΔP , with vapour quality at different mass fluxes for flow boiling of R134a in the different types of fin are presented here.

The experimental data of pressure drop are plotted ΔP versus exit vapour quality x , for flow boiling in the test section in Fig. 6.27 to 6.30 for all fin surfaces.

Fig. 6.27 and to 6.28 presents the results of two offset strip fin surfaces (OSF1 and OSF2) while Fig. 6.29 and 6.30 present the results for two wavy fins surfaces (WF1 and WF2). In general, the two-phase frictional pressure drop of the refrigerant showed strong dependence on mass flux and vapour quality.

6.3.1 Pressure drop characteristics of offset strip fin surfaces.

Experiments were performed on 2 offset strip fin surfaces OSF1 and OSF2. Measured values of the two-phase pressure drop with vapour quality at different mass velocities are plotted in the graphs. Fig. 6.27 and 6.28 shows plotted experimental data of two-phase pressure drop ΔP versus vapour quality x , for flow boiling in the test section.

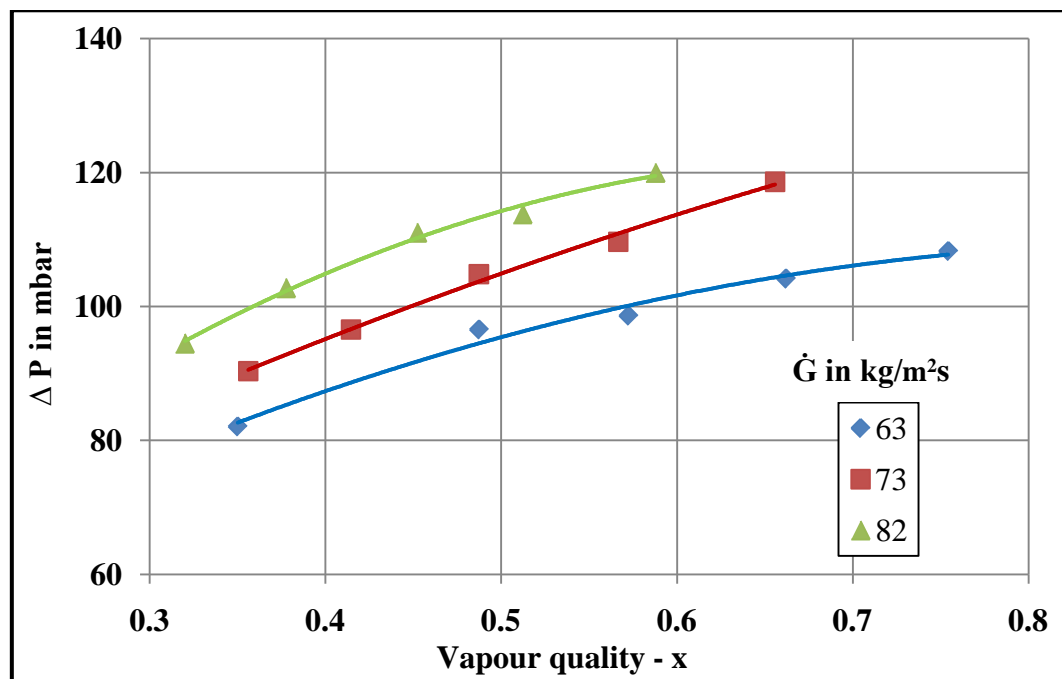


Fig. 6.27: Measured two-phase pressure drop ΔP Vs exit vapour quality x at mass fluxes \dot{G} (63, 73 and 82 kg/m²s) for fin surface OSF1

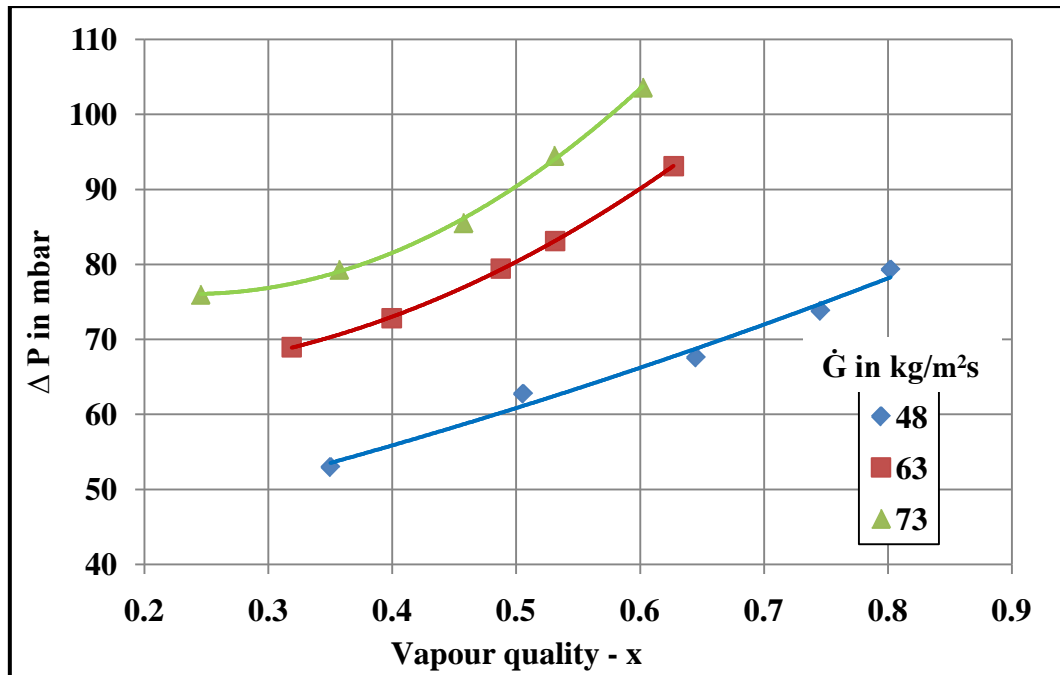


Fig. 6.28: Measured two-phase pressure drop ΔP Vs exit vapour quality x at mass fluxes \dot{G} (48, 63 and 73 kg/m²s) for fin surface OSF2

In Fig. 6.27 and 6.28 the frictional pressure drop of offset strip fin surface for R134a is reported as a function of vapour quality at constant mass flux. The pressure drop is investigated between the inlet and exit of the test section. In general flow pressure drop with fins will be larger than that without fins. From graphs it can be observed that pressure drop increases with both the vapour quality and the mass flux and effect of heat flux is insignificant. The reasons for increase in pressure drop are discussed below.

The pressure drop in the test section is mainly caused by the friction. It is a change of pressure resulting from the energy dissipated in the flow by friction, eddying etc. As the flow goes downstream, vaporization takes place, the density of the liquid-vapour mixture decreases. As a result the flow accelerates much more and frictional pressure drop increases. At low vapour qualities, offset strip fins periodically redirects the flow and increases the two-phase pressure drop somewhat higher than the value caused by wall friction alone. At high vapour qualities, high velocity vapour flow interacts with the fins and causes a larger pressure drop than that of in round tubes

6.3.2 Pressure drop characteristics wavy fin surfaces

Experiments were performed on 2 wavy fin surfaces WF1 and WF2. Measured values of the two-phase pressure drop with vapour quality at different mass velocities are plotted in the graphs. Fig. 6.29 and 6.30 shows plotted experimental data of two-phase pressure drop ΔP versus exit vapour quality x , for flow boiling in the test section.

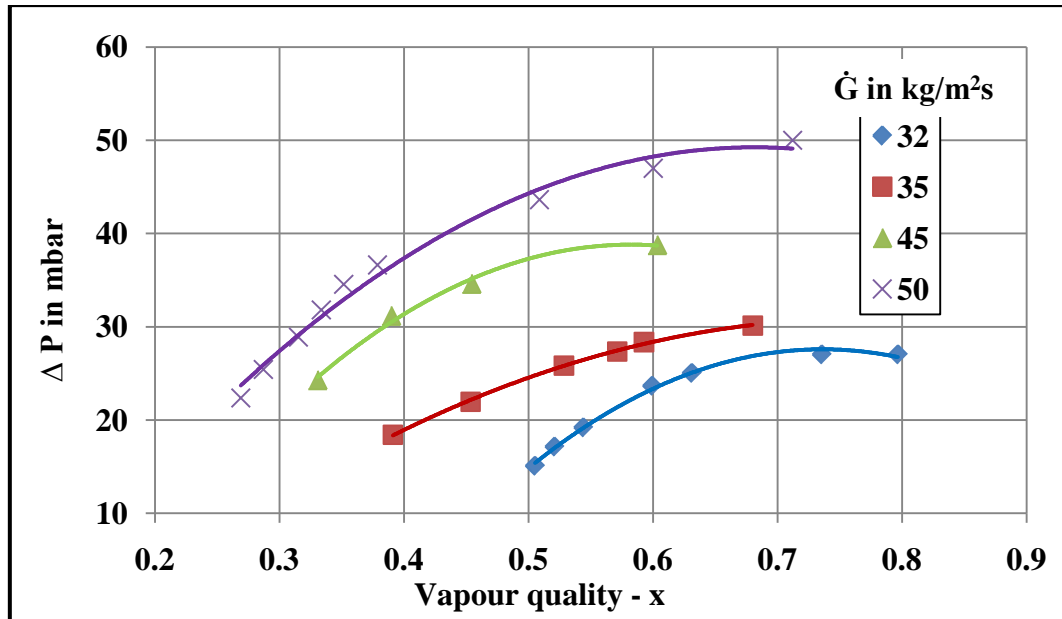


Fig. 6.29: Measured two-phase pressure drop ΔP Vs exit vapour quality x at mass fluxes \dot{G} (32, 35, 45 and 50 kg/m²s) for fin surface WF1

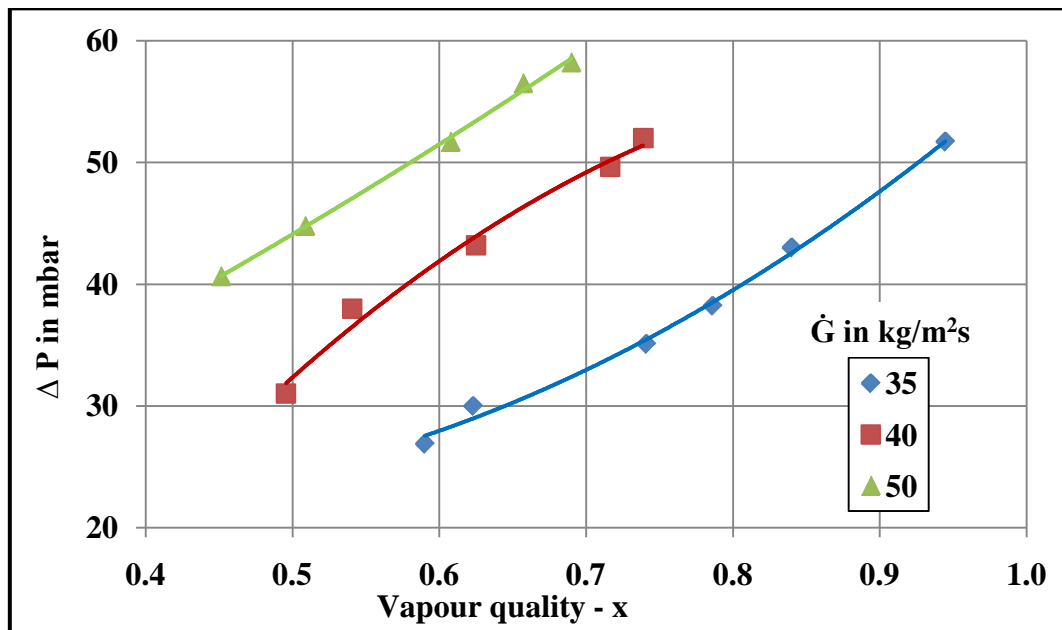


Fig. 6.30: Measured two-phase pressure drop ΔP Vs exit vapour quality x at mass fluxes \dot{G} (35, 40 and 50 kg/m²s) for fin surface WF2

In Fig. 6.29 and 6.30, the frictional pressure drop of wavy fin for R134a is reported as a function of vapour quality at constant mass flux. It can be observed from graphs that pressure drop increases with vapour quality and the mass flux. The reasons for increase in pressure drop are discussed para 6.3.1.

6.4 DEVELOPMENT OF TWO-PHASE CORRELATIONS FOR COMPACT PLATE FIN SURFACES.

Correlations predicting the refrigerant flow boiling heat transfer and two-phase frictional pressure drop in compact plate fin surfaces over evaporators are developed in this section. The heat transfer correlations are based on number of data points, covering the experimental data of R134a. The pressure drop correlations are based on number of data points covering R134a.

6.4.1 Two-phase heat transfer correlations

Local boiling heat transfer coefficient has been correlated in terms of Reynolds number factor, F and Lockhart and Martinelli parameter, X . Reynolds number factor is a function of two-phase forced convective heat transfer coefficient and single phase heat transfer coefficient h_l . The Reynolds number factor has generally been postulated to be a function of the Martinelli parameter X . The measured two-phase forced convective heat transfer data for the two offset strip surfaces and two wavy fin surfaces tested are plotted separately in terms of F and $1/X$ below. Data for which bubble nucleation or partial surface dry out have not been included in the plots.

6.4.1.1 Generation of heat transfer correlation for offset strip fin, OSF1

Experimental two-phase convective boiling heat transfer data for the offset strip surface OSF1, is plotted in terms F and $1/X$ in Fig 6.31.

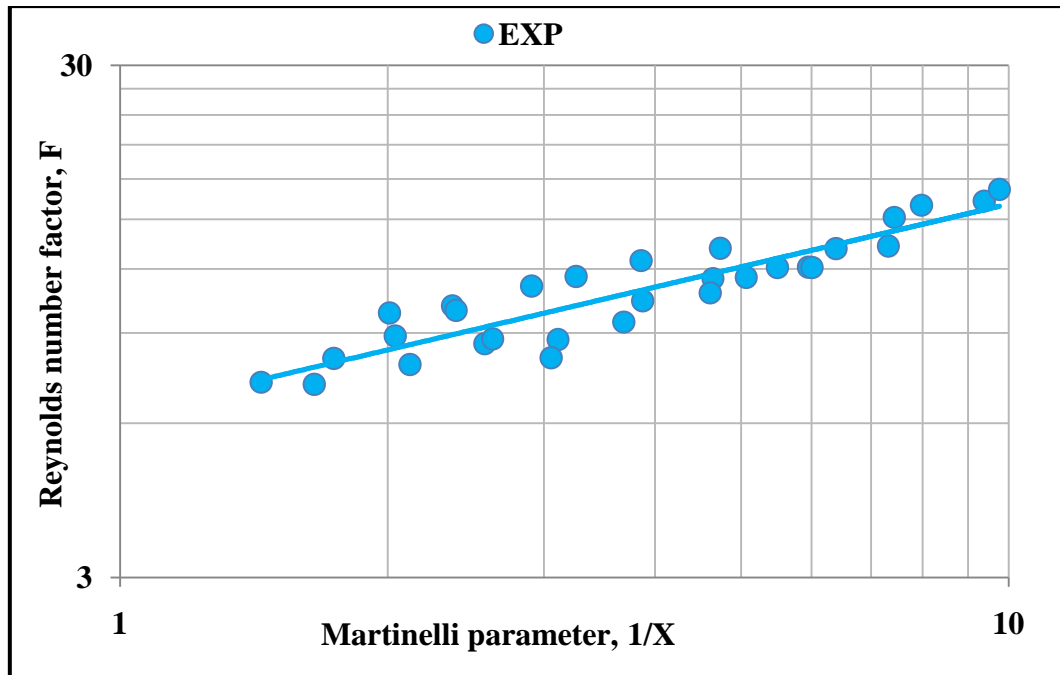


Fig. 6.31: Measured local heat transfer coefficients for convective boiling in OSF1

From the Fig. 6.31 the Reynolds number factor, F for OSF1 (approximate fit to data) is correlated

$$F = \left[1 + \frac{33.3}{X} \right]^{0.5} \quad (6.1)$$

for the case $\frac{1}{X} > 1.0$. Nucleate boiling dominant data, $\frac{1}{X} < 1.0$ has not included in the development of F correlations. With the above correlation, forced convection heat transfer data can be predicted within error of $\pm 7.4\%$.

Convective boiling heat transfer coefficient will not depend on wall superheat where as nucleate boiling heat transfer coefficient is strongly depends on the local wall superheat. Hence, nucleate boiling contribution has to be computed. It is computed separately for primary and secondary surface areas since; temperature of the fin is not uniform. The contribution of nucleate boiling, h_{nb} to the local boiling heat transfer is estimated using Eqn.5.23.

The measured two heat transfer coefficient (h_{tp} Exp) and predicted heat transfer coefficient (h_{tp} Pre) using the correlation Eqn. 6.1 & Eqn.5.23 is plotted in Fig. 6.32.

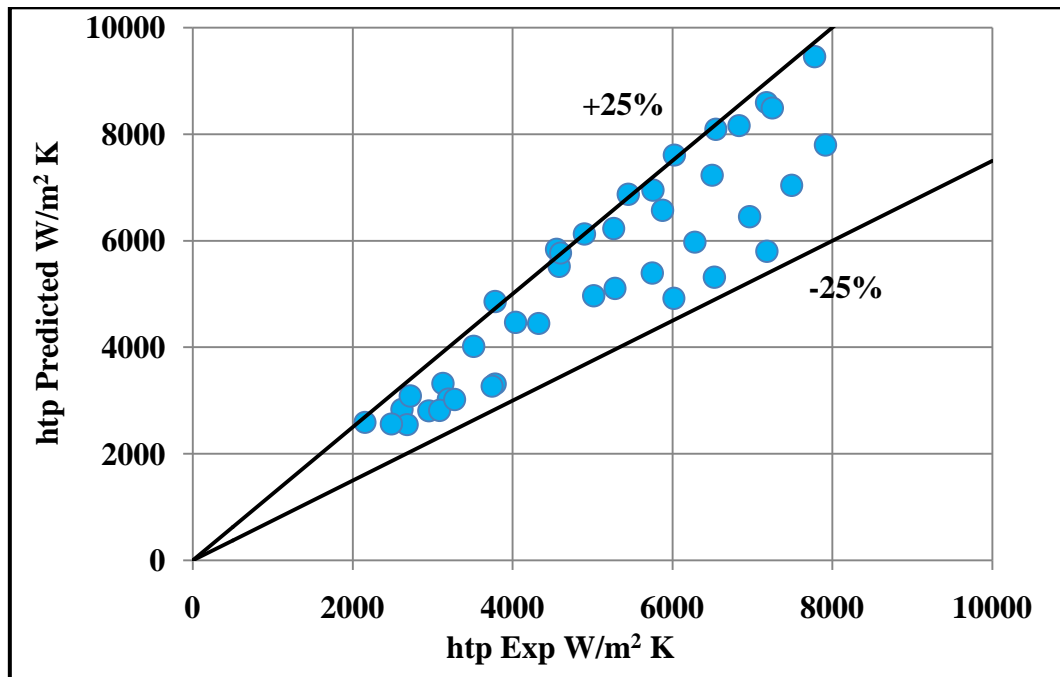


Fig. 6.32: Comparison of measured and predicted two-phase heat transfer coefficient for OSF1.

$h_{tp}Exp$ = Experimentally measured two-phase heat transfer coefficient

$$h_{tp}Pre = F h_l + h_{nb}$$

$$= F h_l + S h_{pb}$$

Where F is estimated from Eqn.6.1

h_l is single phase heat transfer coefficient

S, Suppression factor from Eqn.5.26

h_{pb} from Eqn.5.24

Predicted and experimentally measured values of the local boiling heat transfer coefficient are in good agreement and the data lies within $\pm 25\%$ of the predictions. This difference is unavoidable since the contribution of primary and secondary surfaces areas to the nucleate boiling heat transfer was not able compute separately. Also effect of fins is not able to include in suppression factor estimation. Hence correlation has a tendency to over predict, especially at low quality the contribution of nucleate boiling to the local boiling heat transfer coefficient. The mean difference between the predicted and the experimentally measured local boiling heat transfer coefficients is found 8.44%.

Experimental Reynolds number factor F , is compared with published F correlations in the Fig. 6.33.

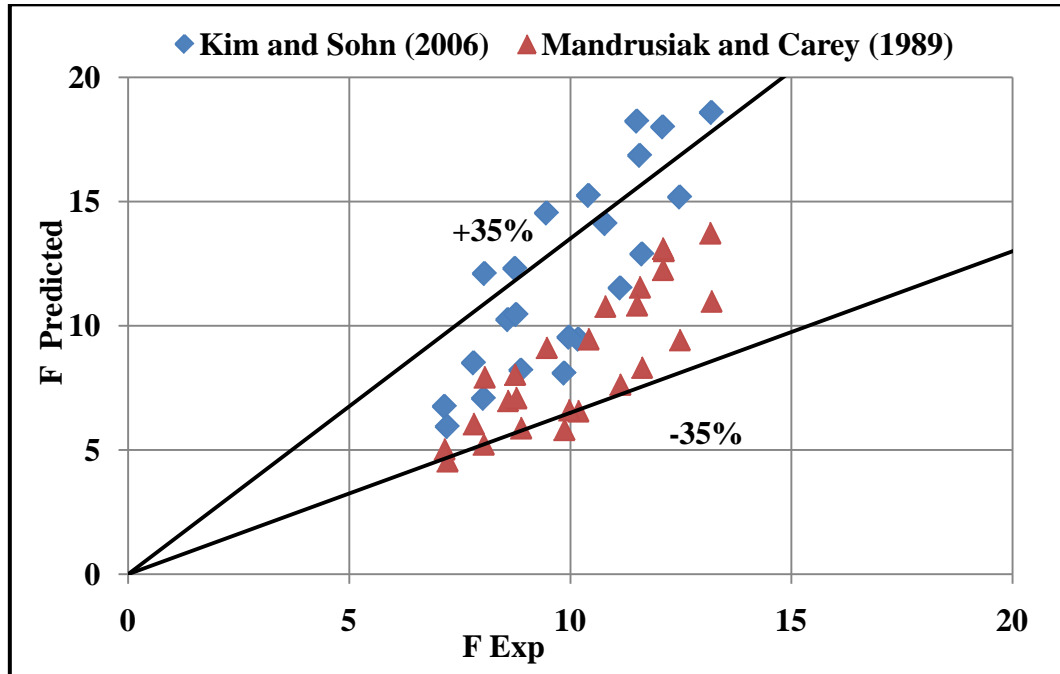


Fig. 6.33: Comparison of OSF1, F data with the predictions of referred correlations

The disagreement between the experimental data and prediction of published correlations is mainly due to difference in geometries of the fins, refrigerant fluids flow passage used. The correlation of Mandrusiak and Carey (1989) under predicts the F value when compared to the experimental values of present study. Mandrusiak and Carey (1989) used copper slab and fin is machined out of it, which is not accurate with one used in industrial applications. The hydraulic diameter fin used was 8.84 mm, where as the hydraulic diameter of present is 1.189. These geometrical differences seem to result in a serious discrepancy in the F . Kim and Sohn (2006) have conducted the experiments at very low vapour quality i.e. <0.3 .

6.4.1.2 Generation of heat transfer correlation for offset strip fin, OSF2

Experimental two-phase convective boiling heat transfer data for the offset strip surface OSF2, is plotted in terms F and $1/X$ in Fig 6.34.

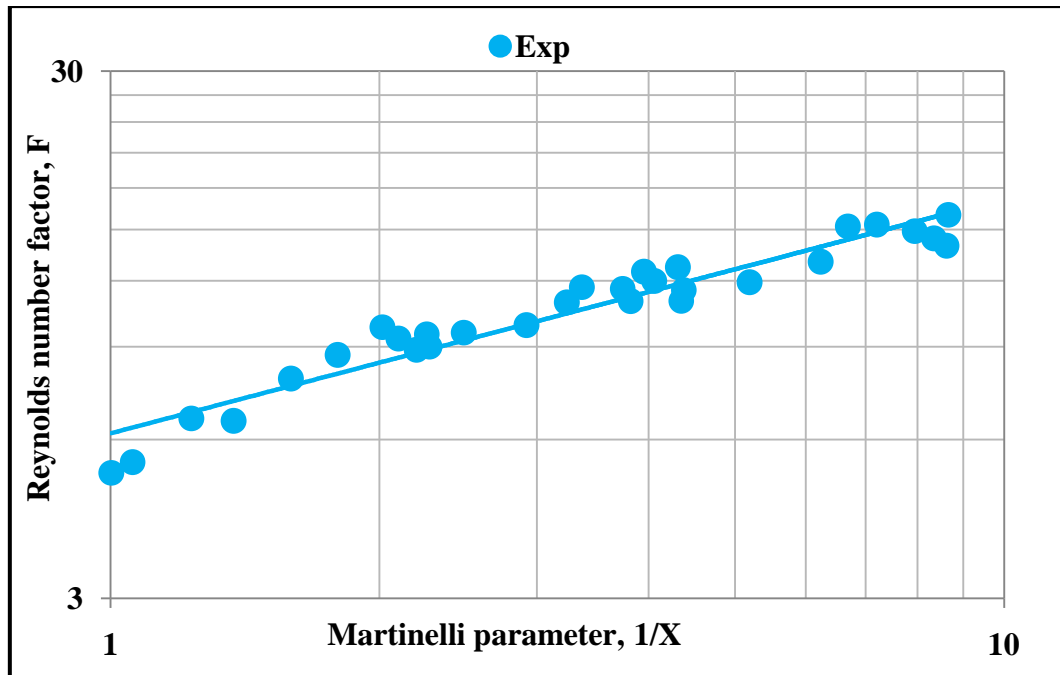


Fig. 6.34: Measured local heat transfer coefficients for convective boiling in OSF2

From the Fig 6.34 the Reynolds number factor, F for OSF2 (approximate fit to data) is correlated as

$$F = \left[1 + \frac{30}{X} \right]^{0.5} \quad (6.2)$$

for the case $\frac{1}{X} > 1.0$. Nucleate boiling dominant data, $\frac{1}{X} < 1.0$ has not included in the development of F correlations. With the above correlation, forced convection heat transfer data can be predicted within error of $\pm 7.04\%$.

The measured two heat transfer coefficient ($h_{tp,Exp}$) and predicted heat transfer coefficient ($h_{tp,Pre}$) using the correlation Eqn. 6.2 & Eqn.5.23 is plotted in Fig. 6.35.

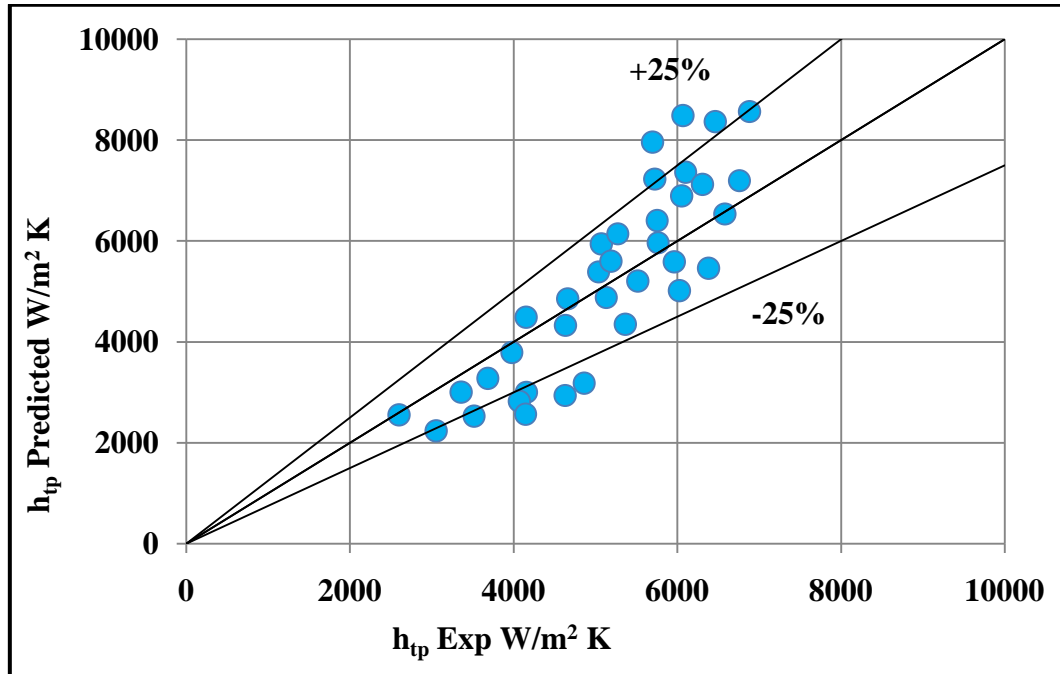


Fig. 6.35: Comparison of measured and predicted two-phase heat transfer coefficient for OSF2.

Predicted and experimentally measured values of the local boiling heat transfer coefficient are in good agreement and 95 % the data lies within $\pm 25\%$ of the predictions. For predictions of F, Eqn.6.2 is used. The mean difference between the predicted and the experimentally measured local boiling heat transfer coefficients is found 5.88%.

Experimental Reynolds number factor F, is compared with published F correlations in the Fig. 6.36.

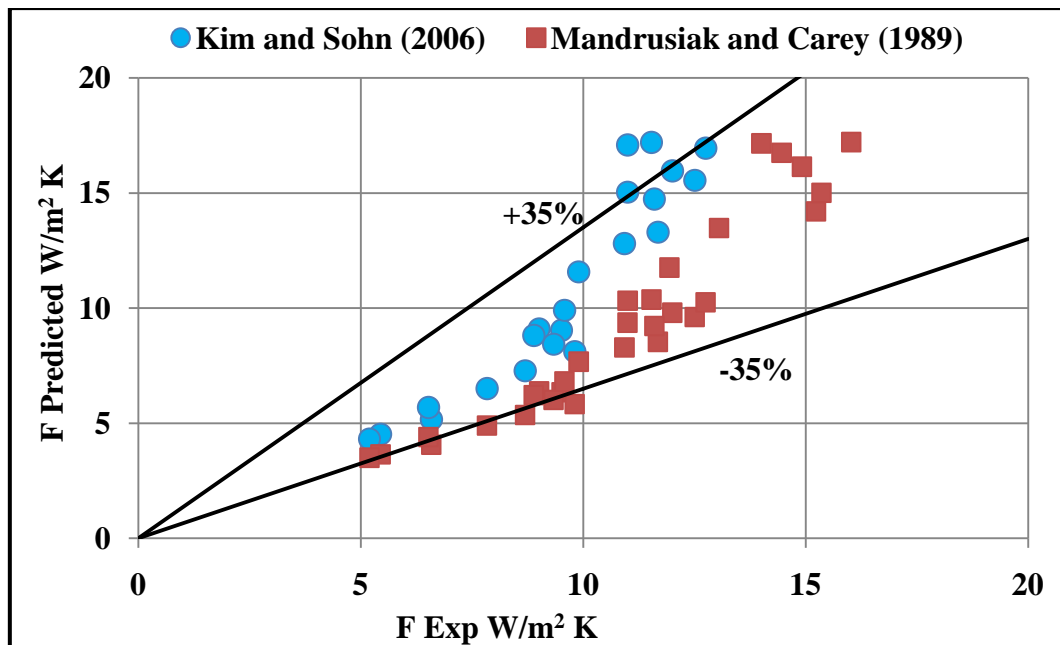


Fig. 6.36: Comparison of OSF2, F data with the predictions of referred correlations.

The disagreement between the experimental data and prediction of published correlations is clearly explained in above, para no.6.4.1.1.

6.4.1.3 Generalized heat transfer correlation for offset strip fin surfaces

A composite plot summarizing forced convective heat transfer data for two offset fin surfaces is shown in Fig. 6.37.

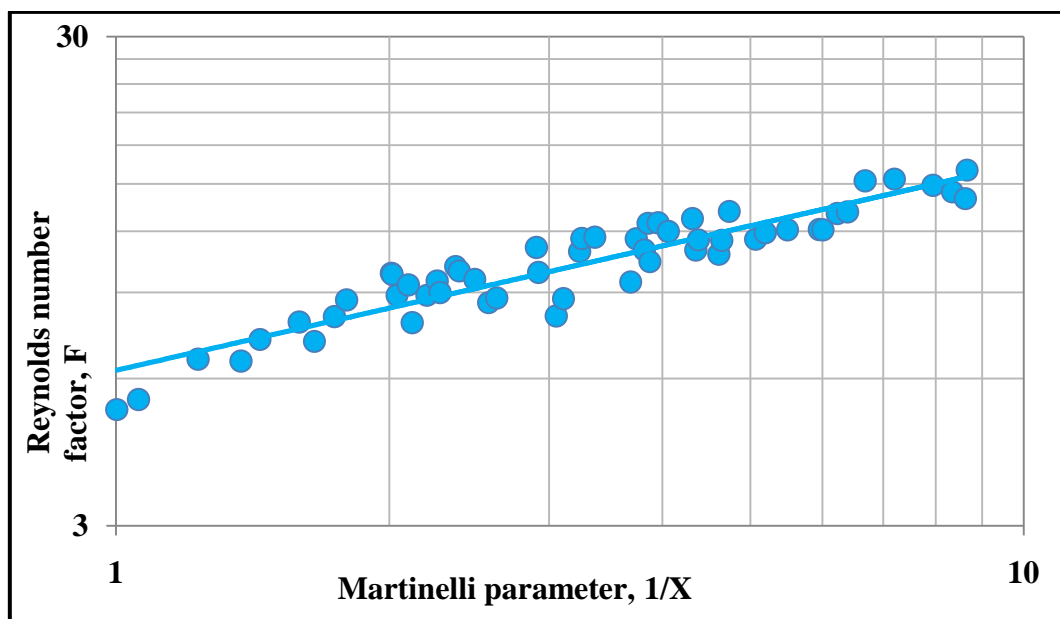


Fig. 6.37: Combined measured local heat transfer coefficients for convective boiling in offset fin surfaces (OSF1 and OSF2).

From the Fig. 6.37 the Reynolds number factor, F(approximate fit to data) is correlated as

$$F = \left[1 + \frac{32}{X}\right]^{0.5} \quad (6.3)$$

for the case $\frac{1}{X} > 1.0$. Data for which the nucleate boiling was dominant, $\frac{1}{X} < 1.0$ has not included in the development of correlations of F. The measured data of both offset strip fin surfaces are reasonably well represented by single correlation. In fact, 90 percent of the heat transfer data shown in Fig. 6.37 lie within ± 10 percent of Eqn.6.3. The results shown above indicate that the convective boiling component of the two-phase heat transfer coefficient for the two offset fin geometries considered here differ only slightly when correlated in terms of F-parameter.

6.4.1.4 Generation of heat transfer correlation for wavy fin, WF1

Experimental two-phase convective boiling heat transfer data for the wavy fin surface WF1 is plotted in terms of F and 1/X in Fig. 6.38 and compared with predictions published.

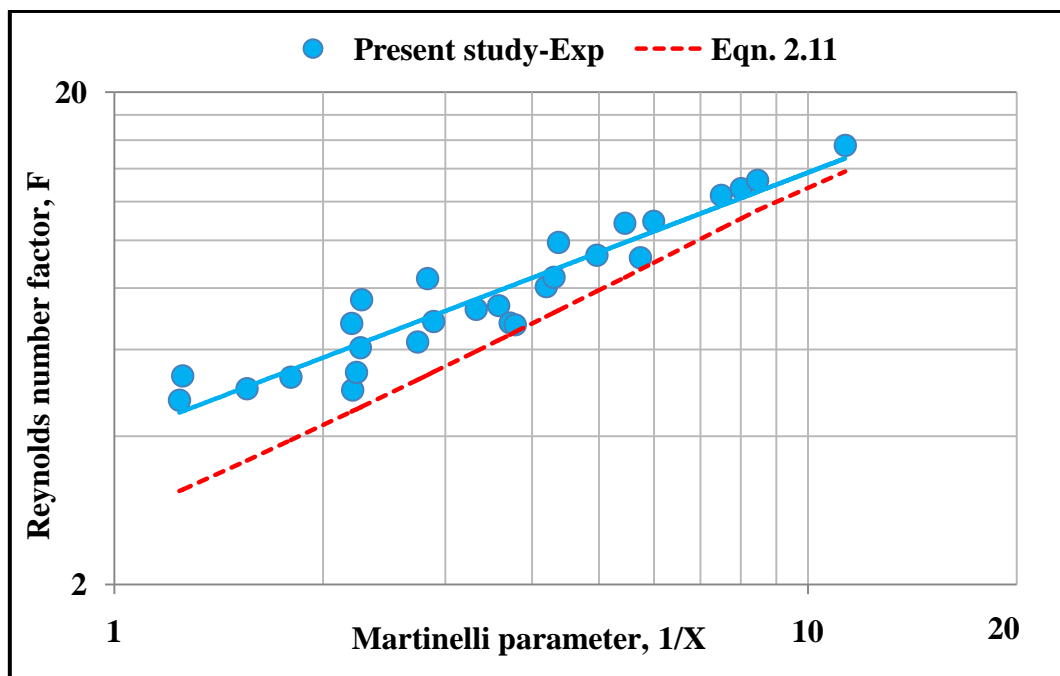


Fig. 6.38: Measured local heat transfer coefficients for convective boiling in WF1 and comparison with predictions reported for round tubes.

From the Fig. 6.38 the Reynolds number factor, F for WF1 (approximate fit to data) is correlated as

$$F = \left[1 + \frac{21}{X}\right]^{0.5} \quad (6.4)$$

for the case $\frac{1}{X} > 1.0$. Nucleate boiling dominant data, $\frac{1}{X} < 1.0$ has not included in the development of F correlations. With the above correlation, forced convection heat transfer data can be predicted within error of $\pm 6.9\%$.

In Fig. 6.38, measured two-phase heat transfer data is compared with round tubes since there are no correlations available for wavy fin surfaces in open literature. The disagreement between the experimental data and the predictions of referred (Eqn.2.11) correlation proposed by Chen (1966) is due to different geometries of the flow passage and refrigerant fluid used. The correlation of Chen (1966) under predicts F compared to the present study. His experimental values of the F, are less than those of the present study. Chen (1966) predicted Reynolds number factor for round tubes, where as present study is for wavy fin geometries. The results shown above indicate that the convective boiling component of the two-phase heat transfer coefficient for the wavy fin geometry is higher than that of the round tubes. This is obvious that wavy fin have higher heat transfer area than round tubes when compared for per unit area. Hence wavy fin exhibits higher heat transfer coefficient than round tubes.

The measured two heat transfer coefficient ($h_{tp,Exp}$) and predicted heat transfer coefficient ($h_{tp,Pre}$) using the correlation Eqn. 6.4 & Eqn.5.23 is plotted in Fig.6.39.

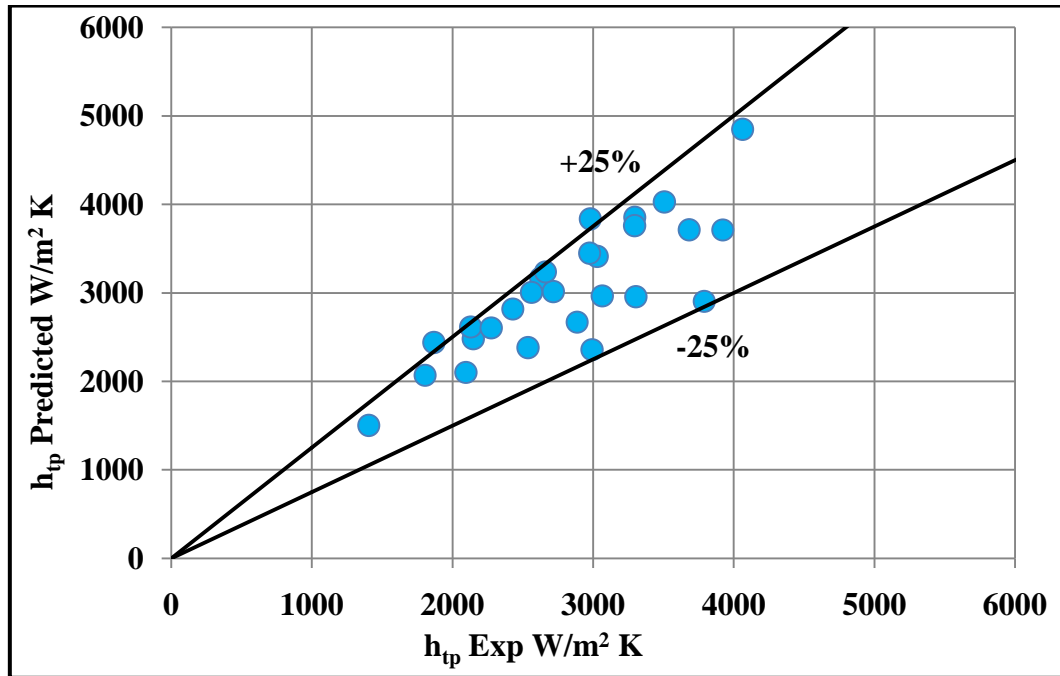


Fig. 6.39: Comparison of measured and predicted two-phase heat transfer coefficient for WF1

Predicted and experimentally measured values of the local boiling heat transfer coefficient are in good agreement and the data lies within $\pm 25\%$ of the predictions. For predictions of F, Eqn. 6.4 is used. This difference is unavoidable since the contribution of primary and secondary surfaces areas to the nucleate boiling heat transfer was not able compute separately. Also effect of fins is not able to include in suppression factor estimation. Hence correlation has a tendency to over predict, especially at low quality the contribution of nucleate boiling to the local boiling heat transfer coefficient. The mean difference between the predicted and the experimentally measured local boiling heat transfer coefficients is found 13.52%.

6.4.1.5 Generation of heat transfer correlation for wavy fin, WF2

Experimental two-phase forced convective boiling heat transfer data for the wavy surface WF2 is plotted in terms of F and $1/X$ in Fig. 6.40 and compared with predictions published.

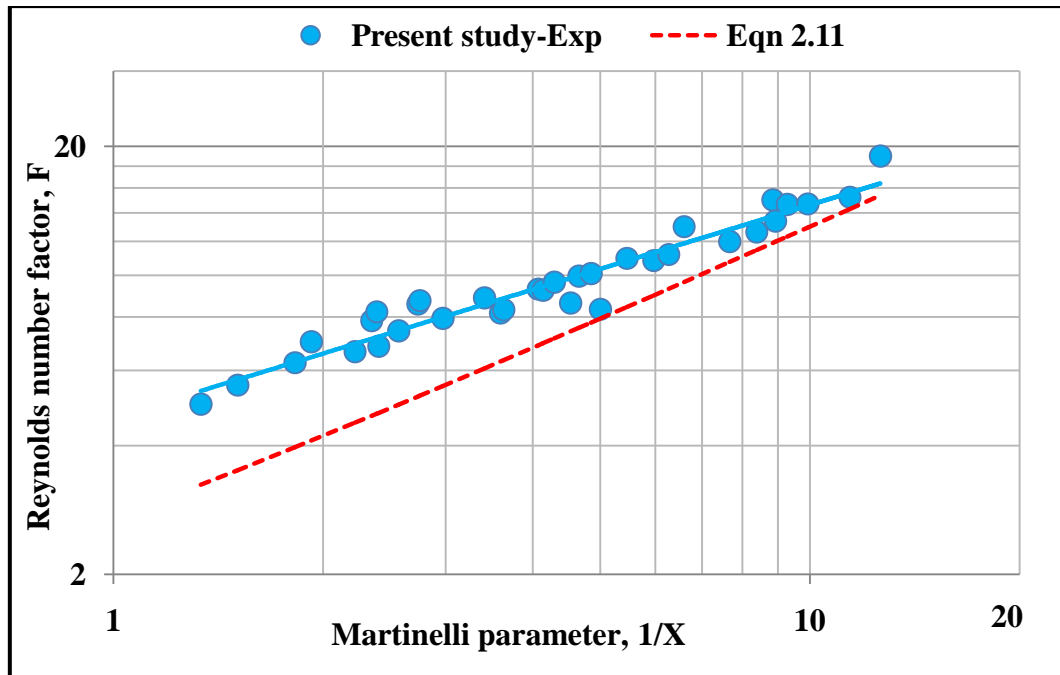


Fig. 6.40: Measured local heat transfer coefficients for convective boiling in WF2 and comparison with predictions reported for round tubes.

From the Fig. 6.40 the Reynolds number factor, F for WF2 (approximate fit to data) is correlated as

$$F = \left[1 + \frac{20}{X} \right]^{0.5} \quad (6.5)$$

for the case $\frac{1}{X} > 1.0$. Nucleate boiling dominant data, $\frac{1}{X} < 1.0$ has not included in the development of F correlations. With the above correlation, forced convection heat transfer data can be predicted within error of $\pm 6.62\%$.

The disagreement between the experimental data and prediction of published correlations is clearly explained in above, para no.6.4.1.4.

The measured two heat transfer coefficient ($h_{tp,Exp}$) and predicted heat transfer coefficient ($h_{tp,Pre}$) using the correlation Eqn. 6.5 & Eqn.5.23 is plotted in Fig.6.41.

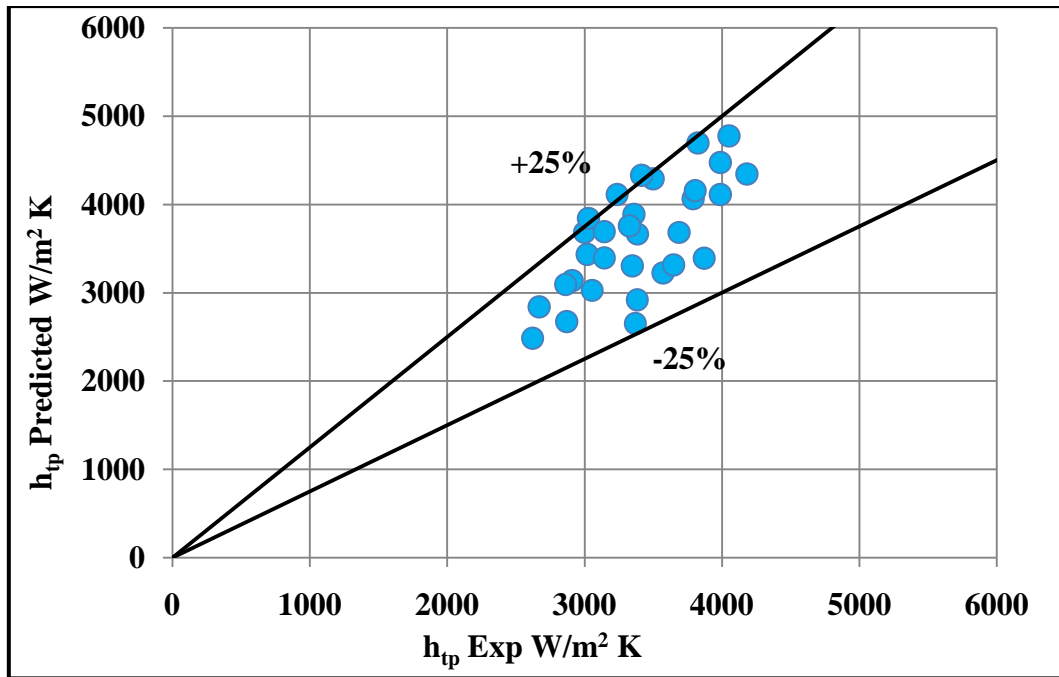


Fig. 6.41: Comparison of measured and predicted two-phase heat transfer coefficient for WF2

Predicted and experimentally measured values of the local boiling heat transfer coefficient are in good agreement and the data lies within $\pm 25\%$ of the predictions. For predictions of F, Eqn.6.5 is used. The mean difference between the predicted and the experimentally measured local boiling heat transfer coefficients is found 9.1%.

6.4.1.6 Generalized correlation for wavy fin surfaces

A composite plot summarizing forced convective heat transfer data for two wavy fin surfaces is shown in Fig. 6.42.

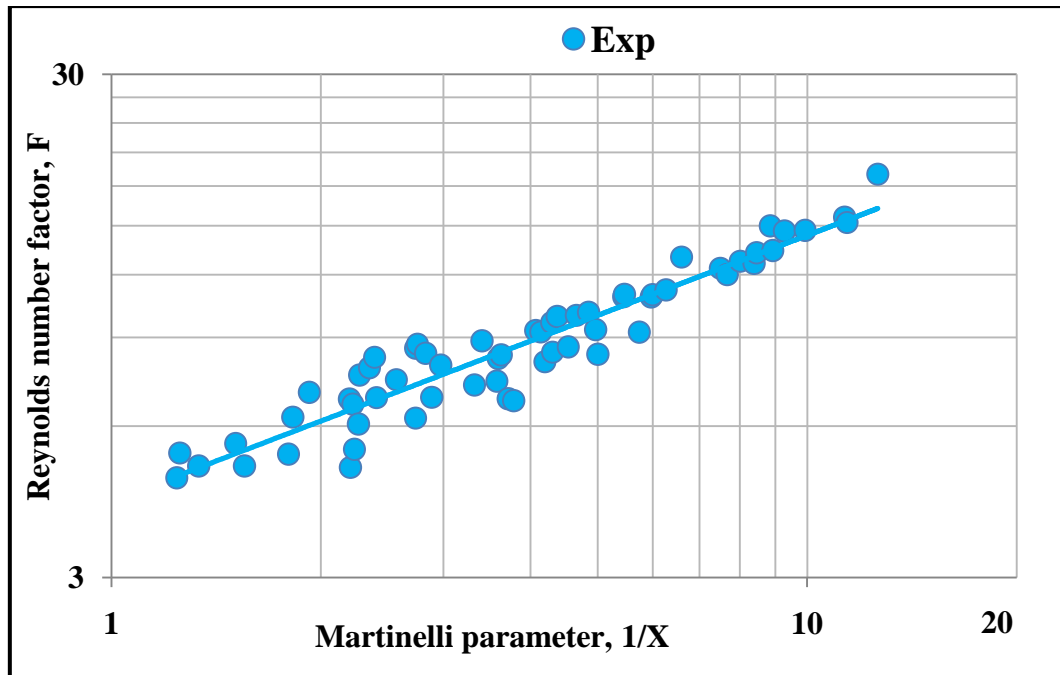


Fig. 6.42: Combined measured local heat transfer coefficients for convective boiling in wavy fin surfaces (WF1 and WF2)

From the Fig 6.42 the Reynolds number factor, F (approximate fit to data) is correlated as

$$F = \left[1 + \frac{20.5}{X} \right]^{0.5} \quad (6.6)$$

for the case $\frac{1}{X} > 1.0$. Data for which the nucleate boiling was dominant, $\frac{1}{X} < 1.0$ has not included in the development of correlations of F . The measured data of both offset strip fin surfaces are reasonably well represented by single correlation. In fact, 90 percent of the heat transfer data shown in Fig. 6.42 lie within ± 10 percent of Eqn. 6.6. The results shown above indicate that the convective boiling component of the two-phase heat transfer coefficient for the two wavy fin geometries considered here differ only slightly when correlated in terms of F -parameter.

6.4.2 Two-phase frictional pressure drop correlations

The two-phase frictional pressure gradient is usually expressed in terms of single-phase pressure gradient for liquid phase flowing alone in the channel. Two-phase pressure drop are plotted in terms of two-phase frictional multiplier ϕ_f and Lockhart and Martinelli parameter $1/X$ for offset strip and wavy fins.

6.4.2.1 Generation of correlation for offset strip fin, OSF1

The measured two-phase pressure drop data for the offset strip surface OSF1 is plotted in terms of ϕ_f and $1/X$ in Fig. 6.43.

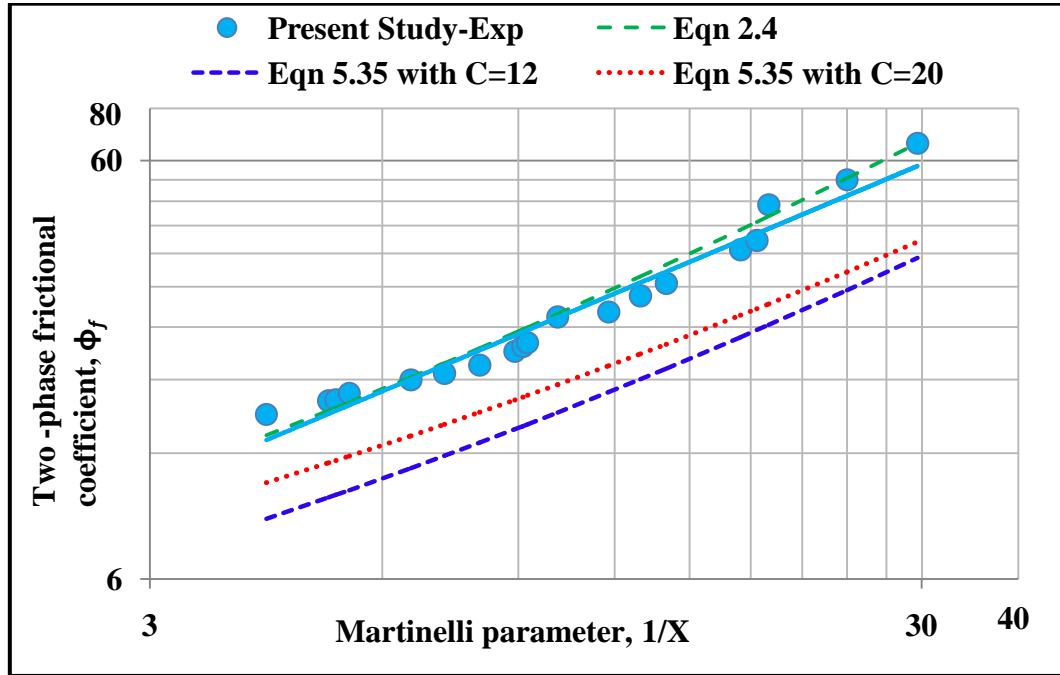


Fig. 6.43: Measured two-phase frictional coefficient for OSF1 and comparison with predictions reported

From the Fig 6.43 the two-phase frictional multiplier, ϕ_f (approximate fit to data) is correlated as

$$\phi_f^2 = 1 + \frac{30.1}{X} + \frac{4}{X^2} \quad (6.7)$$

Measured two-phase frictional data of present study is comparable with Eqn 2.4 proposed by Kim and Sohn (2006) for offset strip fin surface. The small deviation is attributed due to difference in the geometries of the fin. Large deviation between experimental data and the predictions for round tubes by using Lockhart and Martinelli (1949) correlations is observed. As explained by Kim and Sohn (2006) at low vapour qualities, offset strip fins periodically redirects the flow and increases the two-phase pressure drop somewhat higher than the value caused by wall friction alone. At high vapour qualities, high velocity vapour flow interacts with the fins and causes a larger pressure drop than that of in round tubes. Mandrusiak and Carey (1988) reported that at higher vapour qualities fin form drag effects become more significant in offset strip fins. Due to this offset strip fins exhibits two-phase frictional

multiplier more than 50% compared to round tubes under comparable flow conditions. The present study also shows that two-phase frictional multiplier is higher than the round tubes. Experimental data with Eqn.6.7 can be correlated with error bound of $\pm 6.02\%$ for two phase frictional multiplier.

6.4.2.2 Generation of frictional correlation for offset strip fin, OSF2

The measured two-phase pressure drop data for the offset strip surface OSF2 is plotted in terms of ϕ_f and $1/X$ in Fig 6.44.

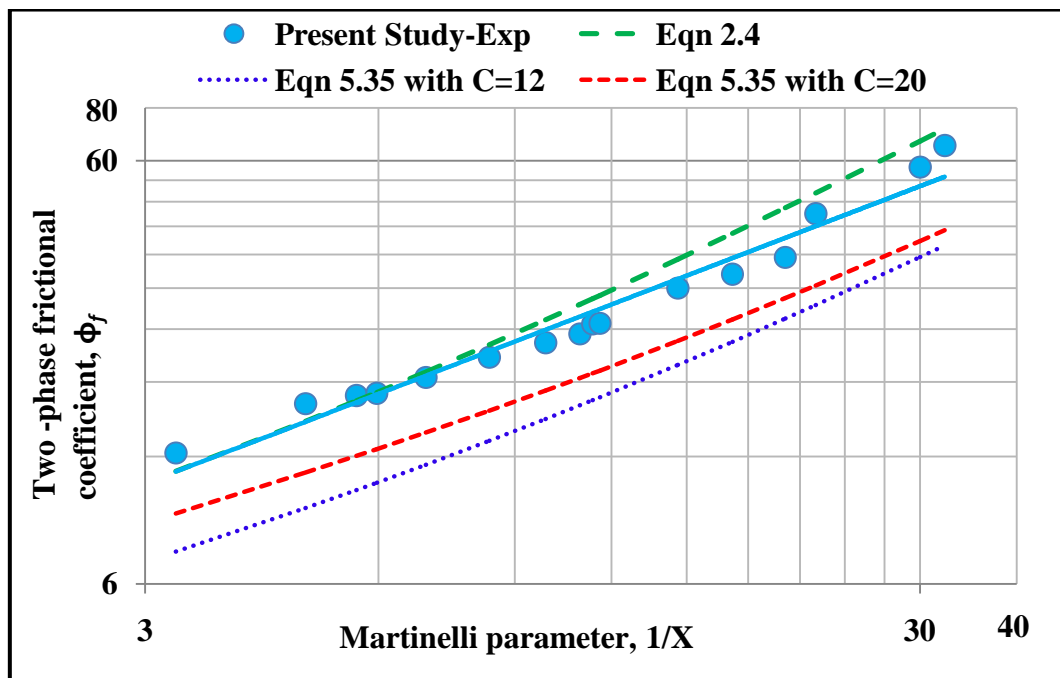


Fig. 6.44: Measured two-phase frictional coefficient for OSF2 and comparison with predictions reported

From the Fig 6.44 the two-phase frictional multiplier, ϕ_f (approximate fit to data) is correlated as

$$\phi_f^2 = 1 + \frac{28}{X} + \frac{3.3}{X^2} \quad (6.8)$$

Disagreement between experimental data and the predictions referred in Fig 6.44 is explained in para no.6.4.2.1.

Experimental data with Eqn.6.8 can be correlated with error bound of $\pm 6.32\%$ for two phase frictional multiplier.

6.4.2.3 Generalized frictional correlation for offset strip fin surfaces

A composite plot summarizing two-phase frictional data for two offset fin surfaces is shown in Fig. 6.45.

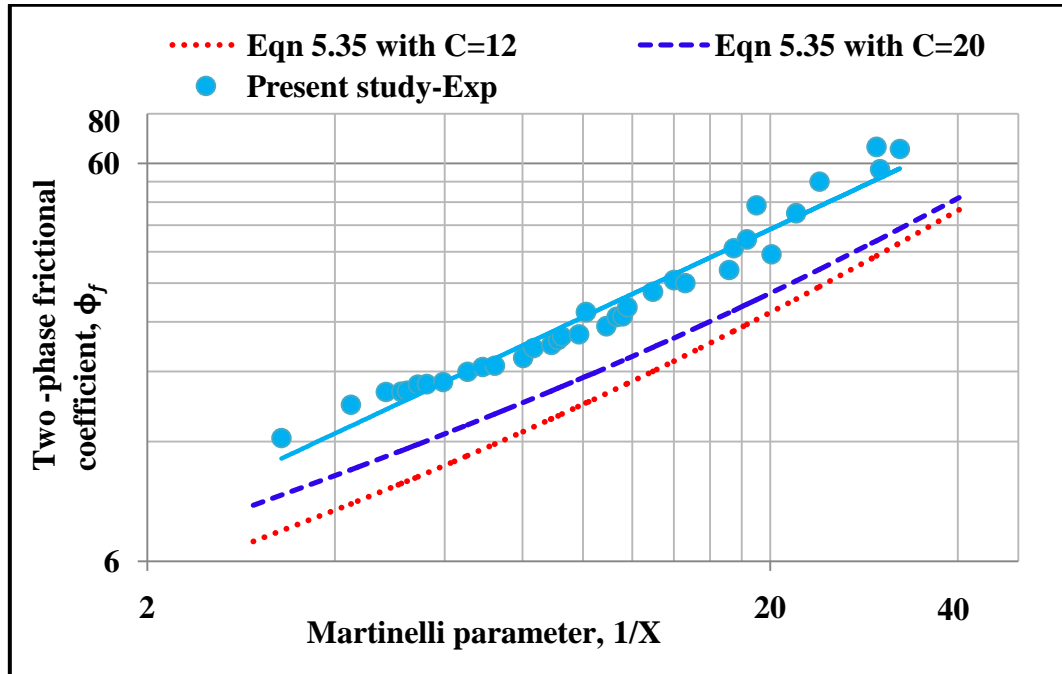


Fig. 6.45: Combined measured two-phase frictional coefficient in offset fin surfaces (OSF1 and OSF2).

From the Fig. 6.45 the two-phase frictional multiplier, ϕ_f (approximate fit to data) is correlated as

$$\phi_f^2 = 1 + \frac{29}{X} + \frac{3.5}{X^2} \quad (6.9)$$

The measured data of both offset strip fin surfaces are reasonably well represented by single correlation. In fact, 90 percent of the heat transfer data shown in Fig. 6.45 lie within ± 10 percent of Eqn.6.9.

6.4.2.4 Generation of frictional correlation for wavy fin, WF1

The measured two-phase pressure drop data for the wavy surface WF1 is plotted in terms of ϕ_f and $1/X$ in Fig. 6.46.

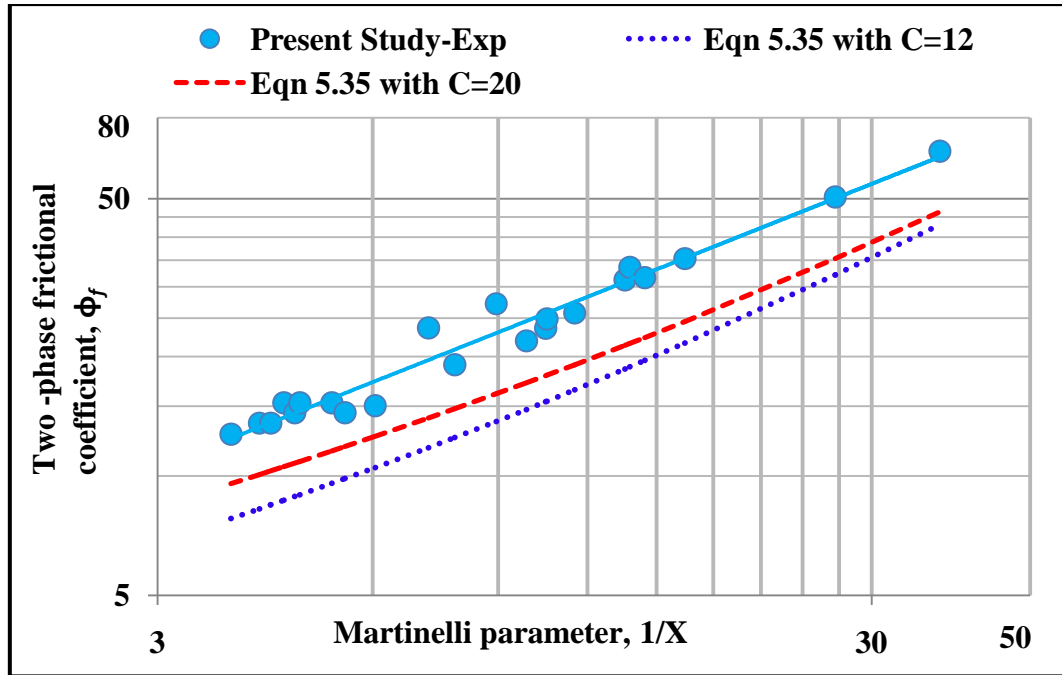


Fig. 6.46: Measured two-phase frictional coefficient for WF1 and comparison with predictions reported.

From the Fig 6.46 ϕ_f (approximate fit to data) is correlated as

$$\phi_f^2 = 1 + \frac{25}{X} + \frac{3}{X^2} \quad (6.10)$$

Experimental data with Eqn.6.10 can be correlated with error bound of $\pm 6.82\%$ for two phase frictional multiplier.

In Fig 6.46, measured two-phase pressure drop data is compared with round tubes since there are no correlations available for wavy fins in open literature. Large deviation between experimental data and the predictions for round tubes by using Lockhart and Martinelli (1949) correlations is observed. This is due to different geometries of the flow passage. Interruption of two-phase flow by wavy fins increases the pressure drop. Fin form drag in the channel with fins gives higher two-phase frictional multiplier than the round tubes.

6.4.2.5 Generation of frictional correlation for wavy fin, WF2

The measured two-phase pressure drop data for the wavy surface WF1 is plotted in terms of ϕ_f and $1/X$ in Fig. 6.47.

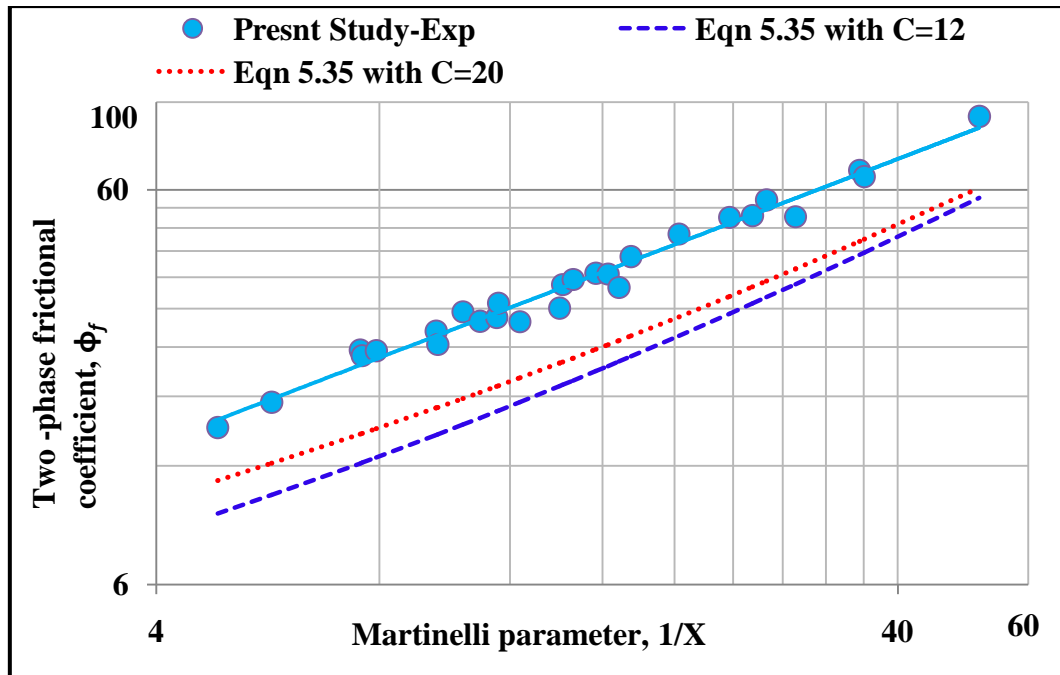


Fig. 6.47: Measured two-phase frictional coefficient for WF2 and comparison with predictions reported.

From the Fig 6.47, ϕ_f (approximate fit to data) is correlated as

$$\phi_f^2 = 1 + \frac{25}{X} + \frac{3.2}{X^2} \quad (6.11)$$

Experimental data with Eqn.6.11 can be correlated with error bound of $\pm 6.52\%$ for two phase frictional multiplier.

6.4.2.6 Generalized frictional correlation for wavy fin surfaces

A composite plot summarizing two-phase frictional data for two wavy fin surfaces is shown in Fig 6.48.

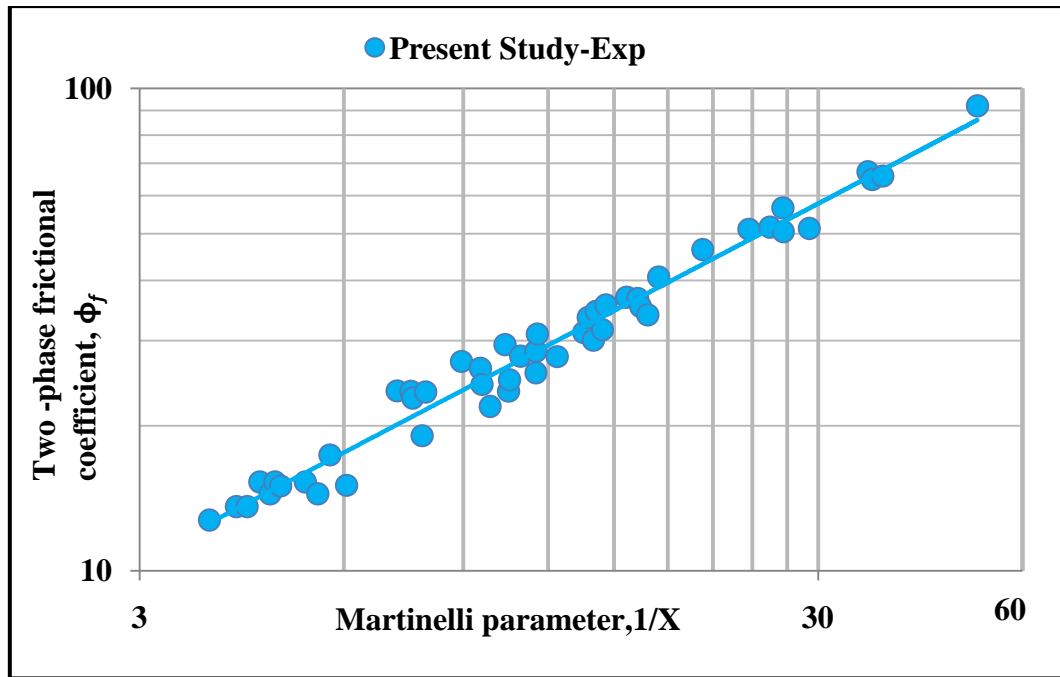


Fig. 6.48: Combined measured two-phase frictional coefficient in wavy fin surfaces (WF1 and WF2).

From the Fig 6.48 the two-phase frictional multiplier, ϕ_f (approximate fit to data) is correlated as

$$\phi_f^2 = 1 + \frac{25}{X} + \frac{3.1}{X^2} \quad (6.12)$$

The measured data of both wavy fin surfaces are reasonably well represented by single correlation. In fact, 90 percent of the heat transfer data shown in Fig. 6.48 lie within ± 10 percent of Eqn.6.12.

6.5 SUMMARY

The effects of flow parameters (mainly q , x , G) on the two-phase heat transfer and frictional pressure drops were analysed for both offset strip and wavy fins in this chapter. Reynolds number factor, F and two-phase frictional multiplier ϕ_f^2 are predicted for both the fins. Generalized correlations have been developed these fin surfaces. The summary of correlations developed for 2 offset strip and 2 wavy fins are presented in Table 6.1

Table 6.1: Summary of correlations developed for offset and wavy fins

Type of Fin surface	Reynolds Number factor, F	Two-phase frictional multiplier, ϕ_f
OSF1	$F = \left[1 + \frac{33.3}{X}\right]^{0.5}$	$\phi_f^2 = 1 + \frac{30.1}{X} + \frac{4}{X^2}$
OSF2	$F = \left[1 + \frac{30}{X}\right]^{0.5}$	$\phi_f^2 = 1 + \frac{28}{X} + \frac{3.3}{X^2}$
Combined equation of OSF1 and OSF2	$F = \left[1 + \frac{32}{X}\right]^{0.5}$	$\phi_f^2 = 1 + \frac{29}{X} + \frac{3.5}{X^2}$
WF1	$F = \left[1 + \frac{21}{X}\right]^{0.5}$	$\phi_f^2 = 1 + \frac{25}{X} + \frac{3}{X^2}$
WF2	$F = \left[1 + \frac{20}{X}\right]^{0.5}$	$\phi_f^2 = 1 + \frac{25}{X} + \frac{3.2}{X^2}$
Combined equation of WF1 and WF2	$F = \left[1 + \frac{20.5}{X}\right]^{0.5}$	$\phi_f^2 = 1 + \frac{25}{X} + \frac{3.1}{X^2}$

CHAPTER 7

CONCLUSIONS AND SCOPE FOR FUTURE WORK

7.1 CONCLUSIONS

Two-phase heat transfer and pressure drop characteristics are studied experimentally on 4 compact plate fin heat exchanger fin surfaces (2 offset strip and 2 wavy fins) for R134a refrigerant. The contributions from the present study are summarized as below.

- Obtained the two phase heat transfer and pressure drop data for offset strip and wavy fin geometries from the experiments.
- Local flow boiling heat transfer and pressure drop characteristics obtained and analysed the trends with respect to vapour quality, mass flux and heat flux. Influence of flow parameters on boiling heat transfer and pressure drops were studied. Two-phase heat transfer and pressure drop coefficient increases with the increase in mass flux and vapour quality and shows a strong dependence on the mass flux and vapour quality and less significance of heat flux.
- Reynolds number factor, F and two-phase frictional multiplier ϕ_f^2 are predicted for both offset strip and wavy fins. Empirical correlations were developed for predicting the refrigerant boiling heat transfer coefficient and two-phase frictional pressure drop for both offset strip and wavy fins. The correlations were developed in terms of Reynolds number (F) and Martinelli parameter (X) for heat transfer and two-phase frictional multiplier ϕ_f^2 and Martinelli parameter X for pressure drop. The developed correlations for R134a are presented in the table below. Among these 4 fins OSF1 showed highest heat transfer coefficient and WF2 showed the lowest pressure drop coefficient. Hence the selection of fin for design of evaporator may be based on applications.

Type of Fin surface	Reynolds Number factor, F	Two-phase frictional multiplier, ϕ_f
OSF1	$F = \left[1 + \frac{33.3}{X}\right]^{0.5}$	$\phi_f^2 = 1 + \frac{30.1}{X} + \frac{4}{X^2}$
OSF2	$F = \left[1 + \frac{30}{X}\right]^{0.5}$	$\phi_f^2 = 1 + \frac{28}{X} + \frac{3.3}{X^2}$
Combined equation of OSF1 and OSF2	$F = \left[1 + \frac{32}{X}\right]^{0.5}$	$\phi_f^2 = 1 + \frac{29}{X} + \frac{3.5}{X^2}$
WF1	$F = \left[1 + \frac{21}{X}\right]^{0.5}$	$\phi_f^2 = 1 + \frac{25}{X} + \frac{3}{X^2}$
WF2	$F = \left[1 + \frac{20}{X}\right]^{0.5}$	$\phi_f^2 = 1 + \frac{25}{X} + \frac{3.2}{X^2}$
Combined equation of WF1 and WF2	$F = \left[1 + \frac{20.5}{X}\right]^{0.5}$	$\phi_f^2 = 1 + \frac{25}{X} + \frac{3.1}{X^2}$

- The experimentally measured flow boiling heat transfer coefficients are compared with the values predicted by correlations. Measured values of local boiling heat transfer can be predicted within $\pm 25\%$ of the correlation proposed in the present study.
- Single-phase refrigerant heat transfer and pressure drop data for a range of fin surfaces using experiments as well as CFD approach obtained. CFD data compared with experiments data and found that CFD results are found in good agreement with experimental results. The deviation is found less than 5%. Hence CFD approach can be used for predicting the j and f data for any other fluids to save the time and cost of experiments.
- Colburn j factor and friction factor f were analyzed using CFD and compared for water and R134a for wavy fin. It is observed that there is no significant variation of ' f ' factor for both liquid water and liquid refrigerant R134a at constant Reynolds number. The difference is found less than 5% for both liquids. However the variation in ' j ' factor is found for water and liquid refrigerant R134a about 15%.
- The generalized correlations for single phase j and f in terms of non-dimensional parameters are developed at Reynolds number range of 100-15000. The effects of fin geometry on the enhanced heat transfer and pressure

drops are investigated. The proposed correlations for wavy and offset fin surfaces are given below.

Wavy fin surface:

Generalized heat transfer correlations non-dimensional parameters for a) R134a:

$$j = 2.989Re^{-0.54241} \alpha^{-0.72276} \beta^{-0.83914} \gamma^{-0.7588} \quad \text{for } 100 \leq Re \leq 1000$$

$$j = 3.245Re^{-0.66388} \alpha^{-0.53614} \beta^{-0.80626} \gamma^{-0.6346} \quad \text{for } 1000 \leq Re \leq 15000$$

b) Water:

$$j = 1.154Re^{-0.65938} \alpha^{-0.96698} \beta^{0.176702} \gamma^{0.28878} \quad \text{for } 100 \leq Re \leq 1000$$

$$j = 0.323Re^{-0.69341} \alpha^{-0.9602} \beta^{0.633246} \gamma^{0.889252} \quad \text{for } 1000 \leq Re \leq 15000$$

Generalized friction correlations in terms of non-dimensional parameters for R134a and Water

$$f = 18.607Re^{-0.59381} \alpha^{-0.088954} \beta^{-0.46976} \gamma^{-0.92621} \quad \text{for } 100 \leq Re \leq 1000$$

$$f = 24.413Re^{-0.46532} \alpha^{-0.226497} \beta^{-0.94256} \gamma^{-1.70937} \quad \text{for } 1000 \leq Re \leq 15000$$

Offset strip fin surface:

Generalized heat transfer correlations for R134a in terms of non-dimensional parameters

$$j = 0.01197 \times Re^{-0.5375} \times \alpha^{0.1212} \times \delta^{-0.1906} \times \epsilon^{-0.8473} \quad \text{for } 100 \leq Re \leq 1000$$

$$j = 0.0099 \times Re^{-0.3744} \times \alpha^{-0.4331} \times \delta^{-0.5475} \times \epsilon^{-0.6931} \quad \text{for } 1000 \leq Re \leq 15000$$

$$f = 0.33648 \times Re^{-0.5909} \times \alpha^{-0.1275} \times \delta^{-0.2356} \times \epsilon^{-0.6108} \quad \text{for } 100 \leq Re \leq 1000$$

$$f = 0.00632 \times Re^{-0.2163} \times \alpha^{0.2253} \times \delta^{-0.3799} \times \epsilon^{-0.9331} \quad \text{for } 1000 \leq Re \leq 15000$$

7.2 SCOPE FOR FUTURE WORK

- Flow visualization of two-phase flow in compact plate fin heat exchangers is a topic rarely addressed and the two-phase flow patterns in this type of channel are very poorly understood. The purpose of flow visualization is to obtain qualitative information of the flow, based on which two-phase flow patterns could be identified. Two-phase flow patterns in conventional pipes are well investigated and documented, but this is not so for plate fin heat exchangers.

- The present work can be extended for other fluids i.e. user friendly refrigerants R236fa, R245fa etc. Also effect of fin geometry (fin height, fin density and fin length) on two-phase heat transfer and pressure drop coefficient can be assessed.

REFERENCES

Journal References

- Asadi, M.(2013).“Studies on Functions of friction and Colburn factors in compact heat exchangers”. *Int. J. Mod. Eng. Sci.*, 2, 17-27.
- Awad, M.M and Muzychka, K.S. (2011).“Models for pressure drop and heat Transfer in air cooled compact wavy fin heat exchangers”. *J. Enhanced Heat Transfer*, 18 (3), 191–207.
- Bennett, D.L., Davis, M.W., Hertzler, B.L. (1980).“The suppression of saturated nucleate boiling by forced convective flow”. *AIChE Symp. Ser.*, 76, 91–103.
- Carey, V.P. (1993).“Two-phase flow in small-scale ribbed and finned passages for compact evaporators and condensers”. *Nucl Eng. Des*, 141, 249–268.
- Carey, V.P. and Mandrusiak, G.D. (1986).“Annular film-flow boiling of liquids in a partially heated vertical channel with offset strip fins”. *Int. J. Heat Mass Transfer*, 29 (6), 927–939.
- Charnay, R., Revellin, R. and Bonjour, J(2015). “Flow boiling heat transfer in mini-channels at high saturation temperatures: Part I – Experimental investigation and analysis of the heat transfer mechanisms”. *Int. J. Heat Mass Transfer*, 87, 636–652.
- Chen, J.C. (1966).“Correlation for boiling heat transfer to saturated fluids in convective flow”. *Ind. Eng. Chem. Process Des. Dev*, 5 (3), 322-339.
- Ciofalo, M., Stasiek, J. And Collins, M.W.(1996).“Investigation of flow and heat transfer in corrugated passages-II; numerical simulations”. *Int. J. Heat Mass Transfer*, 39, 165–192.
- Cooper, M. G. (1984). “Heat flow rates in saturated pool boiling-a wide ranging examination using reduced properties”. *J. Adv. Heat Transfer*, 16,157-239.
- Dong Junqi, Zhang Yi, Li Gengtian and Xu Weiwu, (2013).“Experimental study of wavy fin aluminium plate fin heat exchanger, experimental heat transfer”. *J. Thermal Energy Generation, Transport, Storage and Conversion*, 26, 384-396.
- Feldman, A., Marvillet, C. and Lebouche, M. (2000). “Nucleate and convective boiling in plate in heat Exchangers”. *Int. J. Heat Mass Transfer*, 43, 3433-3442.

- Hamdar, M., Zoughaib, A. and Clodic, D. (2010). "Flow boiling heat transfer and pressure drop pure HFC 152a in a horizontal mini channel". *Int. J. Refrig*, 33, 566-577.
- Han, D.H., Lee, K.J. and Kim, Y.H. (2003). "Experiments on the characteristics of evaporation of R410A in brazed plate heat exchangers with different geometric configurations". *J. Appl. Therm. Eng.*, 23, 1209–1225.
- Hartzog, D.G. and Welmer, R.F. (1977). "Effect of mal-distribution on the performance of multistream multipassage heat exchangers". *J. Adv. Cryo. Eng.*, 18, 52-64.
- Hu, S. and Herold, K.E. (1995). "Prandtl number effect on offset fin heat exchanger performance: experimental results". *Int. J. Heat Mass Transfer*, 38, 1053-1061.
- Hu, S. and Herold, K.E. (1995). "Prandtl number effect on offset fin heat exchanger performance: predictive model for heat transfer and pressure drop". *Int. J. Heat Mass Transfer*, 38 (6), 1043-1051.
- Joshi, H.M. and Webb, R.L. (1987). "Heat transfer and friction in the offset strip fin heat exchanger". *Int. J. Heat Mass Transfer*, 30, 6235-6242.
- Kabelac, S. and Djordjevic, E. (2008). "Flow boiling of R134a and ammonia in a plate heat exchanger". *Int. J. Heat Mass Transfer*, 51, 69-84
- Kandlikar, S. G. (1990). "A general correlations for saturated two-phase flow boiling heat transfer inside a horizontal and vertical tubes". *J. Heat Transfer*, 112.
- Kew, P.A. and Cornwell, K. (1997). "Correlations for the prediction of boiling heat transfer in small-diameter channels". *J. Appl. Therm. Eng.*, 17 (8–10), 705–715.
- Kim, B. and Sohn, B. (2006). "An experimental study of flow boiling in a rectangular channel with offset strip fins". *Int. J. Heat Fluid Flow*, 27, 514– 521.
- Kim, S.M., and Mudawar, I. (2013). "Universal approach to predicting two-phase frictional pressure drop for mini/micro-channel saturated flow boiling". *Int. J. Heat Fluid Flow*, 58, 718– 734.
- Kundu, A., Kumar, R. and Gupta, A. (2014). "Heat transfer characteristics and flow pattern during two-phase flow boiling of R134a and R407C in a horizontal smooth tube". *J. Exp. Therm. Fluid Sci.*, 57, 344–352.

- Lazarek, G.M. and Black, S.H. (1982). "Evaporative heat transfer, pressure drop and critical heat flux in a small vertical tube with R113". *Int. J. Heat Mass Transfer*, 25 (7), 945–960.
- Lee, H.J. and Lee, S.Y. (2001). "Heat Transfer correlations for boiling flows in small rectangular horizontal channels with low aspect ratio". *Int. J. Multiphase Flow*, 27, 2043-2062.
- Lockhart, R.W. and Martinelli, R.C. (1949). "Proposed correlation of data for isothermal two-phase two-component flow in pipes". *Chem. Eng. Prog.* 45, 39–48.
- Longo, G.A., Gasparella, A. and Sartori, R. (2004). "Experimental heat transfer coefficients during refrigerant vaporisation and condensation inside herringbone-type plate heat exchangers with enhanced surfaces". *Int. J. Heat Mass Transfer*, 47, 4125–4136.
- Longo, G.A. and Gasparella, A. (2007). "Refrigerant R134a vaporisation heat transfer and pressure drop inside a small brazed plate heat exchanger". *Int. J. Refrig*, 30, 821–830.
- Mandrusiak, G.D. and Carey, V.P. (1989). "Convective boiling in vertical channels with different offset strip fin geometries". *ASME. J. Heat Transfer*, 111, 156–165.
- Mandrusiak, G.D. and Carey, V.P. (1988). "Pressure drop characteristics of two-phase flow in vertical channels with different offset strip fin geometries". *J. Exp. Therm. Fluid Sci.*, 1, 41–50.
- Mandrusiak, G.D., Carey, V.P. and Xu, X. (1988). "An experimental study of convective boiling in a partially heated horizontal channel with offset strip fins". *ASME. J. Heat Transfer*, 110, 229–236.
- Manglik, R.M and Bergles, A.E. (1995). "Heat transfer and pressure drop correlations for the rectangular off strip fin compact heat exchanger". *J. Exp. Therm. Fluid Sci.*, 10, 171-180.
- Marchitto, A., Devia, F., Fossa, M., Guglielmini, G. and Schenone, C. (2008). "Experiments on two-phase flow distribution inside parallel channels of compact heat exchangers". *Int. J. Multiphase Flow*, 34, 128–144.

- Patankar, S.V., Liu, C.H. and Sparrow, E. (1977).“Fully developed flow and heat transfer in ducts having stream wise-periodic variations of cross sectional area”. *J. Heat transfer*, 99, 180-186.
- Peng, X.F. and Wang, B.X. (1993). “Forced convection and flow boiling heat transfer for liquid flowing through micro-channels”. *Int. J. Heat Mass Transfer*, 36, 3421–3427.
- Prajapati, Y.K, Pathak, M and Khan, M.K (2015). “A comparative study of flow boiling heat transfer in three different configurations of micro-channels”. *Int. J. Heat Mass Transfer*, 85, 711–722.
- Pulvirenti, B., Matalone, A. and Barucca, U. (2010).“Boiling heat transfer in narrow channels with offset strip fins: Application to electronic chipsets cooling”. *J. Appl. Therm. Eng.*, 30, 2138-2145.
- Qu, W. and Mudawar, I. (2003).“Flow boiling heat transfer in two-phase micro-channel heat sinks—I: Experimental investigation and assessment of correlation methods”. *Int. J. Heat Mass Transfer*, 46, 2755–2771.
- Ranganayakulu, C. And Pallavi, P. (2011).“Development of heat transfer coefficient and friction factor correlations for offset fins using CFD”. *Int. J. Numer. Methods Heat Fluid Flow*, 21 (8), 935-951.
- Ranganayakulu, C. and Kabelac, S. (2015). “Boiling of R134a in a plate fin heat exchanger having offset fins”. *ASME. J. Heat Transfer*, 137 (12), HT-14-1235.
- Robertson, J.M. and Lovegrove, P.C. (1983).“Boiling heat transfer with Freon 11 in brazed aluminium plate-fin heat exchangers”. *J. Heat Transfer*, 105, 605–610.
- Saad, S.B, Clement, P., Fourmigue, J. F., Gentric, C. and Leclerc, J.P. (2012). “Single phase pressure drop and two-phase-distributions in an offset strip fin compact heat exchanger”. *J. Appl. Therm. Eng*, 49, 99-105.
- Shah, R.K. and London, A. L. (1969).“Offset rectangular plate-fin surfaces-heat transfer and flow friction characteristics”. *ASME. J. Eng. Power*, 90, 218-228.
- Shah, R.K.(2006).“Advances in science and technology of compact heat exchangers”. *J. Heat Transfer Eng.*, 27(5), 3-22.
- Taboas, F., Valle`s, M., Bourouis, M. and Coronas, A. (2010). “Flow boiling heat transfer of ammonia/water mixture in a plate heat exchanger”. *Int. J. Refrig.*,33,695-705

- Tibirica, C. B. and Ribatski, G. (2010). “Flow boiling heat transfer of R134a and R245fa in a 2.3 mm tube”. *Int. J. Heat Mass Transfer*, 53, 2459-2468.
- Tran, T.N., Wambsganss, M.W. and France, D. M. (1996). “Small circular and rectangular channel boiling with two refrigerants”. *Int. J. Multiphase Flow*, 22 (3), 485–498.
- Vakili, F. F., Agostini, B. and Thome, J. R. (2013). “Experimental study on flow boiling heat transfer of multiport tubes with R245fa and R1234ze (E)”. *Int. J. Refrig*, 36, 335-352.
- Vlasogiannis, P., Karagiannis, G., Argyropoulos, P. and Bontozoglou, V. (2002). “Air–water two-phase flow and heat transfer in a plate heat exchanger”. *Int. J. Multiphase Flow*, 28, 757–772
- Wadekar, V.V. (1991). “Vertical slug flow heat transfer with nucleate boiling”. *ASME. HTD*, 159, 157–161.
- Wadekar, V.V. (1992). “Flow boiling of heptane in a plate-fin heat exchanger passage”. Proc., of the Compact Heat Exchangers for Power and Process Industries, *ASME. HTD*, 201, 1–6.
- Wang, S., Gong, M.Q., Chen, G.F., Sun, Z.H. and Wu, J.F. (2013). “Two-phase heat transfer and pressure drop of propane during saturated flow boiling inside a horizontal tube”. *Int. J. Refrig*.
- Watel , B. (2003). “Review of saturated flow boiling in small passages of compact heat exchangers”. *Int. J. Therm. Sci.*, 42, 107-140.
- Webb, R.L and Gupte, N.S.(1992). “Critical review of correlations for convective vaporization in tubes and tube banks”. *J. Heat Transfer Eng.*, 13 (3), 58-81.
- Wieting, A.R. (1975). “Empirical correlation for heat transfer and flow friction characteristics of rectangular offset-fin plate fin heat exchangers”. *ASME. J. Heat Transfer*, 97, 488-490.
- Xu, Y., Fang, X., Li, G. and Li, D (2015). “An experimental investigation of flow boiling heat transfer and pressure drop of R134a in a horizontal 2.168 mm tube under hyper gravity Part II: Heat transfer coefficient”. *Int. J. Heat Mass Transfer*, 80, 597–604.

Zhang, J., Jaydeep, K. and Manglik, R.M. (2004). “Effect of fin waviness and spacing on the lateral vortex structure and laminar heat transfer in wavy-plate-fin cores”. *Int. J. Heat Mass Transfer*, 47, 1719–1730.

Books

Anderson, J.D. (1995). “*Computational Fluid Dynamics-The Basic with Applications*”. McGraw-Hill Companies Inc, New York.

ASHRAE, (2001). “*Fundamental Handbook*”. American Society of Heating, Refrigerating and Air-Conditioning Engineers, Inc, USA.

Beale, S.B. (1993). “Fluid Flow and Heat Transfer in Tube Banks”, Ph.D. Thesis, Imperial College of Science, Technology and Medicine, London.

Collier, J.G. and Thome, J. R (1994). “*Convective boiling and condensation*”. Oxford University press, New York.

Engineering Equation Solver (EES). F-Chart Software, Madison, USA.

Haseler, L.E. (1993). “*Performance calculation methods for multi stream plate fin heat exchangers Heat exchangers-Theory and practice*”. McGraw Hill, Newyork, 405-506.

Kandlikar, S. G., Shoji, M., and Dhir, V. K. (1999). “*Handbook of Phase change: Boiling and Condensation*”. Taylor and Francis, USA.

Kays, W.H. and London, A.L.(1984). “*Compact Heat Exchangers, (3rd Edn)*”. McGraw-Hill, New York.

Maiti, D.K. (2002). “*Heat transfer and flow friction characteristics of plate-fin heat exchanger surfaces – a numerical study*”. PhD Thesis, IIT Kharagpur, India.

Patankar, S.V. (1980). “*Numerical heat transfer and fluid flow*”. Hemisphere series on computational methods in mechanics and thermal science, Taylor and Francis, 79–86.

Versteeg, H.K. and Malalasekera, W. (1995). “*An Introduction to Computational Fluid Dynamics, the Finite Volume Method*”. Prentice Hall, New York, 62–146.

Conference proceedings

Kandlikar, S. G. And Kuan, W. K. (2006). “*Experimental study on saturated flow boiling critical heat flux in microchannels*”. Proc. ICNMM-2006, 4th Int. Conf. on Nano, Micro and Mini channels, June 19-21, Limerick, Ireland.

Nishikawa, K., Fujita, Y., Ohta, Y., Hidata, S. (1982). “*Effect of the surface roughness on the nucleate boiling heat transfer over the wide range of pressure*”. Proc. 7th Int. Heat Transfer Conf., 4, 61-68

Ranganayakulu, C., Ismail, L.S., Vasudeva Rao, V. And Rajeshwar, S. (2008). “*Optimization of compact plate-fin heat exchanger-a CFD approach*”. Proc., of 19th Nat. Heat and Mass Transfer & 8th ISHMT-ASME Heat Mass Transfer Conf., JNTU, Hyderabad, India.

Ranganayakulu, C., Mersmann, I. and Kabelac, S. (2013). “*Boiling of R134a in a plate fin heat exchanger having offset fins*” Proc., of the 22th Nat. and 11th Int. ISHMT-ASME Heat Mass Transfer Conf., December 28-31, IIT Kharagpur, India.

Robertson, J.M., Wadekar, V.V. (1988). “*Boiling characteristics of cyclohexane in vertical up flow in perforated plate-fin passages*”. 25th Nat. Heat Transfer Conf., Houston, AIChE Sympos. Ser., 84 (263), 120–125.

MEASURING INSTRUMENTS CALIBRATION

A. PRESSURE SENSORS

Pressure sensors are used in test facility are.

- Absolute pressure sensors
- Differential pressure sensors

A.1 Pressure Transducer

Pressure transducers are calibrated using dead weight method.

A.1.1 Instruments required

- a) Pressure transducer / transmitter (Unit under Test)
- b) Power supply: 24V
- c) Voltage standard: NI Multifunction Calibrator, Make: Yokogawa, Model: CA51, S/N:T1F2002, NAL/PR/HSCTF/ C-55, DRUCK / DPI 605 /DPI 610
- d) Pressure standard: Dead weight Pressure Calibrator

A.1.2 Calibration Procedure

Initially the required level of oil is ensured in the calibrator by visual examination. The pressure transmitter to be calibrated is connected to the calibration port of the calibrator. The transmitter is wired through 24V power supply and a 100 ohm resistor to the Multi Function calibrator / DPI 605/610

The priming handle is attached to the location and rotated anti-clock wise completely, after opening the air vent port, the handle is rotated clockwise fully inside to expel the air bubbles formed inside. The same procedure is repeated one more time. Then finally the handle moved out fully by rotating anti-clock wise and air vent port is closed. By using the computer program provided by the calibrator supplier, the weights required to produce required pressure is calculated. Then these weights are kept on the respective pistons (low pressure and High Pressure) as directed by the computer program. Then the pressurizing handle is rotated clock-wise such that the pistons move up and the weights float till the provided mark in the indicating bar.

After the weights are floating slightly rotate the weights and wait for a while. Then measure the electrical output using multifunction calibrator / DPI 605/DPI 610 and compares it with the standard value. If the error in measurement is within the specified limit of the device, then it is accepted and declared as “calibration passed”. If the error is not within the specified limit of the device, then calibration is repeated once again and the measurement is verified further. The results are shown in Table-A1

Table A1: Calibration Report of Pressure Transducer / Transmitter

Unit Under Test (UUT)		Calibrator Information	
Document No: PR/CLOCTER/VCRS/PRT/01		Dead weight Pressure Calibrator	
Make: Measurement Specialties		S/N: 2031811	
Model No: M5156		Cal Ref: NAL/PR/HSCTF/C-56	
S/N: 030108D262, Cal date: 9 MAR 2015			
Date of Next Calibration: 8 MAR 2016			
Calibration Data			
Standard Reading (bar 'g')	Sensor O/P (mA)	Actual Reading (barg)	Error %FS
0.00	4.292	0.007	0.02
5.00	6.263	4.943	-0.13
10.00	8.296	10.033	0.09
15.00	10.275	14.989	-0.02
20.00	12.287	20.027	0.07
25.00	14.286	25.032	0.09
30.00	16.28	30.025	0.07
35.00	18.242	34.938	-0.15
40.00	20.256	39.981	-0.04

A.2 Differential pressure transducer

A.2.1 Instruments required

- a) Pressure transducer / transmitter (Unit under Test)
- b) Power supply: 24V DC
- c) Voltage standard: DRUCK / DPI 605 /DPI 610
- d) Pressure standard: DRUCK / DPI 605 /DPI 610

A.2.2 Calibration Procedure:

Energize with 24V DC power supply and connect transmitter's pressure port to the calibrator and ensure leak proof tightness. After closing Calibrators went port, required value of pressure is applied to the transmitter using its hand priming pump.

The current generated by the transmitter for the applied pressure is read by the DPI 605/610 along with the calibrators known value. The standard value and the measured values are compared for error.

If the error in measurement is within the specified limit of the device, then it is accepted and declared as "calibration passed". If the error is not within the specified limit of the device, then calibration is repeated once again and the measurement is verified further. A typical calibration result is shown in Table A2.

Table A2: Calibration Report of Differential Pressure Transducer

Unit Under Test (UUT)		Calibrator Information	
Document No: PR/CLOCTER/VCRS/DPRT/01		DRUCK / DPI 605 PRESSURE CALIBRATOR	
Make: SENSOCON		S/N: 60505988	
Model No: 251-01		Cal Ref: GTRE Calibration Certificate no.: NAL/CAL/TM/DEC/2013/242(A) dated 24th Dec 2013	
S/N: Q01404, Cal date: 18 DEC 2015		CAL Due: 24th DEC 2015	
Date of Next Calibration: 17 DEC 2016			
Calibration Data			
Standard Reading (psi)	Sensor O/P (mA)	Actual Reading (psi)	Error %FS
0.0000	3.783	-0.022	-0.43
1.0047	7.02	1.001	-0.07
2.0125	10.258	2.025	0.24
3.0288	13.519	3.055	0.52
4.0384	16.682	4.055	0.32
5.0039	19.556	4.963	-0.82

B. FLOW METERS

Two types of flow meters are used in test facility.

- Coriolis mass flow meter
- Turbine flow meter

B.1 Coriolis mass flow meter

B.1.1 Instruments required

- a. Mass flow meter (Unit under Test)
- b. Power supply: 230V
- c. Reference Mass flow Meter: Micro motion, Model No: R050, S/N: 712795
- d. Equipments used: Kerosene Pump, Pressure transmitter to ensure safe pressure limits at the headers, control valves to adjust the flow, on /off valves.
- e. Medium of calibration: kerosene

B.1.2 Calibration Procedure

Start the kerosene pump and then switch on the on-off valve and set the kerosene flow by adjusting the flow control valve. Then close the on-off valve and make the Instruments reading zero. After that open the on-off valve and allow the flow for a predetermined time. Then note down the readings of Reference and UUT meter readings. Then the reading in the flow meters can be compared for errors. Repeat the same procedure for different flow rate till the maximum range of the meter. If the error in measurement is within the specified limit of the device, then it is accepted and declared as “calibration passed”. If the error is not within the specified limit of the device, then calibration is repeated once again and the measurement is verified further. If the same error persists, it is declared as "calibration failed” and discarded from measurements at VCRS. A typical calibration result is shown in Table B1.

Table B1: Calibration report of Coriolis Mass flow meter

Unit Under Test (UUT)		Calibrator Information	
Document No: PR/CLOCTER/VCRS/MF/03		Make: MICROMOTION	
Make: MICROMOTION		Model No: RO50	
Model No: F100S		S/N: 712795	
S/N: 14075013, Cal date: 16 March 2015		Cal Ref: FCRI/OFL/C/2012/021	
Date of Next Calibration: 15 March 2018		Calibrated at FCRI, Palakkad	
Calibration Data			
UUT Meter Reading (kg/min)	Time (min)	Reference Reading (kg/min)	Error %rd
4.75	10.00	4.75	-0.04
10.20	10.00	10.21	-0.05
15.55	10.00	15.54	0.06
20.05	8.00	20.04	0.05
26.23	10.00	26.24	-0.04
31.24	10.00	31.25	-0.03
40.22	8.00	40.23	-0.02
50.60	5.00	50.61	-0.02
60.80	5.00	60.81	-0.02

B.2 Turbine flow meter

B.2.1 Calibration Procedure

The flow meter under test is installed in the metering run of approximate size. Dynamic start-stop method is used in the calibration. Water is allowed collect in the tank which is placed on a weighing scale. The pulses generated by the meter as well as time taken for a fixed quantity of liquid is recorded. Fig.B1 shows calibration certificate of flow meter.

B.2.2 Calculations

$$\text{Calibration factor (Pulses/Litre) } K = \frac{\text{Total pulses}}{\text{volume collected}} \quad (\text{B1.1})$$

$$\text{Average calibration factor} = \frac{K_{\max} + K_{\min}}{2} \quad (\text{B1.2})$$

$$\text{Linearity band} = \frac{K_{\max} - K_{\min}}{\text{Average calibration factor}} * 100 \quad (\text{B1.3})$$

$$\text{Flow rate (LPM)} = \frac{\text{Volume collected}}{\text{Time in sec}} * 60 \quad (\text{B1.4})$$

B.2.3 Sample Calculations

$$\text{Volume of water collected} = 20 \text{ lt}$$

$$\text{Total pulse recorded} = 22272$$

$$\text{Calibration factor} = 1113.60 \text{ pulses/lt}$$

$$\text{Flow rate} = 67.57 \text{ LPM}$$

ROCKWIN FLOW CALIBRATION LABORATORY
TEST CERTIFICATE

Customer: Tecno Lab Equipments, Bangalore
P.O.No. : NAL-15R/2012-13 Dt.18.10.12
W.O.No. : TF-249/12
Calibration Report No: FCL/1212/30

Inst No.: 12634
Model : TFM 1015
Range : 6.6-66 LPM
Date : 07.12.12

Calibration Details:

Total Pulses	Time (Seconds)	Flow Rate Ltr / Min	K Factor Pulses / Ltr
22272	17.76	67.57	1113.6
22217	23.63	50.78	1110.9
22219	34.49	34.79	1111.0
22199	69.76	17.20	1110.0
22172	176.39	6.80	1108.6

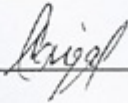
Linearity : +/- 0.23 %

Calibration Factor : 1111.1 Pulses/Litres

REMARKS

Volume: 20 Litres

Calibrated By:
(S.Saigal)



Approved By
(Manoj Kumar)



ROCKWIN FLOWMETER INDIA PVT LTD.
B-24 SITE IV, SAHIBABAD INDL. AREA, GHAZIABAD, DIST. U.P. - 201 010
TEL No.:0120-2895400/01, FAX: 0120-2895450

RCL 4012-G

Fig. B1 : Caibration report turbine flow meter

C. TEMPERATURE SENSORS

Two types of temperature sensors are used in test facility.

- RTD's (Resistance Temperature Detectors)
- Thermocouples

C.1 Resistance Temperature Detectors

Drywell calibrator is used for calibration of RTD's as given the Fig. C1.



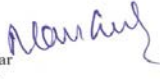
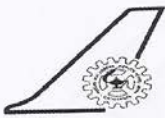
 NABL CERTIFICATE Nos. : C-0314, C-0537, C-0538 As per ISO 17025 : 2005		CALIBRATION REPORT Report No. : C1415/2260/T01 Date of Issue : 26.11.2014 Page : 1 of 1		DIMENSIONS # 128, 19th Cross, 8th Main, CHBS Layout Vijayanagar, Near BDA Complex B E N G A L U R U - 5 6 0 0 4 0 . Phone : 080 - 2314 3921, 2314 3914 E-mail : frontoffice@dimensions-callab.com URL : www.dimensions-callab.com	
1.0 Name and address of the customer	: M/s. NATIONAL AEROSPACE LABORATORIES, NWTC, Belur, Bangalore - 560 037.				
2.0 Customer Reference	: Received thru Delta Systems dated 13.11.2014				
3.0 Date of receipt and condition	: 13.11.2014 :: Satisfactory				
4.0 Description of the instrument	: Temperature Sensor Make : Delta Systems Model : -- Range : -50 to 100°C Calibrated Range: -20 to 100°C SI No : 1411T201 ID. No. : -- Accuracy : Class A Type : PT100				
5.0 Date /s & Place of Calibration	: 13.11.2014 :: Inhouse				
5.1 Due for Calibration	: 12.11.2015				
6.0 Master Used for Calibration	: 1. CHUBE-4 Thermometer Readout (A83732) 2. SPRT (DMN-INS-TM-04)				
7.0 Master's Traceability & Validity	: 1. Traceable to ETDC(Bg)/C-45943 & 30.12.2014 2. Traceable to ARAI/CAL/1301/1927 & 06.02.2015				
8.0 Calibration Procedure No.	: DMN-CPT-003				
9.0 Environmental Conditions	: Temp: 25±2.5°C Humidity: 35 to 65% RH				
10.0 Measurement Uncertainty is reported at 95% confidence level with k = 2.					
RESULTS OF CALIBRATION					
SI No.	STD Reading in °C	DUC Reading in °C	Error Claimed ± in °C	Deviation Observed in °C	Measurement Uncertainty (±) in °C
1	-19.48	-19.45	0.35	0.03	0.2
2	0.72	0.82		0.10	0.2
3	24.93	24.96		0.03	0.2
4	49.87	49.88		0.01	0.2
5	99.99	99.95		-0.04	0.2
Remarks :					
Calibration points are selected as per the customer's request.					
All readings are within the limits as per the Manufacturer's specification.					
Prepared By:				Authorised By:	
				M.R. Magesh Kumar	Technical Manager.

Fig. C1 : Calibration report RTD sensors

C.2 Thermocouples

Drywell calibrator is used for calibration of Thermocouples as given the Fig. C2.

Sample Calibration report of thermocouples is shown in Fig. C3.

Calibration Standards Aerospace Electronics & Systems Division National Aerospace Laboratories (Tel: 080-2508 6575, 6570)	
<i>TEMP/ALD/CS/37</i>	<i>Page 1 of 6</i>

Calibration Report

Calibration of K-Type Thermocouple

Work request from	Head Propulsion		
Date	09/08/2012		

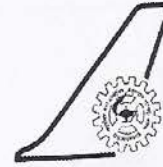
Item Description: K-Type Thermocouple

Serial No. : K-115,K-114, K-117,K-089,K-113,K-157,K-059, K-092,K-060, K-156,K-153,K-155,K-132,K-154,K-128			
Range	-40°C to 100 °C	Tolerance	Not Provided
Date of Calibration	29-08-2012	Calibration Due	29-08-2013
Environmental Conditions	RT: 20 +/-2 °C		

Standard Instruments Used:

<i>Nomenclature</i>	<i>Make/Model</i>	<i>Cal. at</i>	<i>Cal. Validity</i>
Dry Well Calibrator	Hart Scientific/9107	ETDC	30-07-2013
Thermometer Readout	Hart Scientific/1529	ETDC	09-04-2013
PRT	Hart Scientific/5626	ETDC	15-11-2012

Fig. C2 : Caibration standard of Thermocouples



TEMP/ALD/CS/37

Calibration Report

Calibration Results

Sl.No	Set Temp (°C)	Ref Temp (°C)	K-115 (°C)	Error	K-114 (°C)	Error	K-117 (°C)	Error
1	-40	-39.641	-36.95	2.691	-36.96	2.681	-37.00	2.641
2	-30	-29.448	-27.37	2.078	-27.40	2.048	-27.41	2.038
3	-20	-19.409	-17.89	1.519	-17.95	1.459	-17.96	1.449
4	-10	-9.420	-8.39	1.030	-8.39	1.030	-8.38	1.040
5	0	0.419	0.88	0.461	0.85	0.431	1.17	0.751
6	10	10.182	10.45	0.268	10.43	0.248	10.72	0.538
7	20	20.031	19.92	-0.111	19.93	-0.101	20.23	0.199
8	30	29.987	29.67	-0.317	29.72	-0.267	29.95	-0.037
9	40	40.224	39.52	-0.704	39.49	-0.734	39.81	-0.414
10	50	50.010	49.31	-0.700	49.28	-0.730	49.59	-0.420

Fig. C3 : Calibration report of Thermocouples

PUBLICATIONS

Amaranatha Raju, M., Ashok Babu, T.P. and Ranganayakulu, C. (2017). “*Flow boiling heat transfer and pressure drop analysis of R134a in a brazed heat exchanger with offset strip fins*”. J. Heat Mass Transfer., DOI 10.1007/s00231-017-2060-1.

Amaranatha Raju, M., Ashok Babu, T.P. and Ranganayakulu, C. (2015). “*Development of single phase heat transfer correlations for water & R134a in rectangular channel with smooth wavy fin*”. J. Phys Sci. Appl., Vol.5 (3), 199-208.

Amaranatha Raju, M., Ashok Babu, T.P. and Ranganayakulu, C. (2015). “*All electric cooling system for unmanned aircrafts*”. J. Aerosp. Sci. Technol, Vol.67 (4), 488-499.

CURRICULUM VITAE



Name : Muppala. Amaranatha Raju

Registration No. : 092008ME09P08

Department : Mechanical Engineering

Degree Registered : Ph.D

CGPA in Course work : 8.5

Earned credits : 12

Address : **Residence**
405, Sree Sapthagiri Paradise Apartment
KGF Munireddy Layout, Mahadevapura
Bangalore-560 048

Office
Scientist-‘E’
General systems directorate
Aeronautical Development Agency (ADA)
P. B. No.1718, Vimanapura Post
Bangalore-560 017

Email : amaranatha@yahoo.com

Phone No : 9900707180 (Mobile), 080-25087256 (O)

Work Experience : Presently working as Scientist in the Aeronautical Development Agency (ADA), Bangalore and having 15 years work experience in the field of design and development of compact heat exchangers, development of environmental control system for aircraft application and analysis of system performance. I received my bachelor's degree in mechanical engineering from Nagarjuna University, Guntur and Master's degree in Mechanical Engineering from NIT, Trichy. Guided 2 M.Tech students for their academic projects.